

This item was submitted to Loughborough University as a PhD thesis by the author and is made available in the Institutional Repository (<https://dspace.lboro.ac.uk/>) under the following Creative Commons Licence conditions.



For the full text of this licence, please go to:  
<http://creativecommons.org/licenses/by-nc-nd/2.5/>

# **DESIGN ADVANCES OF EMBROIDERED FABRIC ANTENNAS**

By

Shiyu Zhang

A Doctoral Thesis Submitted in Partial Fulfilment of the  
Requirements for the Award of Doctor of Philosophy of  
Loughborough University

April 2014

© by Shiyu Zhang 2014

# Abstract

---

Wearable technology has attracted global attention in the last decade and the market is experiencing an unprecedented growth. Wearable devices are designed to be low-profile, light-weight and integrated seamlessly into daily life. Comfort is one of the most important requirements for wearable devices. Fabric based antennas are soft, flexible and can be integrated into clothing. State of the art textile manufacturing techniques such as embroidery, combined with advanced conductive textile materials can be used to fabricate flexible fabric based on-body antennas.

In this thesis, the feasibility of using computerised embroidery in the fabrication of wearable, flexible yet functional fabric based antennas have been examined. The fabric based antennas are embroidered using conductive threads. The most suitable materials for fabricating embroidered antennas have been identified. The embroidered fabric based antenna systems including transmission lines and low-profile detachable connectors have been fabricated and their RF performances have been tested. The optimal manufacturing parameters related to embroidery such as stitch direction, spacing and length have been examined. The repeatability of embroidered antennas, cost estimation, and complexity of manufacturing process have been clearly presented. The results can be used to inform and provide guidelines for the development of representative products that can be mass manufactured.

A new simulation approach has been introduced to analyse the anisotropic properties of embroidered conductive threads. Simulations and measurements indicate that the performances of embroidered antennas are affected by the anisotropic surface current due to the embroidered stitches. Exploiting the current direction, a novel non-uniform meshed patch antenna has been designed. Representative results show that the non-uniform meshed structure can significantly reduce more than 75% of the usage of conductive materials for the microstrip antennas with negligible effect on the antenna performance.

# Acknowledgements

---

First of all, I would like to give my sincere and foremost gratitude to my supervisors: Mr. Robert Seager, Prof. Yiannis Vardaxoglou and Dr. William Whittow, for their irreplaceable advice, guidance and shared knowledge throughout my PhD. I would also like to express my great appreciation to Dr. Alford Chauraya for the invaluable assistance with the measurements. Without their great support and encouragement, it would be difficult for me to finish this thesis and complete my study satisfactorily.

I am also grateful to Miss. Tessa Acti and Prof. Tilak Dias from Nottingham Trent University for sharing their knowledge of embroidery and fabricating embroidered samples. Their suggestions and contributions were very important in this project.

I would like to thank Dr. James Flint and Dr. Chinthana Panagamuwa who shared their experience which gave me invaluable advice in my research. Also I need to thank the colleagues in CMCR and WiCR labs: Ajit, Aris, Chinwe, Emma, John, Seun, Syed, for their advice, inspiration and friendship.

Last but not least, I would like to thank my parents and all my family members for their encouragements, understanding, and patience during the years of my PhD.



# List of Publications

---

1. S. Zhang, R. Seager, A. Chauraya, W. Whittow, Y. Vardaxoglou, “Non-uniform Meshed Embroidered Patch Antennas”, *2014 IEEE International Symposium on Antennas and Propagation and USNC-URSI Radio Science Meeting*, 2014
2. S. Zhang, R. Seager, A. Chauraya, W. Whittow, Y. Vardaxoglou, “Non-uniform Meshed Microstrip Antennas for Wearable Applications”, *8th European Conference Antennas and Propagation (EuCAP)*, 2014
3. R. Seager, S. Zhang, W. Whittow, A. Chauraya, Y. Vardaxoglou, T. Acti, T. Dias, “Effect of the Fabrication Parameters on the Performance of Embroidered Antennas”, *IET Microwaves, Antennas and Propagation*, Volume 7, Issue 14, 19 November 2013, pp. 1174–1181
4. S. Zhang, A. Chauraya, W. Whittow, R. Seager, T. Acti, T. Dias, Y. Vardaxoglou, “Repeatability of Embroidered Patch Antennas”, *2013 Loughborough Antennas and Propagation Conference (LAPC)*
5. A. Chauraya, R. Seager, W. Whittow, S. Zhang, Y. Vardaxoglou, “Embroidered Frequency Selective Surfaces on Textiles for Wearable Applications”, *2013 Loughborough Antennas and Propagation Conference (LAPC)*
6. R. Seager, A. Chauraya, S. Zhang, W. Whittow, Y. Vardaxoglou, “Flexible Connectors for Fabric Based Systems”, *Electronics Letters*, Volume 49, Issue 22, 24 October 2013, pp.1371-1373
7. A. Chauraya, T. West, R. Seager, W. Whittow, S. Zhang, Y. Vardaxoglou, “Positioner Effects in Measurements of Low-Medium Gain Antennas”, *2013 Antenna Measurement Techniques Association*
8. S. Zhang, A. Chauraya, R. Seager, Y. Vardaxoglou, W. Whittow, T. Acti, T. Dias, “Fully Fabric Knitted Antennas for Wearable Electronics”, *2013 IEEE*

*International Symposium on Antennas and Propagation and USNC-URSI National Radio Science Meeting*

9. S. Zhang, A. Chauraya, W. Whittow, R. Seager, T. Acti, T. Dias, Y. Vardaxoglou, "Embroidered Wearable Antennas Using Conductive Threads with Different Stitch Spacings," *2012 Loughborough Antennas and Propagation Conference (LAPC)*
10. S. Zhang, A. Chauraya, W. Whittow, R. Seager, T. Acti, T. Dias, Y. Vardaxoglou, "Simulation Methodology to Model the Behaviour of Wearable Antennas Composed of Embroidered Conductive Threads," *2012 IEEE International Symposium on Antennas and Propagation and USNC-URSI National Radio Science Meeting*
11. A. Chauraya, S. Zhang, W. Whittow, T. Acti, R. Seager, T. Dias, Y. Vardaxoglou, "Addressing the Challenges of Fabricating Microwave Antennas Using Conductive Threads," *6th European Conference Antennas and Propagation (EuCAP)*, 2012
12. T. Acti, S. Zhang, A. Chauraya, W. Whittow, R. Seager, T. Dias, Y. Vardaxoglou, "High Performance Flexible Fabric Electronics for Megahertz Frequency Communications," *2011 Loughborough Antennas and Propagation Conference (LAPC)*
13. T. Acti, A. Chauraya, S. Zhang, W. Whittow, R. Seager, Y. Vardaxoglou, T. Dias, "Embroidered Wire Dipole Antennas Using Novel Copper Yarns," *IEEE Antennas and Wireless Propagation Letters*, (Submitted May 2014)
14. S. Zhang, R. Seager, A. Chauraya, W. Whittow, Y. Vardaxoglou, "Non-uniform Meshed Microstrip Antennas," *IEEE Transactions on Antennas and Propagation*, (in preparation)

# Acronyms

---

AC	Alternating current
AUT	Antenna under test
BW	Bandwidth
CAD	Computer aided design
CAM	Computer aided manufacturing
CPW	Coplanar Waveguide
dB	Decibels
dBi	Decibels compared to an isotropic radiator
DC	Direct current
EM	Electromagnetic
EU	European Union
FCC	Federal Communication Commission
FDTD	Finite difference time domain
FPGA	Field programmable gate array
GPS	Global Positioning System
ICNIRP	International Commission on Non-Ionizing Radiation Protection
MPA	Microstrip patch antenna
PCB	Printed Circuit Board
PEC	Perfect electrical conductor
PVC	Polyvinyl chloride
RF	Radio Frequency
RFID	Radio frequency identification

## *Acronyms*

---

SAR	Specific absorption rate
SEM	Scanning electron microscope
SMA	SubMiniature version A
SPDR	Split post dielectric resonator
SWNT	Single-walled carbon nanotube
TM	Transverse Magnetic
UHF	Ultra high frequency
VHF	Very high frequency
VNA	Vector Network Analyser
WLAN	Wireless Local Area Network

# List of Symbols

---

$\rho$	Resistivity ( $\Omega\cdot\text{m}$ )
$R$	Resistance ( $\Omega$ )
$R_s$	Resistance of embroidered stitch ( $\Omega$ )
$R_c$	Contact resistance between adjacent embroidered stitches ( $\Omega$ )
$\sigma$	Conductivity (S/m)
$\delta$	Skin depth ( $\mu\text{m}$ )
$\mu_0$	Permeability of free space ( $4\pi \times 10^{-7}$ H/m)
$\mu_r$	Relative permeability
$f$	Frequency (Hz)
$\lambda$	Wavelength (m)
$c$	Free-space velocity of light ( $3 \times 10^8$ m/s)
$f_r$	Resonant frequency (Hz)
$(f_{rc})_{01}$	Resonant frequency of microstrip antenna at $\text{TM}_{01}$ mode (Hz)
$\Delta f$	-3 dB bandwidth (Hz)
$\varepsilon_0$	Permittivity of free space ( $\approx 8.85 \times 10^{-12}$ F/m)
$\varepsilon_r$	Relative permittivity
$\varepsilon_e$	Effective dielectric constant
$\tan \delta$	Loss tangent delta
$h$	Thickness of dielectric substrate (mm)
$Z_0$	Characteristic impedance ( $\Omega$ )
$L_s$	Stitch length (mm)
$T$	Depth of the inserted embroidery (mm)
$L_{total}$	Total length of thread (mm)

## List of Symbols

---

$L_{extra}$	Extra length that compared to the designed length (mm)
$s$	Stitch spacing (mm)
$N$	Number of stitches
$N_{parallel}$	Number of stitches for embroidered transmission line with parallel stitch
$N_{perpendicular}$	Number of stitches for embroidered transmission line with perpendicular stitch
$Q$	Quality factor
$Q_{rad}$	Quality factor due to radiation losses
$Q_c$	Quality factor due to conduction losses
$Q_d$	Quality factor due to dielectric
$Q_{sw}$	Quality factor due to surface wave losses
$L$	Length of microstrip antenna (mm)
$\Delta L$	Extended length of microstrip antenna due to fringing field (mm)
$W$	Width of microstrip antenna (mm)
$d$	Distance from feed position to microstrip antenna edge (mm)
$\omega$	Radian frequency ( $\omega = 2\pi f$ ) (rad/s)
$E$	Electric field intensity (V/m)
$E_x$	Electric field component in x direction (V/m)
$E_y$	Electric field component in y direction (V/m)
$E_z$	Electric field component in z direction (V/m)
$j$	Surface current density (A/m)
$j_x$	Surface current density in x direction (A/m)
$j_y$	Surface current density in y direction (A/m)
$j_z$	Surface current density in z direction (A/m)

## List of Symbols

---

$f_0$	Resonant frequency of empty split post dielectric resonator
$f_s$	Resonant frequency of split post dielectric resonator with fabric sample
$h_s$	Thickness of the fabric sample under test
$K_\epsilon$	Function of relative permittivity and dielectric thickness for a given split post dielectric resonator
$Q_c$	Q factor depending on metal losses for the split post dielectric resonator containing the fabric sample under test
$Q_{c0}$	Q factor depending on metal losses for empty split post dielectric resonator
$Q_{DR}$	Q factor depending on dielectric losses in the split post dielectric resonator
$P_{es}$	Electric energy filling factor of the fabric sample under test
$P_{eDR}$	Electric energy filling factors for the fabric sample contained the split post dielectric resonator
$P_{eDR0}$	Electric energy filling factors for the empty split post dielectric resonator

# List of Figures

---

Figure 1-1 Steve Mann’s wearable computers.....	1-2
Figure 1-2 Smart watch (made by SONY) .....	1-3
Figure 1-3 Programmed LED dress at catwalk (by Hussein Chalayan) .....	1-4
Figure 2-1 Conductive woven fabric from Shieldex.....	2-3
Figure 2-2 A wearable fabric digital television antenna.....	2-3
Figure 2-3 A woven fabric with a vertical conductive path using both conductive and nonconductive yarns .....	2-5
Figure 2-4 Structure of yarns in knitted fabric.....	2-6
Figure 2-5 A monofilament nickel wire sewed onto a cotton fabric made at Nottingham Trent University.....	2-11
Figure 2-6 Zoomed in pictures of two nonconductive threads with 40 µm diameter metal wires twisted around them .....	2-12
Figure 2-7 Sketch of cross section of the single thread of Amberstrand.....	2-14
Figure 2-8 SEM image of unbraided Amberstrand Silver filaments.....	2-15
Figure 2-9 SEM image of single filament of Amberstrand Silver.....	2-16
Figure 2-10 SEM image of broken section of coated layer .....	2-17
Figure 2-11 SEM image of cross section of coated layer .....	2-17
Figure 2-12 Cross sections of filaments in Amberstrand thread.....	2-18
Figure 2-13 Equivalent metallization thickness of (a) cylinder and (b) flattened models of multifilament conductive thread in AC .....	2-20
Figure 2-14 Computerised embroidery machine at Nottingham Trent University .....	2-22



*List of Figures*

---

Figure 2-15 Computerised embroidery machine at Loughborough University.....	2-22
Figure 2-16 Different patterns of embroidered stitches embroidered at Nottingham Trent University.....	2-23
Figure 2-17 Sketch of the lock stitches.....	2-24
Figure 2-18 Model of embroidered conductive thread length using lock stitches...	2-25
Figure 2-19 Embroidered rectangular patch with 0.8 mm stitch spacing .....	2-27
Figure 2-20 Zoomed in view of needle before and after embroidering of conductive yarns.....	2-29
Figure 2-21 Measurement setup for permittivity and loss tangent values of fabric samples .....	2-31
Figure 2-22 Zoomed in view of 0.53 mm thick denim fabric.....	2-33
Figure 2-23 Zoomed in view of 4.30 mm thick felt fabric .....	2-33
Figure 2-24 Zoomed in view of thermal melt copolyamide web strip .....	2-34
Figure 2-25 U.FL low profile connectors .....	2-36
Figure 2-26 Covered low profile U.FL connector with flexible cable .....	2-36
Figure 3-1 Textile transmission lines made out of conductive woven fabric .....	3-2
Figure 3-2 Stitch directions of embroidered transmission lines: (a) perpendicular and (b) parallel.....	3-5
Figure 3-3 Stitch spacings of (a) parallel stitch and (b) perpendicular stitch .....	3-6
Figure 3-4 Zoomed in view of 3 mm wide perpendicular transmission lines with different stitch spacings .....	3-7
Figure 3-5 Zoomed in view of 3 mm wide parallel transmission lines with different stitch spacings.....	3-8

Figure 3-6 Equivalent electrical model of parallel stitched transmission line and zoomed in view .....	3-11
Figure 3-7 Sketches of perpendicular stitch direction transmission lines with different stitch spacing .....	3-12
Figure 3-8 Equivalent electrical model of perpendicular stitched transmission line and zoomed in view .....	3-13
Figure 3-9 Test jig used for embroidered transmission line measurements .....	3-14
Figure 3-10 (a) Zoomed in view of SMA probe pressed down onto the embroidered transmission line (b) Five repeated S11 measurements of the same line .....	3-16
Figure 3-11 (a) Zoomed in view of enlarged contacting area probe pressed down onto the embroidered transmission line (b) Five repeated S11 measurements of the same line .....	3-17
Figure 3-12 S21 of Amberstrand Nickel 166 transmission lines with different stitch directions and spacings .....	3-18
Figure 3-13 S21 of Amberstrand Copper 66 transmission lines with different stitch directions and spacings .....	3-19
Figure 3-14 S21 of Liberator Silver 40 transmission lines with different stitch directions and spacings .....	3-19
Figure 3-15 S11 of embroidered transmission lines with parallel stitch direction ...	3-21
Figure 3-16 S11 of embroidered transmission lines with perpendicular stitch direction .....	3-22
Figure 3-17 Zoomed in view of loop strip .....	3-23
Figure 3-18 Zoomed in view of hook strip .....	3-24

Figure 3-19 Sketch of the cross section of hook and loop connector on gapped transmission line.....3-25

Figure 3-20 (a) Zoomed in view of gapped transmission line with hook attached (b) After loop strips are placed across the gap.....3-26

Figure 3-21 S11 of hook and loop ‘switches’ .....3-27

Figure 3-22 S21 of hook and loop ‘switches’ .....3-27

Figure 3-23 Zoomed in view of electroplated loop strip .....3-28

Figure 3-24 Zoomed in view of electroplated hook strip .....3-29

Figure 3-25 S11 data for all eight hook and loop ‘switches’ .....3-30

Figure 3-26 S21 data for all eight hook and loop ‘switches’ .....3-31

Figure 4-1 Sketch of patches with different stitch directions ..... 4-5

Figure 4-2 Sketch of DC resistance measurement in x and y directions ..... 4-5

Figure 4-3 Geometry and feed position of the embroidered and etched patch antenna ..... 4-7

Figure 4-4 Sketch of upside down embroidered patch antenna on rigid dielectric substrate, with thermal melt adhesive between base fabric and substrate ..... 4-10

Figure 4-5 Measured S11 of four 0.4 mm stitch spacing embroidered patch antenna with different stitch direction and etched copper patch antenna ..... 4-13

Figure 4-6 Measured electric field gain radiation patterns (in dBi) on  $\phi=0^\circ$  plane ..... 4-14

Figure 4-7 Simulation of measurement tower in anechoic chamber ..... 4-15

Figure 4-8 Simulated gain pattern of etched copper patch antenna with measurement tower showing enlarged back lobe (in dBi)..... 4-16

Figure 4-9 Two groups of *identical* embroidered patch antennas with different stitch spacings..... 4-17

Figure 4-10 Measured S11 of eight *identical* embroidered patch antennas with diagonal 0.4 mm stitch spacing ..... 4-19

Figure 4-11 Measured S11 of eight *identical* embroidered patch antennas with diagonal 0.8 mm stitch spacing ..... 4-19

Figure 4-12 Measured dual polarization gain patterns (in dBi) of eight *identical* diagonal stitch antennas with 0.4mm spacing ..... 4-22

Figure 4-13 Measured dual polarization gain patterns (in dBi) of eight *identical* diagonal stitch antennas with 0.8mm spacing ..... 4-22

Figure 4-14 Measured electric field gain pattern (in dBi) of one diagonal stitched antenna with 0.4 mm spacing ..... 4-23

Figure 4-15 Measured electric field gain pattern (in dBi) of one diagonal stitched antenna with 0.8 mm spacing ..... 4-23

Figure 4-16 Simulated solid patch total efficiency with different conductivity values ..... 4-26

Figure 4-17 Microscope image of 0.4 mm spacing vertically embroidered stitches ..... 4-27

Figure 4-18 Horizontal zigzag metal conductor separated by low conductivity “gaps” ..... 4-29

Figure 4-19 Vertical zigzag metal conductor separated by low conductivity “gaps” ..... 4-29

Figure 4-20 Simulated S11 for the patch with horizontal metal conductors separated by different conductivity values ..... 4-30

Figure 4-21 Simulated S11 for the patch with vertical metal conductors separated by different conductivity values ..... 4-30

Figure 4-22 Simulated surface currents for zigzag patch with horizontal conductors separated by a conductivity of  $1 \times 10^5$  S/m..... 4-32

Figure 4-23 Simulated surface currents for zigzag patch with vertical conductors separated by a conductivity of  $1 \times 10^5$  S/m..... 4-32

Figure 4-24 Simulated patch total efficiency for the zigzag patches with low conductivity area compared with homogeneous solid patch antenna with equivalent conductivity..... 4-33

Figure 5-1 Sketch of uniform meshed patch structure ..... 5-3

Figure 5-2 Sketch of non-uniform meshed patch structure..... 5-5

Figure 5-3 Metal coverage of meshed patch with different mesh sizes..... 5-6

Figure 5-4 Simulation of changes in resonant frequency with different mesh sizes of uniform meshed patch antennas..... 5-7

Figure 5-5 S11 of uniform meshed patch antennas with different mesh spaces..... 5-9

Figure 5-6 S11 of non-uniform meshed patch antennas with different mesh spaces 5-9

Figure 5-7 Electric field distribution for the (a)TM<sub>01</sub> and (b)TM<sub>10</sub> mode in the microstrip cavity ..... 5-10

Figure 5-8 Electric fields of solid patch antenna at TM<sub>01</sub> mode..... 5-11

Figure 5-9 Electric fields of 3 mm uniform meshed patch at TM<sub>01</sub> mode..... 5-12

Figure 5-10 Electric fields of 3 mm non-uniform meshed patch at TM<sub>01</sub> mode ..... 5-12

Figure 5-11 *x* direction component of surface current distribution in a solid patch at TM<sub>01</sub> mode ..... 5-13

Figure 5-12  $y$  direction component of surface current distribution in solid patch at  $TM_{01}$  mode ..... 5-14

Figure 5-13 Surface current distribution on solid patch in  $x$  &  $y$  directions at  $TM_{01}$  mode..... 5-14

Figure 5-14  $x$  direction component of surface current distribution in  $3\text{ mm} \times 3\text{ mm}$  uniform meshed patch at  $TM_{01}$  mode..... 5-15

Figure 5-15  $y$  direction component of surface current distribution in  $3\text{ mm} \times 3\text{ mm}$  uniform meshed patch at  $TM_{01}$  mode..... 5-16

Figure 5-16 Current distribution on  $3\text{ mm} \times 3\text{ mm}$  uniform meshed patch in  $x$  &  $y$  directions at  $TM_{01}$  mode..... 5-16

Figure 5-17  $x$  direction component of surface current distribution in  $3\text{ mm}$  space non-uniform meshed patch at  $TM_{01}$  mode..... 5-18

Figure 5-18  $y$  direction component of surface current distribution in  $3\text{ mm}$  space non-uniform meshed patch at  $TM_{01}$  mode..... 5-18

Figure 5-19 Current distribution on  $3\text{ mm}$  space non-uniform meshed patch in  $x$  &  $y$  directions at  $TM_{01}$  mode..... 5-19

Figure 5-20 Simulated electric field gain patterns (in dBi) of solid copper,  $1\text{ mm}$  non-uniform meshed and  $4\text{ mm}$  non-uniform meshed patch antennas..... 5-20

Figure 5-21 Simulated total efficiency as a function of metal surface coverage..... 5-24

Figure 5-22 Effects of conduction loss and dielectric loss on meshed patch antennas ..... 5-28

Figure 5-23 Etched  $1\text{ mm}$  spacing uniform meshed patch antenna ..... 5-29

Figure 5-24 Etched  $1\text{ mm}$  spacing non-uniform meshed patch antenna..... 5-30

Figure 5-25 Measured  $S_{11}$  of etched copper meshed patch antennas ..... 5-30

*List of Figures*

---

Figure 5-26 Measured electric field gain patterns (in dBi) on  $\phi=0^\circ$  plane of etched  
..... 5-32

Figure 5-27 Simulation non-uniform meshed patch antennas with different conductive  
materials and metallization thickness..... 5-34

Figure 5-28 Embroidered 1 mm spaced non-uniform meshed patch on denim fabric  
..... 5-36

Figure 5-29 Measured S11 results of embroidered and etched 1 mm non-uniform  
meshed patch antennas ..... 5-36

Figure 5-30 Measured electric field gain patterns (in dBi) of embroidered 1 mm non-  
uniform meshed patch antenna..... 5-37

Figure 5-31 Embroidered 1 mm non-uniform meshed patch antenna on flexible felt  
substrate..... 5-39

Figure 5-32 Measured S11 of embroidered non-uniform meshed and solid copper tape  
patch antennas on felt substrate..... 5-40

Figure 5-33 Measured electric field gain patterns (in dBi) of copper tape patch  
antenna with felt substrate at 5.08 GHz on ..... 5-41

Figure 5-34 Measured electric field gain patterns (in dBi) of embroidered 1 mm non-  
uniform meshed patch antenna with felt substrate at 4.72 GHz ..... 5-41

Figure A-1 Schematic diagram of a split post dielectric resonator.....A-1

# List of Tables

---

Table 2-1 Summary of approaches for fabricating electro-textiles .....	2-8
Table 2-2 Summary of dielectric properties of nonconductive fabrics.....	2-30
Table 2-3 Dielectric measurements of fabric substrates using split post dielectric resonator.....	2-32
Table 3-1 DC resistance of single thread and embroidered transmission lines .....	3-9
Table 3-2 DC resistance of 5 cm long and 1.6 cm wide hook and loop strip .....	3-25
Table 3-3 DC resistances of 5 cm long and 1.6 cm wide hook and loop before and after electroplating .....	3-29
Table 4-1 Measured DC resistances of Amberstrand Silver patches with different stitch spacings and directions .....	4-6
Table 4-2 Measured results for embroidered patch antennas on RF-45 substrate...	4-12
Table 4-3 Measured results of 0.4 mm stitch spacing embroidered antennas .....	4-20
Table 4-4 Measured results of 0.8 mm stitch spacing embroidered antennas .....	4-20
Table 5-1 Simulation results of uniform meshed patch antenna.....	5-22
Table 5-2 Simulation results of non-uniform meshed patch antennas.....	5-23
Table 5-3 Effects of conduct loss and dielectric loss to meshed patch antennas.....	5-26
Table 5-4 Measured results of meshed patch antennas.....	5-31
Table 5-5 Measured results of etched and embroidered 1 mm non-uniform meshed patch antennas.....	5-37
Table 5-6 Measured copper and embroidered patch antennas on felt substrate .....	5-40



# Contents

---

<b>Summary</b> .....	I
<b>Acknowledgements</b> .....	II
<b>List of Publications</b> .....	III
<b>Acronyms</b> .....	V
<b>List of Symbols</b> .....	VII
<b>List of Figures</b> .....	X
<b>List of Tables</b> .....	XVIII
<b>CHAPTER 1 INTRODUCTION</b> .....	1-1
1.1 Overview of Wearable Communications .....	1-1
1.2 Challenges of Fabric Based Wearable Antennas .....	1-5
1.3 Novel Contributions of this Thesis .....	1-6
1.4 An Overview of this Thesis.....	1-7
References.....	1-9
<b>CHAPTER 2 MATERIALS AND MANUFACTURING TECHNIQUES FOR FABRIC RF SYSTEMS</b> .....	2-1
2.1 Electro-textiles .....	2-1
2.1.1 Fabricating of Electro-textiles.....	2-1
2.1.2 DC and RF Characteristics of Electro-textiles.....	2-9
2.2 Conductive Threads for Embroidery.....	2-10

2.2.1	Fabrication of Conductive Threads.....	2-10
2.2.2	Amberstrand.....	2-13
2.2.3	Conductivity of Amberstrand Threads.....	2-18
2.3	Embroidering Conductive Threads .....	2-21
2.3.1	Computerised Embroidery Machine and Stitch Patterns.....	2-21
2.3.2	Model of Embroidered Stitches .....	2-23
2.3.3	Potential Issues Related to the Embroidery Process .....	2-28
2.4	Dielectric Properties of Fabrics.....	2-29
2.5	Low-profile RF Connectors for Fabric Antennas .....	2-35
2.6	Conclusions .....	2-37
	References.....	2-40

## **CHAPTER 3 EMBROIDERED TRANSMISSION LINES AND**

	<b>FLEXIBLE CONNECTORS .....</b>	<b>3-1</b>
3.1	Embroidered Microstrip Transmission lines.....	3-1
3.1.1	Introduction.....	3-1
3.1.2	Embroidered Stitches of Fabric Transmission Lines.....	3-4
3.1.3	DC Resistance of Embroidered Transmission Lines .....	3-8
3.1.4	RF Measurement Setup for Embroidered Transmission Lines.....	3-14
3.1.5	RF Performance of Embroidered Transmission Lines.....	3-18
3.2	Hook and Loop Connectors.....	3-22
3.2.1	Introduction.....	3-22
3.2.2	DC Resistance of Hook and Loop .....	3-24
3.2.3	RF Performance of Hook and Loop Connectors.....	3-25
3.2.4	Electroplated Hook and Loop Connectors.....	3-28

3.3	Conclusions .....	3-31
	References .....	3-33

**CHAPTER 4 EFFECT OF FABRICATION PARAMETERS ON EMBROIDERED MICROSTRIP ANTENNAS ..... 4-1**

4.1	Introduction .....	4-1
4.2	Sheet Resistance of Embroidered Microstrip Antennas.....	4-4
4.3	RF performance of Embroidered Microstrip Antennas.....	4-7
4.3.1	Fabrication and Feeding.....	4-7
4.3.2	RF performance of Embroidered Microstrip Antennas .....	4-11
4.4	Repeatability of Embroidered Microstrip Antennas .....	4-16
4.5	Simulation Models of Embroidered Microstrip Antennas .....	4-24
4.5.1	Solid Microstrip Antennas with Equivalent Conductivity Values.....	4-24
4.5.2	Anisotropic Microstrip Antennas with Zigzag Patterns .....	4-26
4.6	Conclusions .....	4-34
	References.....	4-37

**CHAPTER 5 MESHED MICROSTRIP ANTENNAS ..... 5-1**

5.1	Introduction .....	5-1
5.2	Non-Uniform Meshed Microstrip Antennas .....	5-4
5.3	Antenna Modes and Surface Current Distribution.....	5-6
5.3.1.	Resonant Frequencies of Meshed Microstrip Antennas .....	5-6
5.3.2.	TM <sub>01</sub> Mode of Meshed Microstrip Antennas.....	5-10

5.3.3.	Surface Current Distribution of Meshed Microstrip Antennas at $TM_{01}$ Mode .....	5-13
5.3.4.	Cross Polarization of Non-Uniform Meshed Microstrip Antennas ...	5-19
5.4	Effect of Metal Coverage of Meshed Microstrip Antennas .....	5-21
5.5	Factors of Losses in Meshed Microstrip Antennas .....	5-25
5.6	Etched Meshed Microstrip Antennas .....	5-29
5.7	Embroidered Non-Uniform Meshed Microstrip Antennas .....	5-33
5.7.1	Skin Effects of Conductive thread on Antenna Efficiency .....	5-33
5.7.2	Measured Results of Embroidered Non-uniform Meshed Microstrip Antennas .....	5-35
5.8	Low Loss Flexible Dielectric Substrate Materials .....	5-38
5.9	Conclusions .....	5-42
	References .....	5-44
 <b>CHAPTER 6 CONCLUSIONS AND FUTURE WORK</b> .....		6-1
6.1	Summary of Research Novelty .....	6-1
6.2	Summary of Results .....	6-2
6.3	Implications for Industry .....	6-4
6.4	Future Work .....	6-5
 <b>APPENDIX A SPLIT POST DIELECTRIC RESONATOR</b> .....		A-1

# Chapter 1

## Introduction

---

### 1.1 Overview of Wearable Communications

The development of wearable antennas over the last decade contributes to the boom of the wide area of wearable personal communications. With the demand for mobility, multi-functionality and also reliability of the mobile computing, the devices are now expected to be lighter, smaller, and more importantly, to be wirelessly networked. Wearable communication is the solution that meets the requirements of convenient, light-weight and “always on”. Wearable devices are portable and can be functioned without the user manipulation. They are capable to be used in a large number of applications including aerospace, health and medical, fitness and wellness, location tracking, harsh environment, military, disabilities, entertainment and fashion [1]–[7].

The growth of the wearable communication market is remarkable. According to the prediction from IHS Electronic and Media, the global wearable technology market will be worth \$30 billion in 2018 [8]. With the development of on-body sensors, sports and health are expected to become two of the largest markets for wearable technology, associated with the personal fitness and wellness which also play a growing role in the wearable health sensor sector. ABI Research forecasts that the total number of wearable devices in sports and health will grow to 169.5 million by 2017, up from 20.77 million in 2011, with 41% compound annual growth rate [9].

Without the physical cables and connectors, the wearable system is lighter and more flexible than the conventional wired system for the user. This is more convenient and

effective for people accessing information on demand. The IEEE standards of wireless communication such as Bluetooth, Zigbee and Local Area Network (LAN) support networked wireless wearable systems. Well-designed and optimized antennas are important for such system in order to provide highly efficient links [10]. High data rates and robust channels are also required for the capability of dealing with increasingly big data [1]. Cellular devices can play the role of a hub or terminal which collect the data from wearable devices, display the information to the users and synchronise with the Internet.

The earliest wearable computer was designed to be hidden behind clothes for the purpose of cheating at the game of roulette [11]. After that, in 1980 Mann built the first wearable device with a wearable antenna on a helmet that provided wireless connecting [12], see Figure 1-1 (a). Then further developments were made to improve the portability of the wearable system. Figure 1-1 (b) to (e) show the route of improvement. As it is shown in the picture, the size of the wearable system including the antenna were minimised due to the demand of mobility and light-weight. The other components such as the processor and the battery were placed on different parts of body separately. Since there is large available area on clothing, the components of the wearable system can be individually placed on different locations of the cloth.



Figure 1-1 Steve Mann's wearable computers [13]

The development of the field programmable gate array (FPGA) and microelectronics have also boosted wearable technology. The electronic components have become significantly smaller. Researchers start integrating the wireless devices including antennas into the accessories such as belts, watches, necklaces and glasses [14]–[18]. These miniature electronics are designed for aiding the cloud computing. Figure 1-2 shows a smart watch [19] as an example of wireless wearable computing. The watch has the functions of music playing, sports monitoring, and can access user accounts on the Internet such as email and social networks. Users can download applications to the watch to personalise their experience.



**Figure 1-2 Smart watch (made by SONY [19])**

On the other hand, comfort is one of the most important requirements for the wearable devices. For this reason, wearable electronics can be made by flexible fabric materials and integrated into clothing. This smart textile made by the advanced electro-textile materials are flexible, light-weight and can be placed closer to the skin which is ideal for building the on-body network systems. Users will not be aware of the antenna due to fabric nature of the wearable antennas. This type of smart textile is ideal for long-term, real-time monitoring such as health care sensors, navigation and fitness monitoring [2], [20]–[23]. Furthermore, since some antennas at MHz spectrum, for

instance VHF (very high frequency) and UHF (ultra high frequency) band, require certain physical sizes, fabric antennas can utilise the available space in the cloth without increasing the volume of the device [24]. There will also be aesthetic advantages of the smart textiles as the design of wearable electronics will add to the cosmetic appeal and can be considered as fashion accessories rather than being hidden. Figure 1-3 shows a programmable LED dress at a fashion show.



**Figure 1-3 Programmed LED dress at catwalk (by Hussein Chalayan [25])**

In this thesis, embroidery will be used to make fabric based wearable antennas. The embroidered antennas are flexible and can be directly embroidered onto the clothes at



the manufacturing stage. Computerised embroidery machines enable the embroidered antennas to be mass manufactured which will reduce the cost of manufacturing wearable antennas.

## 1.2 Challenges of Fabric Based Wearable Antennas

The first challenge comes from the material. As mentioned in Section 1.1, the conventional rigid materials are uncomfortable and not suitable for wearable antennas. To overcome this problem, conductive textile materials can be used to make the conducting elements in wearable antennas to realise the textile features [26]–[29]. Sourcing the most suitable material for fabricating the flexible fabric based wearable antennas is one of the primary targets. However, due to the anisotropic and non-PEC properties of the conductive textiles, the conduction characteristics of electro-textile are different from conventional conductors. Compared with the current in solid conductors, the current in the electro-textile is non-uniform and directional due to the fabric fibres, particular for embroidered conductors. The antenna performance highly depends on the current distribution in the fabric. This anisotropic nature of fabric should be considered at the design stage to optimise the fabric antenna performance.

Another challenge comes from the human body because by definition wearable antennas are placed close to the skin. The performance of these antennas is influenced by the human tissues. Antennas that are near to the body are detuned and their resonant frequencies are different from in free space. The dielectric properties of tissues has been examined by Gabriel *et al.* in [30]–[32]. The results show tissues have high relative permittivity and the values depend on the tissue type. For example at 2.4 GHz, the muscle has a relative permittivity of 52.8 and loss tangent of 0.24; the relative permittivity of fat is 5.3 and loss tangent is 0.15. With increasing frequency, the relative permittivity decreases. Moreover, antennas on different locations on the body perform differently. The relative positions of the transmitting and receiving

antennas have a significant impact on the channels of body centric networks [14], [33]–[35]. Furthermore, the movements of the user and postures will result in bending and twisting of flexible wearable antennas. Previous research indicates that compared with bending on magnetic plane, geometry changing on the electric plane of linearly polarized patch antenna has larger effects on the antennas performance [36], [37]. Generally, antennas with ground planes will be reasonably isolated from the human body and will have less detuning effect.

In addition, some of the radiated energy may be absorbed by the human body. The absorbed energy is most clearly seen as decreased antenna efficiency and distorted radiation patterns. However it is important to evaluate the electromagnetic field absorbed by the body to control the absorption of power below the safety limits [38], [39]. The specific absorption rate (SAR) is the international standard dosimetry parameter used to specify the power absorbed per the unit mass of tissue. In America, the Federal Communications Commission (FCC) requires the SAR level to be below 1.6 W/kg average over 1 g for mobile devices [40], whilst in the Europe Union sets the cap at 2 W/kg averaged over 10 g [41]. Placing an isolating layer between the human body and antennas will reduce the power absorbed by tissues. A larger ground plane for the antenna will further reduce the SAR level [42] at the expense of increasing the antenna size.

### **1.3 Novel Contributions of this Thesis**

The novelties of this thesis are

- (1) Evaluation of the effect of the embroidery parameters on the direct current (DC) and radio frequency (RF) performance of embroidered microstrip antennas and transmission lines [43]–[45]

- (2) Simulation methodologies for modelling embroidered stitches of microstrip antennas have been introduced, the anisotropic properties and the current distribution on embroidered stitches have been analysed [45], [46]
- (3) A non-uniform meshed microstrip antenna with less than 25% metal coverage but without influencing antenna performance has been designed and embroidered [47], [48]
- (4) A detachable and flexible RF connectors made by hook and loop fasten has been presented [49]

## 1.4 An Overview of this Thesis

Chapter 2 will give a brief summary and comparison of electro-textiles manufacturing techniques and state the reason for choosing embroidery to fabricate wearable antennas. The properties of multifilament conductive threads will be presented. Scanning electron microscope images will illustrate the microstructure of these threads. This chapter will also show the schematic of embroidered stitches and estimate the actual length of embroidered threads. The measured dielectric properties of denim and felt will also be presented.

Chapter 3 will demonstrate the effects of embroidered transmission lines on fabrication factors including stitch direction and stitch spacing with different conductive threads. DC resistances and RF scattering parameters are measured to evaluate their performance. A measurement rig and a connection mechanism are designed for repeatable and stable results. Different conductive threads will be compared in this chapter. Amberstrand Silver thread will be selected as the most suitable for embroidered fabric based antennas. Chapter 3 will present a novel detachable, reusable and flexible RF connector which is made from conductive hook and loop.

After comparing the different threads and the stitch parameters in Chapter 2 and Chapter 3, measurements of a set of the embroidered patch antennas will be analysed in Chapter 4. The effects of stitch direction and stitch spacing on microstrip antennas performance including resonant frequency, antenna gain and efficiency will be discussed. The guidelines for choosing the correct fabrication parameters are given. A repeatability test of embroidered patch antennas will be included to show the applicability of embroidery in mass producing wearable antennas. Chapter 4 will introduce a simulation model to represent the behaviour of embroidered stitches. The distorted current which is impacted by the stitch direction and spacing will be illustrated.

Chapter 5 will introduce a novel non-uniform meshed structure of microstrip antennas which can reduce the total length of conductive threads for antenna fabrication. The uniform meshed microstrip antenna will also be represented for a comparison. The meshed patch antennas have comparable gain with the solid patch but with significant reduced area of metal coverage. This will reduce the cost of embroidered patch antennas. The first part of Chapter 5 will cover the simulations, including the surface current distribution, antenna mode analysis, antenna gain and efficiencies of the meshed patch antennas. Then meshed patch antennas etched on conventional rigid laminated will be measured to proof the theory. At the end of Chapter 5, embroidered meshed patch antennas with flexible fabric dielectric substrates will be presented.

Chapter 6 will draw some conclusions and summarise the potential implications for industry. Recommendations for future work will be suggested at the end.

## References

- [1] P. S. Hall and Y. Hao, *Antennas and propagation for body-centric wireless communications*. London, UK: Artech House, 2012.
- [2] A. Pantelopoulos and N. G. Bourbakis, "A Survey on Wearable Sensor-Based Systems for Health Monitoring and Prognosis," *IEEE Transactions on Systems, Man, and Cybernetics, Part C (Applications and Reviews)*, vol. 40, no. 1, pp. 1–12, Jan. 2010.
- [3] T. Kennedy, P. Fink, and A. Chu, "Body-worn e-textile antennas: The good, the low-mass, and the conformal," *IEEE Transactions on Antennas and Propagation*, vol. 57, no. 4, pp. 910–918, 2009.
- [4] P. Massey, "Mobile phone fabric antennas integrated within clothing," in *11th International Conference on Antennas and Propagation (ICAP)*, 2001, pp. 344–347.
- [5] N. H. M. Rais, P. J. Soh, F. Malek, S. Ahmad, N. B. M. Hashim, and P. S. Hall, "A review of wearable antenna," in *Loughborough Antennas & Propagation Conference (LAPC)*, 2009, pp. 225–228.
- [6] J. Lilja, P. Salonen, T. Kaija, and P. de Maagt, "Design and Manufacturing of Robust Textile Antennas for Harsh Environments," *IEEE Transactions on Antennas and Propagation*, vol. 60, no. 9, pp. 4130–4140, Sep. 2012.
- [7] D. Psychoudakis, G. Lee, C. Chen, and J. L. Volakis, "Military UHF Body-Worn Antennas for Armored Vests," in *Proceedings of the Fourth European Conference on Antennas and Propagation (EuCAP)*, 2010, pp. 1–4.
- [8] S. Walker, "Wearable Technology – Market Assessment," *IHS Electronics & Media*, 2013. [Online]. Available: <http://www.ihs.com/pdfs/Wearable-Technology-sep-2013.pdf>. [Accessed: 01-Mar-2014].
- [9] "Wearable Sports and Fitness Devices Will Hit 90 Million Shipments in 2017," *ABI Research*, 2012. [Online]. Available:

- <https://www.abiresearch.com/press/wearable-sports-and-fitness-devices-will-hit-90-mi>. [Accessed: 05-May-2012].
- [10] A. Alomainy, Y. Hao, C. G. Parini, and P. S. Hall, "Comparison Between Two Different Antennas for UWB On-Body Propagation Measurements," *Antennas and Wireless Propagation Letters*, vol. 4, no. 1, pp. 31–34, Dec. 2005.
- [11] E. O. Thorp, "The invention of the first wearable computer," in *Digest of Papers. Second International Symposium on Wearable Computers (Cat. No.98EX215)*, 1998, pp. 4–8.
- [12] S. Mann, "Wearable computing: a first step toward personal imaging," *Computer*, vol. 30, no. 2, pp. 25–32, 1997.
- [13] S. Mann, "Further developments on 'HeadCam': joint estimation of camera rotation+gain group of transformations for wearable bi-foveated cameras," in *IEEE International Conference on Acoustics, Speech, and Signal Processing*, 1997, vol. 4, pp. 2909–2912.
- [14] P. S. Hall, Y. I. Nechayev, A. Alomainy, C. C. Constantinou, C. Parini, M. R. Kamarudin, T. Z. Salim, D. T. M. Hee, R. Dubrovka, A. S. Owadally, A. Serra, P. Nepa, M. Gallo, and M. Bozzetti, "Antennas and propagation for on-body communication systems," *IEEE Antennas and Propagation Magazine*, vol. 49, no. 3, pp. 41–58, Jun. 2007.
- [15] D. Gaspar and A. A. Moreira, "Belt antenna for wearable applications," in *IEEE Antennas and Propagation Society International Symposium*, 2009, pp. 1–4.
- [16] C. Narayanaswami and M. T. Raghunath, "Application design for a smart watch with a high resolution display," in *Digest of Papers. Fourth International Symposium on Wearable Computers*, 2000, pp. 7–14.
- [17] F. Bashir, "Real life applicable fall detection system based on wireless body area network," in *IEEE 10th Consumer Communications and Networking Conference (CCNC)*, 2013, pp. 62–67.

- [18] H. Gamboa, F. Silva, and H. Silva, "Patient tracking system," in *Proceedings of the 4th International ICST Conference on Pervasive Computing Technologies for Healthcare*, 2010, pp. 1–2.
- [19] "SmartWatch." [Online]. Available: <http://www.sonymobile.com>. [Accessed: 05-Feb-2014].
- [20] R. Paradiso, G. Loriga, and N. Taccini, "A wearable health care system based on knitted integrated sensors.," *IEEE transactions on information technology in biomedicine: a publication of the IEEE Engineering in Medicine and Biology Society*, vol. 9, no. 3, pp. 337–344, Sep. 2005.
- [21] P. G. Elliot, E. N. Rosario, B. Rama Rao, R. J. Davis, and N. M. Marcus, "E-textile microstrip patch antennas for GPS," in *Proceedings of the 2012 IEEE/ION Position, Location and Navigation Symposium*, 2012, pp. 66–73.
- [22] "Sports technology: Vital statistics." [Online]. Available: <http://www.economist.com/blogs/babbage/2011/11/sports-technology>. [Accessed: 07-Jan-2014].
- [23] T. Kellomaki, W. G. Whittow, J. Heikkinen, and L. Kettunen, "2.4 GHz plaster antennas for health monitoring," in *Antennas and Propagation, 3rd European Conference on (EuCap)*, 2009, pp. 211–215.
- [24] J. Roh, Y. Chi, J. Lee, Y. Tak, S. Nam, and T. J. Kang, "Embroidered Wearable Multiresonant Folded Dipole Antenna for FM Reception," *IEEE Antennas and Wireless Propagation Letters*, vol. 9, pp. 803–806, 2010.
- [25] H. Chalayan, *Hussein Chalayan*, 1st ed. New York: Rizzoli International Publications, 2011.
- [26] E. R. Post, M. Orth, P. R. Russo, and N. Gershenfeld, "E-broidery: Design and fabrication of textile-based computing," *IBM Systems Journal*, vol. 39, no. 3.4, pp. 840–860, 2000.

- [27] G. F. Eichinger, K. Baumann, T. Martin, and M. Jones, "Using a PCB Layout Tool to Create Embroidered Circuits," in *11th IEEE International Symposium on Wearable Computers*, 2007, pp. 1–2.
- [28] L. Buechley and M. Eisenberg, "Fabric PCBs, electronic sequins, and socket buttons: techniques for e-textile craft," *Personal and Ubiquitous Computing*, vol. 13, no. 2, pp. 133–150, Aug. 2007.
- [29] I. Locher and G. Troster, "Fundamental Building Blocks for Circuits on Textiles," *IEEE Transactions on Advanced Packaging*, vol. 30, no. 3, pp. 541–550, Aug. 2007.
- [30] C. Gabriel, S. Gabriel, and E. Corthout, "The dielectric properties of biological tissues: I. Literature survey," *Physics in Medicine and Biology*, vol. 41, no. 11, pp. 2231–2249, Nov. 1996.
- [31] S. Gabriel, R. W. Lau, and C. Gabriel, "The dielectric properties of biological tissues: II. Measurements in the frequency range 10 Hz to 20 GHz," *Physics in Medicine and Biology*, vol. 41, no. 11, pp. 2251–2269, Nov. 1996.
- [32] S. Gabriel, R. W. Lau, and C. Gabriel, "The dielectric properties of biological tissues: III. Parametric models for the dielectric spectrum of tissues," *Physics in Medicine and Biology*, vol. 41, no. 11, pp. 2271–2293, Nov. 1996.
- [33] M. U. Rehman, Y. Gao, X. Chen, C. G. Parini, and Z. Ying, "Effects of Human Body Interference on the Performance of a GPS Antenna," in *Antennas and Propagation (EuCAP), The Second European Conference on*, 2007, pp. 2–5.
- [34] A. Sani, A. Alomainy, G. Palikaras, Y. Nechayev, C. Parini, and P. S. Hall, "Experimental Characterization of UWB On-Body Radio Channel in Indoor Environment Considering Different Antennas," *IEEE Transactions on Antennas and Propagation*, vol. 58, no. 1, pp. 238–241, Jan. 2010.
- [35] A. Alomainy, Y. Hao, A. Owadally, C. G. Parini, Y. Nechayev, C. C. Constantinou, and P. S. Hall, "Statistical Analysis and Performance Evaluation for On-Body Radio Propagation With Microstrip Patch Antennas," *IEEE*



- Transactions on Antennas and Propagation*, vol. 55, no. 1, pp. 245–248, Jan. 2007.
- [36] P. Salonen and Y. Rahmat-Samii, “Textile antennas: Effects of antenna bending on input matching and impedance bandwidth,” *Aerospace and Electronic Systems Magazine, IEEE*, vol. 22, pp. 10–14, 2007.
- [37] Q. Bai and R. Langley, “Textile antenna bending and crumpling,” in *Antennas and Propagation (EuCAP), Proceedings of the Fourth European Conference on*, 2010, pp. 1–4.
- [38] W. G. Whittow and R. M. Edwards, “A Study of Changes to Specific Absorption Rates in the Human Eye Close to Perfectly Conducting Spectacles Within the Radio Frequency Range 1.5 to 3.0 GHz,” *IEEE Transactions on Antennas and Propagation*, vol. 52, no. 12, pp. 3207–3212, Dec. 2004.
- [39] W. G. Whittow, C. J. Panagamuwa, R. M. Edwards, and J. (Yiannis) C. Vardaxoglou, “The Energy Absorbed in the Human Head Due to Ring-Type Jewelry and Face-Illuminating Mobile Phones Using a Dipole and a Realistic Source,” *IEEE Transactions on Antennas and Propagation*, vol. 56, no. 12, pp. 3812–3817, Dec. 2008.
- [40] Federal Communications Commission (FCC), “Specific Absorption Rate (SAR) for Cellular Telephones.” [Online]. Available: <http://www.fcc.gov/encyclopedia/specific-absorption-rate-sar-cellular-telephones>. [Accessed: 06-Feb-2014].
- [41] International Commission on Non-Ionizing Radiation Protection (ICNIRP), “Health issues related to the use of handheld radio telephones and base transmitters,” *Health Physics*, vol. 70(4), p. 383-387, 1996.
- [42] K. H. Chan, L. C. Fung, S. W. Leung, and Y. M. Siu, “Effect of internal patch antenna ground plane on SAR,” in *17th International Zurich Symposium on Electromagnetic Compatibility*, 2006, pp. 513–516.

- [43] T. Acti, S. Zhang, A. Chauraya, W. Whittow, R. Seager, T. Dias, and Y. Vardaxoglou, “High performance flexible fabric electronics for megahertz frequency communications,” in *Loughborough Antennas & Propagation Conference (LAPC)*, 2011, pp. 1–4.
- [44] S. Zhang, A. Chauraya, W. Whittow, R. Seager, T. Acti, T. Dias, and Y. Vardaxoglou, “Embroidered wearable antennas using conductive threads with different stitch spacings,” in *Loughborough Antennas & Propagation Conference (LAPC)*, 2012, pp. 1–4.
- [45] R. Seager, S. Zhang, A. Chauraya, W. Whittow, Y. Vardaxoglou, T. Acti, and T. Dias, “Effect of the fabrication parameters on the performance of embroidered antennas,” *IET Microwaves, Antennas & Propagation*, vol. 7, no. 14, pp. 1174–1181, Nov. 2013.
- [46] S. Zhang, A. Chauraya, W. Whittow, R. Seager, T. Acti, T. Dias, and Y. C. Vardaxoglou, “Simulation Methodology to Model the Behavior of Wearable Antennas Composed of Embroidered Conductive Threads,” in *IEEE International Symposium on Antennas and Propagation and USNC-URSI National Radio Science Meeting*, 2012, (conference abstract).
- [47] S. Zhang, R. Seager, A. Chauraya, W. Whittow, and Y. Vardaxoglou, “Non-uniform Meshed Microstrip Antennas for Wearable Applications,” in *Antennas and Propagation (EuCAP), 8th European Conference*, 2014
- [48] S. Zhang, R. Seager, A. Chauraya, W. Whittow, and Y. Vardaxoglou, “Non-uniform Meshed Embroidered Patch Antennas,” in *IEEE International Symposium on Antennas and Propagation and USNC-URSI Radio Science Meeting*, 2014, (accepted March, 2014).
- [49] R. D. Seager, A. Chauraya, S. Zhang, W. Whittow, and Y. Vardaxoglou, “Flexible radio frequency connectors for textile electronics,” *Electronics Letters*, vol. 49, no. 22, pp. 1371–1373, Oct. 2013.

# Chapter 2

## Materials and Manufacturing Techniques for Fabric RF Systems

---

### Abstract

This chapter will describe the composition of fabric based antennas including the electro-textile materials with numerous fabrication techniques, flexible fabric dielectric substrates and flexible RF connectors. Techniques for fabricating electro-textiles will be outlined in Section 2.1. Characteristics of the electro-textiles include the DC resistance and RF transmission will be measured. The conductive thread used for the embroidery in this thesis, Amberstrand, will be analysed in Section 2.2. The scanning electron microscope (SEM) images of Amberstrand will also be presented in Section 2.2, which will show the detailed structure of this multifilament conductive thread. Details of embroidered stitches will be shown in Section 2.3. An estimation of thread usage and the materials costs will be introduced. Section 2.4 will present the measured dielectric properties of different fabric dielectric substrates using the split post dielectric resonator. Finally low profile RF connectors for fabric based antennas will be discussed in Section 2.5.

### 2.1 Electro-textiles

#### 2.1.1 *Fabricating of Electro-textiles*

Electro-textile is the conductive fabric which can realise the integration of wearable electronic and RF components into normal cloth but keep the features of light-weight

and flexibility. There are several methods of fabricating the conductive textile materials. General reviews can be found in [1]–[3]. Generally, the conductive textiles can be made by the following four approaches:

- I. Conductive layer coating. The conventional non-conductive natural or synthetic polymer fabrics can be deposited with a conductive layer by chemical approaches such as electroplating. After this processing, the entire surface area of the fabric is conductive on both sides.
- II. Weaving or knitting the fabric by conductive yarn. The fabric is woven or knitted entirely using the conductive yarns but also can be blended with normal nonconductive yarns. Fabric with specific conductive patterns can be realised by using both conductive and nonconductive yarns. The conductive yarns are applied at the step of manufacturing and the post processing is not required.
- III. Printing a conductive layer onto fabric. The conductive layer is printed onto the normal fabric by specialized printing techniques such as inkjet printing and screen printing. In this case, there is an additional conductive layer which is printed by the conductive ink on the fabric.
- IV. Embroidering a conductive layer onto fabric. Similar to the printing approach, there is an additional conductive layer on a base fabric. This conductive layer is created using conductive threads.

For the approach (I), high conductivity metal materials such as copper and silver are eligible for plating onto the normal fabrics [4]. There are several commercially available metallized woven conductive fabrics with the sheet resistance less than  $0.05 \Omega/\text{sq}$  such as Pure Copper Taffeta from Less EMF Inc. [5]; conductive metallized nylon fabric Nora Dell from Shieldex [6]; and Shieldex ripstop/plain weave fabrics [7]. Figure 2-1 shows the Shieldex rolled flexible conductive woven

fabrics. These fabrics have the advantages of a low sheet resistance; flexibility; they are easy to cut and can be sewed like ordinary fabric, which make them good for electromagnetic shielding applications. Several authors have used Nora Dell material and cut them into desired shapes for the conductive layer of wearable antennas [8]–[12]. Figure 2-2 shows a wearable fabric digital television antenna made of Nora Dell in [12]. The flexibility of material enable the antenna be curved and placed on different positions of body.



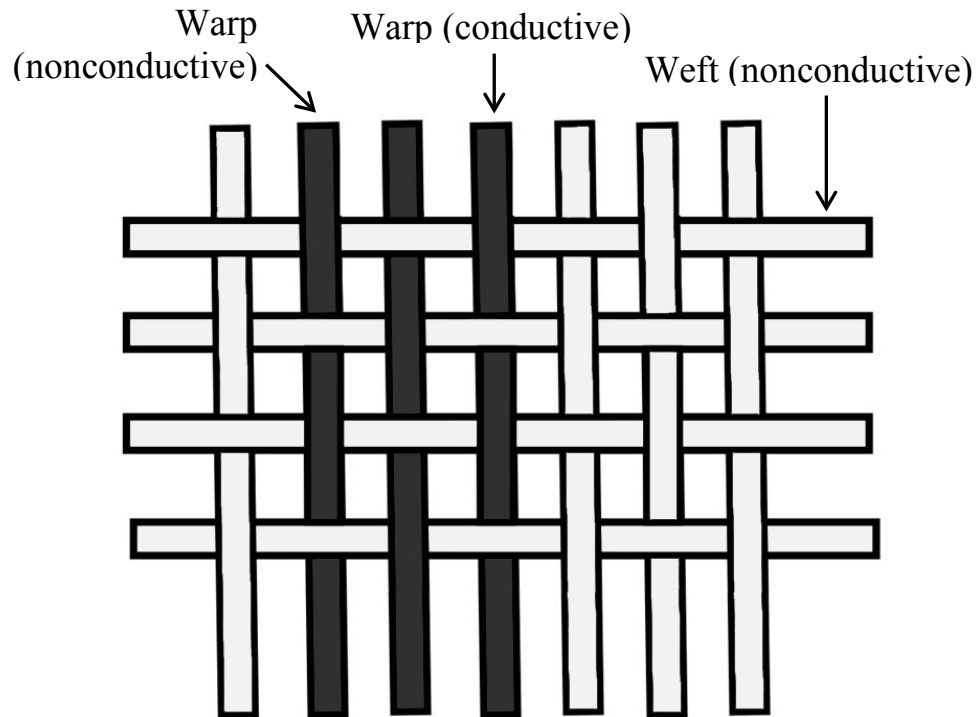
**Figure 2-1 Conductive woven fabric from Shieldex (picture from [7])**



**Figure 2-2 A wearable fabric digital television antenna (picture from [12])**

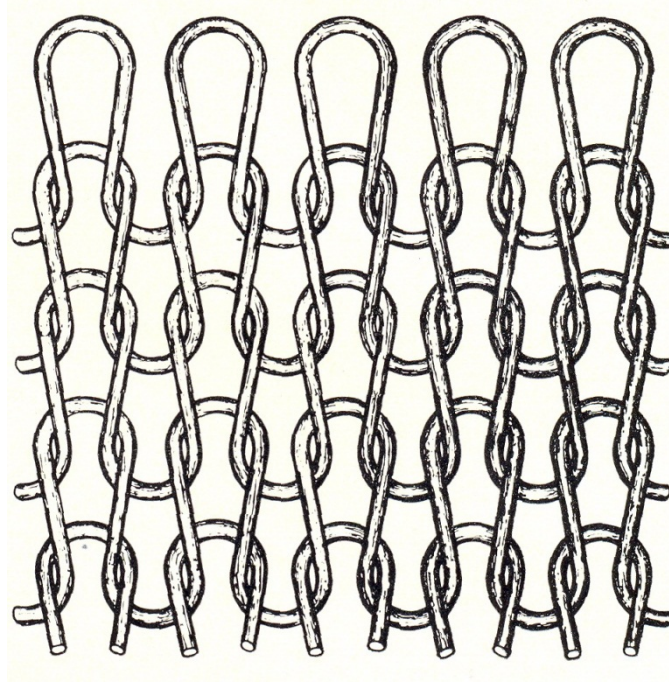
Non-metal conducting materials also can be deposited onto the fabrics. For instance, the single-walled carbon nanotubes (SWNTs) can be coated onto cotton or polyester [13], [14]. After absorbing the aqueous SWNT ink, the textile becomes conductive but without losing flexibility. This is very similar to the dyeing process in the textile industry. The conductivity of the textile can be increased by repeating the dyeing process. Hu *et al.* showed the conductive textile with conductivity of 123 S/cm and sheet resistance less than 1  $\Omega$ /sq by this approach [14]. The SWNT dyed microstrip fabric antenna with a polymer composite substrate was reported in [15].

For approach (II), the conductive fabric can be fabricated by the combination of conductive fibres with or without ordinary fibres using weaving or knitting methods [16]–[22]. Cottet *et al.* reported an woven fabric entirely using the conductive yarns but without revealing the material name [18]. If the fabric is woven with both conductive and nonconductive yarns, the distribution and directions of conductive yarns in the fabric will result in anisotropic conducting properties of fabric because the current only travels on the paths along the conductive strands. The conductive paths may exist in all directions throughout the fabric or only one direction depending on the fabrication method. Figure 2-3 illustrates a fabric woven by weft yarns (longitudinal) and warp yarns (lateral). Only the warp yarns with dark colour are conductive and the yarns with light colour are nonconductive. Clearly the current will only follow the path of warp yarns in the vertical direction. Weaving conductive yarns with nonconductive yarns can create the partly conductive fabric without additional layers, which makes this approach unique compared with others. This feature makes this type of fabric suitable for applications such as electroluminescent [21] that requires a particular conductive path in the fabric without adding thickness. The electro-textile can be woven with plastic optical fibres and normal yarns to guide the optical signal and worked for on-body optical antennas [23].



**Figure 2-3 A woven fabric with a vertical conductive path using both conductive and nonconductive yarns**

Copper-yarn based knitted fabric antennas were reported in 2003 [22]. However, knitted fabrics may present higher anisotropy than woven fabric due to its structure (shown in Figure 2-4) and this anisotropy will be increased with the stretch of the knitted fabric. The knitted fabric is soft with high flexibility and stretchability which result in easy deformation and then change the surface resistance of the fabric sheet. Locher *et al.* reported that the sheet resistance was increased by approximately 4 times due to elongation in one direction of the knitted conductive fabric [17].



**Figure 2-4 Structure of yarns in knitted fabric (picture from [24])**

However, for wearable antennas, there are some drawbacks for the fabrics made by methods (I) and (II): i) in high frequency applications, the antenna size is usually small. Although the conductive woven fabric can be cut into desired shapes, it is still hard to cut small-scale accurately, particularly for the complex patterns; ii) since the patterns are cut from the fabric, there is a wastage after the fabric has been cut, which increases the cost of materials; iii) the conductive fabrics need to be sewed onto the cloth, which requires additional fabrication procedures; iv) due to the characteristic of woven and knitted fabric, the fibres are easy to separate and unravel at the edges of the fabric. Hem is required to prevent this issue. But it is difficult to hem small fabrics and it also increases the production procedures.

The concepts of approaches (III) and (IV) are very similar, i.e. using conductive materials to create a conductive layer on the fabric to form a pre-designed, functional conductive pattern. Both (III) and (IV) can use the state of the art techniques to improve the accuracy of the conductive patterns. Screen printed high frequency systems on cotton have been reported in [25]. Kim *et al.* presented screen printed circuits on various types of fabric [26]. Compared with screen printing, inkjet printing



has the advantages of high speed; no need for a mask; accuracy; reduced material consumption; flexibility of changing design and being environmentally friendly [27]. Inkjet printed antennas on flexible substrate for wearable application can be seen in [27]–[31] and showed good antenna performance. Other applications such as realising parallel plate flexible capacitors on textiles by inkjet printing is described in [32]. However, the printed conductive layer is generally thin (usually micron scale), and hence it is difficult to generate an even thickness printed layer onto the rough and non-continuous textile surface [33]. Multilayer printing can overcome this drawback but the costs will be increased by the number of conductive layers.

Embroidering conductive patterns onto textiles using conductive threads has attracted researchers' attentions in recent years [34]–[50]. The advantages of embroidering conductive threads are promising. Antennas and electronics design can be incorporated into clothing using the state of the art embroidery machines which have already become standard in the textile industry. This will potentially save considerable costs at the mass-manufacturing stage. In addition, there are several commercialised conductive threads such as X-Static [51], Shieldex yarn [52] and Amberstrand [53]. Furthermore, there will be aesthetic advantages as the design will add to the cosmetic apparel rather than being an *added* shape that needs to be hidden. The embroidery stitch density is mentioned in [34]–[36] and the stitch direction which affects the RFID performance at 900 MHz is mentioned in [38] but without extensive analysis on antenna performance. Ukkonen *et al.* pointed out that the antenna impedance is impacted by the stitching technique [34]. The same paper also reported the RFID antenna read range for different stitch densities but with low realised gain. The feasibility of double-layer embroidery for high conductivity radiators and transmission lines was reported in [35]. Moradi *et al.* compared different sewing patterns on the read range of dipole RFID tag antennas [46].

Table 2-1 summarises the comparison of fabricating electro textiles with different approaches. Embroidery, with the balance between cost and performance, shows its potential in mass-manufacturing fabric wearable antennas.

**Table 2-1 Summary of approaches for fabricating electro-textiles**

	<b>Coating or dyeing</b>	<b>Weaving or knitting</b>	<b>Printing</b>	<b>Embroidery</b>
Commercial materials available	<b>Yes</b>	Customised by requirement	Yes, but fewer	<b>Yes</b>
Additional processes (cutting, sewing and hemming)	Yes	Yes	<b>No</b>	<b>No</b>
Waste due to cutting	Yes	Yes	<b>No</b>	<b>No</b>
Accuracy of fabricating small patterns	Low	Medium	<b>Highest</b>	High
Initial investment	<b>Lowest</b>	High	Highest	Medium
Partly conductive fabric without additional layers	No	<b>Yes</b>	No	No
Easy to attach to fabric	<b>Easy</b>	<b>Easy</b>	Difficult	<b>Easy</b>
Stylish	Unattractive	<b>Aesthetic</b>	<b>Aesthetic</b>	<b>Aesthetic</b>
Optimum applications	For large, coarse patterns, and shielding	For customised “in textile” patterns	For small, complex patterns require very high resolution	For small, complex patterns require high resolution
Reference	[4]–[15]	[16]–[24]	[25]–[33]	[32]–[53]

### **2.1.2 DC and RF Characteristics of Electro-textiles**

Electro-textiles are normally constructed with fibres in aligned directions. And therefore, the directions and distribution of conductive yarns in the electro-textile will result in the anisotropic electrical properties as mentioned in Section 2.1.1. It is important to understand the way that the conductive yarns distort the current flow in the electro textiles. For instance, the sheet resistance of the woven conductive fabric is affected by the different weaving angle of the fibres [54], [55]. Banaszczyk *et al.* showed that the current direction and distribution will follow the conductive fibres direction in the electroconductive woven fabric [56], [57].

In the embroidery process, the conductive threads are usually aligned with a preferred direction and spacing which are defined by the embroidery parameter settings. These threads create the paths for the current but the contact points between the adjacent threads also provide alternative paths. More details about the DC performance of embroidered conductive threads will be discussed in Chapter 3 and Chapter 4. Approaches such as two metal electrodes and four points Van der Pauw method can be carried out to measure the sheet resistance of the conductive fabric [58], [59]. Since the measured resistance results will be different when measured from different directions, the sheet resistance measurement will give an indication of the optimum current direction.

Because of the non-continuous and non-uniform structure of the conductive fabric, the RF properties of electro-textiles will be different from a continuous metal sheet. The fibres in the textiles create a huge number of microscopic holes. These holes are distributed in the fabric and introduce air in the fabric which results in a tiny grid structure of the fabric. The undulations of the small scale conductive fibres increase the difficulty of precise modelling of the conductive fabric. Capacitance and inductance will be introduced by the gaps between conductors and the current distribution will be different from the continuous metals. The current paths are distorted by these gaps and the electrical length will be increased. The RF

performance of the fabric transmission lines and antennas are influenced by the spacing between the conductive fibres. The RF properties such as resonant frequency, antenna gain and efficiency of the embroidered transmission lines and antennas will be analysed in Chapter 3, 4 and 5. Furthermore, the coated conductive layer on the conductive fabric is usually on the micron scale and has smaller conductivity than copper. As a result, the conduction loss due to the skin effect is more significant than normal etched conductive metals, particularly at high frequency applications. The skin depth of the conductive thread will be calculated in Section 2.2.3 and the influence of the skin effect on embroidered antenna performance will be analysed in Chapter 5.

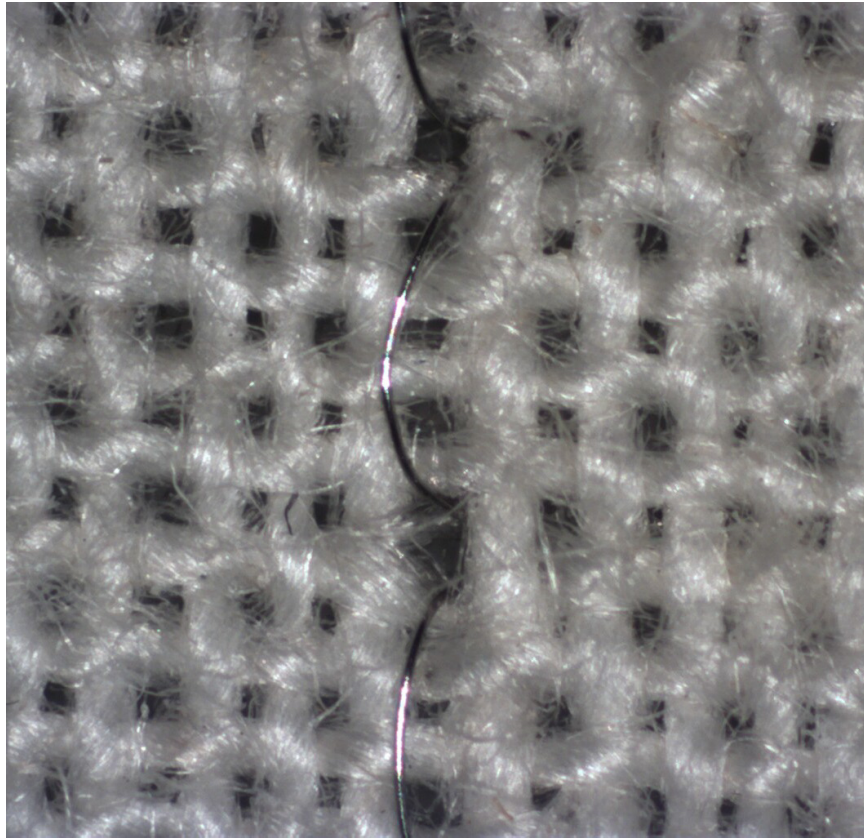
## **2.2 Conductive Threads for Embroidery**

### ***2.2.1 Fabrication of Conductive Threads***

There are three common methods to make conductive threads:

#### **I. Monofilament thread**

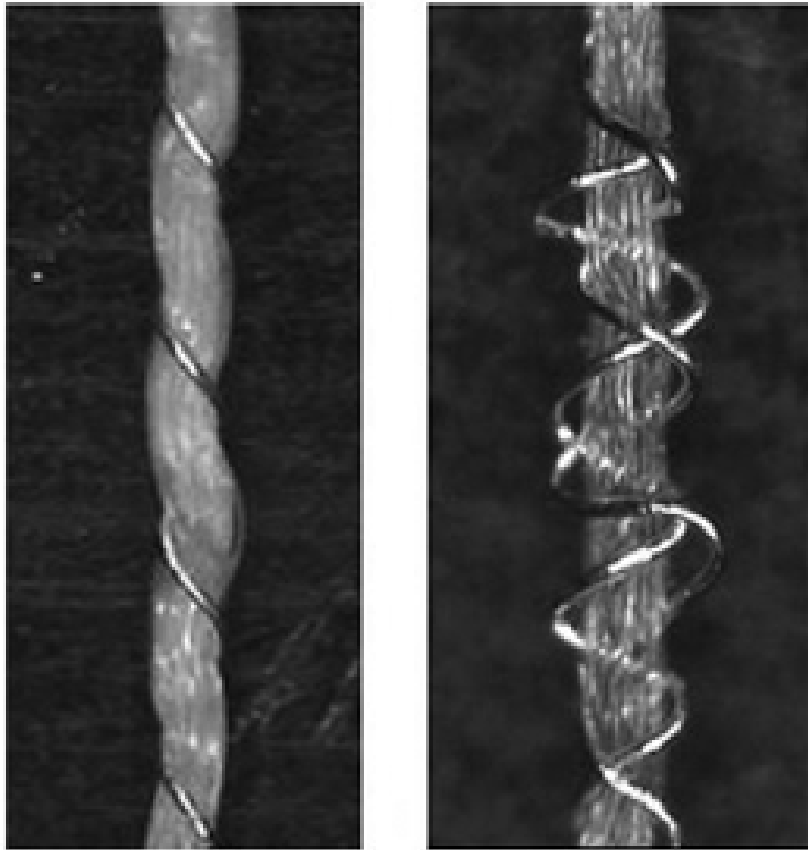
The monofilament conductive thread is usually very similar to a thin metal wire which is solid, and is made by the metal with good ductility and malleability such as copper, silver and nickel. This type of thread has a low resistance due to the solid homogeneous metal structure compared with other same diameter multifilament threads [20]. Figure 2-5 shows a sewed thin nickel wire on a plain woven cotton fabric made at Nottingham Trent University. However, because of the stiffness of the metal wire, they are difficult to embroider by machine and easily break.



**Figure 2-5 A monofilament nickel wire sewed onto a cotton fabric made at Nottingham Trent University**

## II. Dual-filament (hybrid) thread

The hybrid thread is a nonconductive thread which has the conductive wires twisted around it. The core thread provides mechanical strength, flexibility and elasticity [60]. The choice of core nonconductive thread depends on the application. The structures of the hybrid conductive thread are shown in Figure 2-6. However, when high frequency current follows the spun coil structure of the conductive wires, the inductance and capacitance between the spun wires will be generated.



**Figure 2-6 Zoomed in pictures of two nonconductive threads with 40  $\mu\text{m}$  diameter metal wires twisted around them (pictures are from [20])**

### III. Multifilament thread

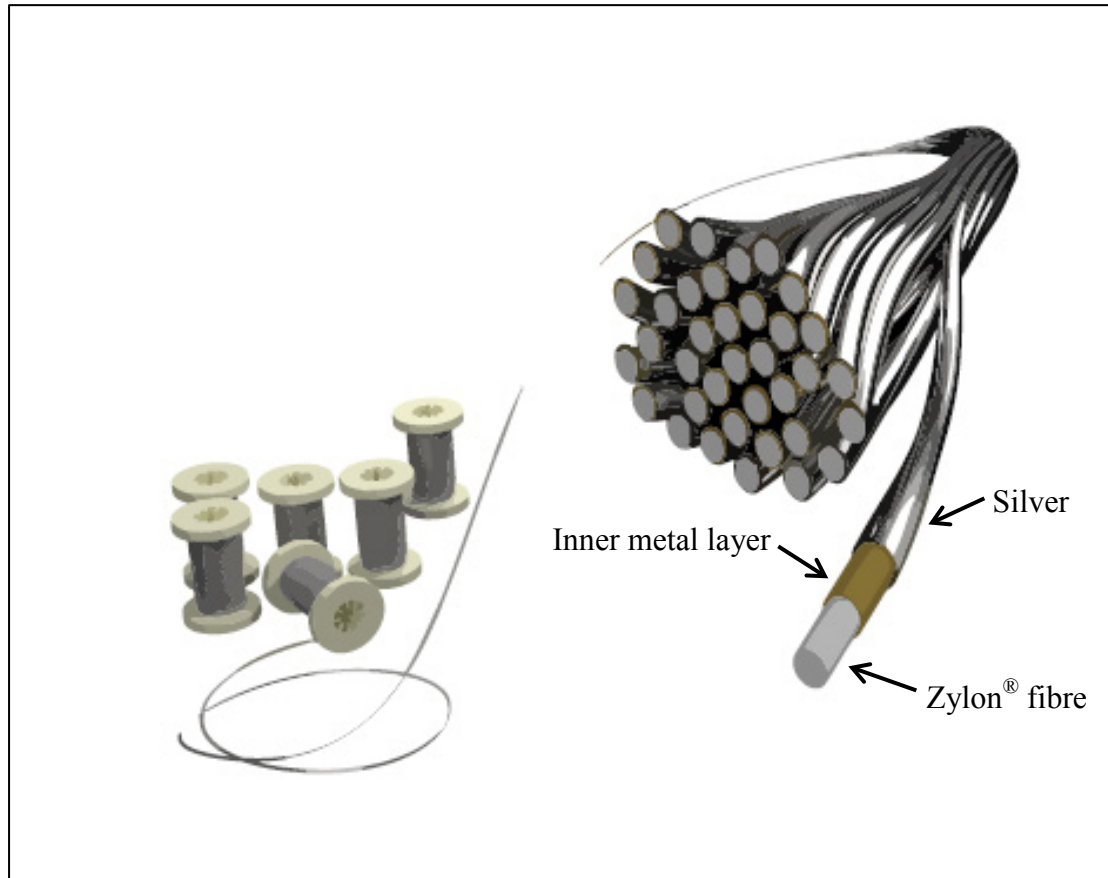
The multifilament thread is a strand which is twisted with a large number of “identical” thin conductive filaments. In general the filaments are made by polymer and chemically coated with a micron scale conductive layer. The diameter of the individual filament including the conductive layer is usually approximately 10 to 20  $\mu\text{m}$ . The conductive layer can be either carbon nanotubes [61] or metal. Due to the difficulty of carbon nanotube process, there is little choice of commercial carbon nanotube coated conductive fibres. However, the options of metal plated conductive threads are wide. The plated material can be chosen from different metals to balance the performance and the cost. An expensive choice such as gold can be applied to achieve good electrical conductivity and bio-compatibility [62]. Normally, silver,

copper and nickel are the options for commercialised products such as X-Static, Shieldex, Amberstrand. This type of conductive thread provides balance between electrical conductivity, mechanical strength and flexibility. However, the coarser conductive threads and threads containing abundant filaments are problematic in embroidery as they have a tendency to become wrapped around the tension devices and may not fit through the eye of the needle. Generally, polymer based conductive threads are easy to embroider due to the physical similarity shared with traditional embroidery threads.

The metal plated conductive threads will be used in fabricating embroidered antennas in this thesis. The coated material and the number of filaments influence both the DC and RF properties of the multifilament conductive threads. The performance of the metal plated threads and the embroidered RF components using these threads including transmission lines and patch antennas will be presented in Chapter 3, 4, and 5.

### **2.2.2 Amberstrand**

In this thesis, conductive thread Amberstrand<sup>®</sup> Silver was used for embroidering the transmission lines and antennas. One single thread of Amberstrand Silver 66 is composed of 66 *identical* filaments, whilst there are 166 filaments in Amberstrand Silver 166 thread. Every single filament is mainly silver coated Zylon<sup>®</sup> fibre (a synthetic polymer material). The cross section of Amberstrand fabric is shown in Figure 2-7. The inner metal layer varies on products.

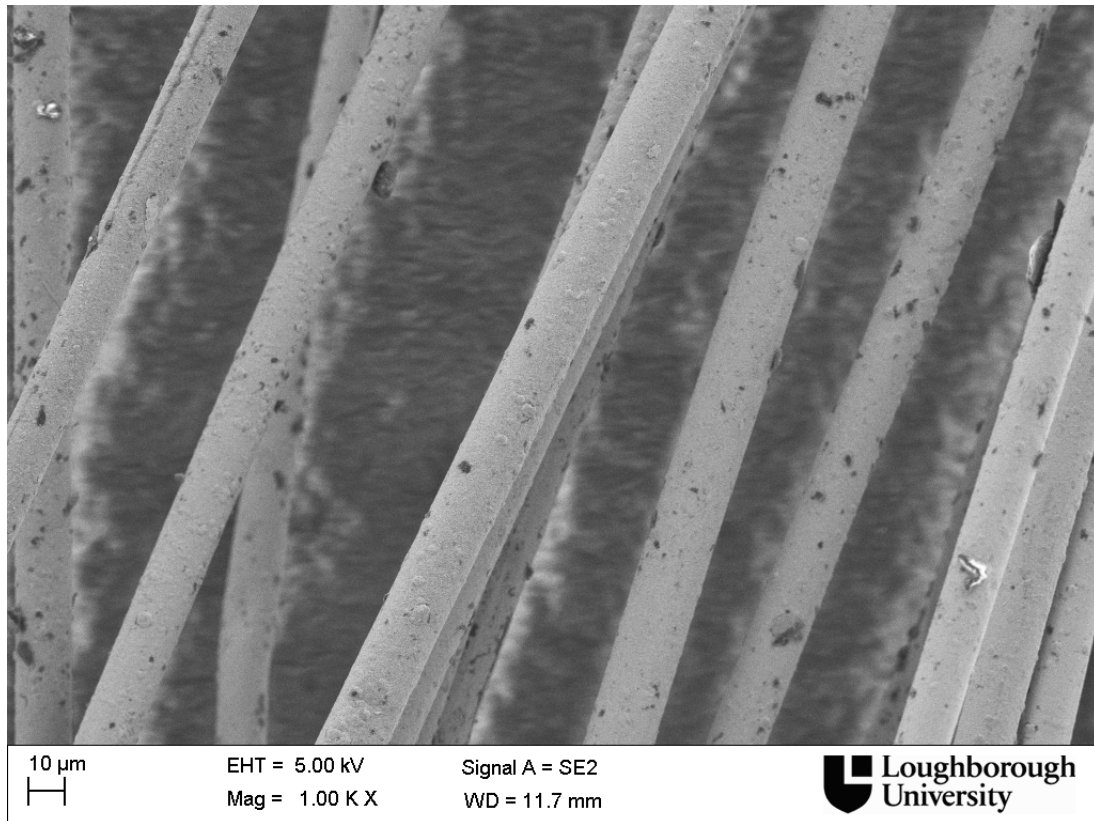


**Figure 2-7 Sketch of cross section of the single thread of Amberstrand (picture from [63])**

Scanning electron microscope (SEM) images of Amberstrand Silver thread with different scales were taken at Loughborough University, shown in Figure 2-8 to Figure 2-11.

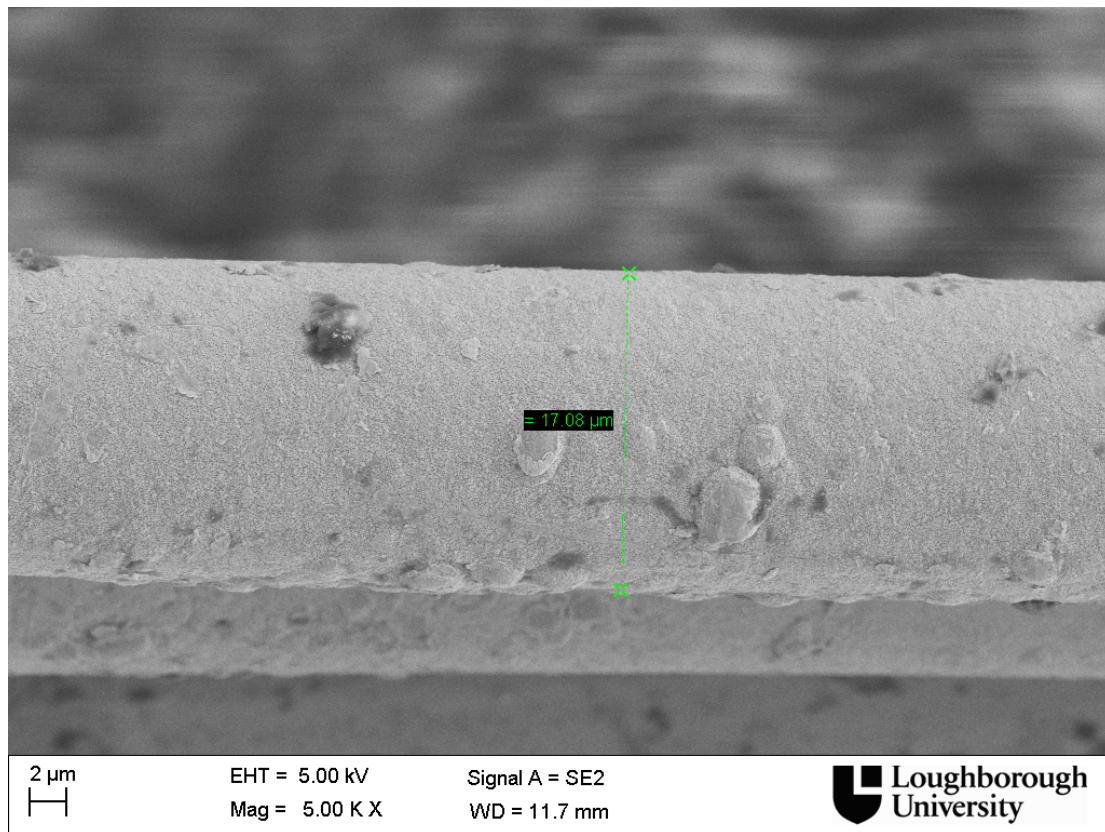
Figure 2-8 shows the SEM image of unbraided Amberstrand Silver filaments. As it can be seen the diameters of the each filament are consistent. Although the coating layer is not perfect smooth, the effect of unsmooth surface will be minimized when the filaments are spun together.





**Figure 2-8 SEM image of unbraided Amberstrand Silver filaments**

Figure 2-9 shows the single filament of Amberstrand Silver. The diameter of the filament is approximate 17  $\mu\text{m}$ . The imperfections of surface are more clearly shown in Figure 2-9.



**Figure 2-9 SEM image of single filament of Amberstrand Silver**

It was noticed that the metallization is not perfect and at some parts the coated layer are broken. Figure 2-10 and Figure 2-11 show the broken sections of metallization and the exposed polymer core underneath (*shiny* part). The metal cladding included both the inner and outer metal layer is approximate 1 μm thickness according to these images. It can be concluded that the coated layer component is approximately 22% of the whole filament by volume.



Figure 2-10 SEM image of broken section of coated layer

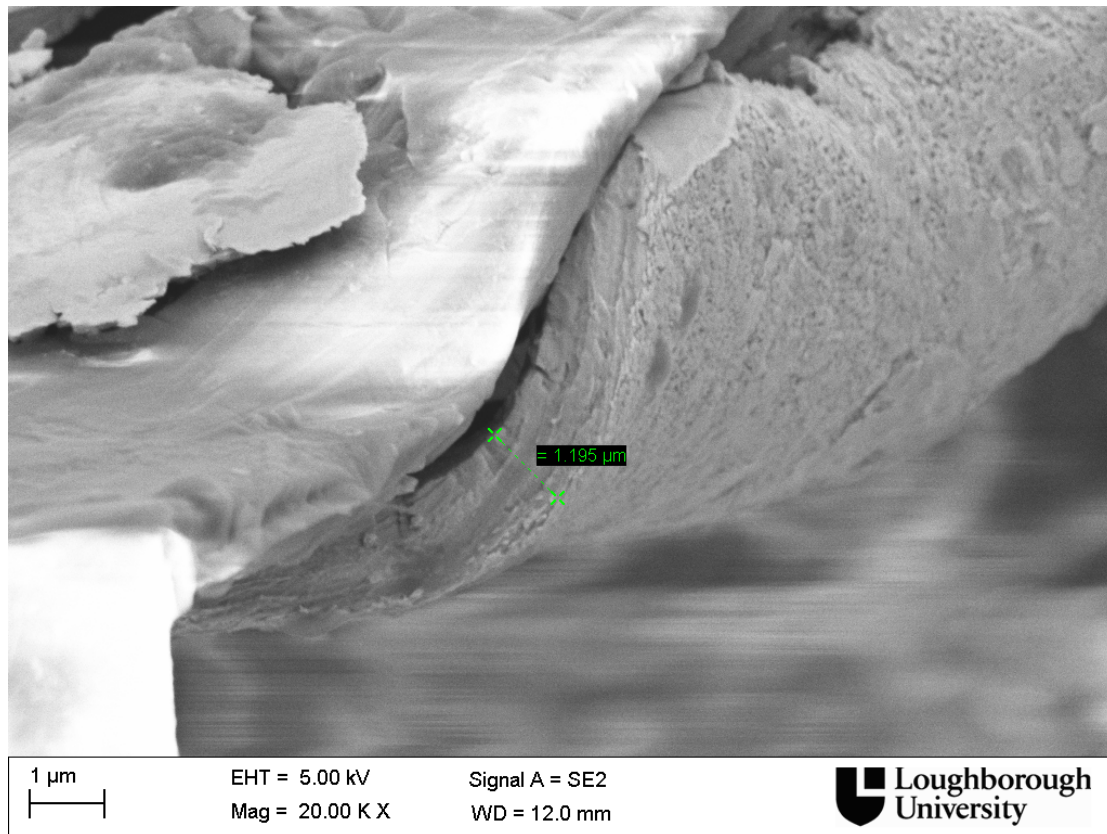
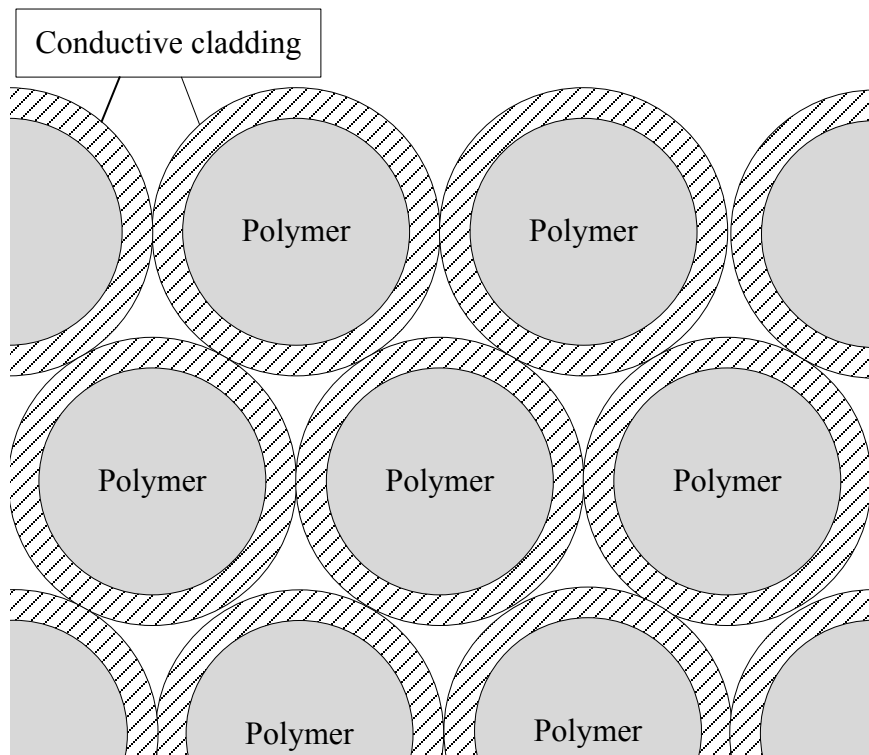


Figure 2-11 SEM image of cross section of coated layer

### 2.2.3 Conductivity of Amberstrand Threads

Section 2.3.1 showed that the metallization of the cladding on the filament is only 1  $\mu\text{m}$  thick. A sketch of the cross section of the thread is shown by Figure 2-12.



**Figure 2-12 Cross sections of filaments in Amberstrand thread**

The area of metal in a single filament is approximately  $50 \mu\text{m}^2$ . Then the total cladding cross section in the entire thread is  $66 \times 50 \mu\text{m}^2 = 3300 \mu\text{m}^2$ . A DC resistance measurement was taken and showed that the resistance of one Amberstrand Silver 66 entire thread is  $2 \Omega$  per imperial foot. This agrees with the datasheet. The equivalent resistivity  $\rho$  of the conducting layer can be obtained from

$$\rho = R \frac{A}{L} \quad (2.1)$$

Where  $L$  is the length of the thread sample,  $R$  is the DC resistance value of the given length of thread sample, and  $A$  is the cross sectional area of the conducting layer.

From (2.1), the calculated resistivity of cladding layer is  $2.2 \times 10^{-8} \Omega \cdot \text{m}$ , The conductivity  $\sigma$  equals to  $1/\rho$  and it is  $4.5 \times 10^7 \text{ S/m}$ . Note this value is smaller than pure silver ( $6.1 \times 10^7 \text{ S/m}$ ) because it is the equivalent conductivity of whole metallization.

At high frequencies, it is necessary to consider the skin effect. The current distribution is non-uniform in the conductor due to skin effect and the resistance of the conductor will be increased. The skin depth  $\delta$  in meters can be obtained from (2.2)

$$\delta = \sqrt{\frac{\rho}{\pi f \mu_r \mu_0}} \quad (2.2)$$

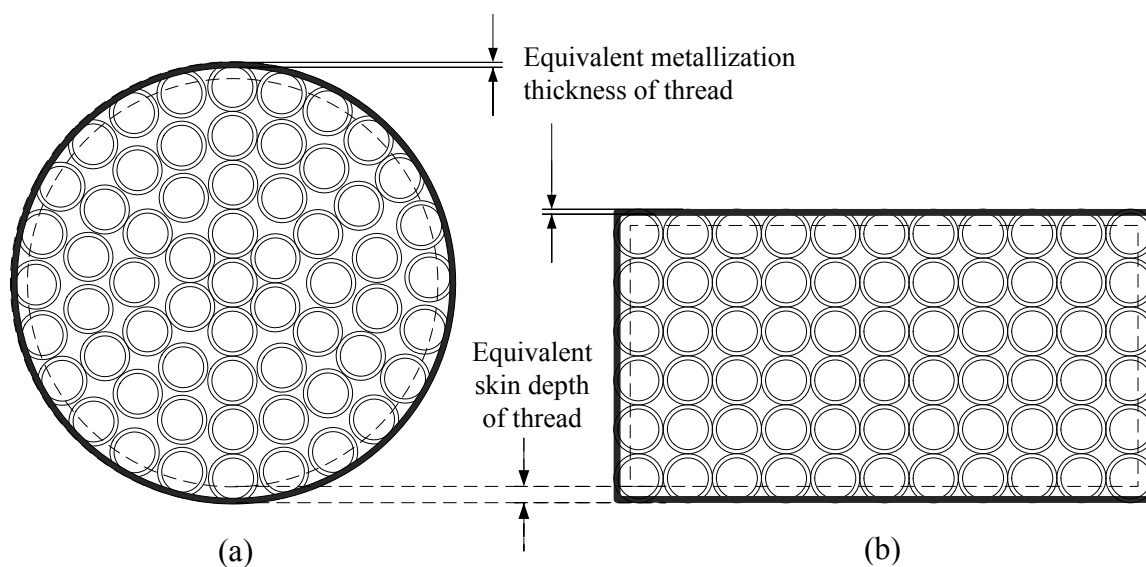
where  $\rho$  is resistivity in  $\Omega \cdot \text{m}$ ,  $f$  is the frequency in Hz,  $\mu_r$  is relative permeability of material, and the  $\mu_0$  is the permeability of free space which equal to  $4\pi \times 10^{-7} \text{ H/m}$ .

The skin depth at 2.4 GHz for copper is 1.332  $\mu\text{m}$ , and for silver is 1.295  $\mu\text{m}$ . The skin depth of the conducting layer on Amberstrand Silver 66 ( $4.5 \times 10^7 \text{ S/m}$ ) is 1.52  $\mu\text{m}$ . As a result the metallization (1  $\mu\text{m}$ ) is smaller than one skin depth. The skin effect will increase the ohmic loss in microstrip antennas and transmission lines and result in reduced efficiency.

However, since the filaments are shorted to each other, they behave like large single conductor. Experimental results showed that the skin effect of the non-spiralled multi-stranded conductor is similar to the single conductor with equal cross sectional area [64]. The skin effect results in the highest current density constraining on the thread surface rather than distributing evenly on each filament. In addition, because the thickness of the cladding layer (1  $\mu\text{m}$ ) is smaller than the skin depth (1.52  $\mu\text{m}$  at 2.4 GHz), the metallization thickness is the limit of the resistance of the thread for AC. Consequently the Amberstrand Silver 66 thread in AC can be treated as a 1  $\mu\text{m}$  thick hollow conductor. The cross sectional area of the hollow cylinder is approximately

$454 \mu\text{m}^2$ , and therefore the resistance of 1 meter thread at 2.4 GHz is approximately 43.5 Ohms (see Figure 2-13 a). When the thread is embroidered onto the fabric, it is flattened due to the tension from stitches. Therefore the cylinder thread will be flattened with increased width (see Figure 2-13 b). For instance, the flattened width of Amberstrand Silver 66 is measured approximately 0.2 mm when embroidered on 0.5 mm thick cotton fabric with 2 mm stitch length. The cross section area of the 0.2 mm wide hollow rectangular bar is approximate  $540 \mu\text{m}^2$  and therefore the resistance of 1 m embroidered Amberstrand Silver 66 is approximately 36.6 Ohms at 2.4 GHz. Note the surface roughness is neglected in these calculations.

It can be seen that the resistance for AC is greater than five times of the DC resistance. The metallization thickness is smaller than the equivalent skin depth up to 5 GHz. When the frequency is higher than 5 GHz, the skin depth is reduced to less than the  $1 \mu\text{m}$  metallization thickness which results in greater resistance for AC. Higher resistance will result in more conduction loss which reduces efficiencies for antennas and transmission lines.



**Figure 2-13 Equivalent metallization thickness of (a) cylinder and (b) flattened models of multifilament conductive thread in AC**



## **2.3 Embroidering Conductive Threads**

### ***2.3.1 Computerised Embroidery Machine and Stitch Patterns***

It can be foreseen that the automatic production of fabric antennas via computerised embroidery machine will boost the development of textile-based wearable electronics and reduce the cost significantly. Figure 2-14 shows the digital controlled embroidery machine at Nottingham Trent University. The embroidered samples in Chapter 2, 3 and 4 were fabricated at Nottingham Trent University by this machine. The antennas in Chapter 5 were embroidered using the embroidery machine at Loughborough University (shown in Figure 2-15). The specifications of antenna geometries can be designed using computer-aided design / computer aided manufacturing (CAD/CAM) software either on a computer or embedded on the embroidery machine. The defining characteristics including dimensions, arrangement, stitch type, stitch direction and stitch spacing of each embroidered objects can be controlled with software for the embroidery machine. This system provides fast and accurate productivity for complex antenna shapes, which reduces the error in manufacturing and improves product quality. The embedded camera with micro-lens above the stitches can assist in inspecting the stitch patterns and the structure of the fabrics.

Figure 2-16 shows different patterns of embroidered stitches. Considering the current flowing path, Satin stitch and Running stitch are used in this thesis. Satin stitch is the zigzag pattern that perpendicular to the designed direction. Usually it creates a bold line. Running stitch is a single line of stitch that follows the designed direction. Clearly the running stitch creates the thinnest line compared with other stitches and uses the least length of thread for the same distance. Comparison between these two stitches will be presented in Chapter 3.

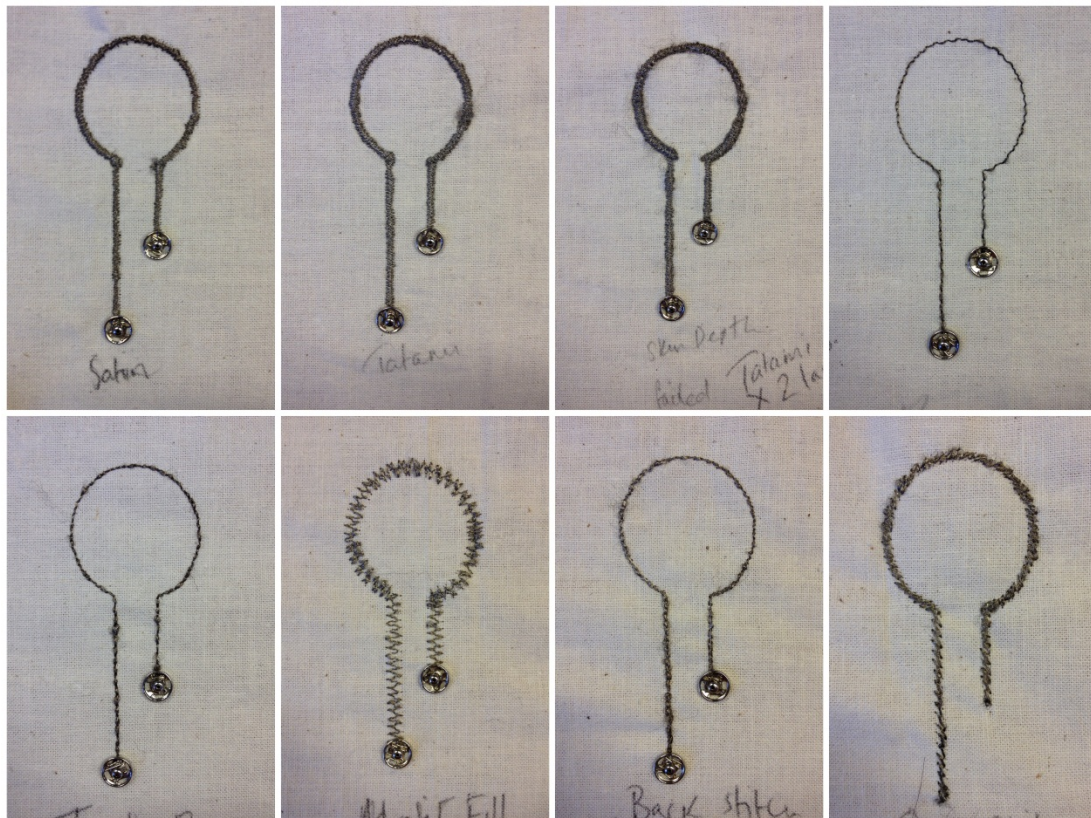


**Figure 2-14 Computerised embroidery machine at Nottingham Trent University  
(model: Barudan BEVT-Z1501CB)**



**Figure 2-15 Computerised embroidery machine at Loughborough University  
(model: Brother Entrepreneur® Pro PR1000e)**



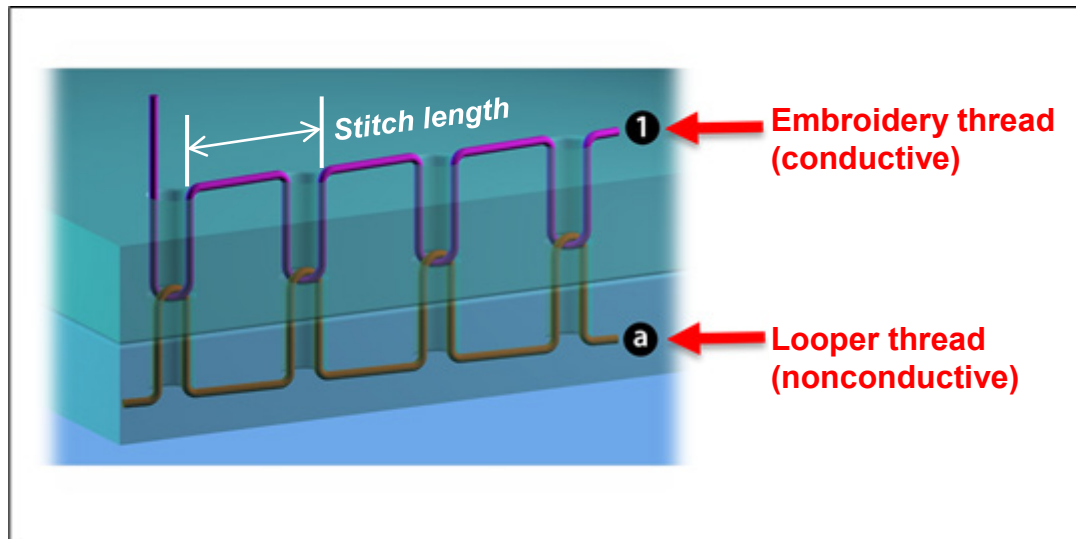


**Figure 2-16 Different patterns of embroidered stitches (from top left: Satin, Tatamin, double layer Tatamin, Running stitch, tripple Running stitch, Hotfill, Back Stitch, and Stem), embroidered at Nottingham Trent University**

### **2.3.2 Model of Embroidered Stitches**

The stitch pattern describes the direction and route of the embroidered thread for creating a shape. The thread needs to be fixed onto the base fabric either by itself or by another thread. There are a variety of different techniques for fixture, but the stitch formation predominantly utilised in this thesis is the ‘lock stitch’ which is the most commonly used in embroidery. The lock stitch is created with a top thread and a looper thread. The top thread runs through a tension system, take-up lever and the eye of the needle. The looper thread is wound onto a bobbin which is inserted into a casing and used in the lower half on the machine. Due to the use of two individual threads which are interlocked during the embroidery process, lock stitching is durable

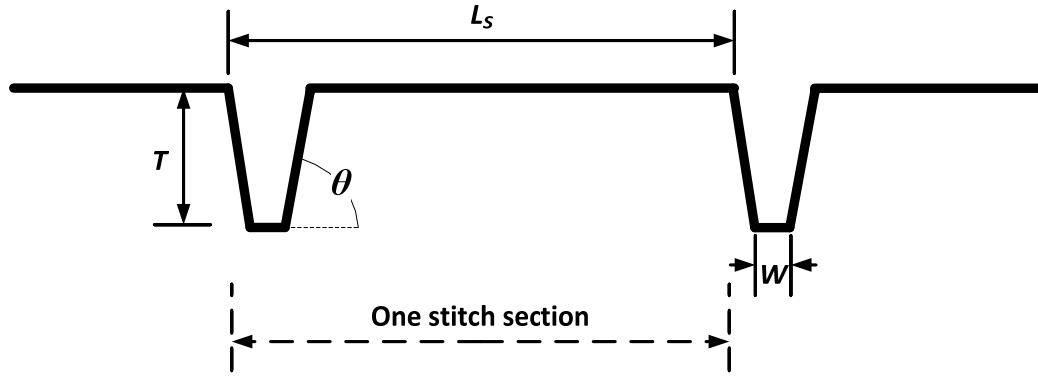
and secure – see Figure 2-17. The conductive layer is embroidered by the conductive thread on the top of a base fabric. A nonconductive thread (usually cotton or polyester yarn) is used to lock the conductive thread via the holes in the fabric. The depths of the holes are equal to the thickness of the fabric.



**Figure 2-17 Sketch of the lock stitches [49]**

As shown in Figure 2-17, the actual usage of the conductive thread is longer than its horizontal length due to the two dimensional structure of the stitches. The depth of the stitch holes in Figure 2-17 are exaggerated as the depth is equal to the thickness of the base fabric which is usually less than 1 mm. The stitch length is the distance between each punch in the direction of stitch running.

In this work, a model was built to estimate the total length of the used thread, see Figure 2-18. Taking running stitch as an example, the diagram illustrates the conductive embroidery thread only.



**Figure 2-18 Model of embroidered conductive thread length using lock stitches**

In Figure 2-18  $L_s$  indicates the stitch length.  $T$  indicates the depth of the inserted embroidery thread.  $T$  depends on the type of thread and base fabric. When Amberstrand is used as embroidery thread and polyester thread is used as looper, the Amberstrand is pulled through the base fabric by the looper threads. Therefore  $T$  equals the base fabric thickness.  $W$  is the width of the lock and is slightly smaller than the width of the hole. The angle  $\theta$  is generated by the lock between top and bottom threads and it can indicate the size of the hole in the base fabric. Generally, the holes are the gaps between the woven yarns and they are insignificant. Therefore  $W$  can approximately represent the width of the hole and the angle  $\theta$  is approximately equal to  $90^\circ$ . Since the diameter of the looper thread is usually much smaller than the conductive thread, and the diameters of the threads will be smaller under the tension,  $W$  is assumed to be approximately equal to twice the diameter of the conductive thread. The curvatures of the thread at the corners are ignored. The length of the used thread in one stitch section  $L_0$  can be calculated by (2.3)

$$L_0 = L_s + 2T \quad (2.3)$$

It is worth noting that there is always one stitch at the end of sewing procedure for the fixture knot. The number of stitches before the finishing stitch can be obtained by (2.4)

$$N = \left\lfloor \frac{L}{L_s} \right\rfloor \quad (2.4)$$

Where  $L$  is the designed length of the line. If the designed length is not the integral multiple of the stitch length, the length of the last stitch and the lock stitch in the last

punch must be add. For a line embroidered with running stitch, the total length of required thread is equal to the sum of total stitch length, the last stitch and the last lock stitch:

$$L_{total} = N \cdot L_0 + (L - N \cdot L_s + 2T) + 2T + W \quad (2.5)$$

By merging equation (2.3), (2.4) and (2.5), the total length of thread can be presented:

$$L_{total} = L + 2(N + 2)T + W \quad (2.6)$$

Since the value of  $W$  is very small compared with total length thus (2.6) can be written as

$$L_{total} = L + 2 \left( \left\lfloor \frac{L}{L_s} \right\rfloor + 2 \right) T \quad (2.7)$$

This can be used for determining the physical and electrical length of the embroidered patterns such as transmission lines or antennas. The extra length that compared to the designed length is determined by

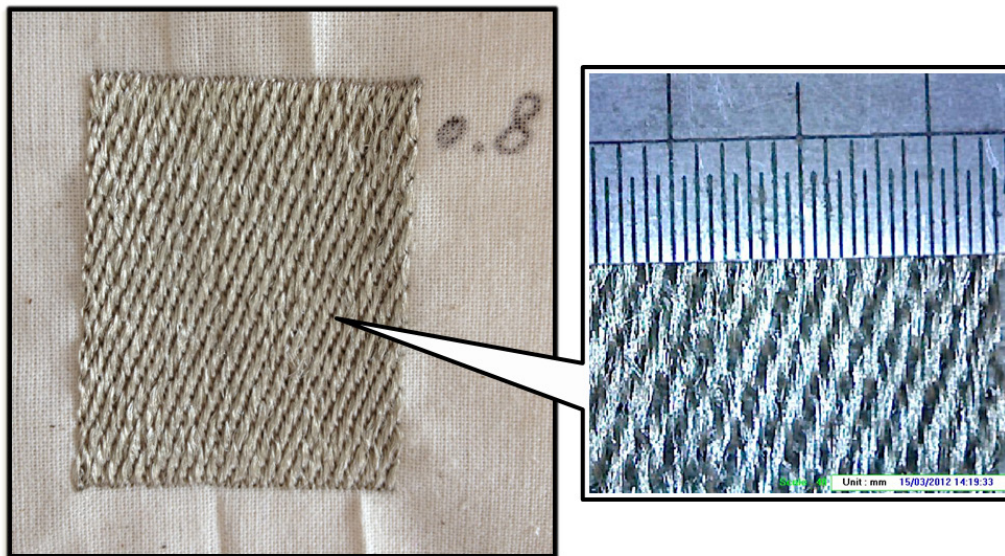
$$\begin{aligned} L_{extra} &= L_{total} - L \\ &= 2 \left( \left\lfloor \frac{L}{L_s} \right\rfloor + 2 \right) T \end{aligned} \quad (2.8)$$

For instance, if a 100 mm long running stitch straight line is embroidered on a 0.5 mm thick cotton fabric with 2 mm stitch length. The total length of the thread is 152 mm. Compared with the designed length of 100 mm, the extra length of thread is 52 mm which is 52% of the designed length.

Equation (2.8) indicates that the extra length depends on the number of stitches and the thickness of base fabric. A thin base fabric will reduce the extra length but may have less mechanical strength. Longer stitch lengths can also reduce the total thread usage but the threads are loosed and wrinkled easily. The optimum base material and

stitch length can provide the balance between the quality of embroidered pattern and the total required length of the conductive thread.

Stitch spacing is another important fabrication parameter when embroidering an area that filled with stitches. The ‘stitch spacing’ indicates the distance between adjacent stitches. As the threads are flattened during embroidery and the filaments may be separated, the adjacent stitches are contacted each other via the loosed filaments. Smaller stitch spacing results in better connection at the cost of longer thread. A 46 mm × 35 mm embroidered rectangular patch antenna on white cotton base fabric with 0.8 mm stitch spacing is shown in Figure 2-19. The running stitch is used for embroidering this pattern and the stitch direction is vertical in the picture. It is estimated that this rectangular patch pattern uses about 3.1 m of thread.



**Figure 2-19 Embroidered rectangular patch with 0.8 mm stitch spacing**

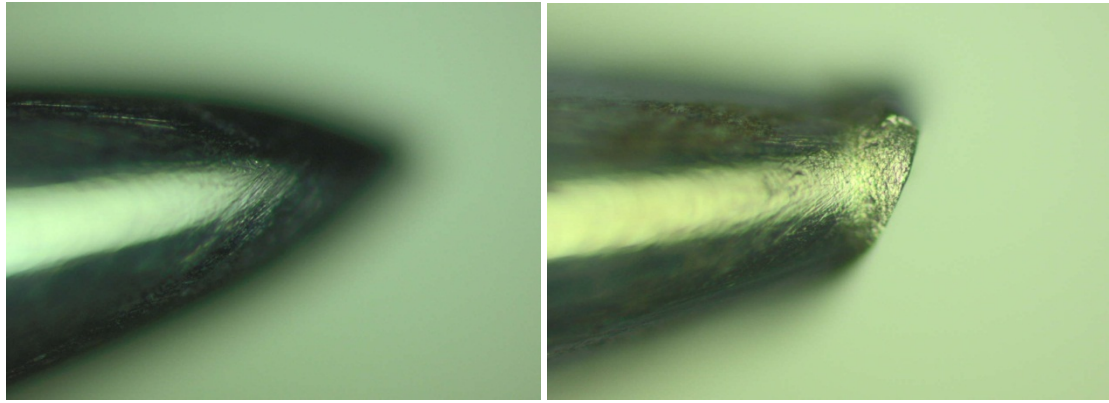
### **2.3.3 Potential Issues Related to the Embroidery Process**

The breakage of the filaments happens during embroidering, particularly for the conductive threads which are stiffer compared with ordinary embroidery threads. This may increase embroidery process difficulty and production costs. The hair-like finer threads can be embroidered at slower speeds in order to minimise the breakages of the conductive threads. In general, polymer based multifilament conductive threads are easy to process compared with metal-filament threads. In addition, the stretching of the base material after embroidery may change the geometrical dimensions. For instance, it has to be carefully designed when embroidering on to the fabric that is more elastic in one direction (for instance, twill). Sourcing the right materials that minimise the stretch is important in embroidered antennas.

To prevent the breakage of the thread, the embroidery stitch patterns and stitch densities had to be processed at lower tensions compared with using normal nonconductive threads. But this resulted in the top thread looping on the fabric surface or the looper thread being pulled through to the fabric front creating a ‘whip stitch’. This may be acceptable for creative aesthetic value; however it is not acceptable when striving to meet the stringent rules for, consistency of an RF transmission line or antenna. High stitch densities would lead to a higher degree of thread breakage.

There are also other factors which could influence the embroidery process. A key factor is the metal surface of the conductive threads which will increase their frictional between the thread and the thread guides on the machine. This also increases the breakage of the filaments. The friction can be reduced by oiling the contact points between the thread and the thread guides on the machine. Higher thread friction could also generate excessive heat at each of the contact points at high machine speeds. Nottingham Trent University also indicated the needles became damaged and pointed out it was mainly due to the coarse nature of the conductive threads utilised, see Figure 2-20.





**Figure 2-20 Zoomed in view of needle before and after embroidering of conductive yarns [49]**

## 2.4 Dielectric Properties of Fabrics

As the electro-textiles are integrated with the normal fabrics, it is crucial to understand the dielectric properties of normal fabrics. These nonconductive fabrics play the role of dielectric substrate or superstrate in the textile based antenna systems. As the textile contains many small air cavities, this microscopic structure makes the dielectric soft and flexible which is suitable for wearable applications. Furthermore, these cavities distributed in the fabric reduce both the dielectric loss and the permittivity. However, the low permittivity of textiles will result in longer effective wavelengths, which usually results in larger antennas.

Several authors measured the permittivity and loss tangent of nonconductive fabrics. However, due to the manufacturing techniques and specifications such as weight, density and dyeing process, some fabrics share the same name but have different dielectric properties (for instance, there are numerous “felt” fabrics with different thicknesses and weights), whilst some fabrics are made from the same raw material but also have different properties (for instance, cotton made denim and canvas). Table 2-2 shows some of the measured results of common fabrics from published papers.

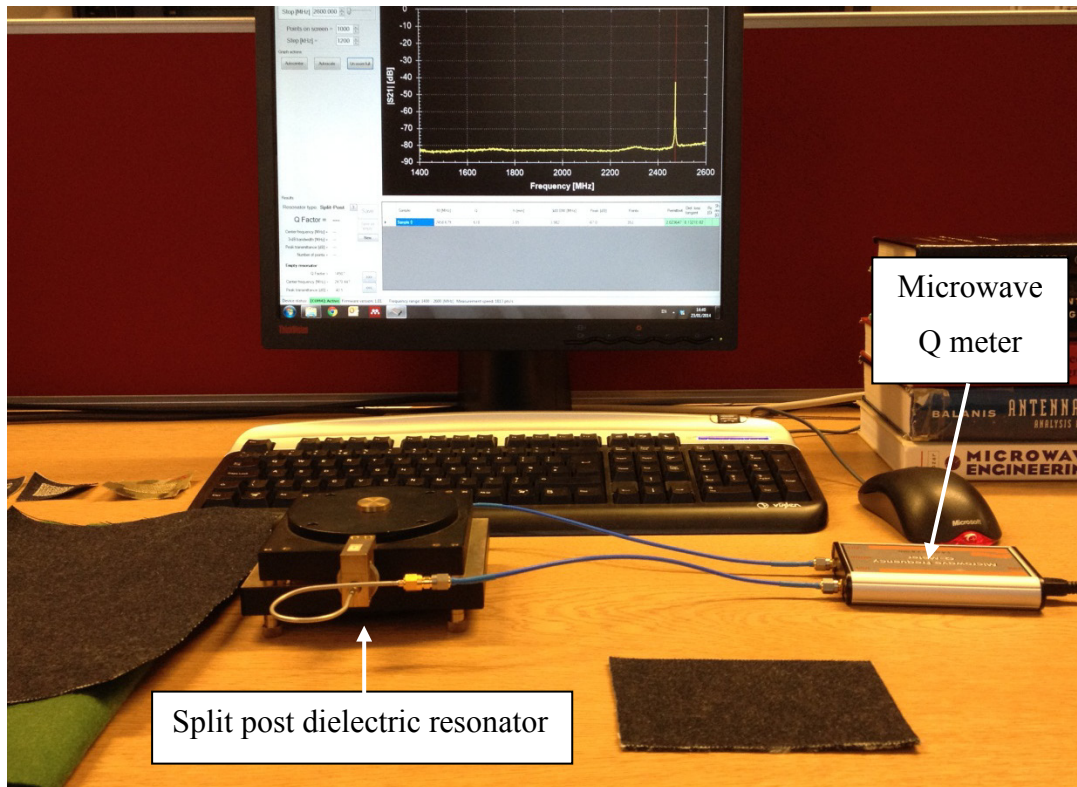
**Table 2-2 Summary of dielectric properties of nonconductive fabrics**

<b>Material</b>	<b>Permittivity</b>	<b>Loss Tangent</b>	<b>Reference</b>
Denim	1.40 to 2.00	0.0140 to 0.0700	[65]–[70]
Cotton	1.54, 1.60	0.0580, 0.0040	[71], [20]
Cordura/Lycra <sup>®</sup>	1.50	0.0093	[20]
Felt	1.36, 1.38	0.0160, 0.0230	[71], [72]
Fleece	1.17, 1.20	0.0035, 0.0040	[72], [71]
Polyester	1.90	0.0045	[20]
Leather	1.80 to 2.95	0.0490 to 0.1600	[66], [71]
Moleskin	1.45	0.0500	[72]
Panama	2.12	0.0018	[72]
Silk	1.20, 1.75	0.0540, 0.0120	[72], [71]
Tween	1.69	0.0084	[72]
Velcro	1.34	0.0060	[68], [73]
Neoprene	5.20	0.0250	[71]

In this work, two common textile materials were measured: denim and felt. There are several of methods available to determine the dielectric properties. For instance, by measuring the dielectric loaded resonant cavities, the Nicholson-Ross-Weir (NRW) conversion [74]–[77] can be used to convert the measured scattering parameters to the permittivity and permeability. However, the normal waveguide cavity method requires the materials under test to be flat and precisely fill the waveguide without wrinkling and air gap. This is difficult for fabric materials. And therefore the split post dielectric resonator method was used in this work.



The measurement setup is shown by Figure 2-21. The microwave Q meter in Figure 2-21 is a device that can measure the S21 results of split post dielectric resonator without a vector network analyser (VNA). By measuring the quality factors (Q) of the empty resonator and with the dielectric material in the resonator, the permittivity and loss tangent can be calculated [78], [79]. Details of the method are shown in Appendix A.



**Figure 2-21 Measurement setup for permittivity and loss tangent values of fabric samples**

The Q factor is obtained by measuring the -3 dB bandwidth of the S21 using the Q meter.

$$Q = \frac{f_r}{\Delta f} \quad (2.13)$$

Where  $f_r$  is the resonant frequency and the  $\Delta f$  is the -3 dB bandwidth.

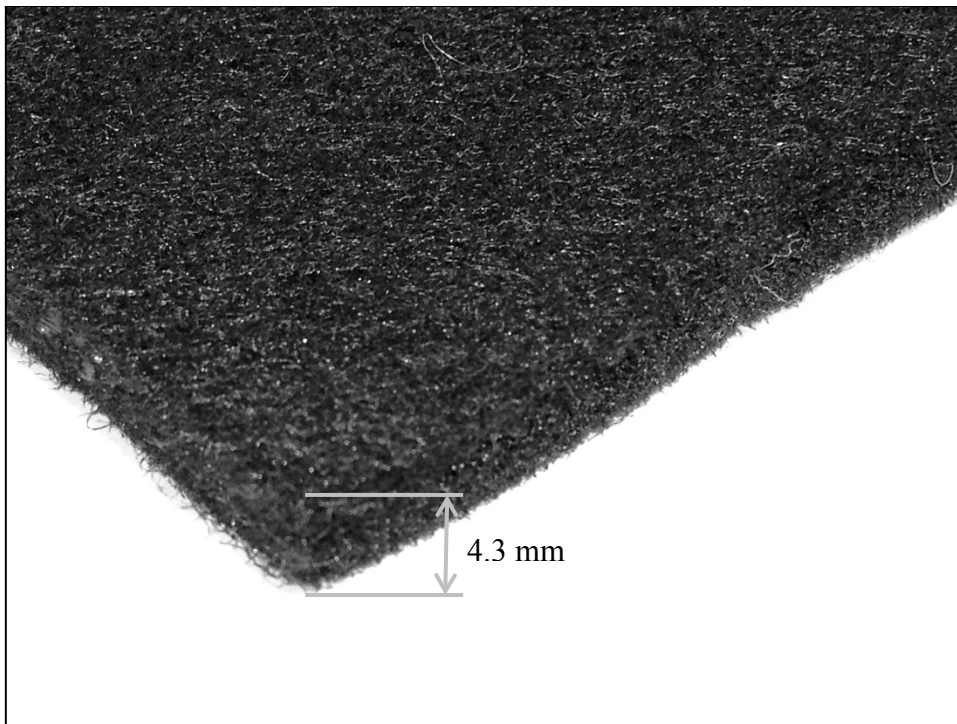
Table 2-3 contains the dielectric measurement results of denim (see Figure 2-22) and felt (Figure 2-23). The thermal melt adhesive web is used in this work for attaching multiple layers of fabric. A zoomed in view of the hemming web strip is shown in Figure 2-24. This thermal melt adhesive is made from 100% copolyamide and is widely used for textile adhesive such as hemming. The melting temperature is 105 – 120 °C. This thin and low density adhesive material introduces additional air holes in the cloth fabric. The impact of melted copolyamide web on its permittivity and loss tangent was also measured. The results are shown in Table 2-3. The melted web between two layers of denim is 0.05 mm thick. The hemming web reduces both the permittivity and loss tangent of the two layers of denim. On the other hand, the permittivity and loss tangent of the black felt is the smallest. Particularly the loss tangent of felt is smaller than the low-loss rigid dielectric substrate RF-45. This indicates that thick fabric material such as felt with a large number of air voids has low loss tangent and can be used for dielectric substrate for microstrip antennas.

**Table 2-3 Dielectric measurements of fabric substrates using split post dielectric resonator**

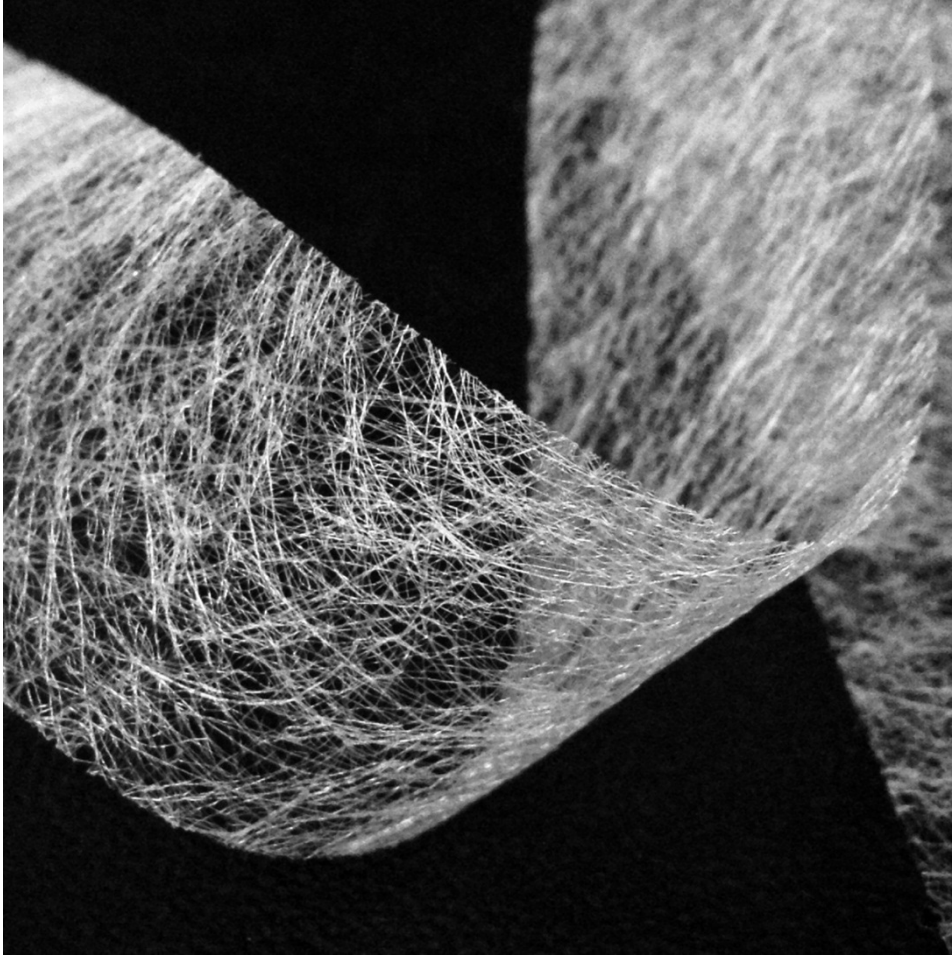
	Thickness (mm)	$\epsilon_r$	$\tan\delta$
Single layer denim	0.53	1.97	0.0737
2 layers of denim (no adhesive)	1.10	1.92	0.0751
2 layers of denim with copolyamide web	1.15	1.85	0.0526
4 layers of denim with copolyamide web	2.24	1.90	0.0661
Black felt	4.30	1.22	0.0022
Taconic RF-45 rigid substrate	1.57	4.50	0.0037



**Figure 2-22 Zoomed in view of 0.53 mm thick denim fabric**



**Figure 2-23 Zoomed in view of 4.30 mm thick felt fabric**



**Figure 2-24 Zoomed in view of thermal melt copolyamide web strip**

The black felt will be used for dielectric substrate of embroidered patch antenna in Chapter 5 because of its lowest loss tangent. However due to the low relative permittivity and thickness, the antenna size has to be increased compared with high permittivity substrates.

## 2.5 Low-profile RF Connectors for Fabric Antennas

A miniature connector with a standard interface is desirable to maintain the flexibility and comfort of wearable devices. The basic requirements for the wearable antenna connectors are being low-profile and having a small mounting area. They can be either permanent or detachable depending on the application. Wearable electronics such as microchips can be permanently ironed onto the high temperature resistant metallised fabric circuit substrates [80], [81]. The chips can also be sewed onto the fabric using conductive threads [82]–[84]. A note of caution must be sounded that the fabric based antennas and electronics may touch and be shorted each other due to the fold of textile fabrics and results in unwanted short circuit. Generally, it will be beneficial for the wearable electronics to have shorter connectors or cables to reduce the effects of bending and folding. Placing the fabric antenna on the positions with less fabric fold and additional protection layer on conductive textile will also prevent the fabric based wearable antennas and electronics from being shorted.

The U.FL connector is an ultra-small, low profile coaxial connector [85] (shown in Figure 2-25). After the 90° plug is fitted in the receptacle, the height of the plug is 2 mm including receptacle base, and the mounting area is 7-8 mm<sup>2</sup>. With a diameter of 0.81 mm flexible cable connected, this U.FL connector is ideal for realising low profile connections for fabric-based antennas. Figure 2-26 shows the back-side of an embroidered dipole antenna with the U.FL connector and a thin flexible cable. The plug is covered by the fabric and therefore will not attract user's attention. The SubMiniature version A (SMA) connector at the other end of the cable can be replaced by another U.FL connector depends on the device at the other end. The disadvantage of this connector comes from the cable loss which is dependent on the cable diameter. At 3 GHz the smallest cable loss is 0.28 dB per centimetre for the thickest cable of 1.37 mm diameter whilst the largest loss is 0.65 dB per centimetre for the thinnest diameter of 0.81 mm. Minimising the lengths of the cables in wearable applications will reduce the losses and also improve the compactness of the devices. Embroidered dipole antennas connected to the U.FL connectors and flexible lightweight cables can be seen in [86].





Figure 2-25 U.FL low profile connectors (picture from [85])



Figure 2-26 Covered low profile U.FL connector with flexible cable

Detachable conductive fasteners that provide both mechanical and electrical connections will be beneficial to the fabric based wearable antennas and electronics. It allows antennas and electronics to be replaced or removed from the wearable systems on demand. A novel conductive hook and loop connectors for RF application will be developed and measured in Chapter 3. The hook and loop is detachable and flexible connections which links two pieces of electronics. Moreover due to the flat structure of the hook and loop strip, it can be fabricated as transmission lines.

## **2.6 Conclusions**

This chapter has summarised and compared the current techniques of fabricating electro-textiles i.e. coating, weaving, printing and embroidery. These techniques have their own advantages in different wearable applications. Conductive layer coated fabric sheet is suitable for large continuous conductive shapes or EMC shielding. It is also the most widely available type of conductive fabric due to the low technical challenge compared with other three techniques. Woven conductive fabrics can be customised for special requirements and weaving conductive yarns with normal nonconductive yarns can create “in textile” conductive paths which are suitable for particular applications such as electroluminescence. Printing is the most accurate approach with the highest resolution of conducting patterns. However, the cost of the specialised conductive ink and the difficulty of applying it onto the fabric limit its applicability. Embroidery on the other hand, has reasonable resolution and also benefits from the large number of commercially available conductive threads. These features make embroidery become the choice of fabricating textile based antennas in this thesis with bespoke designs and a balance between performance and cost.

Three types of conductive threads based on the composition of the filaments are compared. The multifilament conductive thread is chosen in this thesis for embroidery as it is easier to be embroidered than the monofilament and dual-filament threads by

using the computerised embroidery machine. The SEM images of the Amberstrand indicated the thickness of the metal cladding to be 1  $\mu\text{m}$  and its diameter of a single filament to be 17  $\mu\text{m}$ . The conductivity of the Amberstrand Silver thread was estimated from the SEM images. The skin effect should be accounted for high frequency applications as the metallization on the filament is thin.

The key factors of embroidery including stitch patterns and stitches types have been presented in this chapter. Lock stitch is applied for fixing the conductive thread onto the base fabric. The accurate length of conductive thread was estimated based on the schematic of the lock stitch. The model indicates that the total usage of the thread is longer than designed length and the extra length can be determined by the thickness of the base fabric and the selected stitch length.

Nonconductive fabric materials can be used as flexible dielectric substrates. These dielectric characteristics of the nonconductive normal fabric were measured using the split post dielectric resonator method. The thermal melt copolyamide can be used as adhesive for creating substrates with multiple layers. The measured low loss tangent of the nonwoven fabric black felt indicate that it can be used for the substrate for the microstrip antenna to reduce the dielectric loss.

Ultra-small, low profile coaxial U.FL connectors were considered. The tiny semi detachable connector can be hidden under the fabric layers unobtrusively. With the thin coaxial cable of diameter less than 1 mm, the U.FL connector can be used for connection between fabric antennas and wearable electronic devices for maintaining flexibility. The cable loss will be reduced with thicker cables and the cable length should be minimised.



Recent literature shows the feasibility of embroidering wearable antennas using conductive threads. However, fabrication specifications such as embroidery parameters, conductive threads choosing, connections and cost of production which link to the mass-manufacturing have not been completely analysed and evaluated. This thesis tackles and emphasises on investigating the optimal manufacturing parameters with the balance between performance and cost of production. The effects of embroidery parameters on both DC and RF performances of embroidered transmission lines and antennas will be critical compared in Chapter 3 and 4. The guideline of embroidering conductive patterns and choosing the suitable thread is given in this thesis. In addition, the connection between RF source and embroidered components is needed to be further developed based on previous researches. Detachable and reusable connectors are desirable for fabric based wearable antennas. Chapter 3 will present a connector providing repeatable RF measurements. Novel detachable conductive hook and loop RF connectors will also be showed in Chapter 3. Furthermore, although previous researches have showed the anisotropic characteristic of conductive textiles, detailed surface current distribution on textile that linked to RF performance has not been analysed. This thesis investigates the effect of embroidered stitches on the surface current that influenced the RF performance of embroidered transmission lines and microstrip antennas. The anisotropic characteristic of embroidered stitches will be illustrated in Chapter 3, 4 and 5.

## References

- [1] R. Salvado, C. Loss, R. Gonçalves, and P. Pinho, “Textile materials for the design of wearable antennas: a survey.,” *Sensors (Basel, Switzerland)*, vol. 12, no. 11, pp. 15841–57, Jan. 2012.
- [2] T. F. Kennedy, P. W. Fink, A. W. Chu, and G. F. Studor, “Potential space applications for body-centric wireless and e-textile antennas,” in *IET Seminar on Antennas and Propagation for Body-Centric Wireless Communications*, 2007, pp. 77–83.
- [3] U. Möhring, S. Gimpel, A. Neudeck, W. Scheibner, and D. Zschenderlein, “Conductive, sensorial and luminescent features in textile structures,” in *Applied Wearable Computing (IFAWC), 3rd International Forum on*, 2006, pp. 1–6.
- [4] S. Q. Jiang, E. Newton, C. W. M. Yuen, and C. W. Kan, “Chemical silver plating and its application to textile fabric design,” *Journal of Applied Polymer Science*, vol. 96, no. 3, pp. 919–926, May 2005.
- [5] LessEMF, “Pure Copper Polyester Taffeta Fabric.” [Online]. Available: <http://www.lessemf.com/fabric.html#1212>. [Accessed: 20-Mar-2013].
- [6] “Nora Dell.” [Online]. Available: [http://www.shieldextrading.net/pdfs/NoraDell CR.pdf](http://www.shieldextrading.net/pdfs/NoraDell%20CR.pdf). [Accessed: 12-Dec-2013].
- [7] Shieldex Trading, “Woven Fabrics.” [Online]. Available: [http://www.shieldextrading.net/woven\\_fabrics.html](http://www.shieldextrading.net/woven_fabrics.html). [Accessed: 10-Jan-2013].
- [8] J. Lilja and P. Salonen, “Textile material characterization for SoftWear antennas,” in *IEEE Military Communications Conference (MILCOM)*, 2009, pp. 1–7.

- [9] M. Klemm and G. Troester, "Textile UWB Antennas for Wireless Body Area Networks," *IEEE Transactions on Antennas and Propagation*, vol. 54, no. 11, pp. 3192–3197, Nov. 2006.
- [10] T. Kennedy, P. Fink, and A. Chu, "Body-worn e-textile antennas: The good, the low-mass, and the conformal," *IEEE Transactions on Antennas and Propagation*, vol. 57, no. 4, pp. 910–918, 2009.
- [11] J. A. Dobbins, A. W. Chu, P. W. Fink, T. F. Kennedy, G. Y. Lin, M. A. Khayat, and R. C. Scully, "Fabric equiangular spiral antenna," in *IEEE Antennas and Propagation Society International Symposium*, 2006, pp. 2113–2116.
- [12] D. L. Paul, C. Jayatissa, G. S. Hilton, and C. J. Railton, "Conformability of a textile antenna for reception of digital television," *Loughborough Antennas & Propagation Conference*, pp. 225–228, Nov. 2010.
- [13] M. Panhuis, J. Wu, S. A. Ashraf, and G. G. Wallace, "Conducting textiles from single-walled carbon nanotubes," *Synthetic Metals*, vol. 157, no. 8–9, pp. 358–362, May 2007.
- [14] L. Hu, M. Pasta, F. La Mantia, L. Cui, S. Jeong, H. D. Deshazer, J. W. Choi, S. M. Han, and Y. Cui, "Stretchable, porous, and conductive energy textiles.," *Nano letters*, vol. 10, no. 2, pp. 708–14, Feb. 2010.
- [15] Y. Bayram, N. A. Kotov, and J. L. Volakis, "E-Textile Conductors and Polymer Composites for Conformal Lightweight Antennas," *IEEE Transactions on Antennas and Propagation*, vol. 58, no. 8, pp. 2732–2736, Aug. 2010.
- [16] E. R. Post, M. Orth, P. R. Russo, and N. Gershenfeld, "E-broidery: Design and fabrication of textile-based computing," *IBM Systems Journal*, vol. 39, no. 3.4, pp. 840–860, 2000.
- [17] I. Locher, M. Klemm, and T. Kirstein, "Design and characterization of purely textile patch antennas," *IEEE Transactions on Advanced Packaging*, vol. 29, no. 4, pp. 777–788, 2006.

- [18] D. Cottet, J. Grzyb, T. Kirstein, and G. Troster, "Electrical characterization of textile transmission lines," *Advanced Packaging, IEEE Transactions on*, vol. 26, no. 2, pp. 182–190, 2003.
- [19] E. J. Power and T. Dias, "Knitting of electroconductive yarns," in *Eurowearable*, 2003, pp. 55–60.
- [20] Y. Ouyang and W. J. Chappell, "High frequency properties of electro-textiles for wearable antenna applications," *Antennas and Propagation, IEEE Transactions on*, vol. 56, no. 2, pp. 381–389, 2008.
- [21] S. Gimpel, U. Mohring, H. Muller, A. Neudeck, and W. Scheibner, "Textile-Based Electronic Substrate Technology," *Journal of Industrial Textiles*, vol. 33, no. 3, pp. 179–189, Jan. 2004.
- [22] P. Salonen and L. Hurme, "A novel fabric WLAN antenna for wearable applications," in *IEEE Antennas and Propagation Society International Symposium. Digest. Held in conjunction with: USNC/CNC/URSI North American Radio Sci. Meeting (Cat. No.03CH37450)*, vol. 2, pp. 700–703.
- [23] K. J. Noh, Y. K. Son, B. S. Kim, and I. Cho, "Wearable network using Optical e-Textile Antenna for NLOS," in *IEEE International Conference on Consumer Electronics (ICCE)*, 2012, pp. 556–557.
- [24] Wikipedia, "Knitting." [Online]. Available: <http://en.wikipedia.org/wiki/Knitting>. [Accessed: 20-Mar-2013].
- [25] I. Locher and G. Troster, "Screen-printed Textile Transmission Lines," *Textile Research Journal*, vol. 77, no. 11, pp. 837–842, Nov. 2007.
- [26] Y. Kim, H. Kim, and H. Yoo, "Electrical Characterization of Screen-Printed Circuits on the Fabric," *IEEE Transactions on Advanced Packaging*, vol. 33, no. 1, pp. 196–205, Feb. 2010.
- [27] A. Chauraya, W. G. Whittow, J. C. Vardaxoglou, Y. Li, R. Torah, K. Yang, S. Beeby, and J. Tudor, "Inkjet printed dipole antennas on textiles for wearable

- communications,” *IET Microwaves, Antennas & Propagation*, vol. 7, no. 9, pp. 760–767, Jun. 2013.
- [28] M. M. Tentzeris, R. Vyas, V. Lakafosis, A. Traille, H. Lee, E. Gebara, and M. Marroncelli, “Inkjet-printed RFIDs for wireless sensing and anti-counterfeiting,” in *6th European Conference on Antennas and Propagation (EuCAP)*, 2012, pp. 3481–3482.
- [29] Y. Li, R. Torah, S. Beeby, and J. Tudor, “Inkjet printed flexible antenna on textile for wearable applications,” in *Textile Institute World Conference, Selangor, Malaysia*, 2012.
- [30] A. Rida, R. Vyas, and M. M. Tentzeris, “Conductive Inkjet-Printed Antennas on Flexible Low-Cost Paper-Based Substrates for RFID and WSN Applications,” *IEEE Antennas and Propagation Magazine*, vol. 51, no. 3, pp. 13–23, Jun. 2009.
- [31] M. Mäntysalo and P. Mansikkamäki, “An inkjet-deposited antenna for 2.4 GHz applications,” *AEU - International Journal of Electronics and Communications*, vol. 63, no. 1, pp. 31–35, Jan. 2009.
- [32] Y. Li, R. Torah, S. Beeby, and J. Tudor, “An all-inkjet printed flexible capacitor on a textile using a new poly(4-vinylphenol) dielectric ink for wearable applications,” in *IEEE Sensors*, 2012, pp. 1–4.
- [33] S. Merilampi, T. Björninen, V. Haukka, P. Ruuskanen, L. Ukkonen, and L. Sydänheimo, “Analysis of electrically conductive silver ink on stretchable substrates under tensile load,” *Microelectronics Reliability*, vol. 50, no. 12, pp. 2001–2011, Dec. 2010.
- [34] L. Ukkonen, L. Sydänheimo, and Y. Rahmat-Samii, “Sewed textile RFID tag and sensor antennas for on-body use,” in *6th European Conference on Antennas and Propagation (EuCAP)*, 2012, pp. 3450–3454.

- [35] Z. Wang, L. Zhang, D. Psychoudakis, and J. L. Volakis, "GSM and Wi-Fi textile antenna for high data rate communications," in *Proceedings of the IEEE International Symposium on Antennas and Propagation*, 2012, vol. 3, pp. 1–2.
- [36] L. Zhang, Z. Wang, and J. L. Volakis, "Embroidered textile circuits for microwave devices," *Proceedings of the IEEE International Symposium on Antennas and Propagation*, pp. 1–2, Jul. 2012.
- [37] S. Zhang, A. Chauraya, W. Whittow, R. Seager, T. Acti, T. Dias, and Y. Vardaxoglou, "Embroidered wearable antennas using conductive threads with different stitch spacings," in *Loughborough Antennas & Propagation Conference (LAPC)*, 2012, pp. 1–4.
- [38] J. Choi, Y. Kim, K. Lee, and Y. C. Chung, "Various wearable embroidery RFID tag antenna using electro-thread," in *IEEE Antennas and Propagation Society International Symposium*, 2008, pp. 1–4.
- [39] Z. Wang, L. Zhang, Y. Bayram, and J. L. Volakis, "Embroidered e-fiber-polymer composites for conformal and load bearing antennas," in *IEEE Antennas and Propagation Society International Symposium*, 2010, pp. 1–4.
- [40] T. Maleszka and P. Kabacik, "Bandwidth properties of embroidered loop antenna for wearable applications," in *European Wireless Technology Conference (EuWIT)*, 2010, pp. 89–92.
- [41] Z. Wang, L. Zhang, Y. Bayram, and J. L. Volakis, "Multilayer printing of embroidered RF circuits on polymer composites," in *IEEE International Symposium on Antennas and Propagation (APS/URSI)*, 2011, pp. 278–281.
- [42] L. Zhang, Z. Wang, D. Psychoudakis, and J. L. Volakis, "E-fiber electronics for body-worn devices," in *6th European Conference on Antennas and Propagation (EuCAP)*, 2012, pp. 760–761.
- [43] Z. Wang, L. Zhang, Y. Bayram, and J. L. Volakis, "Embroidered Conductive Fibers on Polymer Composite for Conformal Antennas," *IEEE Transactions on Antennas and Propagation*, vol. 60, no. 9, pp. 4141–4147, Sep. 2012.

- [44] J. L. Volakis, L. Zhang, Z. Wang, and Y. Bayram, "Embroidered flexible RF electronics," in *IEEE International Workshop on Antenna Technology (iWAT)*, 2012, pp. 8–11.
- [45] Z. Wang, L. Zhang, D. Psychoudakis, and J. L. Volakis, "Flexible textile antennas for body-worn communication," in *IEEE International Workshop on Antenna Technology (iWAT)*, 2012, vol. 4, pp. 205–208.
- [46] E. Moradi, T. Bjorninen, L. Ukkonen, and Y. Rahmat-Samii, "Effects of Sewing Pattern on the Performance of Embroidered Dipole-Type RFID Tag Antennas," *IEEE Antennas and Wireless Propagation Letters*, vol. 11, pp. 1482–1485, 2012.
- [47] K. Koski, E. Koski, T. Björninen, A. A. Babar, L. Ukkonen, L. Sydanheimo, and Y. Rahmat-Samii, "Practical read range evaluation of wearable embroidered UHF RFID tag," in *Proceedings of the IEEE International Symposium on Antennas and Propagation*, 2012, pp. 1–2.
- [48] E. Koski, K. Koski, T. Bjorninen, A. A. Babar, L. Sydanheimo, L. Ukkonen, and Y. Rahmat-Samii, "Fabrication of embroidered UHF RFID tags," in *Proceedings of the IEEE International Symposium on Antennas and Propagation*, 2012, pp. 1–2.
- [49] T. Acti, S. Zhang, A. Chauraya, W. Whittow, R. Seager, T. Dias, and Y. Vardaxoglou, "High performance flexible fabric electronics for megahertz frequency communications," in *Loughborough Antennas & Propagation Conference (LAPC)*, 2011, pp. 1–4.
- [50] Y. Ouyang and W. Chappell, "Measurement of electrotiles for high frequency applications," in *IEEE MTT-S International Microwave Symposium Digest*, 2005, pp. 1679–1682.
- [51] "X-Static." [Online]. Available: <http://www.noblebiomaterials.com/category2.asp?itemid=212>. [Accessed: 12-Dec-2012].

- [52] “Shieldex.” [Online]. Available: <http://www.statex.biz/index.php/en/?lang=en>. [Accessed: 12-Dec-2013].
- [53] “AmberStrand® fiber.” [Online]. Available: <http://www.metalcladfibers.com/amberstrand-fiber/>. [Accessed: 12-Dec-2013].
- [54] J. Azoulay, “Anisotropy in electric properties of fabrics containing new conductive fibers,” *IEEE Transactions on Electrical Insulation*, vol. 23, no. 3, pp. 383–386, Jun. 1988.
- [55] H. Shimasaki, T. Nakagawa, and M. Akiyama, “Measurement of the surface resistance of conductive textiles at microwave frequency,” in *Asia Pacific Microwave Conference*, 2009, pp. 2580–2583.
- [56] J. Banaszczyk, G. De Mey, A. Schwarz, and L. Van Langenhove, “Current Distribution Modelling in Electroconductive Textiles,” in *14th International Conference on Mixed Design of Integrated Circuits and Systems*, 2007, pp. 418–423.
- [57] J. Banaszczyk, G. De Mey, and A. Schwarz, “Current Distribution Modelling in Electroconductive Fabrics,” *Fibres & Textiles in Eastern Europe*, vol. 17, no. 2, pp. 28–33, 2009.
- [58] V. Der Pauw, “A method of measuring specific resistivity and Hall effect of disc of arbitrary shape,” *Philips Research Reports*, vol. 13, pp. 1–9, 1958.
- [59] I. Kazani, G. De Mey, C. Hertleer, J. Banaszczyk, A. Schwarz, G. Guxho, and L. Van Langenhove, “Van Der Pauw method for measuring resistivities of anisotropic layers printed on textile substrates,” *Textile Research Journal*, vol. 81, no. 20, pp. 2117–2124, Sep. 2011.
- [60] A. Schwarz, L. Cuny, C. Hertleer, F. Ghekier, I. Kazani, G. De Clercq, G. De Mey, and L. Van Langenhove, “Electrical circuit model of elastic and conductive yarns produced by hollow spindle spinning,” *Materials Technology: Advanced Performance Materials*, vol. 26, no. 3, pp. 121–127, 2011.



- [61] M. Miao, “Electrical conductivity of pure carbon nanotube yarns,” *Carbon*, vol. 49, no. 12, pp. 3755–3761, Oct. 2011.
- [62] A. Schwarz, J. Hakuzimana, A. Kaczynska, J. Banaszczyk, P. Westbroek, E. McAdams, G. Moody, Y. Chronis, G. Priniotakis, G. De Mey, D. Tseles, and L. Van Langenhove, “Gold coated para-aramid yarns through electroless deposition,” *Surface and Coatings Technology*, vol. 204, no. 9–10, pp. 1412–1418, Jan. 2010.
- [63] Syscom Advanced Materials, “Metal clad fibers.” [Online]. Available: <http://www.metalcladfibers.com/metal-clad-fibers/>. [Accessed: 02-Jan-2014].
- [64] A. E. Kennelly, F. A. Laws, and P. H. Pierce, “Experimental Researches on Skin Effect in Conductors,” *Transactions of the American Institute of Electrical Engineers*, vol. XXXIV, no. 2, pp. 1953–2021, Jul. 1915.
- [65] B. Sanz-Izquierdo and J. C. Batchelor, “A Dual Band Belt Antenna,” in *International Workshop on Antenna Technology: Small Antennas and Novel Metamaterials*, 2008, pp. 374–377.
- [66] D. Gaspar and A. A. Moreira, “Belt antenna for wearable applications,” in *IEEE Antennas and Propagation Society International Symposium*, 2009, pp. 1–4.
- [67] B. Sanz-Izquierdo, J. C. Batchelor, and M. I. Sobhy, “Compact UWB Wearable Antenna,” in *Loughborough Antennas and Propagation Conference (LAPC)*, 2007, pp. 121–124.
- [68] B. Sanz-Izquierdo, J. C. Batchelor, and M. I. Sobhy, “Button antenna on textiles for wireless local area network on body applications,” *IET Microwaves, Antennas & Propagation*, vol. 4, no. 11, pp. 1980–1987, 2010.
- [69] S. W. Harmer, N. Rezgui, N. Bowring, Z. Luklinska, and G. Ren, “Determination of the complex permittivity of textiles and leather in the 14–40 GHz millimetre-wave band using a free-wave transmittance only method,” *IET Microwaves, Antennas & Propagation*, vol. 2, no. 6, pp. 606–614, 2008.

- [70] B. Sanz-Izquierdo, L. Wu, J. C. Batchelor, and P. R. Young, "Textile integrated waveguide slot antenna," in *IEEE Antennas and Propagation Society International Symposium*, 2010, pp. 1–4.
- [71] S. Bashir, "Design and synthesis of non uniform high impedance surface based wearable antennas," PhD thesis, School of Electronic, Electrical and Systems Engineering, Loughborough University, Loughborough, 2009.
- [72] S. Zhu and R. Langley, "Dual-band wearable textile antenna on an EBG substrate," *Antennas and Propagation, IEEE Transactions on*, vol. 57, no. 4, pp. 926–935, 2009.
- [73] B. Sanz-Izquierdo, F. Huang, and J. C. Batchelor, "Small size wearable button antenna," in *First European Conference on Antennas and Propagation (EuCAP)*, 2006, pp. 1–4.
- [74] N. G. Alexopoulos, C. A. Kyriazidou, and H. F. Contopanagos, "Effective Parameters for Metamorphic Materials and Metamaterials Through a Resonant Inverse Scattering Approach," *IEEE Transactions on Microwave Theory and Techniques*, vol. 55, no. 2, pp. 254–267, Feb. 2007.
- [75] A. Boughriet, C. Legrand, and A. Chapoton, "Noniterative stable transmission/reflection method for low-loss material complex permittivity determination," *IEEE Transactions on Microwave Theory and Techniques*, vol. 45, no. 1, pp. 52–57, 1997.
- [76] A. M. Nicolson and G. F. Ross, "Measurement of the Intrinsic Properties of Materials by Time-Domain Techniques," *IEEE Transactions on Instrumentation and Measurement*, vol. 19, no. 4, pp. 377–382, 1970.
- [77] W. B. Weir, "Automatic measurement of complex dielectric constant and permeability at microwave frequencies," *Proceedings of the IEEE*, vol. 62, no. 1, pp. 33–36, 1974.
- [78] J. Krupka, "Measurements of the complex permittivity of microwave circuit board substrates using split dielectric resonator and reentrant cavity techniques,"

- in *Seventh International Conference on Dielectric Materials, Measurements and Applications*, 1996, pp. 21–24.
- [79] J. Krupka, A. P. Gregory, O. C. Rochard, R. N. Clarke, B. Riddle, and J. Baker-Jarvis, “Uncertainty of complex permittivity measurements by split-post dielectric resonator technique,” *Journal of the European Ceramic Society*, vol. 21, no. 15, pp. 2673–2676, Jan. 2001.
- [80] I. Locher and G. Troster, “Fundamental Building Blocks for Circuits on Textiles,” *IEEE Transactions on Advanced Packaging*, vol. 30, no. 3, pp. 541–550, Aug. 2007.
- [81] L. Buechley and M. Eisenberg, “Fabric PCBs, electronic sequins, and socket buttons: techniques for e-textile craft,” *Personal and Ubiquitous Computing*, vol. 13, no. 2, pp. 133–150, Aug. 2007.
- [82] H. S. Lee, “Wearable Personal Network Based on Fabric Serial Bus Using Electrically Conductive Yarn,” *ETRI Journal*, vol. 32, no. 5, pp. 713–721, Oct. 2010.
- [83] T. Linz, C. Kallmayer, R. Aschenbrenner, and H. Reichl, “Embroidering Electrical Interconnects with Conductive Yarn for The Integration of Flexible Electronic Modules into Fabric,” *Ninth IEEE International Symposium on Wearable Computers (ISWC’05)*, pp. 86–91, 2005.
- [84] T. Linz, C. Kallmayer, R. Aschenbrenner, and H. Reichl, “Fully Integrated EKG Shirt based on Embroidered Electrical Interconnections with Conductive Yarn and Miniaturized Flexible Electronics,” *International Workshop on Wearable and Implantable Body Sensor Networks (BSN’06)*, pp. 23–26, 2006.
- [85] Hirose Electric Group, “U.FL Series.” [Online]. Available: <http://www.hirose-connectors.com/connectors/H203SeriesCategorySearch.aspx?cat=03>. [Accessed: 01-May-2013].

- [86] T. Acti, A. Chauraya, S. Zhang, W. Whittow, R. Seager, Y. Vardaxoglou, T. Dias, “Embroidered Wire Dipole Antennas Using Novel Copper Yarns”, IEEE Antennas and Wireless Propagation Letters, (Submitted May 2014)

# Chapter 3

## Embroidered Transmission Lines and Flexible Connectors

---

### Abstract

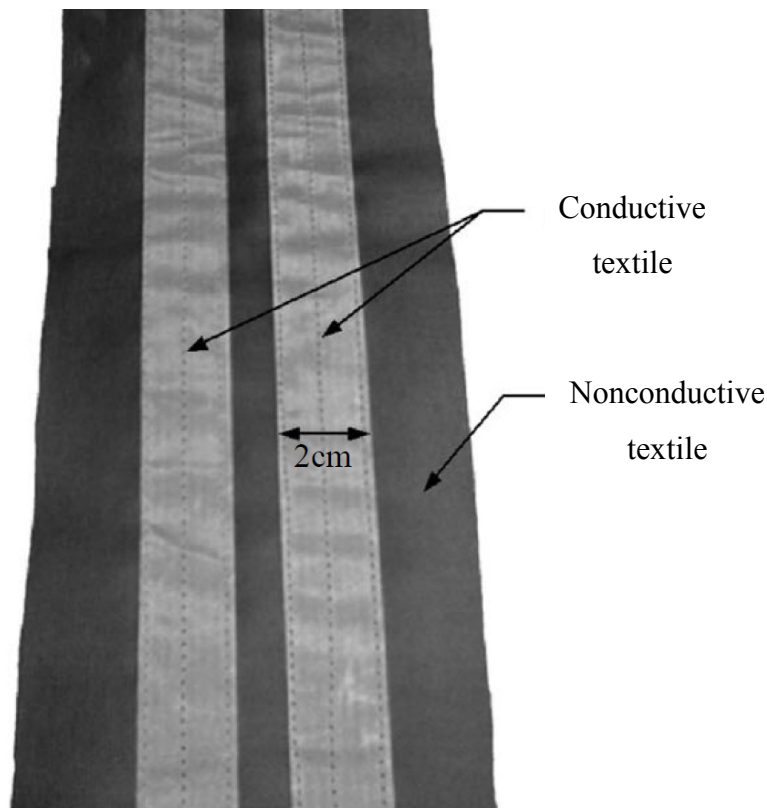
This chapter will discuss the effects of embroidery factors (i.e. stitch directions, stitch spacings and number of filaments) on embroidered transmission lines. Section 3.1.2 will represent the details of embroidered stitch directions and spacings. Measured DC resistance results of embroidered transmission lines with different embroidery factors will be shown in Section 3.1.3. A measurement system for repeatability and stabilisation will be shown in Section 3.1.4. Section 3.1.5 will represent the measured RF S-parameters results of the embroidered transmission lines. The optimal choice of conductive thread for RF electronics will be outlined in this chapter. Meanwhile, the feasibility of RF connectors made from hook and loop transmission lines will also be presented in Section 3.2. The conductive hook and loop connectors are detachable and reusable which is advantageous for wearable electronics applications. Improving both the DC and RF performance of hook and loop using electroplating will be shown in Section 3.2.4.

### 3.1 Embroidered Microstrip Transmission lines

#### 3.1.1 *Introduction*

In wearable applications, conductive textile can provide the functions of signal transmission but do not affect the users' comfort. Several authors have discussed

fabricating transmission lines by using conductive fabric materials [1]–[4]. The textile transmission lines can be made from conductive threads using embroidery, knitting, or twisting with normal yarns. Figure 3-1 shows the textile transmission lines in [1]. The transmission lines are made out of conductive ripstop fabrics and sewed onto a nonconductive textile substrate. This chapter mainly focus on embroidered transmission lines. State of the art embroidery technique reduces the manufacturing process such as cutting and sewing. Multifilament conductive threads are used for embroidering the textile transmission lines. The appropriate thread should have both good conductivity and mechanical strength.



**Figure 3-1 Textile transmission lines made out of conductive woven fabric  
(picture from [1])**

For high frequency applications the evaluation of conductive yarns are based on the transmission and reflection coefficients. The conduction loss and dielectric loss also have to be considered [5], [6]. The conduction loss depends on the conductivity of the

conductor and the frequency. The skin effect has to be considered at high frequency applications [7]. However the conductivity of commercial conductive fabrics are much lower than copper. Ouyang *et al.* reported some of the multifilament thread have effective conductivities approximately from  $1 \times 10^4$  S/m to  $5 \times 10^4$  S/m [8], [9]. Although the conductive textile has high resistivity and complex surface compared with metal, a good conductive fabric still can provide reliable RF performance [3]. The dielectric loss is influenced by the substrate height, dielectric constant, and dissipation factor. High conductive fabrics based on low loss soft materials with reasonable return loss have been reported by [10]–[13]. In addition, the multiple layered dielectrics are very common in wearable applications and the effective dielectric properties have to be taken into account in the design [14], [15]. Additionally, the environment such as humidity may also affect the characteristic of the fabric substrate materials [16]. It is important to consider the effect of humidity on fabric based RF system performance. The textile transmission lines and antennas will benefit from a waterproof protective layer.

Previous research showed that the weaving angles of woven conductive fabric influence the current distributions in the electro-textile [17], and the measured sheet resistances were varied with different directions on the anisotropic conductive fabrics [18]. Furthermore, Cottet *et al.* showed that the RF performance of fabric transmission lines made by woven fabric were affected by the fibre structure and line length [19].

In this chapter, the textile transmission lines were made using standard industrial computerised embroidery machines at Nottingham Trent University. To minimise the number of variables, the rigid substrate FR4 ( $\epsilon_r = 4.5$ , loss tangent = 0.019, 1.6 mm high) along with a solid copper ground plane were used for dielectric substrate. The characteristic impedance of the microstrip lines can be obtained from the width of the microstrip line  $W$ , the height of the substrate  $h$  and the effective dielectric constant  $\epsilon_e$ , see equations in [20]

$$Z_0 = \begin{cases} \frac{60}{\sqrt{\epsilon_e}} \ln \left( \frac{8h}{W} + \frac{W}{4h} \right) & \text{for } W/h \geq 1 \\ \frac{120\pi}{\sqrt{\epsilon_e} [W/h + 1.393 + 0.677 \ln(W/h + 1.444)]} & \text{for } W/h \leq 1 \end{cases} \quad (3.1)$$

$$\epsilon_e = \frac{\epsilon_r + 1}{2} + \frac{\epsilon_r - 1}{2} \frac{1}{\sqrt{1 + 12h/W}} \quad (3.2)$$

For a given characteristic impedance which is 50  $\Omega$  in this case, the width of the transmission line  $W$  can be calculated as in equation (3.3),

$$W = \begin{cases} \frac{8he^A}{e^{2A} - 2} & \text{for } W/h < 2 \\ \frac{2h}{\pi} \left[ B - 1 - \ln(2B - 1) + \frac{\epsilon_r - 1}{2\epsilon_r} \left\{ \ln(B - 1) + 0.39 - \frac{0.61}{\epsilon_r} \right\} \right] & \text{for } W/h > 2 \end{cases} \quad (3.3)$$

Where

$$A = \frac{Z_0}{60} \sqrt{\frac{\epsilon_r + 1}{2} + \frac{\epsilon_r - 1}{\epsilon_r + 1} \left( 0.23 + \frac{0.11}{\epsilon_r} \right)}$$

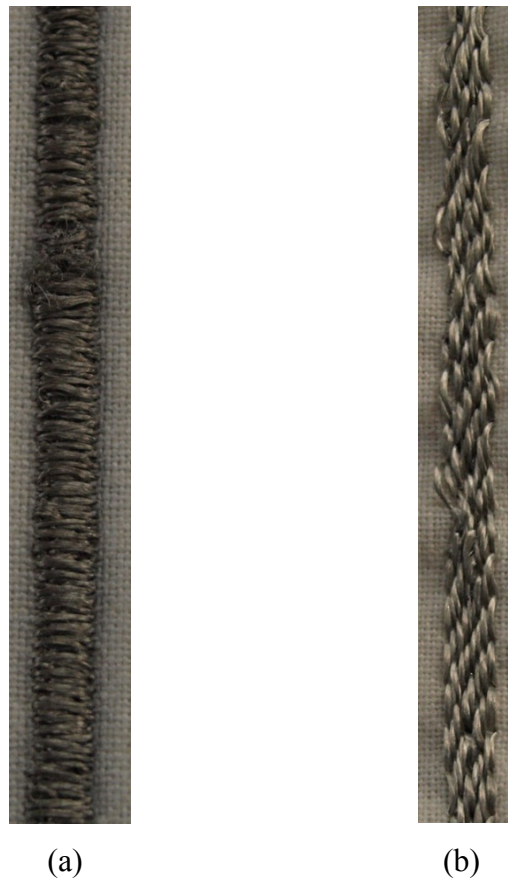
$$B = \frac{377\pi}{2Z_0\sqrt{\epsilon_r}}$$

From (3.3), the width of the microstrip lines is calculated as 3 mm with the 1.6 mm FR4 substrate.

### 3.1.2 Embroidered Stitches of Fabric Transmission Lines

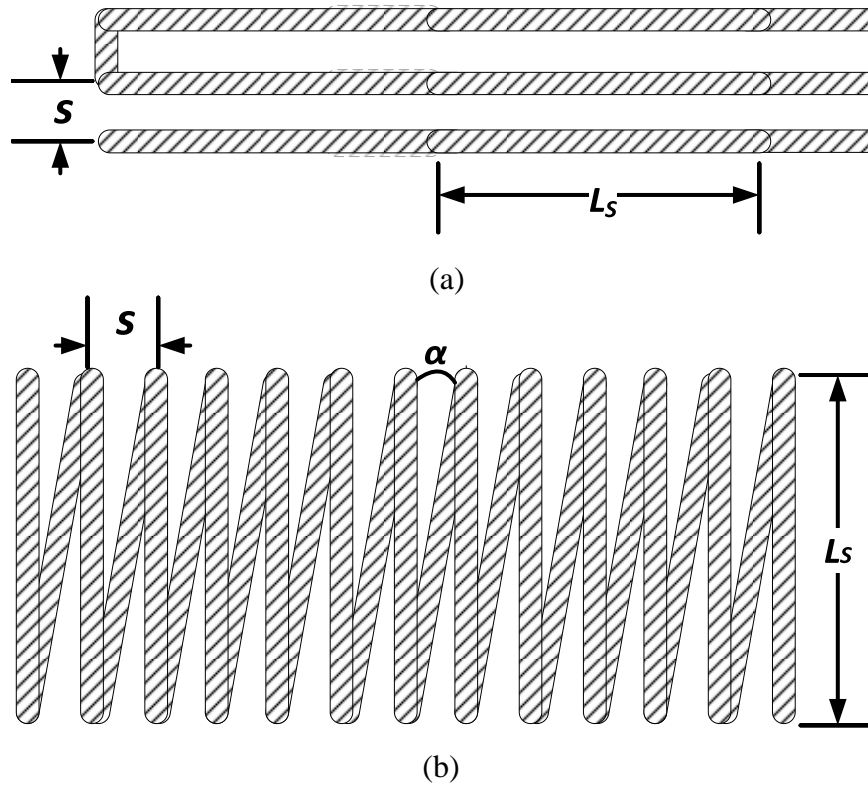
As was mentioned in Chapter 2, there are several types of stitch that can be chosen for embroidering fabric based electrical patterns. Satin stitch and running stitch were used to embroider the transmission lines in this chapter. The stitch direction can be either perpendicular or parallel to the line direction. Figure 3-2 shows the two stitch directions. The transmission line with perpendicular stitch direction is embroidered by the Satin stitch, whilst the line with parallel stitch direction is embroidered by running stitch. A comparison will be analysed to evaluate the performance of different stitch directions for embroidering transmission lines.





**Figure 3-2** Stitch directions of embroidered transmission lines: (a) perpendicular and (b) parallel

The stitch spacing indicates the distance between two parallel stitches, usually in millimetres. The stitch spacings  $s$  and stitch length  $L_s$  of perpendicular and parallel stitches are shown in Figure 3-3. The adjacent stitches may connect with each other via the loose fibres if the stitches are close enough. Larger stitch spacings require less thread but the connection between neighbouring stitches will be poorer. The embroidered transmission lines in this chapter are made by using stitch spacings of 0.4 mm and 0.8 mm.



**Figure 3-3** Stitch spacings of (a) parallel stitch and (b) perpendicular stitch

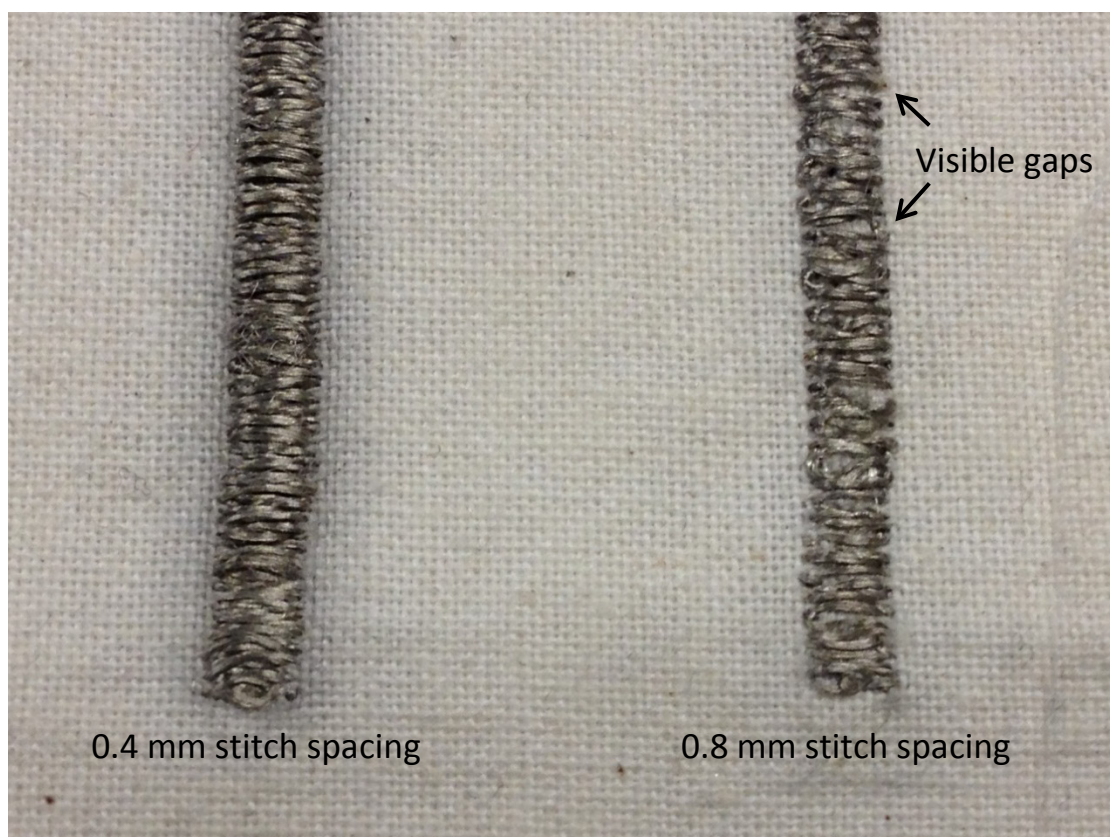
The total length of used thread depends on the stitch length  $L_s$  and the stitch spacing  $s$ . For very close stitch spacing,  $\alpha$  is approximately  $0^\circ$  thus  $\cos \alpha = 1$ . As the stitch length equals to the width of the transmission line (see Figure 3-2), the number of the stitches  $N$  can be obtained by

$$\text{Parallel stitch} \quad N_{parallel} = \left\lceil \frac{L}{L_s} \right\rceil \cdot \left( \left\lceil \frac{L_s}{s} \right\rceil + 1 \right) \quad (3.4)$$

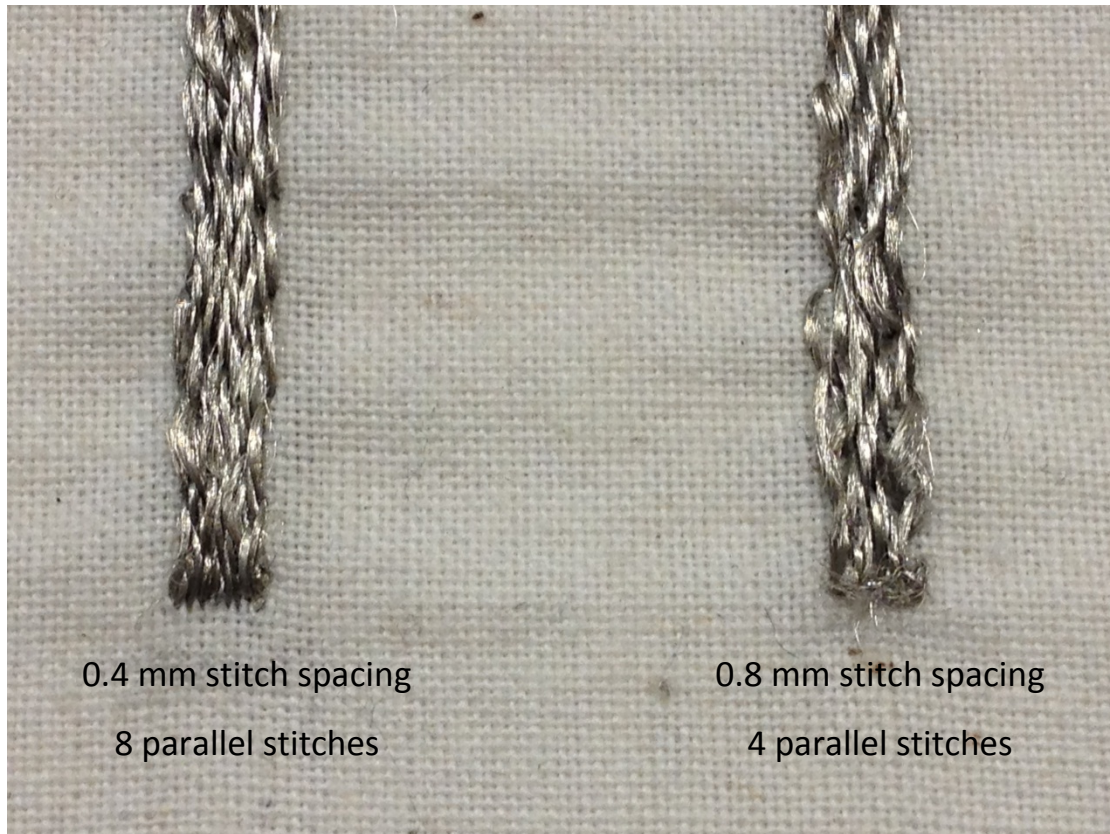
$$\text{Perpendicular stitch} \quad N_{perpendicular} = 2 \left\lceil \frac{L}{s} \right\rceil + 1 \quad (3.5)$$

Where  $L$  is the length of the transmission line. A 3 mm wide 100 mm long transmission line with 0.4 mm stitch spacing requires 272 parallel embroidered stitches or 501 perpendicular embroidered stitches. If the stitch spacing equals to 0.8 mm, this transmission line needs 136 parallel stitches or 251 perpendicular stitches. Therefore, perpendicular stitch directions require more stitches and have longer thread, which means higher material costs.

The zoomed in details of the transmission lines are shown in Figure 3-4 and Figure 3-5. As is shown by Figure 3-4, some visible gaps in between the adjacent stitches can be observed on the 0.8 mm spacing perpendicular stitched transmission line. These gaps are related to the stitch spacing but it is difficult to quantify the gaps when the stitch spacing is small. It can be seen in Figure 3-5 that the 0.4 mm stitch spacing parallel transmission line has 8 parallel stitches whilst 0.8 mm stitch spacing parallel transmission line has 4 parallel stitches.



**Figure 3-4 Zoomed in view of 3 mm wide perpendicular transmission lines with different stitch spacings**



**Figure 3-5 Zoomed in view of 3 mm wide parallel transmission lines with different stitch spacings**

### ***3.1.3 DC Resistance of Embroidered Transmission Lines***

Three materials were used to make the fabric transmission lines: i) Amberstrand<sup>®</sup> Copper 66; ii) Amberstrand<sup>®</sup> Nickel 166; and iii) Liberator<sup>®</sup> Silver 40. These materials are manufactured by Syscom Advanced Materials [21]. The figures in the names indicate the number of filaments that each thread contains. Their names indicate the main consist of conductive material (i.e. copper, nickel or silver) in the coated layer on the filaments. Parallel and perpendicular stitch directions were applied with different stitch spacings. The DC resistances of the 10 mm long and 3 mm wide transmission lines were measured and the results are shown in Table 3-1.

**Table 3-1 DC resistance of single thread and embroidered transmission lines**

Thread	Resistivity for the coated material ( $\Omega \cdot m$ )	DC resistance of 100 mm single thread ( $\Omega$ )	Stitch direction \backslash Stitch spacing	DC resistance of transmission line ( $\Omega$ )	
				0.4 mm	0.8 mm
Liberator Silver 40	Silver, $1.59 \times 10^{-8}$	4.3	Perpendicular	8.8	23.8
			Parallel	0.6	1.1
Amberstrand Copper 66	Copper, $1.68 \times 10^{-8}$	0.8	Perpendicular	5.5	6.6
			Parallel	0.2	0.3
Amberstrand Nickel 166	Nickel, $6.99 \times 10^{-8}$	0.3	Perpendicular	0.3	1.0
			Parallel	0.1	0.2

### I. Stitch direction

First of all, it is clear that in all cases the parallel embroidered transmission lines have lower DC resistance than the same stitch spacing perpendicular lines. This shows that lower surface resistance can be obtained when the stitch direction is parallel with the direction of the line. The stitch direction is a more important parameter than the stitch spacing.

### II. Number of filaments

Table 3-1 indicates that a thread that contains more filaments has a lower resistance. The Amberstrand Nickel 166 thread is composed of 166 fibres and has the lowest DC resistance. The resistance of Liberator Silver 40 is the highest and it has the least filaments (40), even though ‘nickel’ is the worst conductor of the three and ‘silver’ is the best conductor. The same conclusion was also true with transmission lines, i.e.

lines made by using threads with larger numbers of filaments with the same stitch direction or stitch spacing have lower DC resistances.

It is to be noticed that the resistance of the 0.4 mm spacing perpendicular Amberstrand Nickel 166 transmission line is approximately equal to the resistance of single thread of the same material. Therefore, large numbers of filaments with small stitch spacing can reduce the total series contact resistance to equal to the resistance of single thread.

### III. Stitch spacing

Secondly, resistances of parallel stitches are smaller than the single thread regardless of stitch spacings. Moreover the DC resistances of the 0.8 mm spacing parallel lines are approximately twice of the 0.4 mm parallel lines. For instance, the resistance of Liberator Silver with 0.4 mm stitch spacing in the parallel direction is 0.6  $\Omega$  and the resistance of the same material and stitch direction but 0.8 mm spacing is 1.1  $\Omega$ . Consequently the equivalent circuit of the parallel stitched line is a parallel circuit and the resistance of the circuit is approximately doubled when the number of current paths are halved (i.e. stitch spacing is doubled).

The electrical equivalent model of transmission line with parallel stitches is shown in Figure 3-6, where  $R_s$  indicates the resistance of each single stitch and it is determined by each single stitch length.  $R_c$  represents the contact resistance between two adjacent stitches and it is determined by the stitch spacing. It is worth noting that the  $R_s$  values are not all identical due to the stitch tension and embroidery accuracy. This is also true with  $R_c$ . However, the difference between  $R_s$  is very small and can be neglected. Therefore it can be assumed that the value of  $R_s$  is constant. Moreover, the influence of  $R_c$  is negligible for this parallel circuit as the major current follows the direction of the stitches. The total resistance of the transmission line  $R_{total}$  can be approximately determined by (3.6).

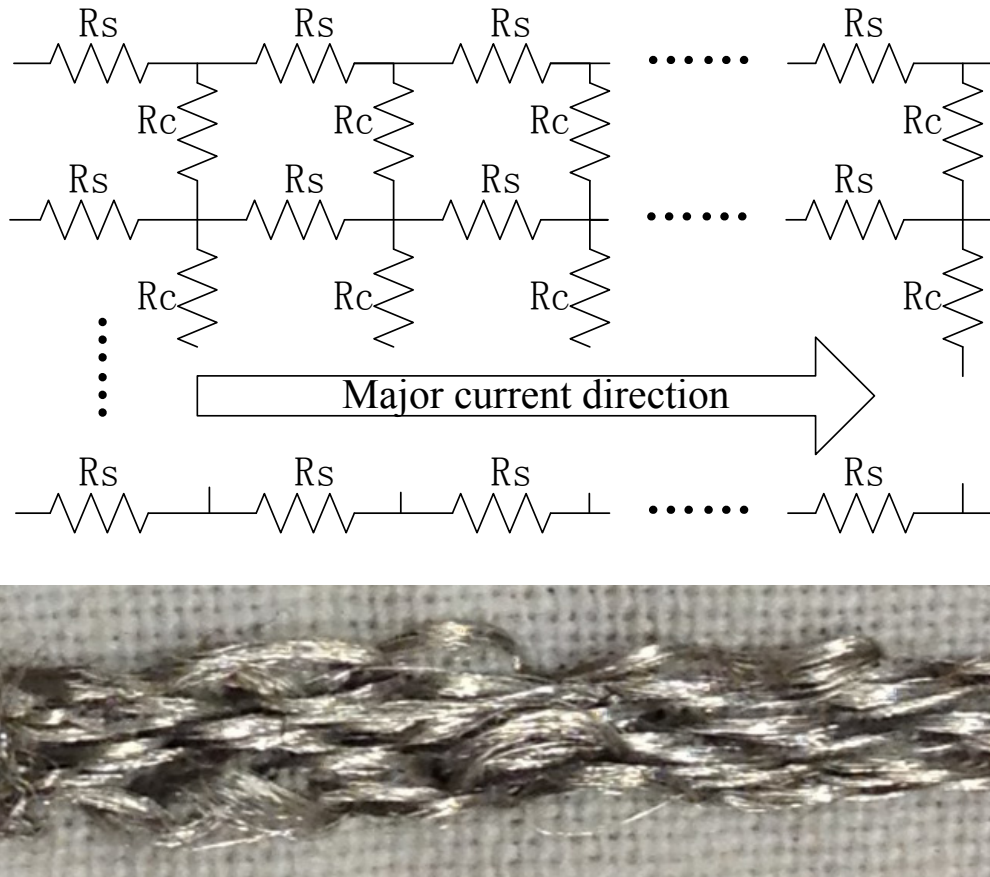


$$R_{total} = \frac{1}{n} \left[ \frac{L}{L_s} \right] R_s \quad (3.6)$$

and  $n$  means the number of parallel stitches.  $n$  can be obtained by (3.7)

$$n = \frac{W}{s} \quad (3.7)$$

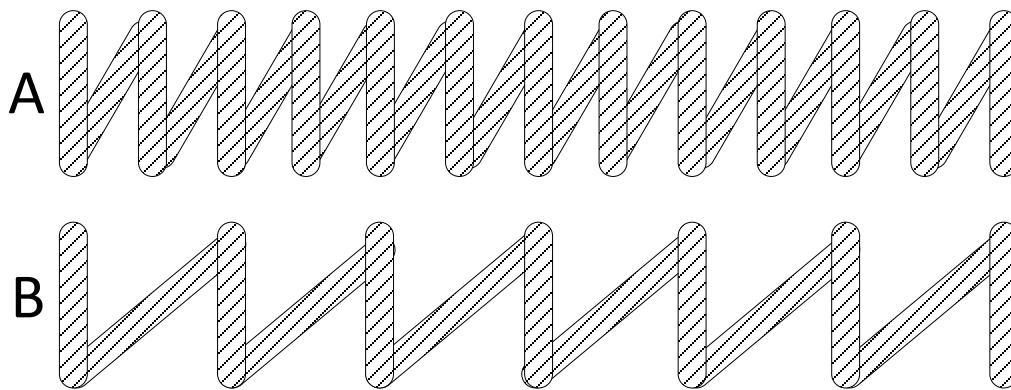
where  $W$  is the width of the transmission line and  $s$  is the stitch spacing.



**Figure 3-6 Equivalent electrical model of parallel stitched transmission line and zoomed in view**

On the other hand, all the perpendicular stitches (apart from 0.4 mm spacing Amberstrand Nickel 166) have higher resistance than the single thread. This indicates that i) either the current mainly travels along the stitches in a zigzag route which is much longer than the length of the transmission line and therefore has a larger resistance; ii) or the major current crosses over the gap between the adjacent stitches via the connected fibres and  $R_c$  is larger than  $R_s$ . If the major current component

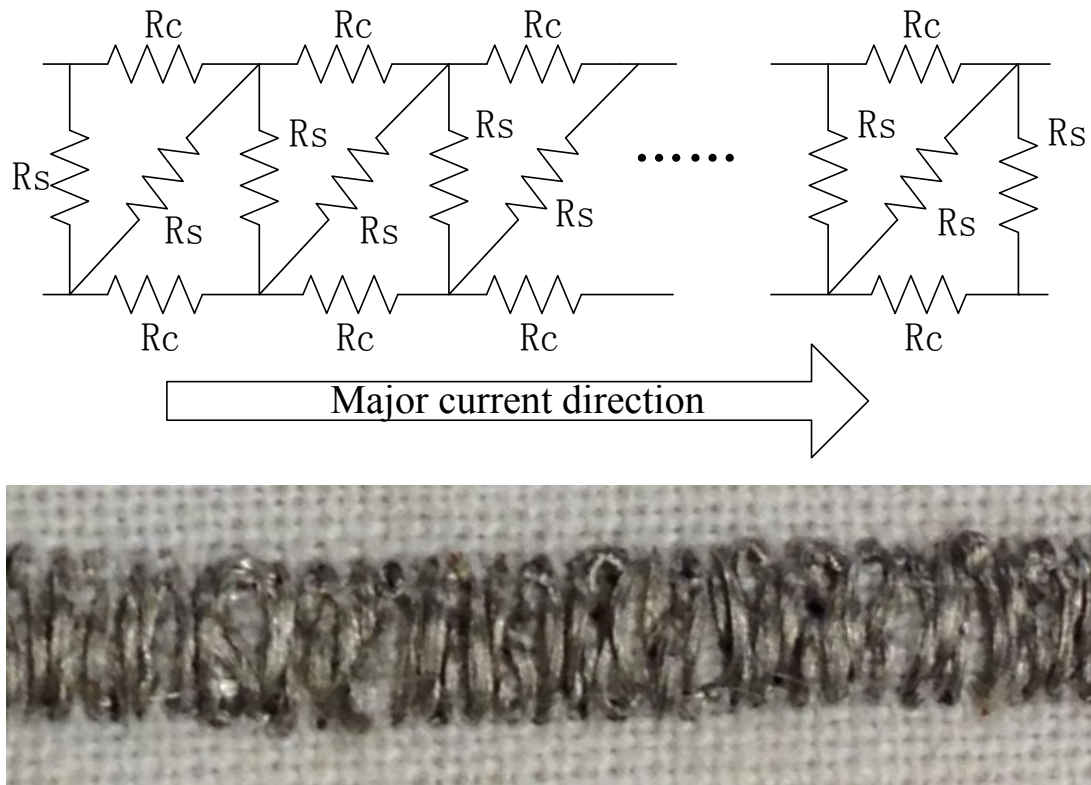
travels via the zigzag path, the resistance of larger stitch spacing lines should be less than the closer stitch spacing lines because the wider stitch spacing lines has a shorter total length of thread (see Figure 3-7, Zigzag line B has a shorter total length and is supposed to have smaller total resistance than A). However, Table 3-1 shows that lines with greater stitch spacings have higher DC resistances, particularly for Liberator Silver 40 and Amberstrand Nickel 166. The resistances of the transmission lines of these two materials with perpendicular stitch are increased by three times when stitch spacings are doubled. This indicates that the main current does not follow along the zigzag trace but crosses over neighbouring stitches.



**Figure 3-7 Sketches of perpendicular stitch direction transmission lines with different stitch spacing**

The equivalent electrical model of the transmission line with perpendicular stitches is shown in Figure 3-8. The resistance of perpendicularly stitched transmission line is determined by the contact resistance  $R_c$ , as embroidered transmission lines with smaller stitch spacings have lower resistances. Large stitch spacings lead to poor connection between stitches and increase  $R_c$ , also high chance result in disconnection between adjacent stitches (see Figure 3-4 and Figure 3-8).





**Figure 3-8 Equivalent electrical model of perpendicular stitched transmission line and zoomed in view**

Assuming all the stitches contact each other by consistent  $R_c$ , and every  $R_s$  is equal, the  $R_{total}$  can be determined by (3.8)

$$R_{total} = \frac{(N-1)(N-2)R_c R_s}{(N-1)R_c + 4(N-2)R_s} \quad (3.8)$$

Where  $N$  is the total number of stitches and it varies inversely with the stitch spacing.

In conclusion, the desired embroidery parameters for fabric transmission lines, listed in order of importance for minimising the DC resistance, are i) parallel stitch direction; ii) higher number of fibres within a single thread; and iii) smaller stitch spacings.

### 3.1.4 RF Measurement Setup for Embroidered Transmission Lines

The embroidered transmission lines were placed on the 1.6 mm rigid FR4 substrate ( $\epsilon_r = 4.5$ , loss tangent = 0.019) with a solid copper ground plane to minimise the variations. Two SubMiniature version A (SMA) connectors were contacted to the ends of the fabric transmission line by applying pressure to achieve a good connection. Soldering was not used to avoid the damage the fabric samples. This test jig eliminates the wrinkles of the fabric and flattens the surface which provides stability for the measurement. The SMAs were connected to the vector network analyser for S-parameter measurements. The measurement setup and test jig are shown in Figure 3-9.

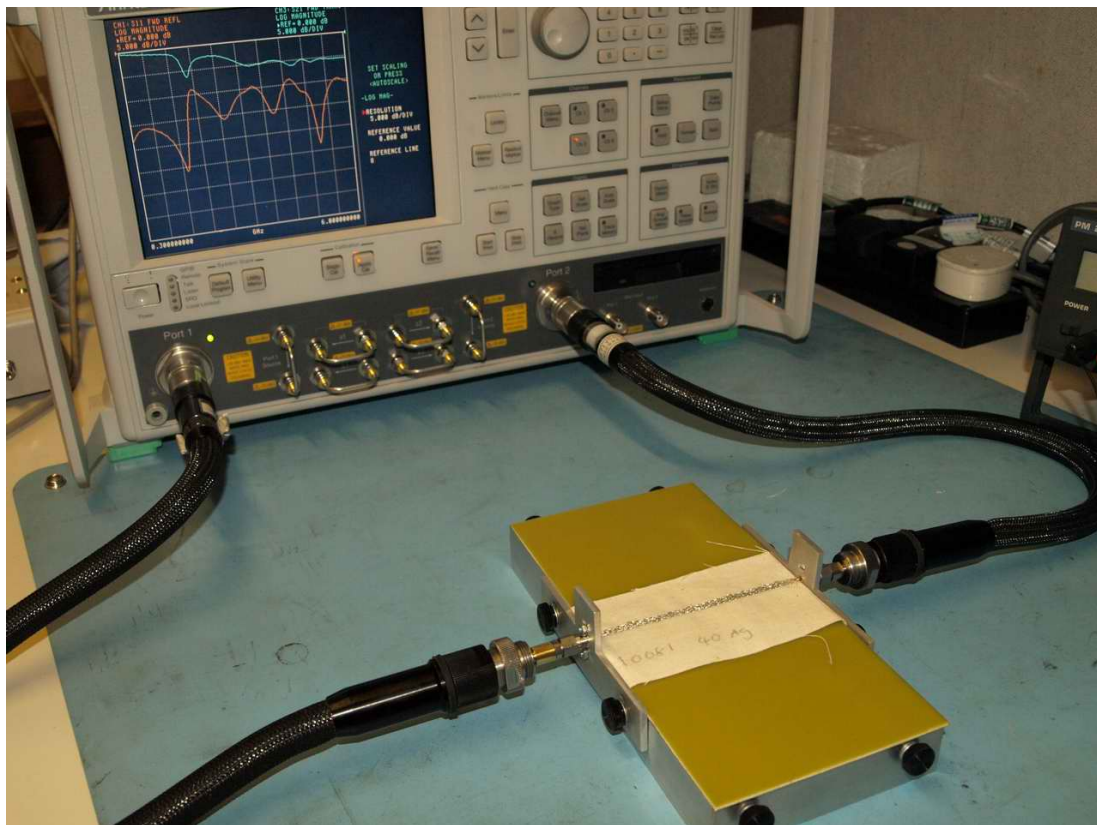
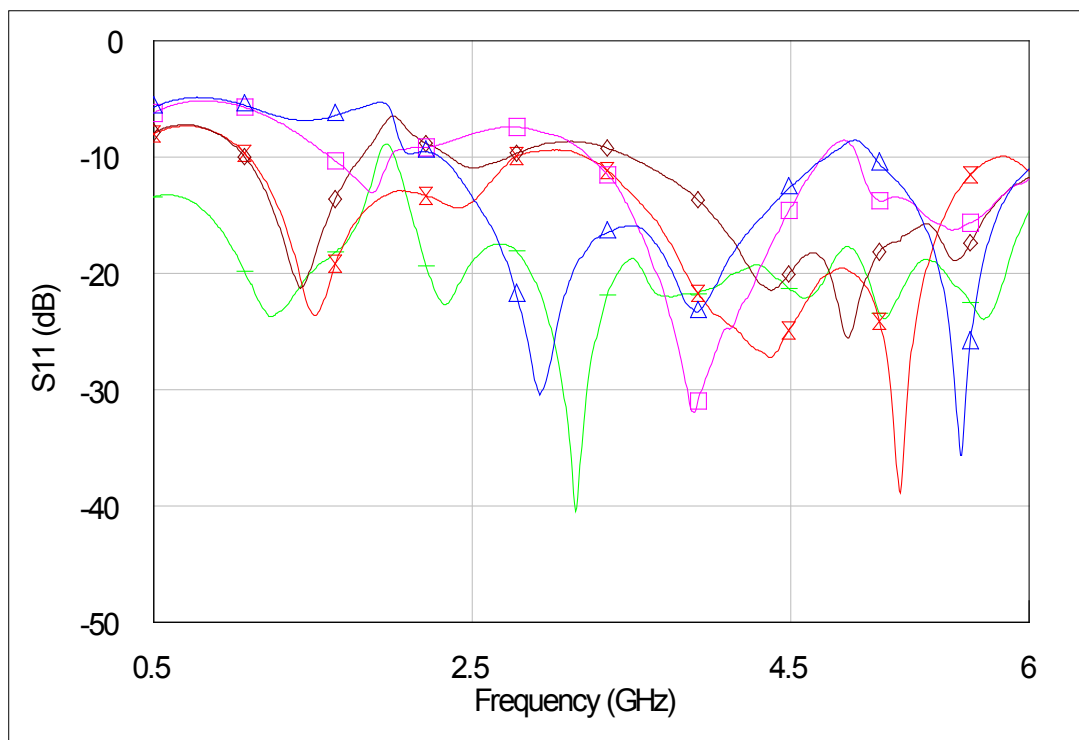


Figure 3-9 Test jig used for embroidered transmission line measurements

Repeatability is important to evaluate the performance of the fabric transmission lines. To test that, five repeated measurements were made with the Amberstrand Copper 66. Initially, the probes of the SMA connectors were directly contacted to the thread, see Figure 3-10 (a). The measured S11 results are shown in Figure 3-10 (b). It can be seen that the repeatability was poor. The connection between probes and the fabric transmission lines was easily changed due to the softness of fabric fibres. It was hypothesised that flattened probes with an enlarged contacting area would improve the repeatability. A small piece of 3 mm wide copper patch was soldered onto the probe of the SMA connectors, see Figure 3-11 (a). This small patch increases contacting area between the probe and the fabric transmission line. Figure 3-11 (b) shows five repeated S11 measurements using the enlarged contact area connectors. The results indicate the improvement in the repeatability of the measurement jig.



(a)



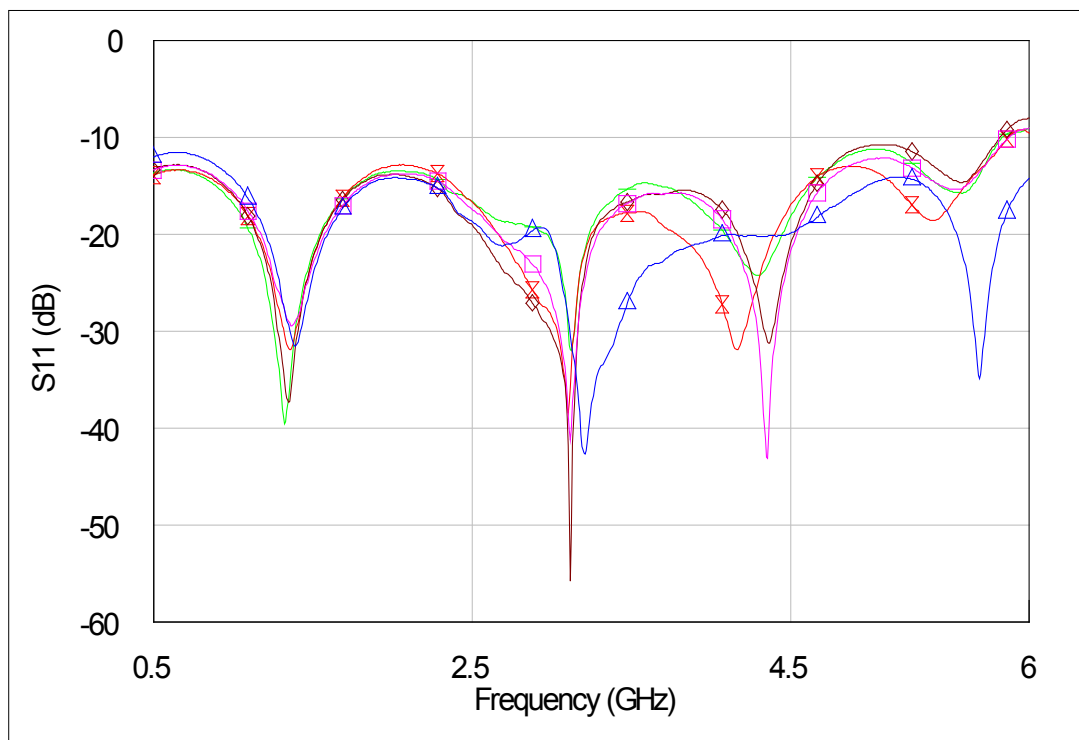
(b)

**Figure 3-10 (a) Zoomed in view of SMA probe pressed down onto the embroidered transmission line**

**(b) Five repeated S11 measurements of the same line**



(a)



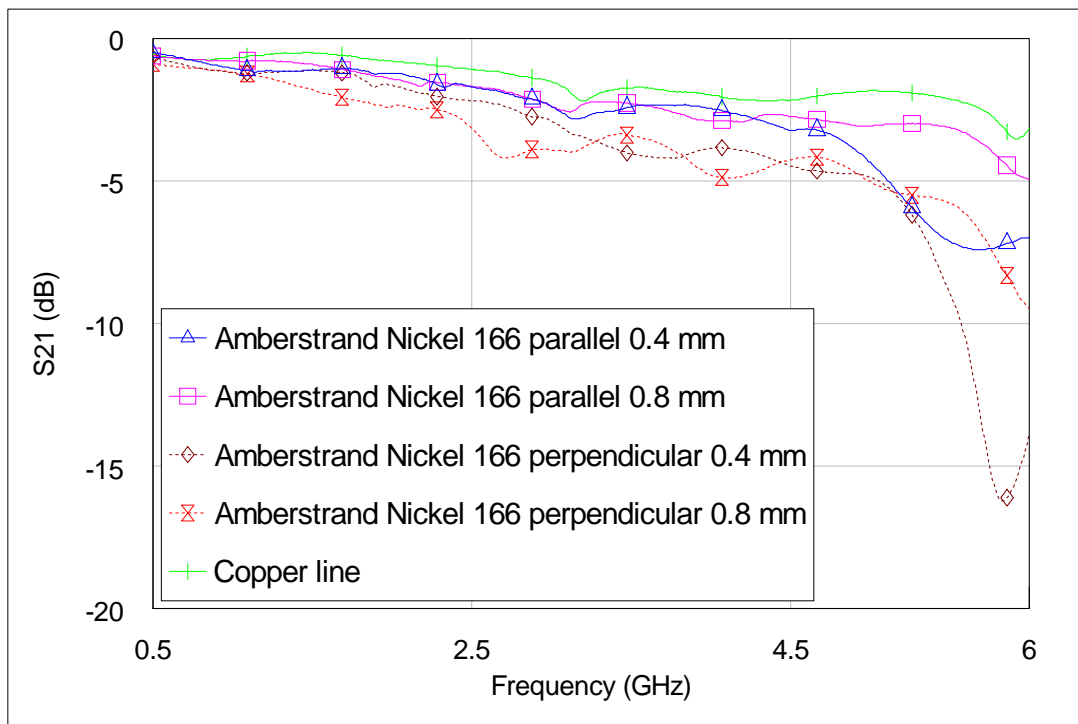
(b)

**Figure 3-11 (a) Zoomed in view of enlarged contacting area probe pressed down onto the embroidered transmission line**

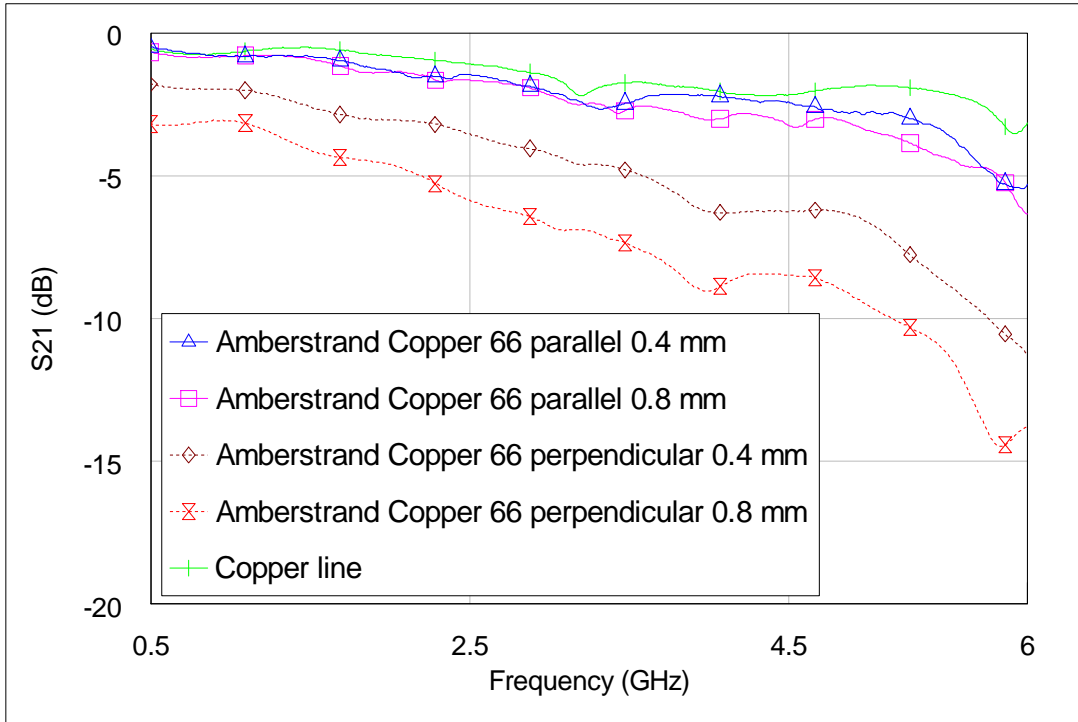
**(b) Five repeated S11 measurements of the same line**

### 3.1.5 RF Performance of Embroidered Transmission Lines

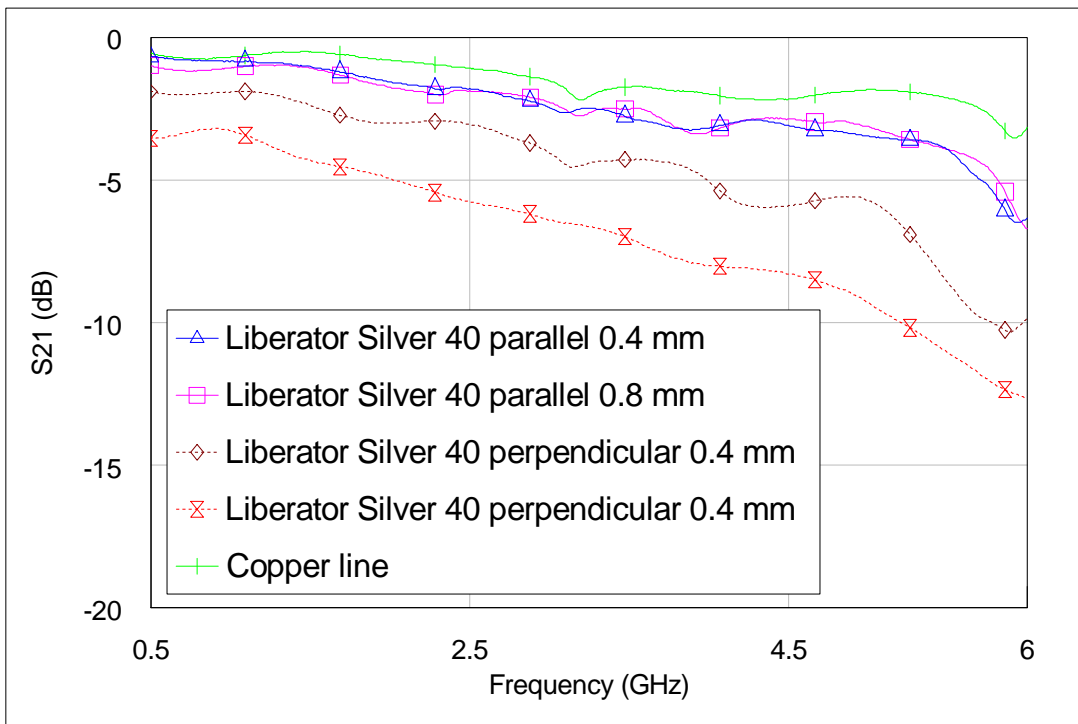
Embroidered transmission lines made from different conductive threads with different stitch spacings and directions were tested using the measurement jig in Section 3.1.4. Insertion losses were measured to evaluate the RF performance of these fabric transmission lines. A copper foil made microstrip line with the same dimensions was placed on the same FR4 substrate with the same base fabric (cotton) in between as a comparison. Figure 3-12 to Figure 3-14 show the measured S21 results of the embroidered transmission lines.



**Figure 3-12 S21 of Amberstrand Nickel 166 transmission lines with different stitch directions and spacings**



**Figure 3-13 S21 of Amberstrand Copper 66 transmission lines with different stitch directions and spacings**



**Figure 3-14 S21 of Liberator Silver 40 transmission lines with different stitch directions and spacings**

### I. Stitch direction

All the parallel stitched lines have better S21 values than the perpendicular stitch lines regardless of stitch spacing, this can be seen from Figure 3-12 to Figure 3-14. The difference of S21 between parallel embroidered lines and copper line is less than 1 dB up to 5 GHz (or up to 4.5 GHz with Liberator). Thus parallel stitches are preferable due to the low insertion loss. More precisely, approximately 2 dB insertion loss are observed by all the parallel stitched lines up to 2.5 GHz, and around 5-6 dB of insertion loss are obtained at 6 GHz. It is worth noting that the insertion losses of different stitch spacings for the parallel lines are very similar, i.e. less than 1 dB difference for all the threads below 4.7 GHz.

### II. Stitch spacing

The variation of S21 of the perpendicular stitched lines with different stitch spacings is more significant than the parallel stitched lines. For the same thread, perpendicular stitched transmission lines with 0.4 mm stitch spacings have lower insertion loss (apart from Amberstrand Nickel 166, lower insertion loss is true up to 2.8 GHz). This is expected as the closer stitch spacing lines have lower DC resistances which results in lower conduction loss.

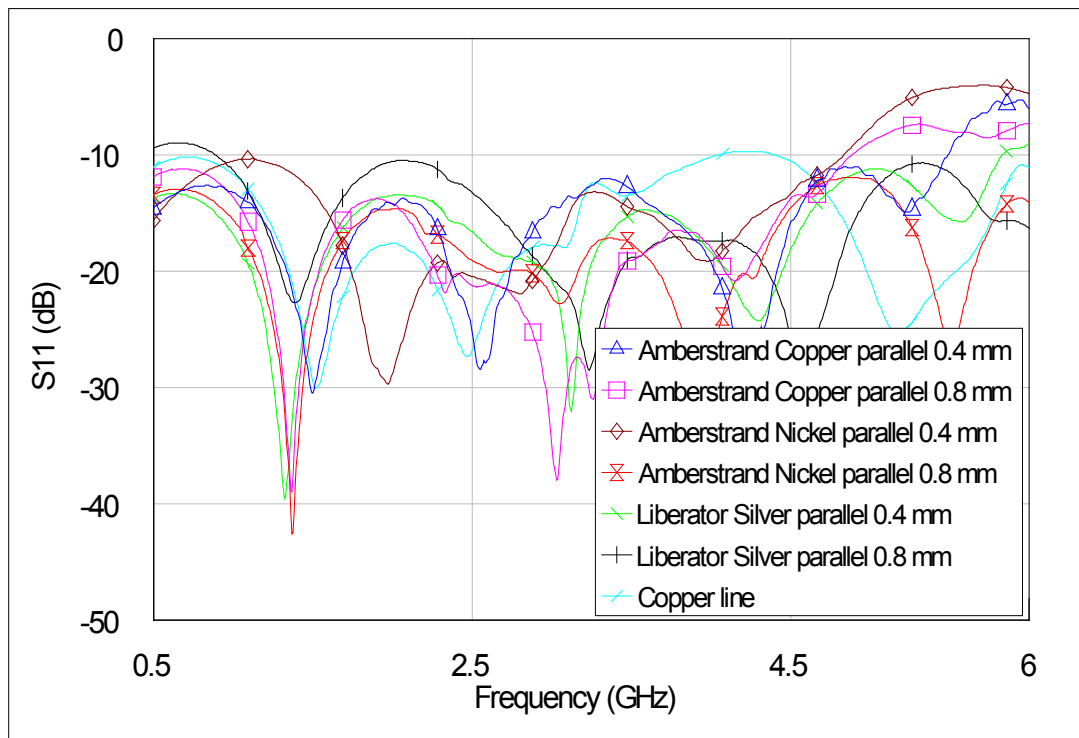
### III. Number of filaments

The difference between the Amberstrand Nickel 166 perpendicular 0.4 mm stitch spacing and 0.8 mm stitch spacing is shown in Figure 3-12. Compared with other two threads with perpendicular stitch direction, the difference between Amberstrand Nickel 166 perpendicular 0.4 mm spacing and 0.8 mm spacing is smaller. It is less than 1 dB up to 5 GHz. Meanwhile when the frequency is lower than 2.8 GHz, the difference of S21 between Amberstrand Nickel 166 perpendicular 0.4 mm spacing and parallel 0.4mm spacing is less than 1 dB. The insertion losses of the same stitch spacing perpendicular Amberstrand Copper 66 (shown in Figure 3-13) and Liberator-Silver-40 (shown in Figure 3-14) are very similar, but they are larger than the

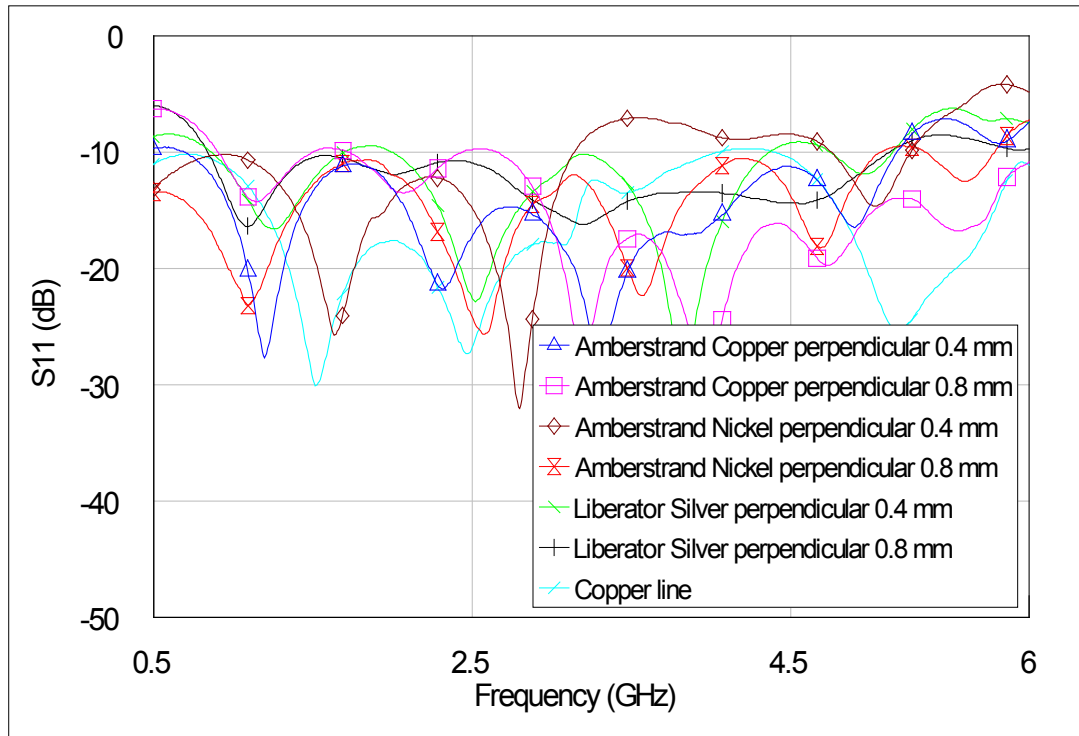


insertion losses of Amberstrand Nickel 166 perpendicular lines. Therefore, threads with larger number of filaments can improve the insertion loss of perpendicular stitched transmission lines.

Measured S11 results of parallel and perpendicular direction transmission lines are shown in Figure 3-15 and Figure 3-16 respectively. Both stitch directions give reasonable S11 results and this indicates that the reduced S21 is due to the losses along the line.



**Figure 3-15 S11 of embroidered transmission lines with parallel stitch direction**



**Figure 3-16 S11 of embroidered transmission lines with perpendicular stitch direction**

The DC and RF results of embroidered transmission lines indicate that higher DC resistance of the transmission line results in higher insertion losses. The impacts on the DC resistance and insertion loss of the fabric transmission lines, in order of importance for RF performance are: i) stitch direction; ii) number of filaments; and iii) stitch spacing.

## 3.2 Hook and Loop Connectors

### 3.2.1 Introduction

A major issue of most wearable applications is connecting the standard electronic circuit to the fabric antenna. A rigid socket in the cloth will affect users' activities and

comfort. Using a flexible connector and the transmission lines will be the optimal solution for certain applications. Hook and loop is largely used in clothing industry as the fastener instead of laces, zips, or buttons. The zoomed in views of the loop and the hook strip are shown in Figure 3-17 and Figure 3-18 respectively. Usually the loop has a large number of flexible and randomly orientated fibres whilst the hook has uniform rigid upside down ‘fishhooks’ in alignment. After being pressed together, the hook catches the fibres on the loop. The hook and loop can be made from conductive materials and form a flexible electric connector [22]. Patents have been filed to use conductive hook and loop for providing flexible electrical connections [23]–[25]. Some authors have addressed the problem of commercial reusable connections for low frequency control signals [26], [27]. In this work, conductive hook and loop will be examined as a connection mechanism for high frequency applications [28]. This hook and loop connector is detachable which allows the antennas or electronics to be reused, washed or replaced.



**Figure 3-17** Zoomed in view of loop strip



**Figure 3-18 Zoomed in view of hook strip**

### ***3.2.2 DC Resistance of Hook and Loop***

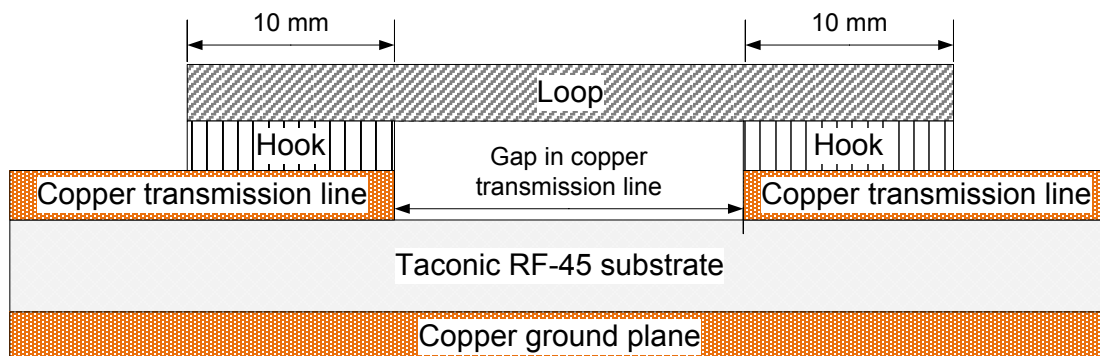
The DC resistances of 5 cm long and 1.6 cm wide hook and loop strips were measured. The results are shown in Table 3-2. The resistance of the back side of hook is the lowest and the hook side is slightly higher. The resistances of hook strips are lower than the loop. After been pressing the loop and hook together, the resistance of the ‘middle’ is measured by inserting the probe of the meter into the middle of the connected hook and loop, the resistance is similar as the reverse side of hook.

**Table 3-2 DC resistance of 5 cm long and 1.6 cm wide hook and loop strip**

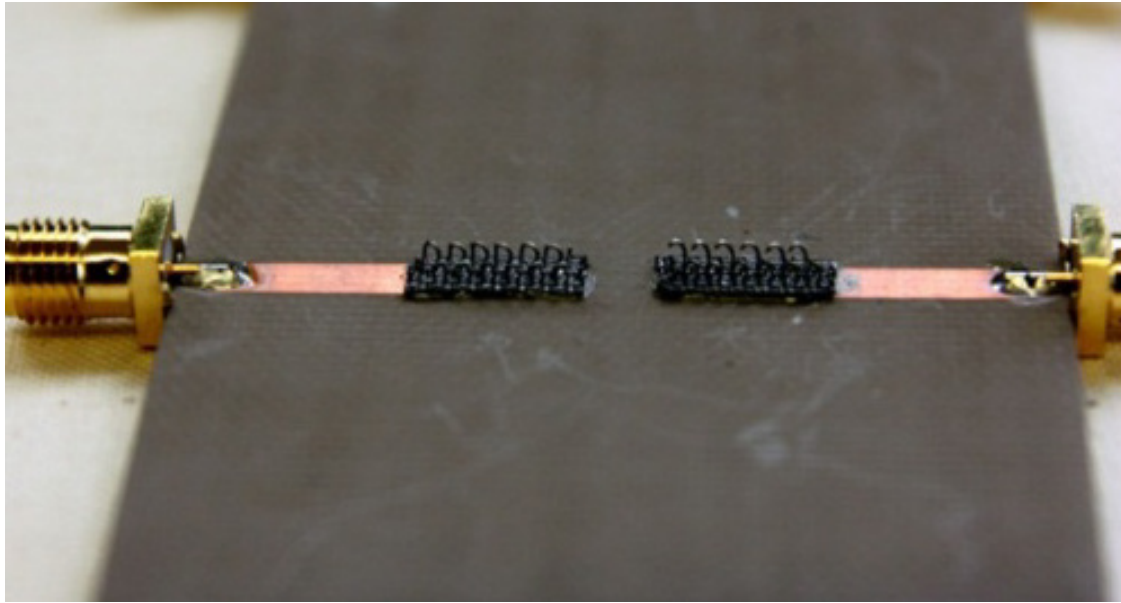
	Individual strip				When pressed together		
	Loop	Hook	Back of loop	Back of hook	Back of loop	Back of hook	Middle
DC resistance in $\Omega$	1.13	0.52	1.78	0.50	1.76	0.50	0.54

### 3.2.3 RF Performance of Hook and Loop Connectors

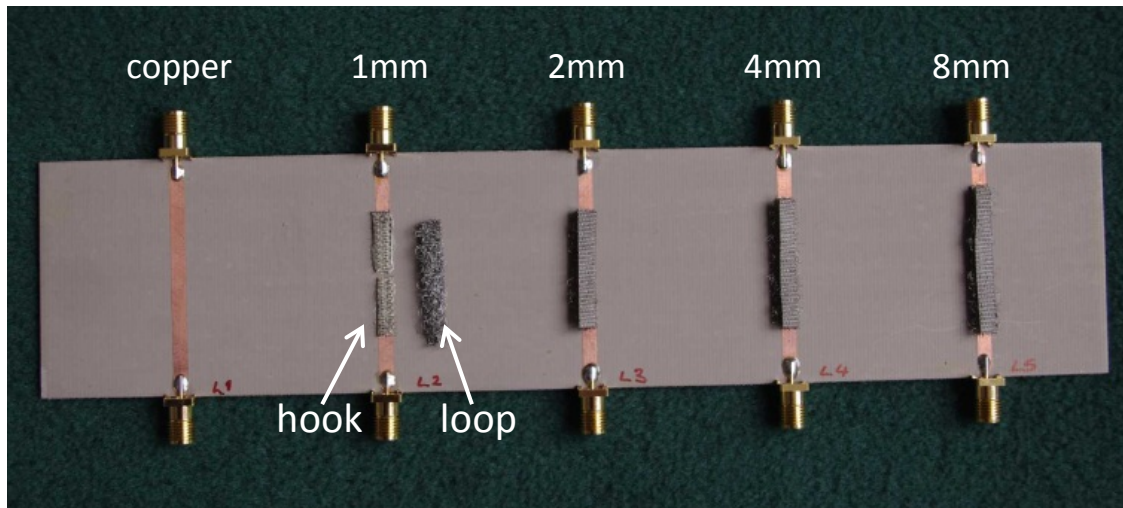
Five 3 mm × 50 mm printed transmission lines were made on the 1.57 mm high low loss substrate Taconic RF-45 ( $\epsilon_r = 4.5$  and  $\tan\delta = 0.0037$ ). All the lines are designed to be approximately 50  $\Omega$ . One of transmission lines was a continuous copper line and the rest had a gap divided every transmission line into two parts. The cross section of each gapped transmission line is shown in Figure 3-19. The test jig is shown in Figure 3-20. On top of the gapped microstrip lines there are two 10 mm long and 3 mm wide hook strips (see the zoomed in view in Figure 3-20) affixed to the microstrip using a conductive epoxy. The loop component was used to bridge the gap. A continuous copper line without gap was used as a comparison. The measurements demonstrated the insertion loss in the loop section and the interconnection between the two component parts that made the assessment of the ‘switch’ with two contacts. The envisaged connectors can be sewed onto transmission lines using conductive yarn in the production process.



**Figure 3-19 Sketch of the cross section of hook and loop connector on gapped transmission line**



(a)



(b)

**Figure 3-20 (a) Zoomed in view of gapped transmission line with hook attached  
(b) After loop strips are placed across the gap, figures indicate sizes of the gaps in transmission lines**

The measured  $S_{11}$  and  $S_{21}$  results are shown in Figure 3-21 and Figure 3-22 respectively. The results show that below 2 GHz, the  $S_{11}$  results of with the hook and loop transmission lines are almost identical. The  $S_{11}$  values are approximately 10 dB worse than the continuous copper line. The  $S_{21}$  values of the hook and loop transmission lines are approximately -2dB when the frequency is below 2 GHz. The insertion loss is increased with larger gap sizes. It is to be noted that the number of

transitions between the hook and the loop is twice that envisaged in the final application as a connector between traditional electronics and a fabric system.

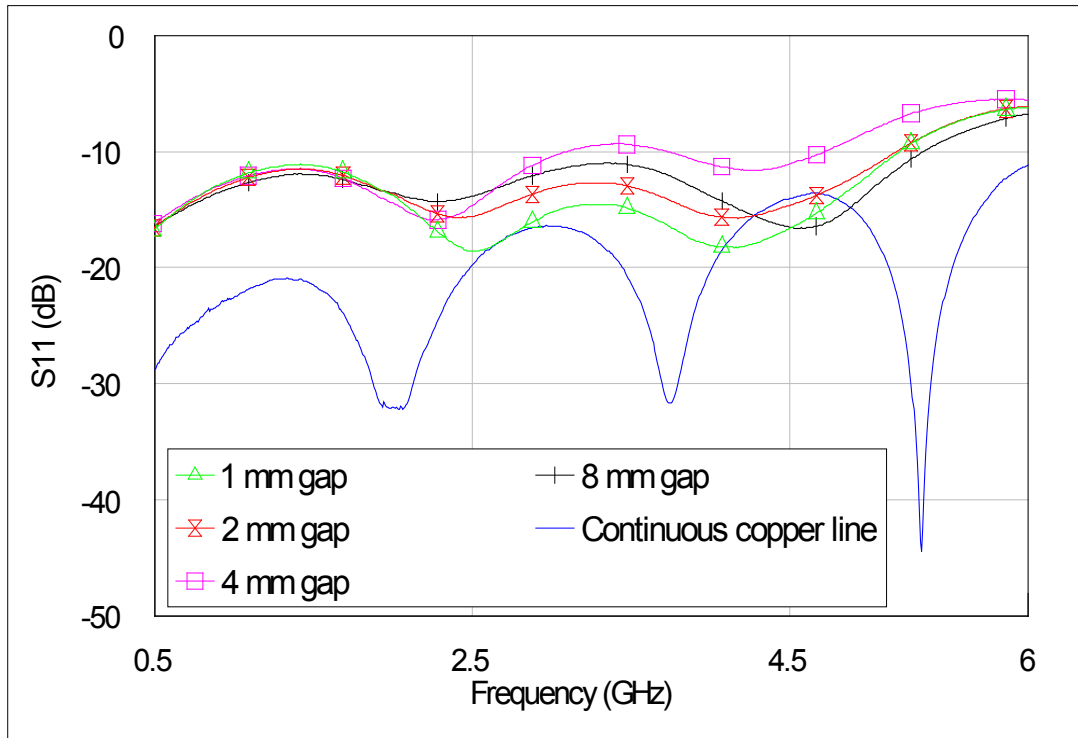


Figure 3-21  $S_{11}$  of hook and loop 'switches'

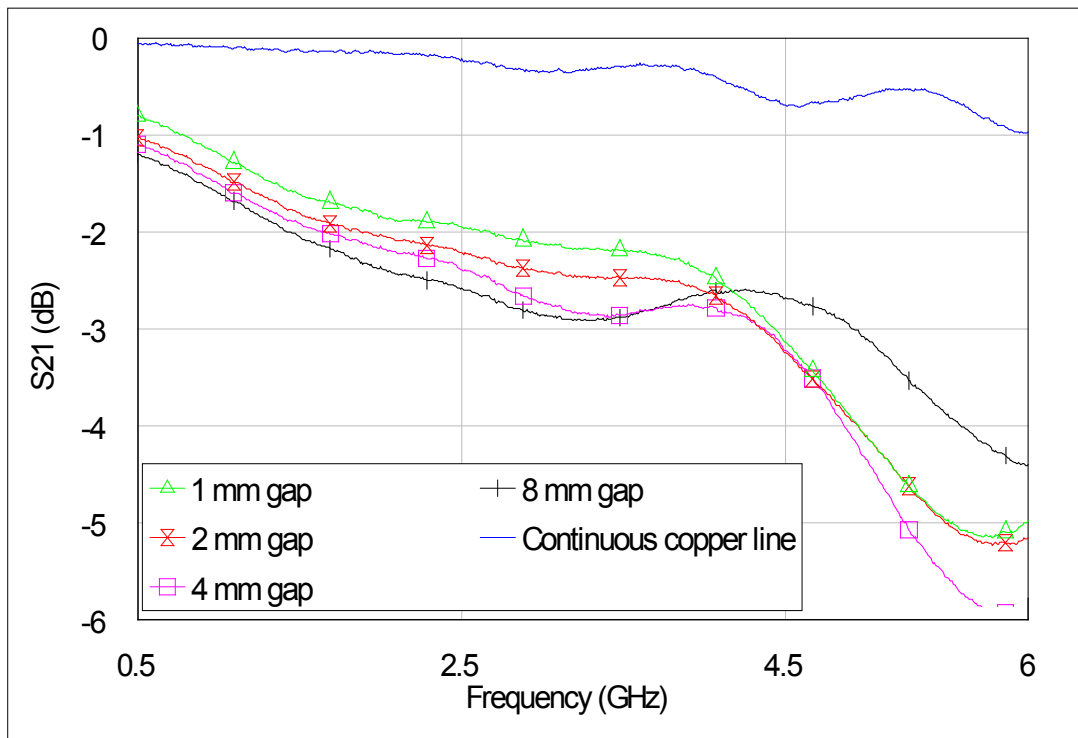


Figure 3-22  $S_{21}$  of hook and loop 'switches'



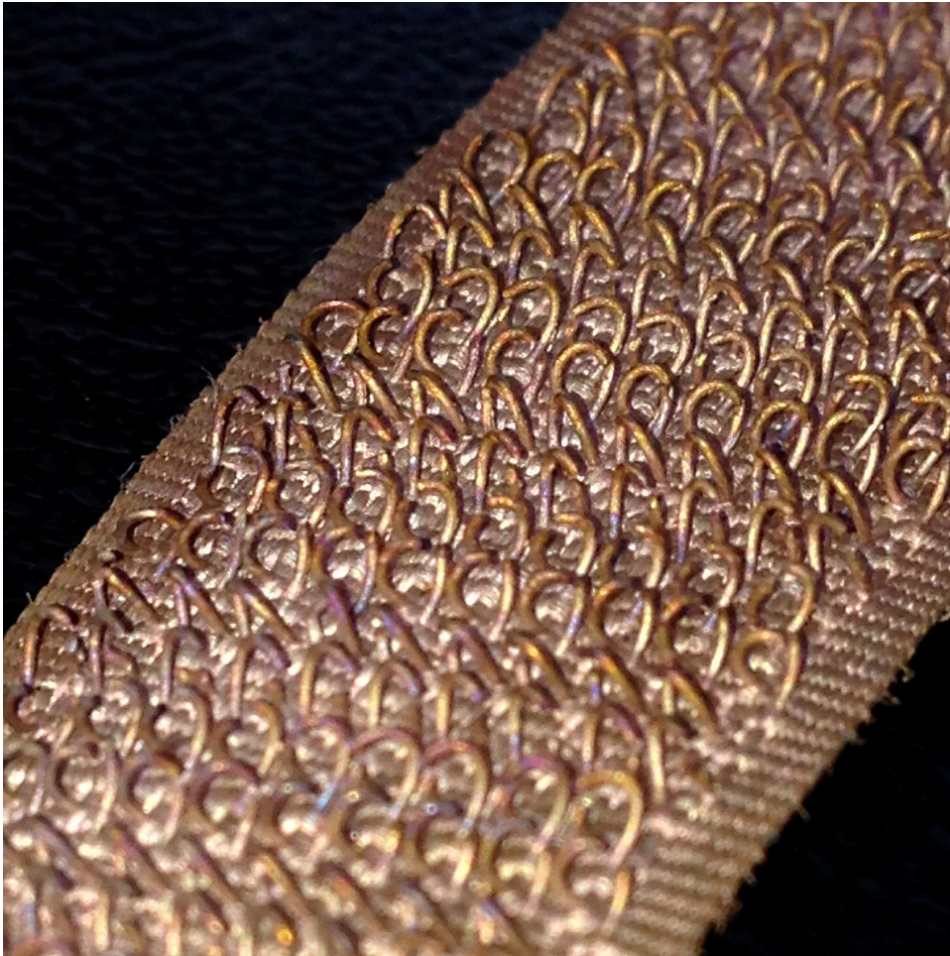
### **3.2.4 Electroplated Hook and Loop Connectors**

Electroplating using a copper solution has been carried to increase the conductivity of the hook and loop, see Figure 3-23 and Figure 3-24. The improvements in the DC resistance can be seen in Table 3-3. The electroplating improves the conductivity of hook and loop significantly. The resistances of hook and loop after electroplating are reduced to less than 10% of the original value. However, the electroplating process used here stiffened the loop component. In future, increasing the conductivity at the manufacturing stage could remove the need for electroplating.



**Figure 3-23 Zoomed in view of electroplated loop strip**



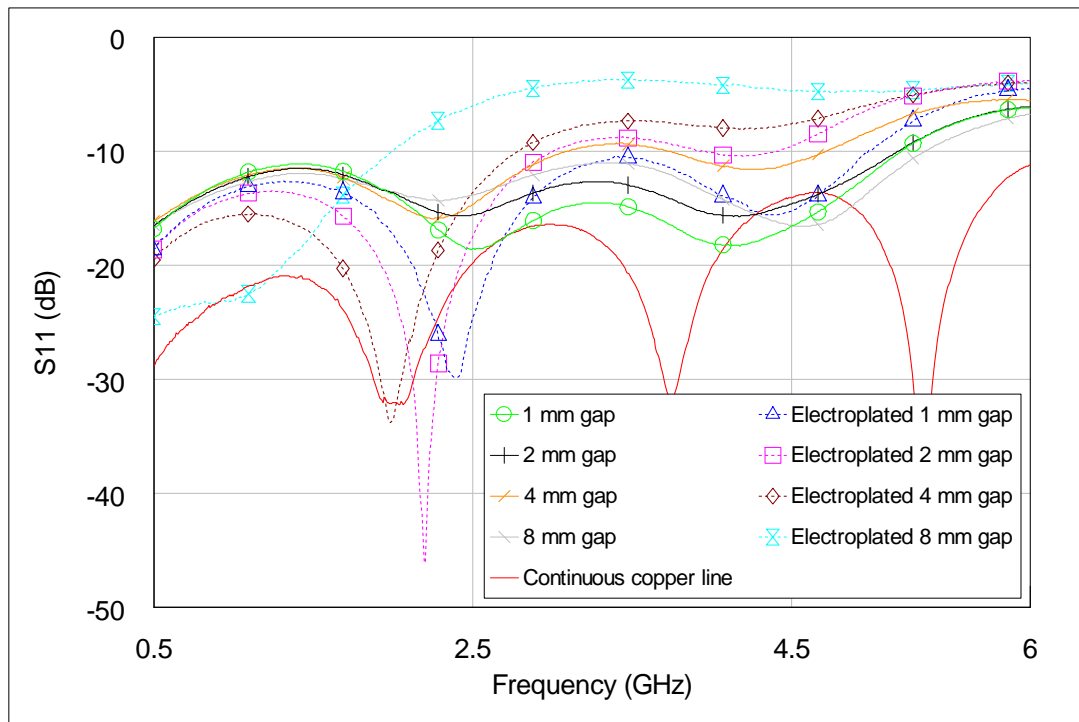


**Figure 3-24 Zoomed in view of electroplated hook strip**

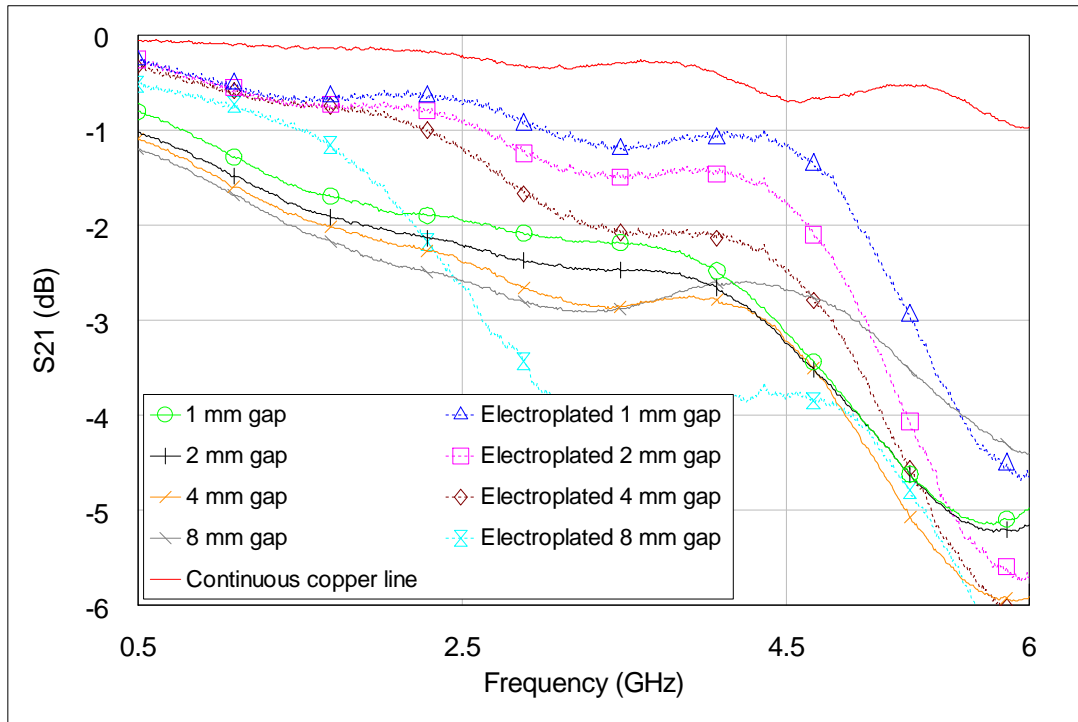
**Table 3-3 DC resistances of 5 cm long and 1.6 cm wide hook and loop before and after electroplating**

		DC resistance in $\Omega$	
		Front side	Back side
Untreated	Loop	1.13	1.78
	Hook	0.53	0.50
60 minutes electroplating	Loop	0.12	0.11
	Hook	0.03	0.03

Figure 3-25 shows the S11 results of all the eight hook and loop transmission lines compared with the continuous copper line. It can be seen that up to 2.7 GHz all the hook and loop ‘switches’ (apart from electroplated 8 mm gap) have the S11 values less than -10 dB which provides a reasonable impedance match. Figure 3-26 shows the comparison of S21 results of hook and loop ‘switches’. The insertion losses are better with smaller gaps. Furthermore the electroplating reduced the hook and loop insertion loss up the 5 GHz (except for the 8 mm gap line). The S21 of the electroplated hook and loop on 8 mm gap line is worse than the untreated hook and loop when frequency is higher than 2 GHz, but it is better than the untreated one when frequency below 2 GHz. Overall the added conductivity given by the electroplating has improved the insertion loss.



**Figure 3-25 S11 data for all eight hook and loop ‘switches’**



**Figure 3-26 S21 data for all eight hook and loop ‘switches’**

### 3.3 Conclusions

In this chapter the DC and RF performance of embroidered microstrip transmission lines made from conductive threads were measured. The presented results show that conductive threads can be used to embroider transmission lines for RF applications. The insertion loss of the embroidered transmission lines are less than 2 dB below 2.5 GHz and are less than 5 dB up to 6 GHz when using parallel stitches.

Generally, parallel stitch direction (i.e. same direction as signal transmission) is highly recommend for fabricating transmission lines and it is the most effective way to obtain low DC resistance and low RF loss. When the parallel stitch direction is applied, the impact from other factors (i.e. stitch spacing, number of filaments, and

coating materials) can be minimised. Threads that contain more filaments also have the advantage in terms of reducing resistance and insertion loss. Closer stitch spacing improves the connection between adjacent threads, which lowers the contact resistance. The coating material has less effect on DC and RF performance compared with stitch spacing, stitch direction and number of filaments. However, it worth noting that nickel may cause allergic dermatitis when prolonged contact with the skin. Fabric antennas made by nickel thread need to be isolated from skin for wearable applications.

The results of the hook and loop demonstrate the feasibility of using them as detachable connectors. The hook and loop ‘switch’ have the advantages of low-profile and easily applied on textile compared with conventional RF connectors. The ‘switch’ format used here will give a higher insertion loss than one would expect to find in a connector using hook and loop. The use of electroplating has indicated that higher conductivities will extend the frequency range of the connectors. Electroplating the hook and loop with copper has produced a significantly lower insertion loss of around 1 dB below 2 GHz. If a 2 dB insertion loss is deemed acceptable then a frequency range up to 4 GHz may be considered.

A reusable connector allows electronics to be removed from a fabric system for security or other reasons such as washing. This concept is useful and important addition to textile RF systems. A wider transmission line would practically works better with the hook and loop connectors proposed. This fits well with textiles where relative permittivities are generally relatively low and this leads to wider 50  $\Omega$  transmission lines.

## References

- [1] M. Chedid, I. Belov, and P. Leisner, “Experimental analysis and modelling of textile transmission line for wearable applications,” *International Journal of Clothing Science and Technology*, vol. 19, no. 1, pp. 59–71, 2007.
- [2] J. Leśnikowski, “Textile Transmission Lines in the Modern Textronic Clothes,” *Fibres & Textiles in Eastern Europe*, vol. 19, no. 6 (89), pp. 89–93, 2011.
- [3] R. Shaw, B. Long, D. Werner, and A. Gavrin, “The characterization of conductive textile materials intended for radio frequency applications,” *Antennas and Propagation Magazine, IEEE*, vol. 49, no. 3, pp. 28–40, 2007.
- [4] J. Leśnikowski and M. Tokarska, “Modelling of selected electric properties of textile transmission lines using neural networks,” *Textile Research Journal*, Jul. 2013.
- [5] G. Kompa, *Practical Microstrip Design and Applications*. Boston: Artech House, 2005.
- [6] R. Torres-Torres and V. H. Vega-Gonzalez, “An approach for quantifying the conductor and dielectric losses in PCB transmission lines,” in *18th IEEE Conference on Electrical Performance of Electronic Packaging and Systems*, 2009, pp. 235–238.
- [7] M. Steer, *Microwave and RF Design: A Systems Approach*. Raleigh: SciTech Publishing Inc, 2010.
- [8] Y. Ouyang and W. J. Chappell, “High frequency properties of electro-textiles for wearable antenna applications,” *Antennas and Propagation, IEEE Transactions on*, vol. 56, no. 2, pp. 381–389, 2008.
- [9] Y. Ouyang and W. Chappell, “Measurement of electrotexiles for high frequency applications,” in *IEEE MTT-S International Microwave Symposium Digest*, 2005, pp. 1679–1682.

- [10] P. Salonen, Y. Rahmat-Samii, H. Hurme, and M. Kivikoski, "Effect of conductive material on wearable antenna performance: a case study of WLAN antennas," *IEEE Antennas and Propagation Society Symposium, 2004.*, no. 1, pp. 455–458 Vol.1, 2004.
- [11] H. Visser and A. Reniers, "Textile antennas, a practical approach," in *The Second European Conference Antennas and Propagation (EuCAP)*, 2007, pp. 1–8.
- [12] M. Klemm, I. Locher, and G. Troster, "A novel circularly polarized textile antenna for wearable applications," in *Wireless Technology, 7th European Conference on*, 2004, pp. 285–288.
- [13] S. Zhu and R. Langley, "Dual-band wearable textile antenna on an EBG substrate," *Antennas and Propagation, IEEE Transactions on*, vol. 57, no. 4, pp. 926–935, 2009.
- [14] E. Tuncer and D. P. Neikirk, "Highly accurate quasi-static modeling of microstrip lines over lossy substrates," *Microwave and Guided Wave Letters, IEEE*, vol. 2, no. 10, pp. 409–411, 1992.
- [15] R. Lawton and W. Anderson, "Two-layer dielectric microstrip line structure: SiO<sub>2</sub> on Si and GaAs on Si: modeling and measurement," *IEEE Transactions on Microwave Theory and Techniques*, vol. 36, no. 4, pp. 785–789, Apr. 1988.
- [16] C. Hertleer, A. Van Laere, H. Rogier, and L. Van Langenhove, "Influence of Relative Humidity on Textile Antenna Performance," *Textile Research Journal*, vol. 80, no. 2, pp. 177–183, Sep. 2009.
- [17] J. Banaszczyk, G. De Mey, and A. Schwarz, "Current Distribution Modelling in Electroconductive Fabrics," *Fibres & Textiles in Eastern Europe*, vol. 17, no. 2, pp. 28–33, 2009.
- [18] I. Kazani, G. De Mey, C. Hertleer, J. Banaszczyk, A. Schwarz, G. Guxho, and L. Van Langenhove, "Van Der Pauw method for measuring resistivities of

- anisotropic layers printed on textile substrates,” *Textile Research Journal*, vol. 81, no. 20, pp. 2117–2124, Sep. 2011.
- [19] D. Cottet, J. Grzyb, T. Kirstein, and G. Troster, “Electrical characterization of textile transmission lines,” *Advanced Packaging, IEEE Transactions on*, vol. 26, no. 2, pp. 182–190, 2003.
- [20] D. M. Pozar, *Microwave Engineering*, 3rd ed. New York: Wiley, 2005.
- [21] Syscom Advanced Materials, “Metal clad fibers.” [Online]. Available: <http://www.metalcladfibers.com/metal-clad-fibers/>. [Accessed: 02-Jan-2014].
- [22] LessEMF.com, “Conductive Hook and Loop Fastenerle.” [Online]. Available: <http://www.lessemf.com/fabric.html#207> . [Accessed: 03-Jun-2013].
- [23] A. F. Levin and P. D. Levin, “Anti bed wetting device,” US patent, Patent No. 4191950 A, March, 4, 1980.
- [24] J. Adams and J. Wolf, “Electromechanical device for mounting an electronic assembly on a mounting rack, in particular for mounting a display instrument recessed in a dashboard,” US Patent, Patent No.6697262 B2, February, 24, 2004.
- [25] B. Kim, Y. Son, J. Sunwoo, H. Jeong, and I. Cho, “Velcro Connector,” US Patent, Patent No. 7753686 B2, July, 13, 2010.
- [26] B. S. Kim, H. S. Shin, Y. K. Son, I. Cho, and H. S. Lee, “Interfacing Mobile Devices with Electronic Textiles Using Spatial Information,” in *15th Annual International Symposium on Wearable Computers*, 2011, pp. 111–112.
- [27] H. S. Lee and I. Cho, “Drop-n-Play: A new device interface for iPod jackets,” in *Digest of Technical Papers International Conference on Consumer Electronics (ICCE)*, 2010, pp. 183–184.
- [28] R. D. Seager, A. Chauraya, S. Zhang, W. Whittow, and Y. Vardaxoglou, “Flexible radio frequency connectors for textile electronics,” *Electronics Letters*, vol. 49, no. 22, pp. 1371–1373, Oct. 2013.

# Chapter 4

## Effect of Fabrication Parameters on Embroidered Microstrip Antennas

---

### Abstract

This chapter discusses the simulated and measured rectangular microstrip patch antennas produced using embroidery techniques. Section 4.2 will show the effects of stitch direction and stitch spacing on the surface resistance of the patch. The effects on the resonant frequency, gain and efficiency of the embroidered antennas will be described in Section 4.3. The repeatability measurements of embroidered patch antennas will be included in Section 4.4. The analysis of the currents flow in the microstrip antennas and how it be influenced by the stitch direction and spacing will be illustrated in Section 4.5. Two different simulation approaches for these antennas will be discussed and linked to measurement results, pointing to a simplified model for simulating embroidered patch antennas. Section 4.6 will give the guidelines for choosing the correct fabrication parameters such as stitch spacing and direction. In this chapter, the antennas have a standard rigid microwave substrate to reduce the number of variables.

### 4.1 Introduction

Smart cloths that have integrated fabric based wearable antennas meets the requirements of being compact, mobile, discreet and always-on [1]–[4]. Multiple on body wearable antennas can be connected and build the body-centric wireless network to provide both mobility and functionality [5]. Flexible conductive materials can be



used for fabricating fabric based wearable antennas which are suitable for various applications. Well-designed fabric based wearable antennas are low-profile and hands-free which is qualified in harsh environments [6]. Hertleer *et al.* reported a wearable antenna integrated into protective clothing for fire fighters [7]. Flexible GPS antenna that can be integrated into cloth is presented in [8]. Manzari *et al.* have investigated passive textile RFID antenna for body-centric systems [9]. Fabric antenna that used for on-body sensor application can be seen in [10]. Textile antenna can be taken out of device and integrated into cloth to reduce the size and weight of the receiver unit. This feature is particularly beneficial for the applications with large antenna such as personal satellite communication [11].

However, the cost of the specialised antennas is concerned by the manufactures and slows down the market growth. Labours, materials, equipment and production times are the major issues in fabric based antennas production and added to the costs. Modern computerised embroidery machines are accurate and efficient in sewing complicated patterns and can be used for high frequency components fabrication. This will facilitate the integration of fabric antennas into clothing and lower the cost of manufacturing. In order to investigate the feasibility of manufacturing fabric based antenna systems, this chapter analyses the effect of the embroidery parameters including stitch spacing and stitch direction on the embroidered patch antennas performance.

The accuracy, adaptability, and flexibility of the computerised embroidery make it eligible to fabricate flexible electronics with complicated patterns [12]–[25]. Due to the features of the embroidered stitches, the embroidered antennas are different from the antennas made from conventional conductive materials. In Chapter 3, the embroidered microstrip transmission lines were examined. The stitch direction is the dominant embroidery parameter that influences the RF performance. Choi *et al.* examined the stitch directions of embroidered RFID tags [12]. The effects of the density of embroidered stitches on the read range of two arms RFID antennas were reported in [13]. Wang *et al.* reported the feasibility of increasing conductivity of

embroidered radiators by using double layers of embroidery [14]. Moradi *et al.* compared different sewing patterns on the read range of dipole RFID tag antennas [22]. However, more detailed study on embroidered factors is needed to investigate the principle of embroidered radiation elements. In this chapter, the effects of stitch direction and spacing on embroidered patch antenna are compared together. The optimum parameters in embroidered antennas manufacturing are determined.

The major difference between conventional copper based and fabric based antennas is the conductive surface of the conventional copper antenna is continuous, which easily achieves high conductivity and uniform electromagnetic fields, yielding high efficiency antennas. Creating a highly efficient fabric based antenna is a challenge due to the discontinuous and anisotropic surface. Some authors have reported fabric based antenna efficiency, for example, Locher *et al.* reported an efficiency of 45% for a knitted fabric antenna [26] and a 78% efficiency for a fabric antenna is achieved by involving conductive metal wire woven into the fabric [27]. However, the including of metal wires increases the manufacturing process and reduces the flexibility of the fabric. Embroidery using conductive thread can achieve both high conductivity and flexibility. In this chapter, silver coated Amberstrand thread will be used for embroidering microstrip antennas. The scanning electron microscope (SEM) image of unbraided Amberstrand Silver yarn shows the diameter of individual fibres is approximately 17  $\mu\text{m}$ . Details can be seen in Chapter 2.

In the embroidery process, the conductive yarns are usually aligned in a preferred direction and spacing which are defined by the embroidery parameter settings. It is vital to understand the way that the conductive yarns distort the current flow in the antenna at its operation frequency. The angle between fibres direction and test electrodes affects surface resistance of the conductive fabric [28]. Charging from different directions on conductive fabric will results in different sheet resistance values. Banaszczyk *et al* reported the current distribution in DC condition on the conductive woven fabric and pointed out that the sheet resistance of fabric is impacted

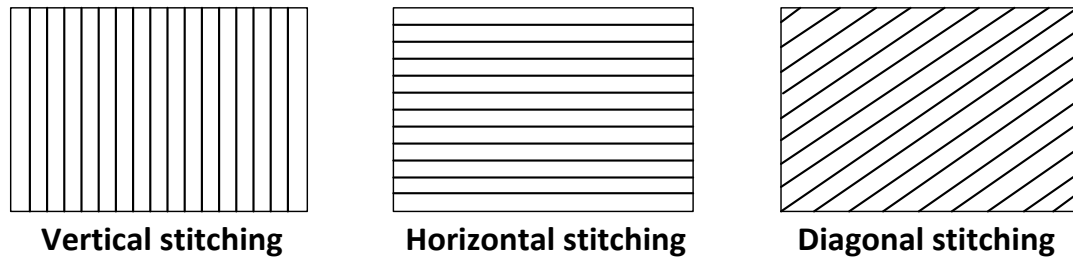
by the fibre direction, current direction and the contact resistance [29]. Approaches such as two metal electrodes and Van der Pauw method can be carried out to measure the sheet resistance of conductive fabric [30], [31]. The two electrode bars approach will be used to measure the surface resistance of the embroidered patches in the Section 4.2.

In addition, the adjacent threads will not touch each other along their full lengths, the structure may have a significant percentage of air voids which also depends on the diameter of the yarns and the stitch spacing. Some of the loose filaments might cross the air gap and connect the adjacent stitches. However, the contact resistance depends on the number of contacted filaments and is generally larger than the resistance of thread as seen from DC measurements in Chapter 2. The analysis of the gaps is vital to embroidered antenna performance and the effects of these gaps between conductive threads will be present in Section 4.5. Due to these limitations, it is not easy to define an electromagnetic model that accurately describes the properties of the embroidered fabric antennas. Two approaches will be discussed in this chapter to emulate the structure of the fabricated antenna.

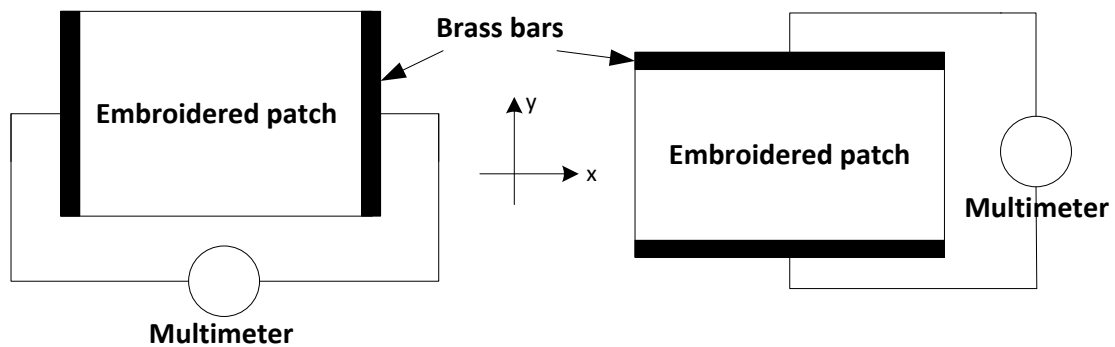
## **4.2 Sheet Resistance of Embroidered Microstrip Antennas**

In this section, rectangular patches were embroidered with three different stitch directions (vertical, horizontal and diagonal); and four stitch spacings (0.4mm, 0.6mm, 0.8mm and 1mm). The dimensions of embroidered patches were 37 mm by 28 mm. Silver coated Amberstrand yarn with the lock stitch was used. The three stitch directions are shown in Figure 4-1. It should be noted, in this context, that the diagonal stitching aligns with the corner to corner diagonal. Two brass bars were connected to the ends of the measurement cables of a digital multimeter in its

resistance mode, and the bars gave an even pressure and good contact over the length/width of the patches. Note connecting the bars together gave zero ohm resistance. Figure 4-2 illustrates the DC resistance measured by two brass bars in  $x$  and  $y$  directions.



**Figure 4-1 Sketch of patches with different stitch directions**



**Figure 4-2 Sketch of DC resistance measurement in  $x$  and  $y$  directions**

The measured DC resistance values are shown in Table 4-1. It is clear that the current prefers to follow the stitch direction rather than jump between threads, particularly with larger stitch spacings. This agrees with the conclusion of the transmission line measurements in Chapter 3. However, the effect of different stitch spacing on the sheet resistances is not very clear in this DC measurement due to the small values of the resistance and the potential parasitic contact resistance between the bars and fabric samples. The antenna gain measurements in Section 4.3 will analyse the influence of different stitch spacings on RF performance.

**Table 4-1 Measured DC resistances of Amberstrand Silver patches with different stitch spacings and directions**

Stitch spacing (mm)	Stitch direction	DC resistance of embroidered patch ( $\Omega$ )	
		Measured in x direction	Measured in y direction
0.4	Diagonal	0.02	0.22
	Horizontal	0.01	0.13
	Vertical	0.19	0.03
0.6	Diagonal	0.01	0.15
	Horizontal	0.00*	0.11
	Vertical	0.44	0.00*
0.8	Diagonal	0.01	0.23
	Horizontal	0.01	0.16
	Vertical	0.18	0.00*
1.0	Diagonal	0.02	0.44
	Horizontal	0.01	0.21
	Vertical	0.26	0.01

\*the resistances were smaller than 0.005  $\Omega$ .

## 4.3 RF performance of Embroidered Microstrip Antennas

### 4.3.1 Fabrication and Feeding

Reducing the unknown changes in variables gives efficient analysis of determining the effects of embroidery parameters on the antenna RF performance. Therefore, rigid substrate with solid ground planes and semi rigid coaxial cable was used to minimise the number of variations. Compared with microstrip line feed [32], the probe feed offers a more flexible way to obtain the optimum impedance match. As the input impedance is determined by the feed location, moving the embroidered patch along the symmetric line can modify the impedance matching. This will reduce the return loss due to the miss match. The geometry and the feed position of the patch antenna are shown in Figure 4-3.

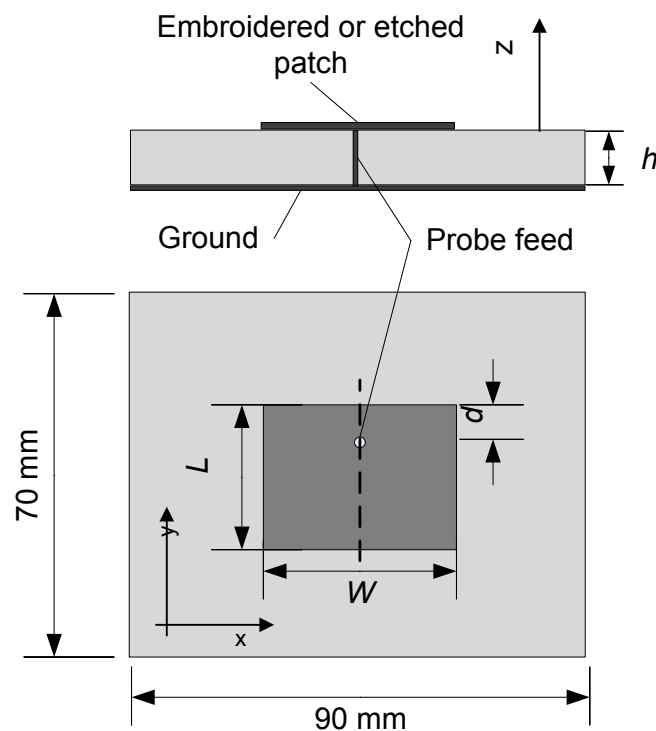


Figure 4-3 Geometry and feed position of the embroidered and etched patch antenna

The design equations for a rectangular patch antenna are given by [33], [34]:

For high antenna efficiency, the width of the patch  $W$  is

$$W = \frac{c}{f_r} \sqrt{\frac{2}{\epsilon_r + 1}} \quad (4.1)$$

where  $c$  is the free-space velocity of light,  $f_r$  is the resonant frequency of the patch antenna in Hz.

The resonant frequency of the rectangular patch antenna at the dominant  $TM_{01}$  mode is determined by its effective length  $L_{eff}$  which can be obtained by (4.2)

$$L_{eff} = L + 2\Delta L \quad (4.2)$$

where  $L$  is the physic length of the patch and  $\Delta L$  is the extended length due to the fringing field. The extension of the length  $\Delta L$  is given by (4.3)

$$\Delta L = 0.412h \frac{(\epsilon_e + 0.3) \left( \frac{W}{h} + 0.264 \right)}{(\epsilon_e - 0.258) \left( \frac{W}{h} + 0.8 \right)} \quad (4.3)$$

where the effective dielectric constant  $\epsilon_e$  can be obtained by equation (3.2).

For the dominant  $TM_{01}$  mode, the resonant frequency of the rectangular patch antenna is given by (4.4)

$$\begin{aligned} (f_{rc})_{01} &= \frac{1}{2L_{eff} \sqrt{\epsilon_e} \sqrt{\mu_0 \epsilon_0}} \\ &= \frac{1}{2(L + 2\Delta L) \sqrt{\epsilon_e} \sqrt{\mu_0 \epsilon_0}} \end{aligned} \quad (4.4)$$

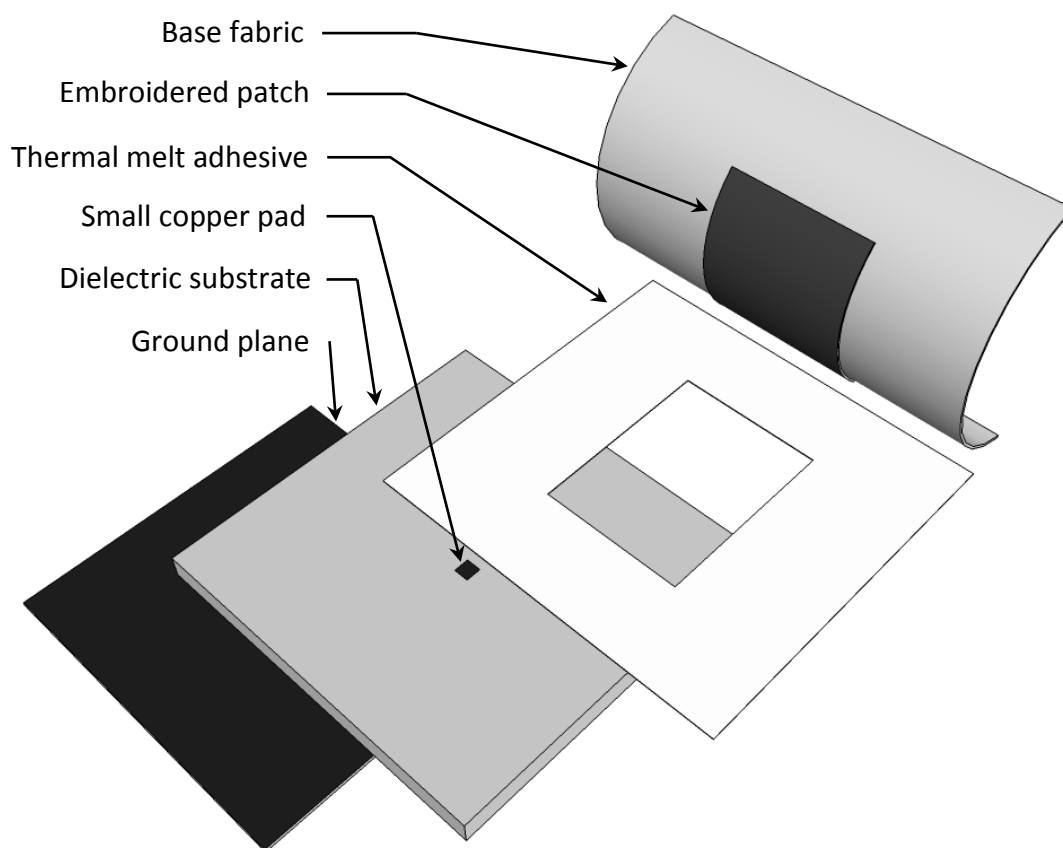
The feed point determines the input impedance. A feed point that is situated along the  $W/2$ , the higher order mode will be suppressed and only  $TM_{01}$  mode is excited. The distance from the edge to the point  $d$  is approximately given by (4.5)

$$d = \frac{L}{2\sqrt{\epsilon_r}} \quad (4.5)$$

The patch antennas in this chapter were designed to work at 2.4 GHz. They were placed on the 90 mm  $\times$  70 mm,  $h=1.57$  mm low loss Taconic RF - 45 substrate ( $\epsilon_r = 4.5$  and  $\tan\delta = 0.0037$ ) with a copper ground plane. Therefore embroidered patch antenna dimensions were determined as  $W=37$  mm and  $L = 28$  mm. The theoretical feed point  $d$  is 9.5 mm away from the edge. An etched copper patch with the same dimensions was made for comparison.

Since the conductive threads were embroidered only on one side of the base fabric, the embroidered patches were placed upside down (see Figure 4-4) to eliminate of additional layer between embroidered radiation element and a substrate. The thermal melt adhesive web was used for fixing the base fabric on the substrate. A hole is cut at the centre of the thermal melt adhesive to avoid isolating the embroidered patch from the feed pad. Simulations indicated that the very thin base fabric layer of cotton ( $\epsilon_r = 1.6$ ,  $\tan\delta = 0.04$  and 0.5 mm height) as superstrate has negligible effect on resonate frequency and antenna efficiency.





**Figure 4-4 Sketch of upside down embroidered patch antenna on rigid dielectric substrate, with thermal melt adhesive between base fabric and substrate**

A  $50 \Omega$  coaxial was used to feed the antenna. The feed position of the copper patch was chosen from the theoretical best impedance match point. A small copper pad ( $3 \text{ mm} \times 3 \text{ mm}$ ) was connected to the coaxial probe where the feed via emerged from the substrate. The embroidered patches were placed against the pad which gives good contact between probe and embroidered patch. However, the theoretical feed position did not give good impedance for the embroidered patch antennas. The feed point need to be adjusted manually to obtain the optimum impedance match. In practice, it is found that the feed point should be placed closer to the top  $W$  edge for better matching.

### **4.3.2 RF performance of Embroidered Microstrip Antennas**

The antennas were measured in the anechoic chamber measuring approximately  $7 \times 7 \times 3 \text{ m}^3$  at Loughborough University. Two-Antenna Method [33] is employed for measuring the gain and radiation pattern of the antenna under test (AUT). The AUT is mounted on the positioner and rotated in azimuth (theta) and elevation (phi) plane. A linearly polarised standard horn antenna with known gain is placed approximately 3.7 m away from the centre of the positioner rotation platform with the same height of the AUT. A VNA was connected to both the AUT and horn antenna. The measurement frequency range of this chamber is from 30 kHz to 6 GHz. Visual Basic software was adopted as measurement control program that enable the AUT 360° fully rotate in both theta and phi planes. The total efficiencies and gain quoted were obtained with a full three dimensional (3D) scan of the radiation fields, and included the return loss.

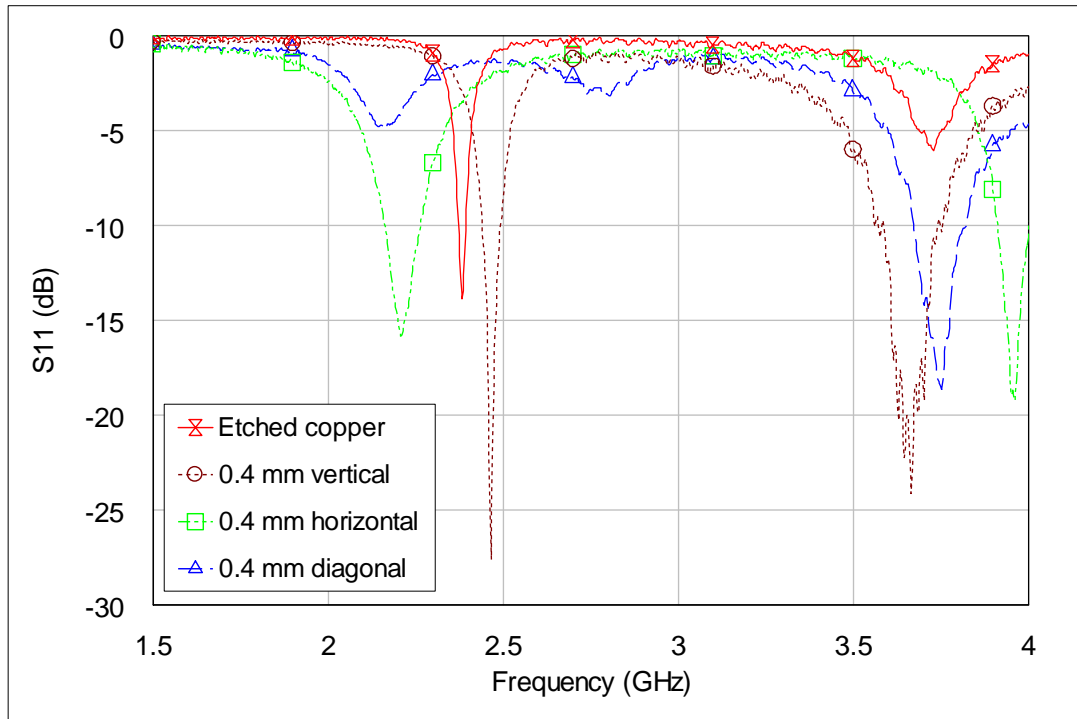
The measured results are summarised in Table 4-2. The gain and efficiency results indicates that the vertical thread orientation is the preferred direction for the first radiation mode and the results show that higher gain and efficiency values are obtained with smaller stitch spacing antennas. The diagonal stitch direction antennas tend to perform better than the horizontal ones. It is likely that this is because there is a component of the current flowing in the vertical direction. The resonant frequencies for the horizontal and diagonal patches are lower than those for the vertical stitch direction. This indicates that the increased current path lengths of the embroidered patches and the anisotropic nature of the textile surface may increase the inductance and capacitance which also could lower the resonant frequency.

In all but three cases in Table 4-2, the S11 values for Amberstrand show a better match than for the etched copper patch. This is most likely because the feed positions of the embroidered antennas were adjusted to give optimum match as far as possible. This was not the case with the etched copper patch.

**Table 4-2 Measured results for embroidered patch antennas on RF-45 substrate**

Antenna		Resonant Frequency (GHz)	S11 (dB)	Gain (dBi)	Directivity (dBi)	Total efficiency (%)
Etched Copper		2.40	-24.5	6.5	7.4	80.4
0.4 mm spacing	Vertical	2.47	-27.9	4.9	7.7	52.5
	Horizontal	2.21	-16.0	-1.0	7.1	15.4
	Diagonal	2.40	-15.8	2.4	7.5	30.4
0.6 mm spacing	Vertical	2.50	-17.6	4.2	7.2	48.9
	Horizontal	2.11	-12.3	-2.0	6.9	12.3
	Diagonal	2.18	-15.9	-1.2	7.3	13.8
0.8 mm spacing	Vertical	2.51	-24.6	3.6	7.4	42.1
	Horizontal	1.91	-11.0	-6.2	7.1	4.3
	Diagonal	2.06	-15.6	-1.3	6.1	17.7
1.0 mm spacing	Vertical	2.57	-14.4	-1.6	7.1	13.2
	Horizontal	1.77	-16.5	-7.8	7.5	2.9
	Diagonal	2.00	-12.4	-1.3	6.2	16.8

Figure 4-5 shows the S11 values of the four antennas described in the previous paragraph. The etched copper patch antenna has the highest Q from this figure. The vertical stitch direction follows this. Both of these two antennas show a very good impedance match (Copper: S11 = -24.5 dB at 2.38 GHz and Vertical stitch direction: S11 = -27.6 dB at 2.47 GHz respectively). The resonant frequency of horizontal stitch direction patch reduces to 2.2 GHz but it still has S11 of -16 dB acceptable impedance match. However the impedance match of the diagonal stitch direction patch is poor, at 2.16 GHz resonant frequency the S11 equals to -5 dB.



**Figure 4-5 Measured S11 of four 0.4 mm stitch spacing embroidered patch antenna with different stitch direction and etched copper patch antenna**

Figure 4-6 (a) to (c) shows the electric field on  $\phi = 0^\circ$  plane for three 0.4 mm stitch spacing embroidered patch antennas with different stitch directions. Figure 4-6 (d) shows radiation patterns on the same plane of the etched copper antenna. For the dominated mode, which is accepted as the normal radiation mode of a patch antenna, the vertically directional stitches are parallel with the major current flow direction. The polarisation purity for the vertical stitched patch antenna is in excess of 27 dB on boresight. This is significantly worse than the 35 dB of etched copper antenna. The polarisation purity for the horizontal stitch direction is decreased to approximately 23 dB. The embroidered patch with diagonal stitch direction has approximately 8 dB polarisation purity. This is caused by current flowing along the diagonal threads and also crossing the adjacent stitches, which causes the two polarisations to come close together in terms of magnitude. It can be summarised that the stitch direction which distorts the major current flowing direction of a patch antenna could reduce the polarisation purity level.

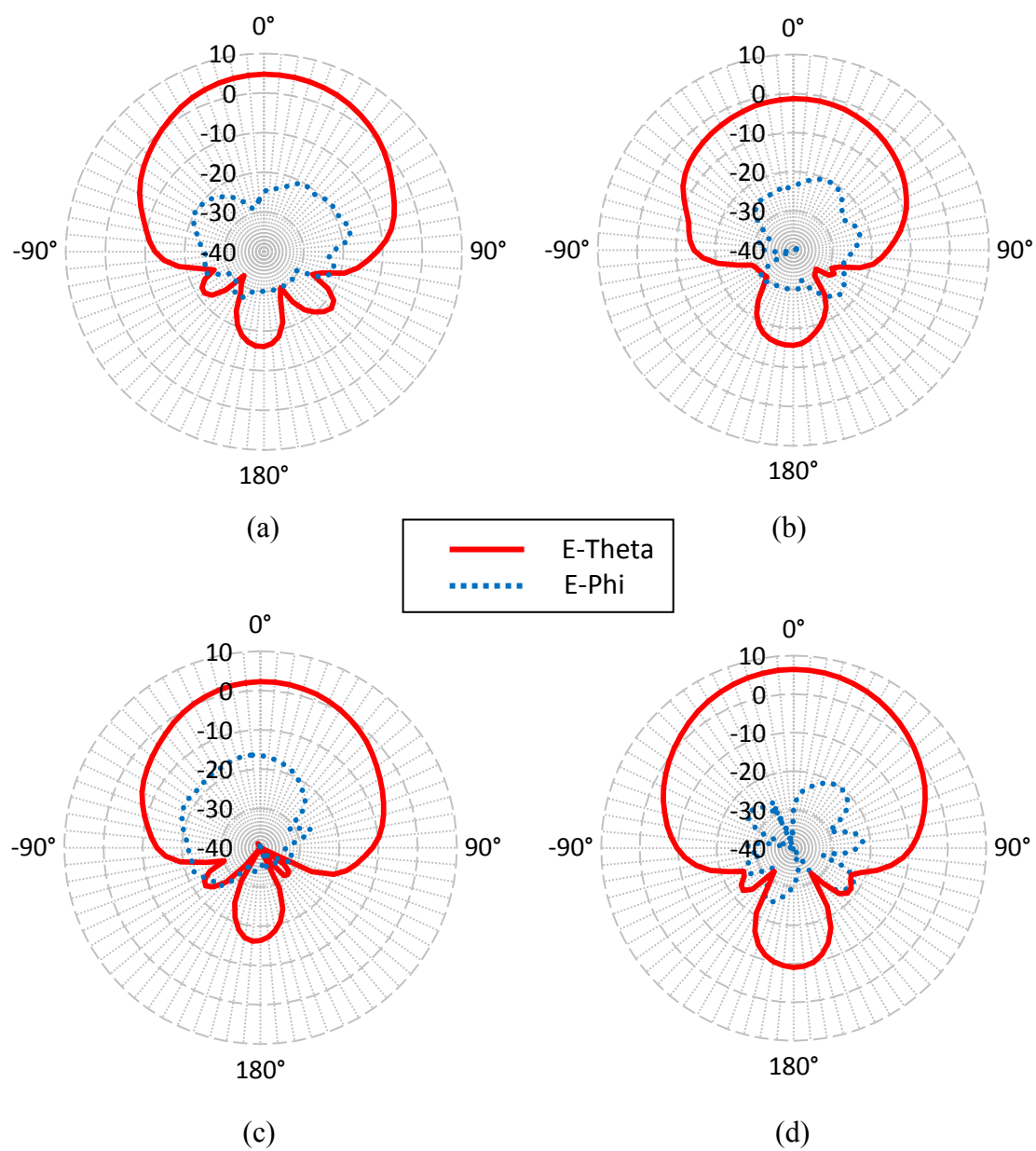


Figure 4-6 Measured electric field gain radiation patterns (in dBi) on  $\phi=0^\circ$  plane

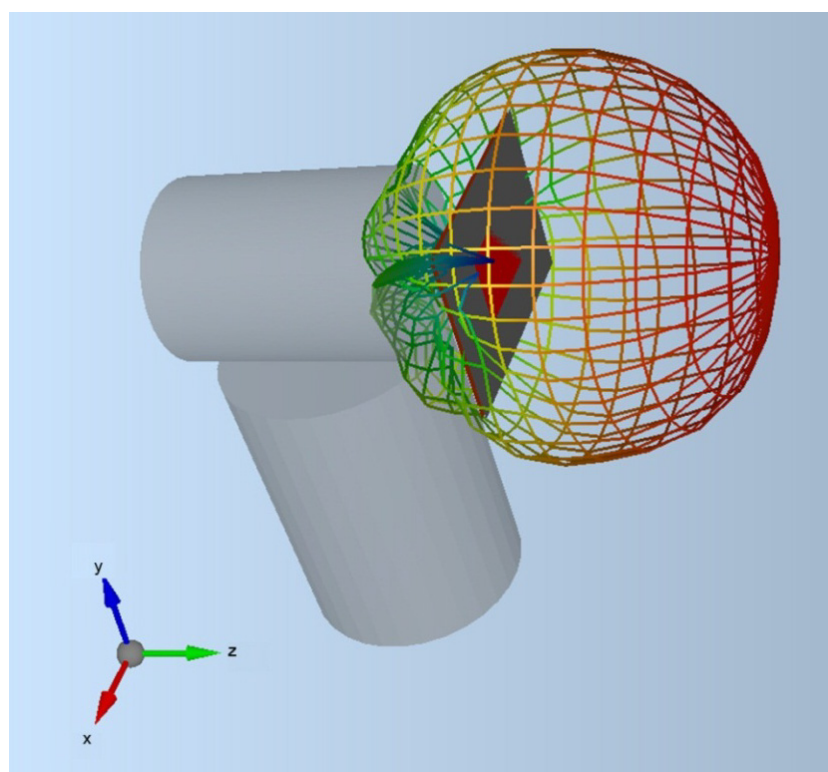
(a) Vertical 0.4mm stitch spacing embroidered patch antenna at 2.47 GHz

(b) Horizontal 0.4mm stitch spacing embroidered patch antenna at 2.21 GHz

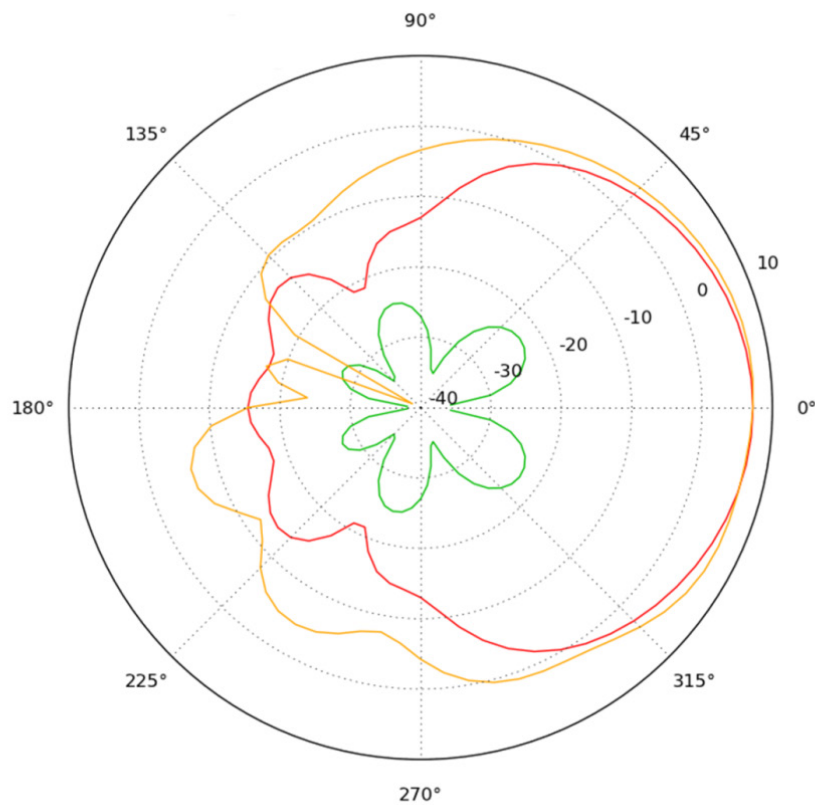
(c) Diagonal 0.4mm stitch spacing embroidered patch antenna at 2.40 GHz

(d) Etched copper patch antenna at 2.40 GHz

There is a back lobe that is larger than would be desirable. It is believed that this is partly caused by the small ground plane (90 mm × 70 mm) and partly by the measurement tower in the chamber. The tower is made out a range of dielectric materials but mainly of polyvinyl chloride (PVC). Simulations including a model of the measurement tower were carried out to test this hypothesis. IMST Empire XCcel software which uses the Finite Difference Time Domain method (FDTD) was used to simulate the measurement environment. Figure 4-7 shows the copper microstrip antenna placed in front of the positioner with dielectric constant equals to 2.91 and loss tangent = 0.025. Figure 4-8 illustrates the simulated radiation pattern of the solid copper patch antenna with the enlarged back lobe due to the positioner. The measured antenna efficiency in this anechoic chamber with this positioner is approximately 3% less than the simulation [35]. However, for the embroidered fabric antennas, the stitch direction also influences the size of the back lobe. The vertical stitch direction has the smallest back lobe of the three embroidered antennas and the diagonal stitch direction is the worst of the three. A note of caution must be sounded here as the ground plane will appear to have a slightly different size for each measurement as the frequencies are different.



**Figure 4-7 Simulation of measurement tower in anechoic chamber**



**Figure 4-8 Simulated gain pattern of etched copper patch antenna with measurement tower showing enlarged back lobe (in dBi)**

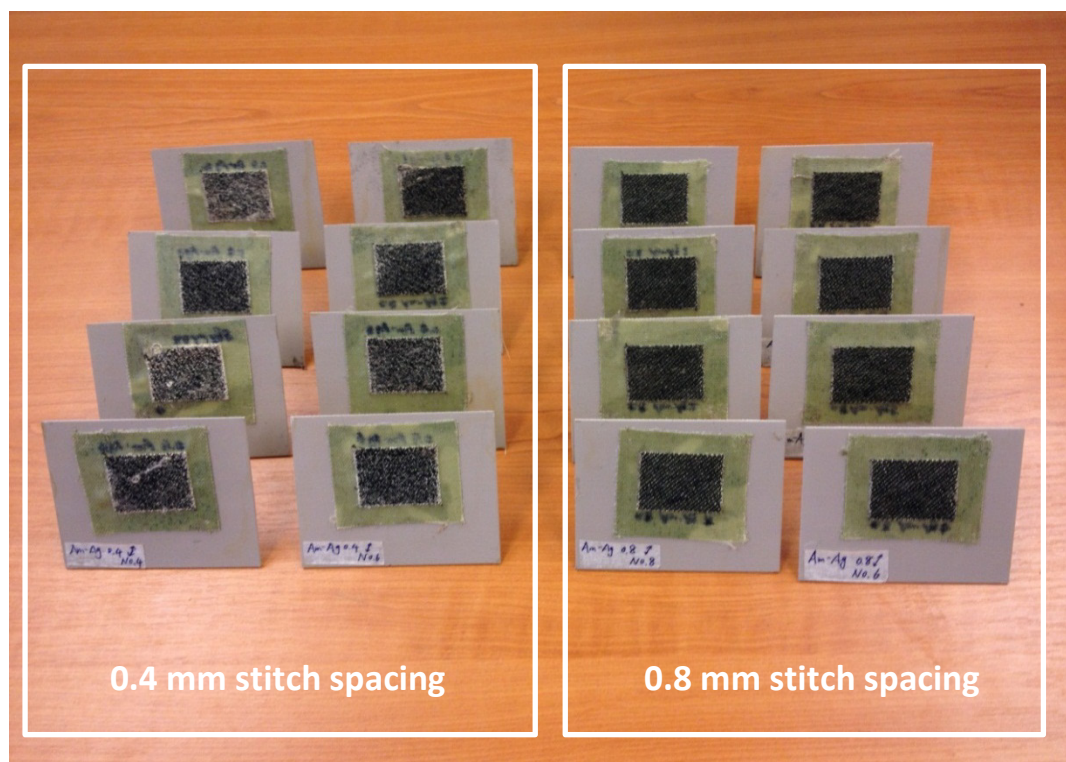
- : E-theta on  $\phi=0^\circ$ ; — : E-phi on  $\phi=0^\circ$**
- : E-theta on  $\phi=90^\circ$ ; E-phi on  $\phi=90^\circ < -40$  dBi**

#### **4.4 Repeatability of Embroidered Microstrip Antennas**

Since embroidered pattern can be mass manufactured, it also worthwhile to investigate the consistency of the embroidery process parameters in textile antenna fabrication. Therefore, a repeatability measurement analysis was made in order to find out the variation of numerous *identical* antennas. Two groups of embroidered antennas with diagonal stitch direction were made by Nottingham Trent University: one group had 0.4 mm stitch spacing and the other group had 0.8 mm spacing. Each group had eight antennas which were designed and embroidered identically by the same machine and

setup. The diagonally embroidered patch has the most complex current distribution, i.e. components in the vertical, horizontal, diagonal directions. Therefore this stitch direction is informative for this repeatability study. This study is principally focused on the consistency of the embroidered process, as a result the rigid substrate with copper ground plane was used to reduce the unwanted variations. In real fully fabric antennas, the variation will be larger.

These antennas were embroidered using the same Amberstrand Silver thread in this chapter and the low loss rigid Taconic RF-45 substrate was used. The feeding point in this repeatability test is chosen as the best impedance match position for the first embroidered sample. Then the same feed position was applied for the rest of the samples. The feed positions of the 0.4 mm spacing patches and the 0.8 mm spacing patches were chosen separately. An etched copper patch antenna with the same dimensions was made as a comparison. Figure 4-9 shows the 16 embroidered patch antennas.



**Figure 4-9 Two groups of *identical* embroidered patch antennas with different stitch spacings**



All the 16 fabric antennas were well matched at the resonant frequencies. Figure 4-10 and Figure 4-11 show the measured S11 results of the 0.4 mm and 0.8 mm stitch spacing antennas respectively. It can be seen that the resonant frequencies changed with different samples. The intersection of the S11 curves (i.e. the frequency that was covered by all the bandwidths) reveals the repeatability of the operation frequency. More precisely, the 0.4 mm stitch spacing group has a repeatable -5 dB bandwidth of 96 MHz whilst the 0.8 mm stitch spacing group has 101 MHz repeatable -5 dB bandwidth. Therefore the repeatability of the 0.4 mm and 0.8 mm spacing stitches at the -5 dB level are similar. However, the 0.4 mm spacing group does not have repeatable -10 dB bandwidth results whilst the repeatable -10 dB bandwidth of 0.8 mm spacing is 26 MHz. This indicates the 0.8 mm stitch spacing group has better repeatability than 0.4 mm stitch spacing group at -10 dB level.

The measured antenna parameters are shown in Table 4-3 and Table 4-4. The standard deviation of 0.4 mm stitch spacing resonant frequencies is 0.04 GHz and the standard deviation of 0.8 mm is 0.01 GHz. The deviation of the resonant frequencies is influenced by the slightly changed dimensions of the patches due to the embroidery precision and the different tensions of the stitches affect the intend geometry. The 0.4 mm spacing strains tighter than the 0.8 mm, this affects the size of the antenna more significantly. The etched copper patch with the same dimension operates at 2.38 GHz which is close to the 0.4 mm spacing patches.

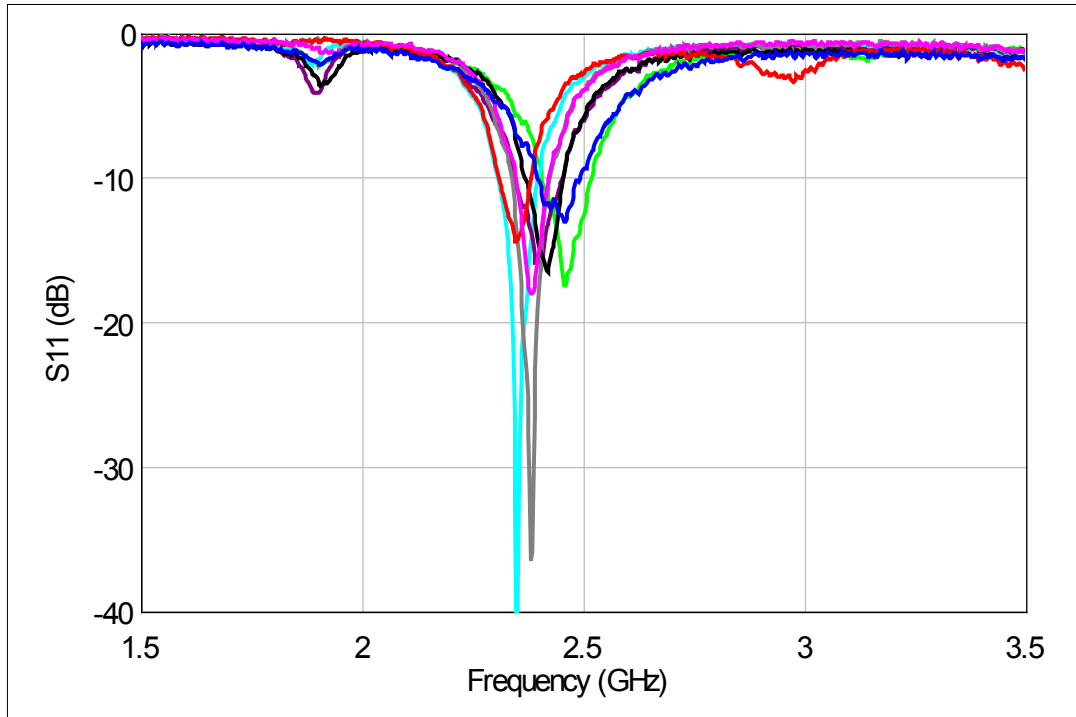


Figure 4-10 Measured S11 of eight *identical* embroidered patch antennas with diagonal 0.4 mm stitch spacing

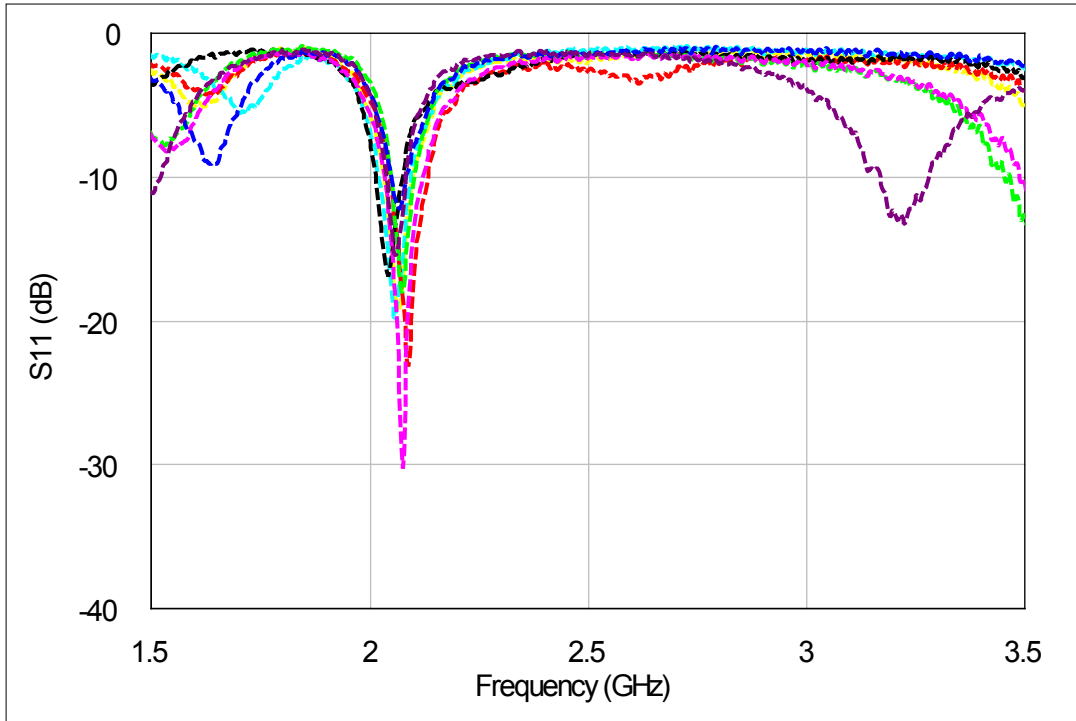


Figure 4-11 Measured S11 of eight *identical* embroidered patch antennas with diagonal 0.8 mm stitch spacing

**Table 4-3 Measured results of 0.4 mm stitch spacing embroidered antennas**

Antenna	Resonant frequency (GHz)	10dB bandwidth (MHz)	Peak gain (dBi)	Total efficiency (%)
1	2.38	73	2.3	30.2
2	2.42	86	2.0	27.9
3	2.46	116	2.2	27.4
4	2.38	86	2.8	34.1
5	2.40	110	2.4	30.4
6	2.35	90	2.5	31.4
7	2.46	111	2.1	28.0
8	2.35	72	2.1	28.1
<b>Average</b>	<b>2.40</b>	<b>93</b>	<b>2.3</b>	<b>29.7</b>
Standard deviation	0.04	16	N/A	2.2
Etched copper	2.40	22	6.5	80.7

**Table 4-4 Measured results of 0.8 mm stitch spacing embroidered antennas**

Antenna number	Resonant frequency (GHz)	10dB bandwidth (MHz)	Peak gain (dBi)	Total efficiency (%)
1	2.06	73	0.1	20.8
2	2.08	53	0.2	22.1
3	2.04	62	-0.5	18.7
4	2.08	74	-1.7	16.1
5	2.09	87	-0.7	17.6
6	2.06	75	-1.8	15.4
7	2.07	65	-1.1	16.3
8	2.07	34	-1.4	14.6
<b>Average</b>	<b>2.07</b>	<b>70</b>	<b>-0.8</b>	<b>17.7</b>
Standard deviation	0.01	15	N/A	2.5
Etched copper	2.40	22	6.5	80.7

Patches with 0.8 mm stitch spacing have narrower bandwidths than the patches with 0.4 mm stitch spacing. The average 10 dB bandwidths are 70 MHz for 0.8 mm spacing and 93 MHz for 0.4 mm spacing. The bandwidth of etched copper patch is 22 MHz which is smaller than all the diagonally embroidered patches. However, as shown in Figure 4-5, vertically embroidered patches have similar bandwidth as solid copper patch and horizontal stitch has the largest bandwidth. Generally lossy patch antennas have large bandwidth.

The antenna gain is reduced when the distance between stitches is increased. All the antenna gains of the 0.4 mm stitch spacing samples are larger than the 0.8 mm spacing samples. The total efficiency has a similar trend as the gain: the average total efficiencies of 0.4 mm and 0.8mm stitch spacing are 29.7 % and 17.7 % respectively. The standard deviations of their efficiencies are 2.2 % and 2.5 % respectively.

Figure 4-12 and Figure 4-13 show the dual polarization gain patterns on the  $\phi = 0^\circ$  and  $\phi = 90^\circ$  planes of all the 0.4mm and 0.8mm spacing embroidered antennas at their resonant frequencies, which clearly illustrate the high repeatability of the embroidered patches. Figure 4-14 and Figure 4-15 represent the electric field plot of one antenna in each stitch spacing group. It is noticed that the cross-polarization level is increased with stitch spacing, i.e. the 0.8 mm stitch spacing antennas have higher cross-polarization level than the 0.4 mm spacing antennas.

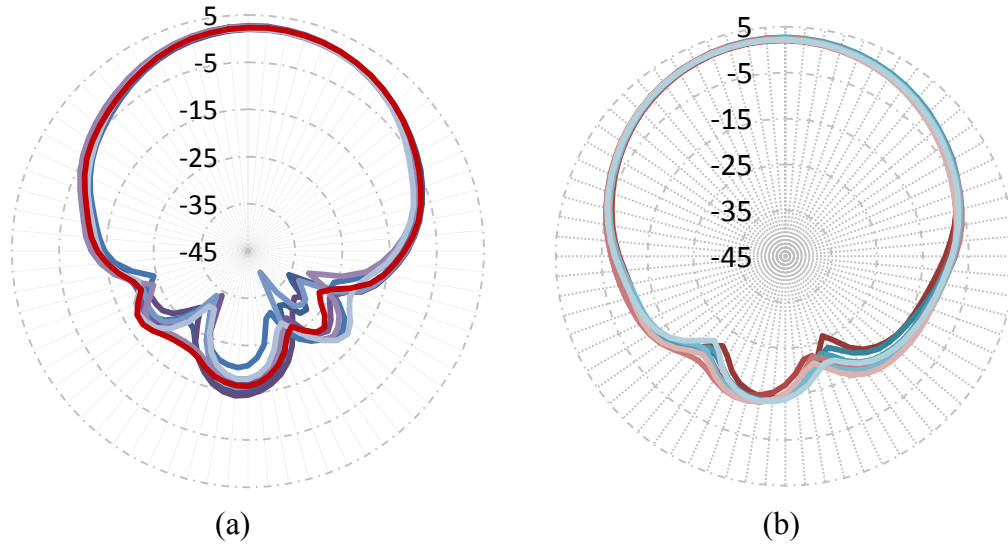


Figure 4-12 Measured dual polarization gain patterns (in dBi) of eight *identical* diagonal stitch antennas with 0.4mm spacing on (a)  $\phi = 0^\circ$  and (b)  $\phi = 90^\circ$

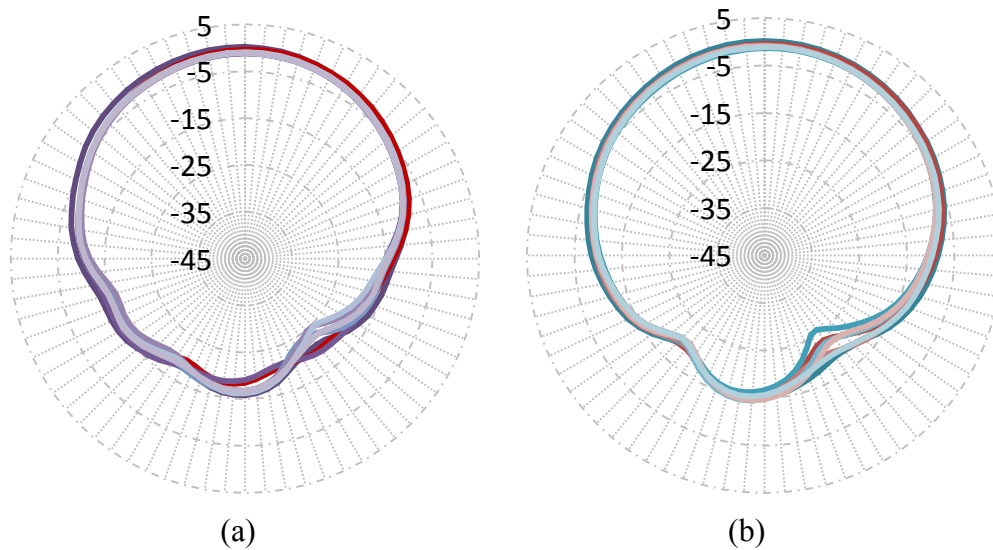


Figure 4-13 Measured dual polarization gain patterns (in dBi) of eight *identical* diagonal stitch antennas with 0.8mm spacing on (a)  $\phi = 0^\circ$  and (b)  $\phi = 90^\circ$

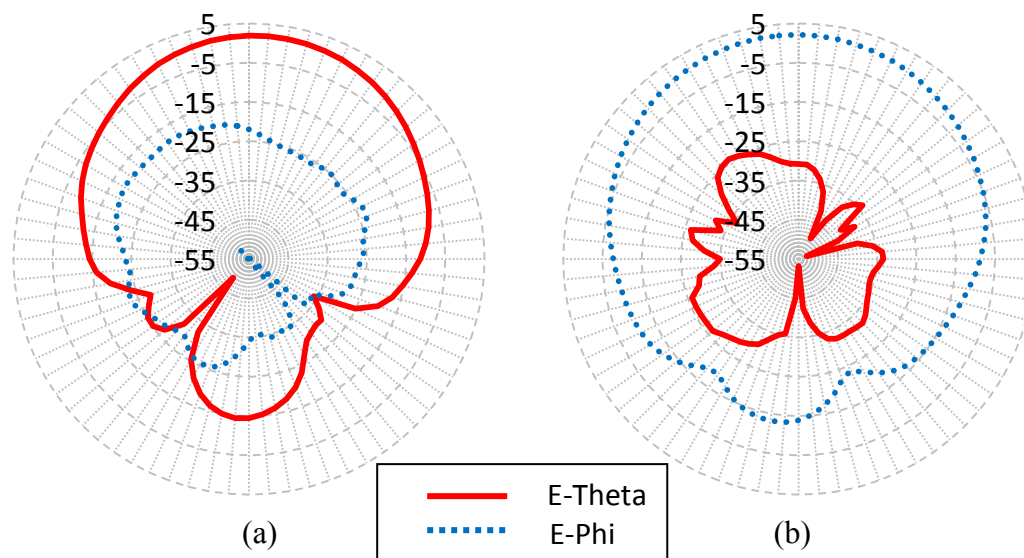


Figure 4-14 Measured electric field gain pattern (in dBi) of one diagonal stitched antenna with 0.4 mm spacing on (a)  $\phi = 0^\circ$  and (b)  $\phi = 90^\circ$

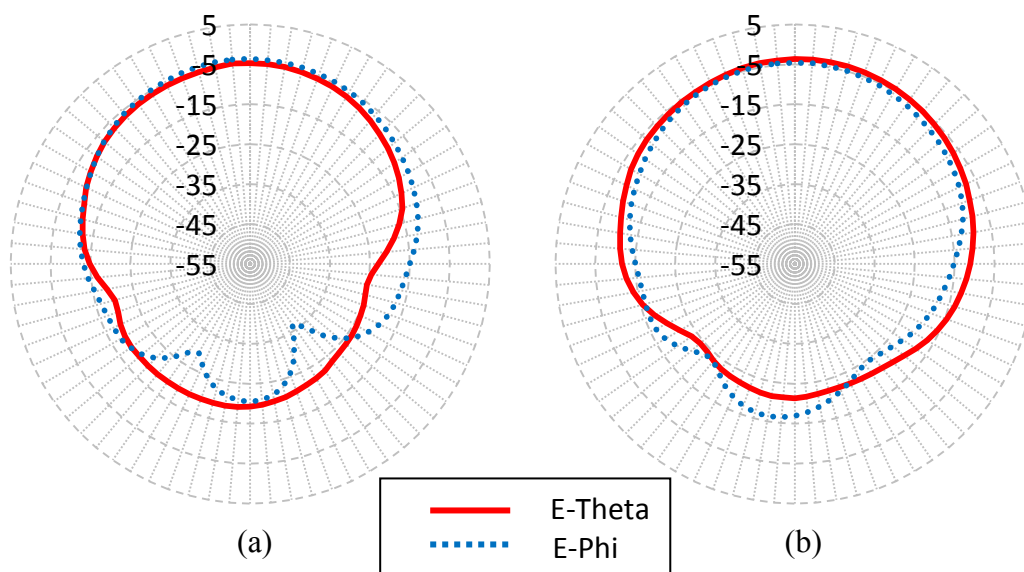


Figure 4-15 Measured electric field gain pattern (in dBi) of one diagonal stitched antenna with 0.8 mm spacing on  $\phi = 0^\circ$  (a) and (b)  $\phi = 90^\circ$

## **4.5 Simulation Models of Embroidered Microstrip Antennas**

In this thesis IMST Empire XCcel (FDTD), was used to model the problems. Two different approaches were taken to modelling the embroidered fabric antennas. The first approach represents in Section 4.5.1 considered the embroidered patch as a solid patch antenna with homogeneous equivalent conductivity values. The second method simulated the anisotropic characteristic of the embroidered threads and will be shown in Section 4.5.2.

### **4.5.1 Solid Microstrip Antennas with Equivalent Conductivity Values**

The losses of patch antennas can be represented by the quality factor. It is composed of radiation loss, conduction loss, dielectric loss and surface wave loss [33]. The total quality factor  $Q$  is influenced by all of these losses

$$\frac{1}{Q} = \frac{1}{Q_{rad}} + \frac{1}{Q_c} + \frac{1}{Q_d} + \frac{1}{Q_{sw}} \quad (4.6)$$

Where  $Q_{rad}$  is the quality factor due to radiation losses

Where  $Q_c$  is the quality factor due to conduction losses

Where  $Q_d$  is the quality factor due to dielectric

Where  $Q_{sw}$  is the quality factor due to surface wave losses

For the very thin substrates (substrate height  $h \ll$  wavelength), the surface wave loss can be neglected. And the  $Q_{rad}$  is inversely proportional to the height of the substrate.

$$Q_{rad} = \frac{2\omega\epsilon_r}{hG_t/l} K \quad (4.7)$$

Where  $G_t/l$  is the total conductance per unit length of the radiation aperture and for a rectangular aperture operation in the dominant mode

$$K = \frac{L}{4} \quad (4.8)$$

$$G_t = \frac{G_{rad}}{W} \quad (4.9)$$

The Q factor of conduction loss and dielectric loss can be presented

$$Q_c = h\sqrt{\pi f \mu \sigma} \quad (4.10)$$

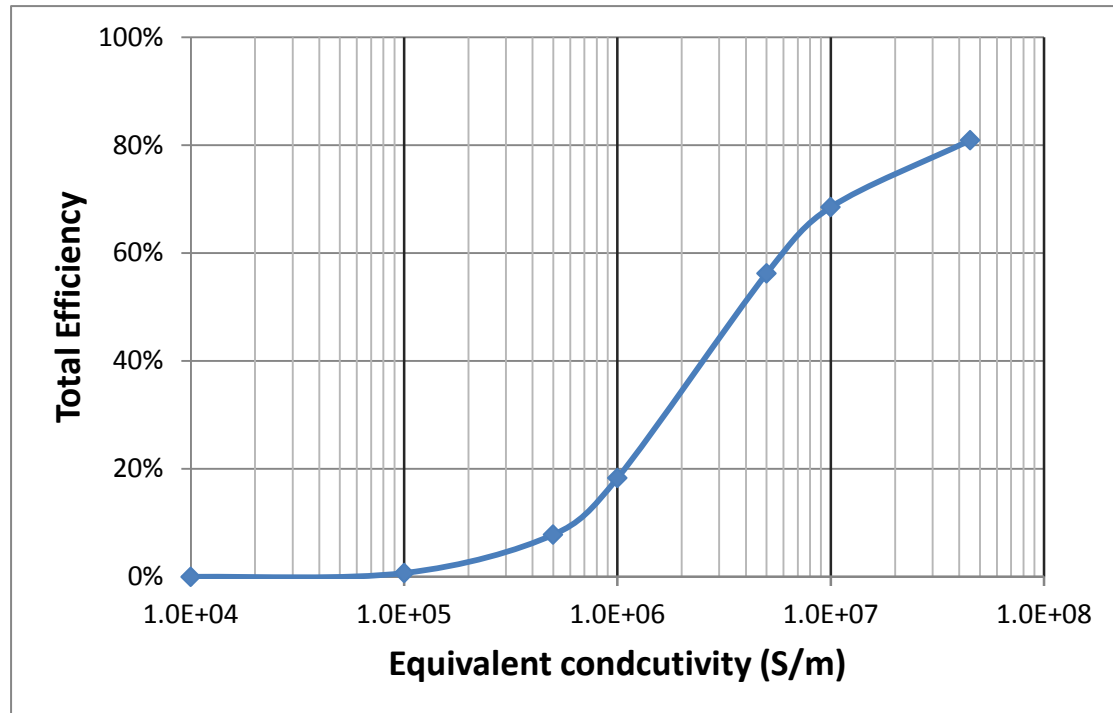
$$Q_d = \frac{1}{\tan \delta} \quad (4.11)$$

Where  $\sigma$  is the conductivity of the conductors and the  $\tan\delta$  is the loss tangent of the substrate. From (4.10) it can be seen that low conductivity of the conductors will increase the conduction loss and (4.11) indicates the dielectric loss is determined by the  $\tan \delta$  value of substrate.

In this chapter, since the embroidered patches and etched patch were placed on the same substrate, the major factor that resulted in low efficiency of embroidered antennas is the conduction loss. In Chapter 2, the metallization of conductive thread was observed approximately 1  $\mu\text{m}$ , and the conductivity of the Amberstrand Silver cladding layer is  $4.5 \times 10^7$  S/m. The reduced conductivity and thin metallization have significant effects on the antenna efficiencies. Figure 4-16 shows simulated total efficiencies of 1  $\mu\text{m}$  metallization continuous surface solid patch with different conductivity values.

The simulated results indicate that the patch antenna with an equivalent conductivity of  $2 \times 10^6$  S/m obtains 50% radiation efficiency which is the efficiency of 0.4 mm vertical embroidered patch antenna. The reduction of efficiency is more significant as the conductivity decreases. The equivalent conductivity value is lower than the calculated conductivity of silver cladding in Chapter 2 ( $4.5 \times 10^7$  S/m). Since the embroidered patch is a discontinuous surface and the adjacent stitches are not fully connected, the equivalent conductivity of the embroidered patch is lower than the silver cladding layer due to the non-uniform surface.





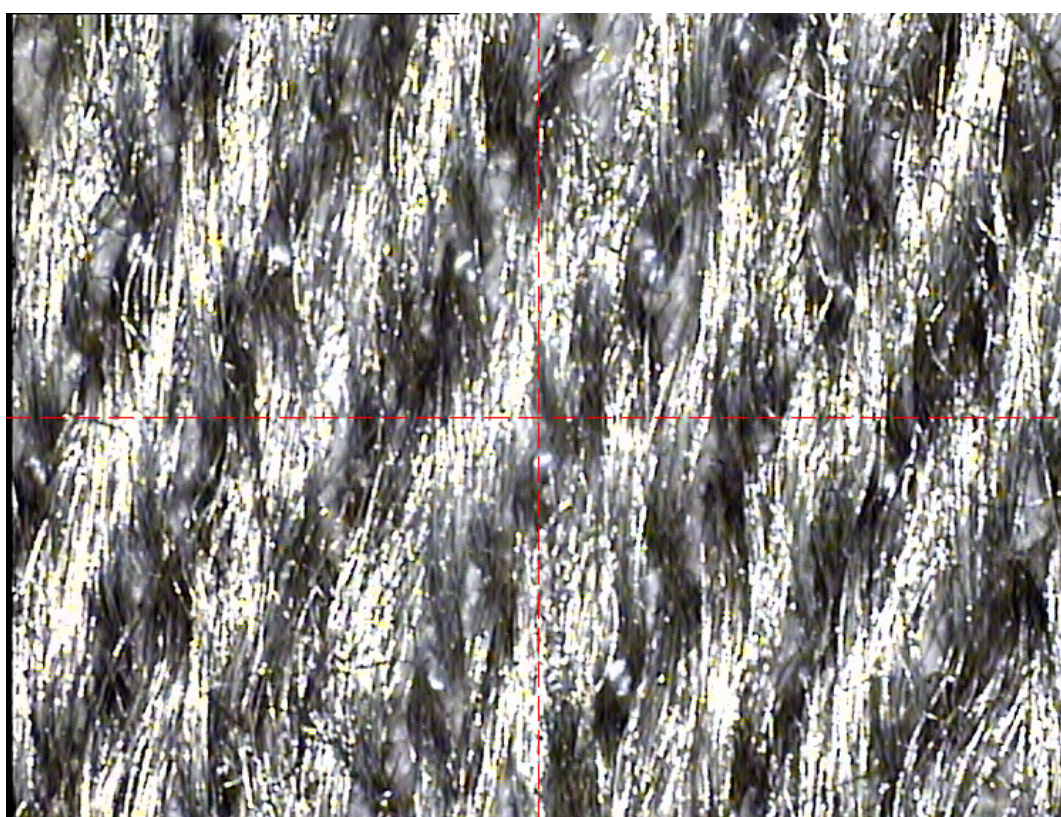
**Figure 4-16 Simulated solid patch total efficiency with different conductivity values**

However, the equivalent conductivity approach is not capable to illustrate the surface current flow on different stitch directions as the conductor surface in this method is continuous. The measured results in Section 4.3.2 showed that different stitch directions impact the resonant frequency and antenna efficiency of embroidered patch antennas. More details are needed to link the antenna performance with the surface current which is guided by the stitch direction.

#### **4.5.2 Anisotropic Microstrip Antennas with Zigzag Patterns**

The complicated anisotropic fibres in the fabric can cause unwanted higher modes and switch the fabric antenna to different frequencies. The polarisation purity is also influenced by the surface current distribution. It is essential to model and understand the interconnection between adjacent conductive threads of embroidered patches. Figure 4-17 shows the zoomed in picture of the air voids of a 0.4 mm spacing

Amberstrand Silver 166 embroidered patch. It clearly illustrates the conductive threads are aligned in the vertical direction with gaps between adjacent threads. DC resistance measurement in Section 4.2 indicated that the resistance in the vertical direction is much smaller than in the horizontal direction. It is believed that the current is guided by the stitch direction and it affects the antenna radiation performance. Consequently, the second approach of modelling embroidered patch antennas using a zigzag conductive line was introduced.

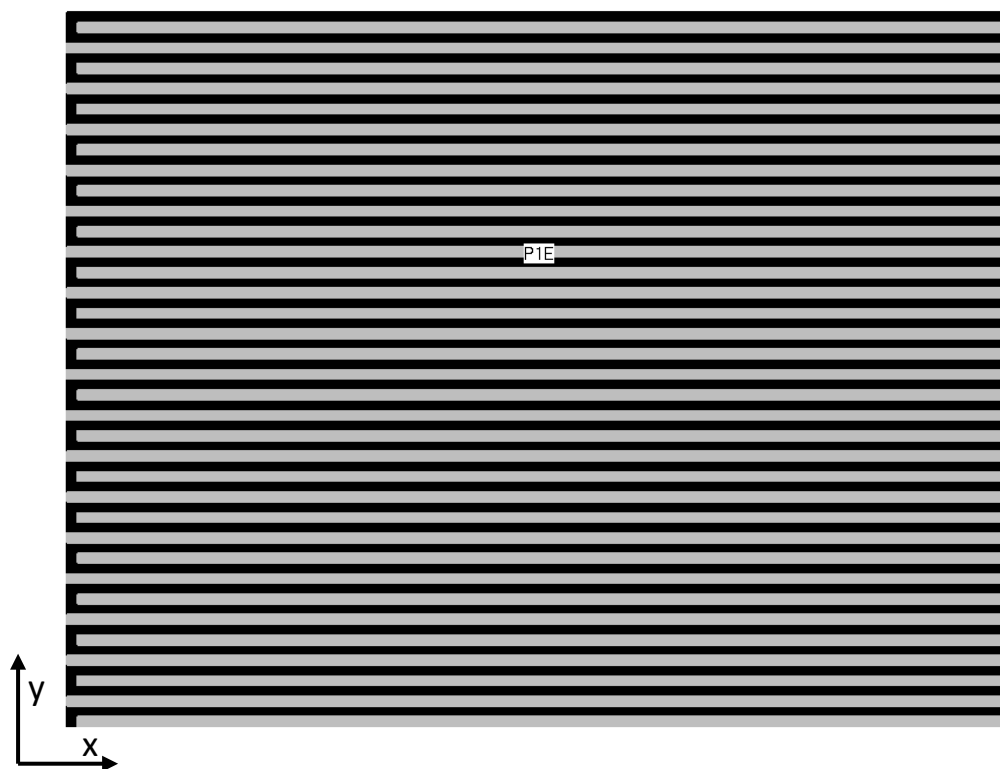


**Figure 4-17 Microscope image of 0.4 mm spacing vertically embroidered stitches (shinning parts are conductive threads)**

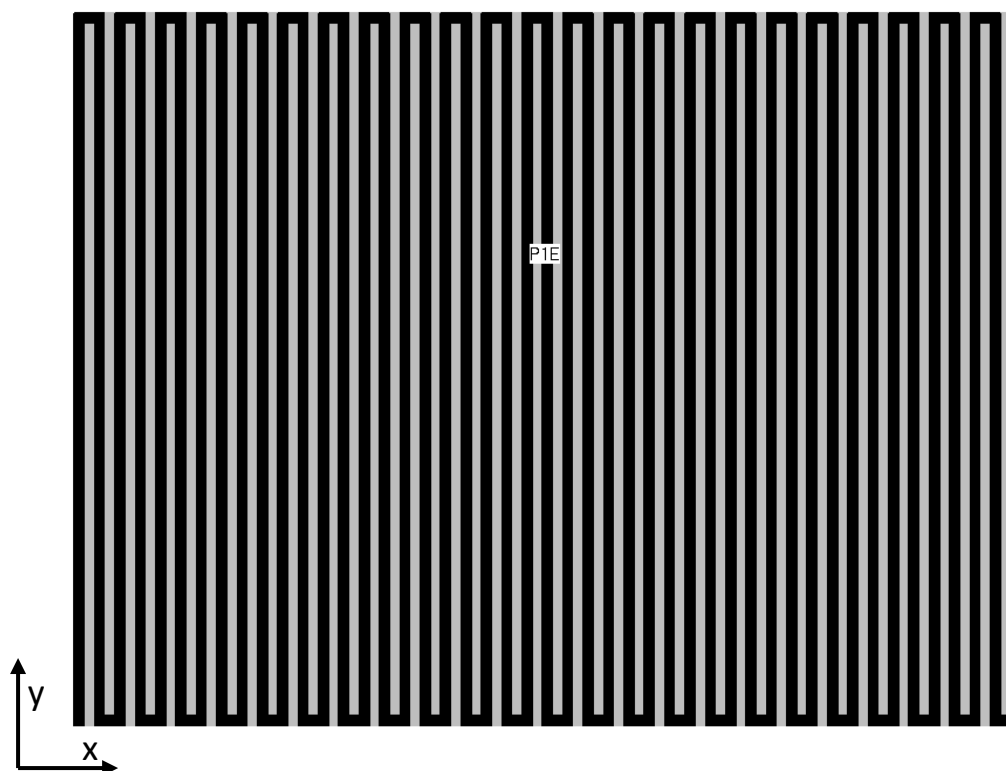
The second approach was to model a zigzag pattern which simulated the conductive thread across the patch area. This zigzag patch had the same dimension as the solid patch (38mm × 27 mm) and it was placed on the dielectric substrate with the same specifications. Then the lower conductivity strips were placed between the adjacent

threads to model the gap that was partly filled by contacted filaments. Figure 4-18 and Figure 4-19 show the zigzag structures of horizontal and vertical threads. It worth noting that without the lower conductivity material, the structure behaved like a meandered wire rather than a patch. A range of lower conductivity values have been considered to find out the contact resistances between the threads. The high and low conductivity threads filled the rectangular area of the patch. This is a simplified model as in reality the interconnection between the adjacent conductive threads is non-uniform or will vary due to the embroidery process. The metallization thicknesses of both high and low conductivity area are  $1\ \mu\text{m}$  which equals to the thickness of the metal cladding layer in Amberstrand Silver thread. The widths of the high conductivity threads and the low conductivity area were  $0.4\ \text{mm}$  and they were estimated from microscope images (see Figure 4-17). The sheet resistances of vertical zigzag patch and horizontal zigzag patch should be equal due to same widths of high and low conductivity areas. This approach represents the surface current on different zigzag directions which simulates the current on embroidered patch antennas.

The simulated S11 results for the zigzag modelling approach are shown in Figure 4-20 and Figure 4-21. In this simulation, the conductivity of the good conductor is used  $4.5 \times 10^7\ \text{S/m}$  which equals to estimated conductivity of the metal cladding on Amberstrand Silver (details can be seen in Chapter 2). The conductivity of the low conductivity “gaps” varies from  $1 \times 10^2\ \text{S/m}$  to  $4.5 \times 10^7\ \text{S/m}$ . Figure 4-20 indicates that with the horizontal zigzag good conductor, the conductivity of the low conductivity area “gaps” must be at least  $1 \times 10^6\ \text{S/m}$  to maintain the antenna resonant frequency at 2.4 GHz. On the other hand, Figure 4-21 shows that the low conductivity “gaps” in the vertical direction zigzag patch has to be larger than  $1 \times 10^3\ \text{S/m}$ . The S11 results show the losses are increased with the reduced conductivity of the “gaps”. It is worth noting that the skin depth with conductivity =  $1 \times 10^6\ \text{S/m}$  at 2.4 GHz is approximately  $10\ \mu\text{m}$  which is greater than the metallization.



**Figure 4-18 Horizontal zigzag metal conductor (black) separated by low conductivity “gaps” (grey), the ‘PIE’ indicates the feed position**



**Figure 4-19 Vertical zigzag metal conductor (black) separated by low conductivity “gaps” (grey), the ‘PIE’ indicates the feed position**

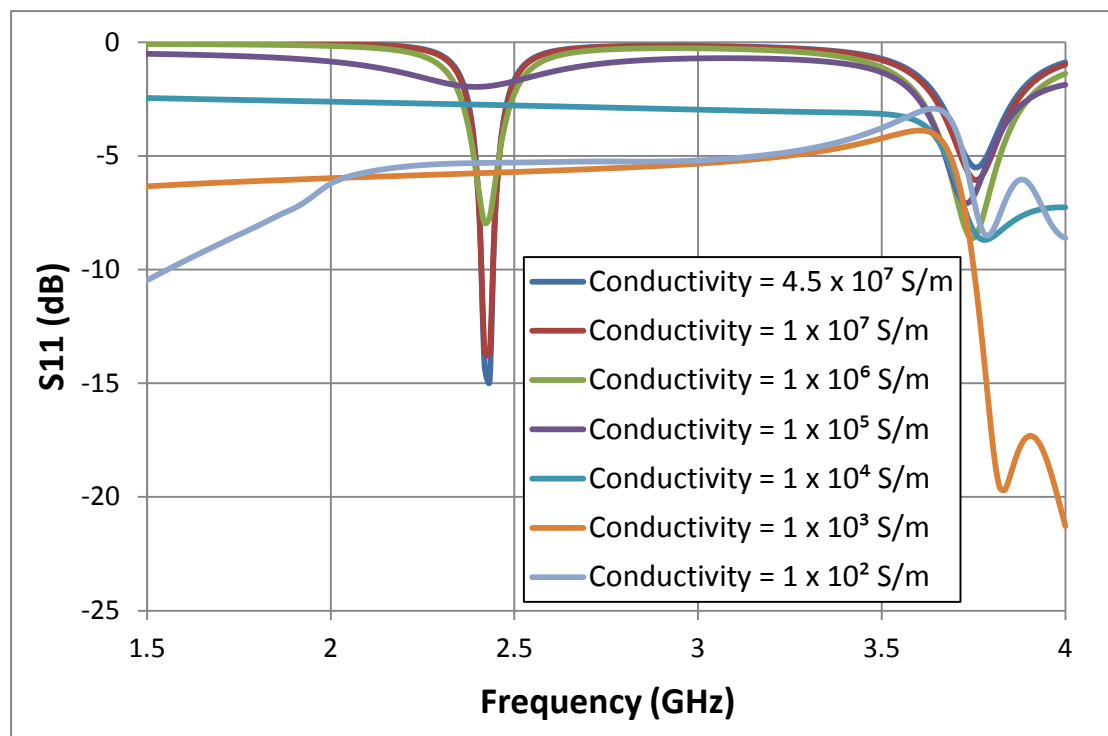


Figure 4-20 Simulated S11 for the patch with horizontal metal conductors separated by different conductivity values

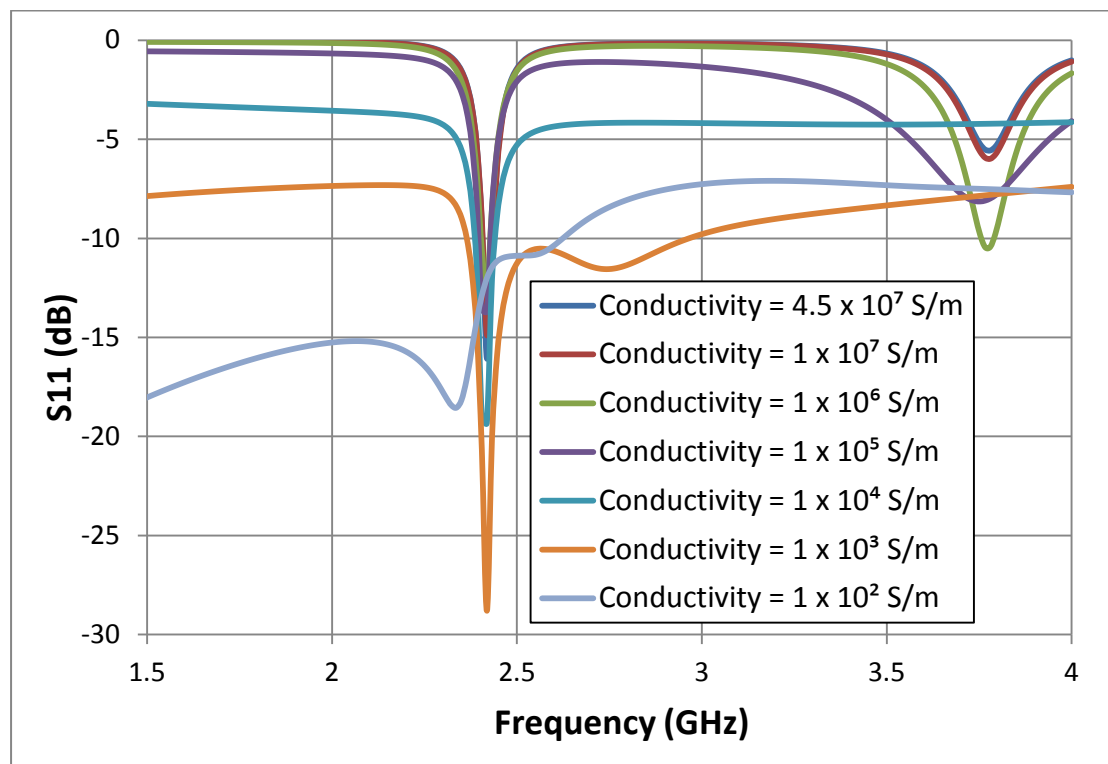


Figure 4-21 Simulated S11 for the patch with vertical metal conductors separated by different conductivity values

As shown in Figure 4-20 the conductivity value of the lower conductivity area must be at least  $1 \times 10^6$  S/m to make the horizontal zigzag patches function as antenna. The simulation of current distribution of conductivity lower than  $1 \times 10^6$  S/m will illustrate the effect of the low conductivity “gaps”. The different current patterns and current directions of the patches separated by  $1 \times 10^5$  S/m low conductivity area are shown in Figure 4-22 and Figure 4-23. It can be seen that the current on the horizontal conductors are more horizontally orientational than on the vertical conductors. The current distribution and directions on the patch with vertical conductors are very similar to the dominant mode of the solid rectangular patch antenna. The current distribution simulation results show that the low conductivity area “detours” the current. The current goes along the direction of good conductors and “bypass” the low conductivity area. This changes the impedance of the patch and increases the effective sheet resistance of the patch. The impact on the current is more significant for the patch with horizontal conductors which is orthogonal to the dominant current direction, which increases the conduction loss and results in increased losses. However, compared with the solid patch antenna, the S11 results indicate that the resonant frequency is not changed by the zigzag threads. Furthermore, the resonant frequencies of zigzag patches are not changed by different conductivity values of the “gaps”. This is different from the measurement results in Section 4.3 and 4.4 which show that the larger stitch spacing results in lower resonant frequency. Therefore, the lower conductivity area which simulates the connected adjacent threads by loose filaments is not the case in real embroidered antennas. The nonconductive air voids between adjacent threads will reduce the resonant frequency. Further analysis will be discussed in Chapter 5.



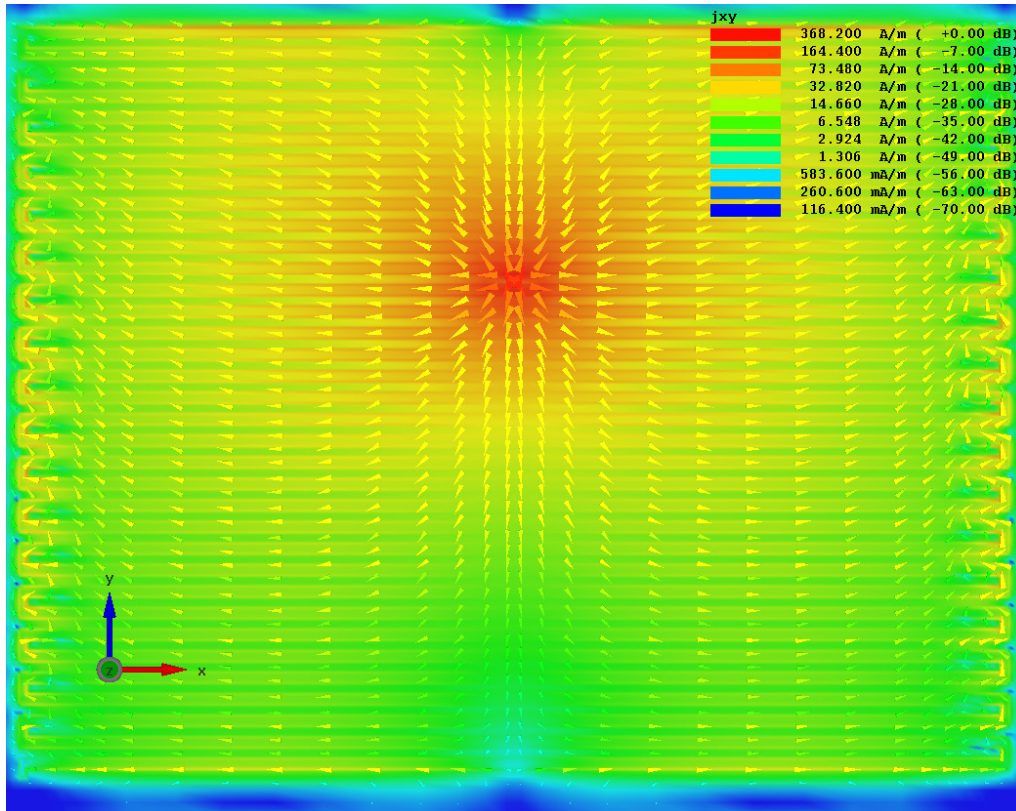


Figure 4-22 Simulated surface currents for zigzag patch with horizontal conductors separated by a conductivity of  $1 \times 10^5$  S/m

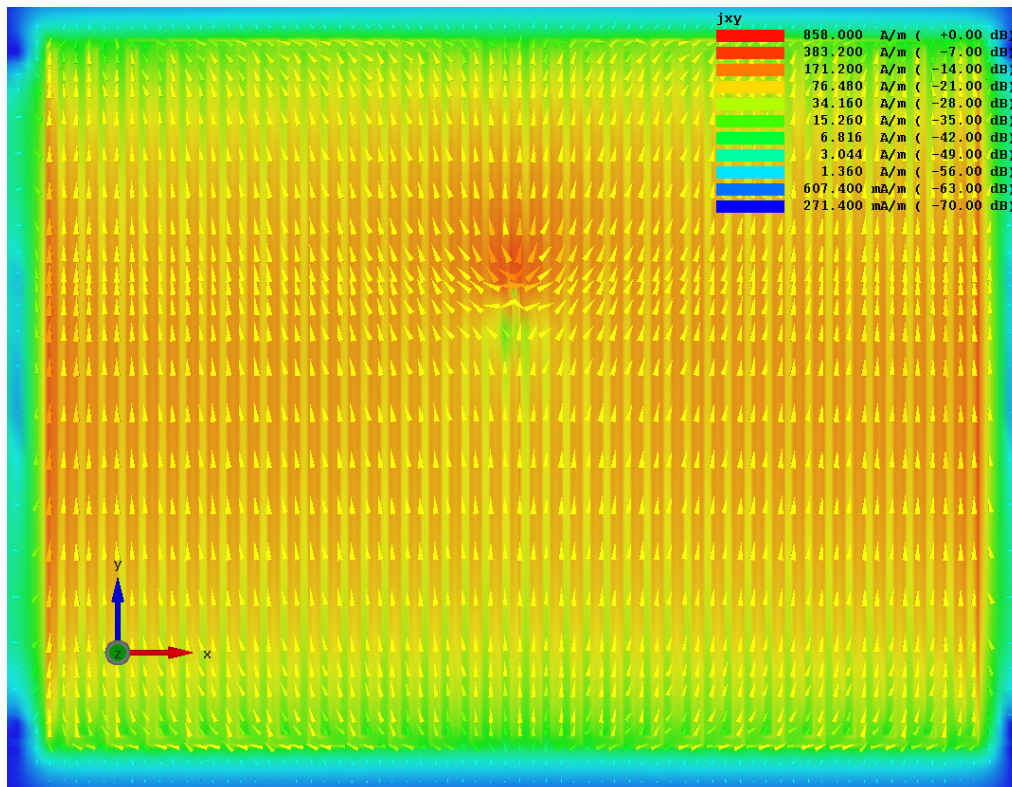


Figure 4-23 Simulated surface currents for zigzag patch with vertical conductors separated by a conductivity of  $1 \times 10^5$  S/m

The simulated total efficiencies of the solid, horizontally zigzag and vertically zigzag patch antennas with different conductivity values are shown in Figure 4-24. For the zigzag patches, only the conductivity values of the ‘gaps’ are changed, the conductivity of the zigzag metal threads is constant ( $4.5 \times 10^7$  S/m) and higher than the “gaps”. Figure 4-24 indicates that lower conductivity reduces the antenna efficiency. As shown with the solid patch, the equivalent conductivity has a direct effect on the antenna efficiency. The results show that the zigzag patches have higher efficiencies than the homogeneous solid patch with the conductivity equals to the “gaps” of zigzag patches. The higher conductivity “fibres” yield a lower equivalent surface resistance than the solid patch and reduce the conduction loss of the zigzag patches. For the same high and low conductivity area ratio, the vertical zigzag outperforms the horizontal zigzag antennas. This agrees with the measured results in Section 4.3. The measured efficiencies of 0.4 mm vertical and horizontal embroidered patches are 52.5% and 15.4% respectively. According to the simulated results, the conductivity of 0.4 mm spacing gap is approximately from  $3 \times 10^4$  S/m to  $2 \times 10^5$  S/m.

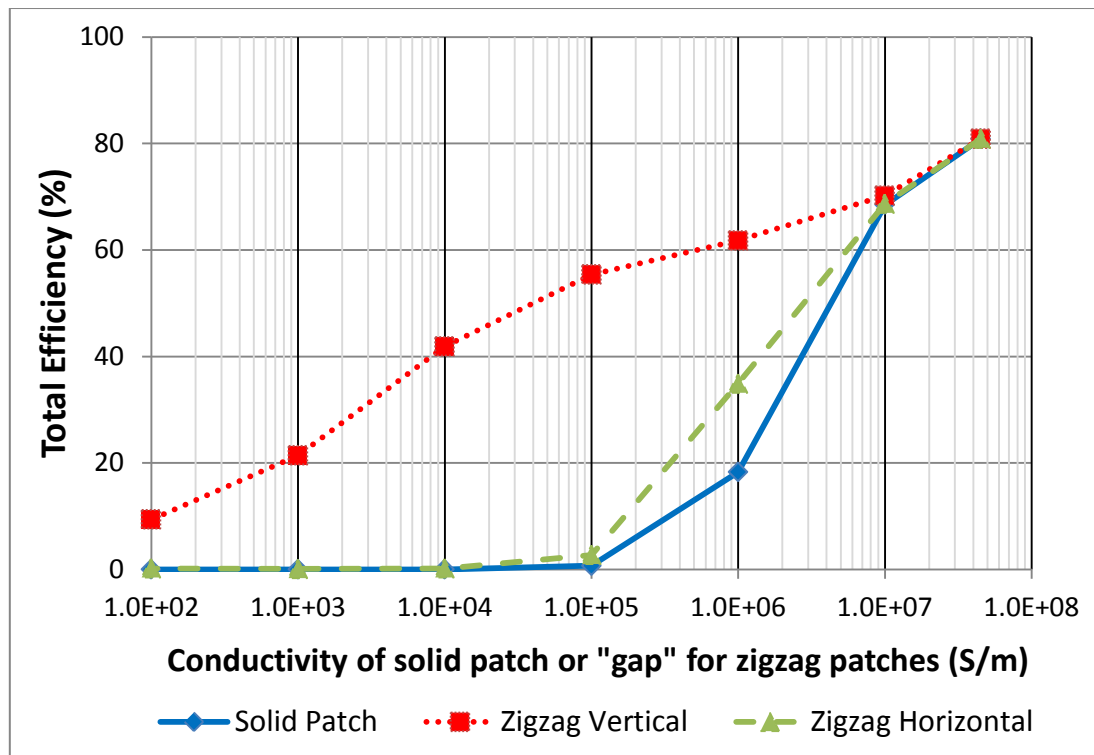


Figure 4-24 Simulated patch total efficiency for the zigzag patches with low conductivity area compared with homogeneous solid patch antenna with equivalent conductivity



Consequently, this simplified model indicates that the embroidered patch antenna performance is majorly determined by the direction of the stitches. The low conductivity area can represent the connection between adjacent stitches and closer stitches have better connection between each other. The conclusions from simulated results lead to a requirement for a calculation of effective conductivities that takes the stitch direction and the stitch spacing into account.

## **4.6 Conclusions**

This chapter has focused on the issues arising from the fabrication of fabric based antennas using embroidery technology. Microstrip patch antennas were considered here although many other antennas will also play roles in fabric and flexible systems. The results presented in this chapter point to the feasibility and practicality of manufacturing the fabric based antennas by embroidery. The Amberstrand Silver embroidered patch antennas on the conventional dielectric substrate with copper ground plane have been measured to show an efficiency of 52.5%, compared to 80% for an equally dimensioned copper patch antenna.

The surface resistances of embroidered patches with different stitch directions and spacings were examined by the two-electrode method measurement, and it indicated that the surface resistances are significantly influenced by the stitch direction. This approach can be used as a quick indicator for the sheet resistance of embroidered stitches. Embroidered patch antennas with low sheet resistance in the direction of major current of dominant mode will have higher antenna efficiency.

The antenna measurements reinforce the conclusions being drawn from of the DC results with respect to stitch spacing and direction. Stitch spacing has an effect on

antenna efficiency and the challenge is to balance the required performance with the cost of fabricating the antennas. Currently, Amberstrand Silver 66 costs approximately £1 per metre. High quantity production and development in the manufacture techniques may reduce these costs. A patch antenna in this chapter with 0.4 mm stitch spacing and vertical stitch direction contains approximately 4 m of conductive thread.

In this chapter, efficiencies of embroidered patch antennas with different stitch spacing and direction were measured. The embroidered patch with 0.4 mm stitch spacing and stitch direction parallel to current direction at dominant mode has the highest antenna efficiency of 52.5% which is 27.9% lower than the same dimension etched copper patch antenna at the corresponding dominant mode frequency. The efficiency of the 0.4 mm stitch spacing with stitch perpendicular to dominant mode current direction patch is 15% lower than the parallel stitched patch with the same stitch spacing. Both of the parallel and perpendicular embroidered patches can obtain better than 20 dB polarisation purity. The diagonal stitch direction antenna with 0.4 mm stitch spacing shows a 30% efficiency with polarisation purity of approximately 9 dB. The diagonal stitches results in vertical and horizontal directed current component which produced the high cross polar content. It is preferred that the stitch direction is parallel to the major current flow direction at the frequency of the desired radiation mode. Therefore, the current direction and stitch direction should be taken into account when embroidering antennas.

The repeatability study was carried out to investigate the variation of the fabrication parameters. The results show that deviation of the antenna resonant frequency is larger with smaller stitch spacing. The enlarged stitch spacing lowers the antenna resonant frequency. The bandwidths of the embroidered antennas are wider than the etched copper patch, and closer stitches offers higher antenna gain. Patches with smaller stitch spacings have better repeatability of gain and efficiency. The repeatability results also

confirmed that embroidered patch antennas with smaller stitch spacing have better polarization purity and denser stitches have less effect on the surface current path.

Simulations using simple simplified models of the embroidered threads have been presented. The patch antenna was modelled as a continuous zigzag good conductor separated by lower conductivity sections. The low conductivity area represents the interconnection between adjacent threads. The simulation of surface current distribution on horizontal zigzag tracks indicates that the current preferentially follows the actual fibres directions rather than jumps across the low conductivity “gaps”. This simulation model confirmed the measured results which indicate that the thread should be aligned with the dominant current flow for the optimal results.

## References

- [1] B. Gupta, S. Sankaralingam, and S. Dhar, “Development of wearable and implantable antennas in the last decade: A review,” in *10th Mediterranean Microwave Symposium*, 2010, pp. 251–267.
- [2] N. H. M. Rais, P. J. Soh, F. Malek, S. Ahmad, N. B. M. Hashim, and P. S. Hall, “A review of wearable antenna,” in *Loughborough Antennas & Propagation Conference (LAPC)*, 2009, pp. 225–228.
- [3] T. Kennedy, P. Fink, and A. Chu, “Body-worn e-textile antennas: The good, the low-mass, and the conformal,” *IEEE Transactions on Antennas and Propagation*, vol. 57, no. 4, pp. 910–918, 2009.
- [4] J. C. G. Matthews and G. Pettitt, “Development of flexible, wearable antennas,” in *3rd European Conference on Antennas and Propagation (EuCAP)*, 2009, pp. 273–277.
- [5] P. S. Hall and Y. Hao, *Antennas and propagation for body-centric wireless communications*. London, UK: Artech House, 2012.
- [6] J. Lilja, P. Salonen, T. Kaija, and P. de Maagt, “Design and Manufacturing of Robust Textile Antennas for Harsh Environments,” *IEEE Transactions on Antennas and Propagation*, vol. 60, no. 9, pp. 4130–4140, Sep. 2012.
- [7] C. Hertleer, H. Rogier, L. Vallozzi, and L. Van Langenhove, “A Textile Antenna for Off-Body Communication Integrated Into Protective Clothing for Firefighters,” *IEEE Transactions on Antennas and Propagation*, vol. 57, no. 4, pp. 919–925, Apr. 2009.
- [8] P. G. Elliot, E. N. Rosario, B. Rama Rao, R. J. Davis, and N. M. Marcus, “E-textile microstrip patch antennas for GPS,” in *Position Location and Navigation Symposium (PLANS), IEEE/ION*, 2012, pp. 66–73.

- [9] S. Manzari, C. Occhiuzzi, and G. Marrocco, “Feasibility of Body-Centric Systems Using Passive Textile RFID Tags,” *IEEE Antennas and Propagation Magazine*, vol. 54, no. 4, pp. 49–62, Aug. 2012.
- [10] L. Zhang, Z. Wang, and J. L. Volakis, “Textile Antennas and Sensors for Body-Worn Applications,” *IEEE Antennas and Wireless Propagation Letters*, vol. 11, pp. 1690–1693, 2012.
- [11] E. Kaivanto, J. Lilja, M. Berg, E. Salonen, and P. Salonen, “Circularly polarized textile antenna for personal satellite communication,” in *Proceedings of the Fourth European Conference on Antennas and Propagation (EuCAP)*, 2010, pp. 1–4.
- [12] J. Choi, Y. Kim, K. Lee, and Y. C. Chung, “Various wearable embroidery RFID tag antenna using electro-thread,” in *IEEE Antennas and Propagation Society International Symposium*, 2008, pp. 1–4.
- [13] L. Ukkonen, L. Sydanheimo, and Y. Rahmat-Samii, “Sewed textile RFID tag and sensor antennas for on-body use,” in *6th European Conference on Antennas and Propagation (EuCAP)*, 2012, pp. 3450–3454.
- [14] Z. Wang, L. Zhang, D. Psychoudakis, and J. L. Volakis, “GSM and Wi-Fi textile antenna for high data rate communications,” in *Proceedings of the IEEE International Symposium on Antennas and Propagation*, 2012, vol. 3, pp. 1–2.
- [15] S. Zhang, A. Chauraya, W. Whittow, R. Seager, T. Acti, T. Dias, and Y. Vardaxoglou, “Embroidered wearable antennas using conductive threads with different stitch spacings,” in *Loughborough Antennas & Propagation Conference (LAPC)*, 2012, pp. 1–4.
- [16] Z. Wang, L. Zhang, Y. Bayram, and J. L. Volakis, “Embroidered e-fiber-polymer composites for conformal and load bearing antennas,” in *IEEE Antennas and Propagation Society International Symposium*, 2010, pp. 1–4.

- [17] T. Maleszka and P. Kabacik, “Bandwidth properties of embroidered loop antenna for wearable applications,” in *European Wireless Technology Conference (EuWIT)*, 2010, pp. 89–92.
- [18] L. Zhang, Z. Wang, D. Psychoudakis, and J. L. Volakis, “E-fiber electronics for body-worn devices,” in *6th European Conference on Antennas and Propagation (EuCAP)*, 2012, pp. 760–761.
- [19] Z. Wang, L. Zhang, Y. Bayram, and J. L. Volakis, “Embroidered Conductive Fibers on Polymer Composite for Conformal Antennas,” *IEEE Transactions on Antennas and Propagation*, vol. 60, no. 9, pp. 4141–4147, Sep. 2012.
- [20] J. L. Volakis, L. Zhang, Z. Wang, and Y. Bayram, “Embroidered flexible RF electronics,” in *IEEE International Workshop on Antenna Technology (iWAT)*, 2012, pp. 8–11.
- [21] Z. Wang, L. Zhang, D. Psychoudakis, and J. L. Volakis, “Flexible textile antennas for body-worn communication,” in *IEEE International Workshop on Antenna Technology (iWAT)*, 2012, vol. 4, pp. 205–208.
- [22] E. Moradi, T. Bjorninen, L. Ukkonen, and Y. Rahmat-Samii, “Effects of Sewing Pattern on the Performance of Embroidered Dipole-Type RFID Tag Antennas,” *IEEE Antennas and Wireless Propagation Letters*, vol. 11, pp. 1482–1485, 2012.
- [23] K. Koski, E. Koski, T. Björninen, A. A. Babar, L. Ukkonen, L. Sydanheimo, and Y. Rahmat-Samii, “Practical read range evaluation of wearable embroidered UHF RFID tag,” in *Proceedings of the IEEE International Symposium on Antennas and Propagation*, 2012, pp. 1–2.
- [24] T. Acti, S. Zhang, A. Chauraya, W. Whittow, R. Seager, T. Dias, and Y. Vardaxoglou, “High performance flexible fabric electronics for megahertz frequency communications,” in *Loughborough Antennas & Propagation Conference (LAPC)*, 2011, pp. 1–4.

- [25] Y. Ouyang and W. Chappell, "Measurement of electrotiles for high frequency applications," in *IEEE MTT-S International Microwave Symposium Digest*, 2005, pp. 1679–1682.
- [26] I. Locher, M. Klemm, and T. Kirstein, "Design and characterization of purely textile patch antennas," *IEEE Transactions on Advanced Packaging*, vol. 29, no. 4, pp. 777–788, 2006.
- [27] Y. Ouyang and W. J. Chappell, "High frequency properties of electro-textiles for wearable antenna applications," *Antennas and Propagation, IEEE Transactions on*, vol. 56, no. 2, pp. 381–389, 2008.
- [28] J. Azoulay, "Anisotropy in electric properties of fabrics containing new conductive fibers," *IEEE Transactions on Electrical Insulation*, vol. 23, no. 3, pp. 383–386, Jun. 1988.
- [29] J. Banaszczyk, G. De Mey, A. Schwarz, and L. Van Langenhove, "Current Distribution Modelling in Electroconductive Textiles," in *14th International Conference on Mixed Design of Integrated Circuits and Systems*, 2007, pp. 418–423.
- [30] V. Der Pauw, "A method of measuring specific resistivity and Hall effect of disc of arbitrary shape," *Philips Research Reports*, vol. 13, pp. 1–9, 1958.
- [31] I. Kazani, G. De Mey, C. Hertleer, J. Banaszczyk, A. Schwarz, G. Guxho, and L. Van Langenhove, "Van Der Pauw method for measuring resistivities of anisotropic layers printed on textile substrates," *Textile Research Journal*, vol. 81, no. 20, pp. 2117–2124, Sep. 2011.
- [32] A. Chauraya, S. Zhang, W. Whittow, T. Acti, R. Seager, T. Dias, and Y. C. Vardaxoglou, "Addressing the challenges of fabricating microwave antennas using conductive threads," in *6th European Conference on Antennas and Propagation (EuCAP)*, 2012, pp. 1365–1367.
- [33] C. A. Balanis, *Antenna Theory: Analysis and Design*, 3rd ed. New York: Wiley, 2005.

- [34] P. B. R. Garg Inder Bahl, A. Ittipiboon, *Microstrip Antenna Design Handbook*. Norwood: Artech House Antennas and Propagation Library, 2000.
- [35] A. Chauraya, T. West, R. Seager, W. Whittow, S. Zhang, and Y. Vardaxoglou, “Positioner Effects in Measurements of Low-Medium Gain Antennas,” in *Antenna Measurement Techniques Association Annual Symposium*, 2013.



# Chapter 5

## Meshed Microstrip Antennas

---

### Abstract

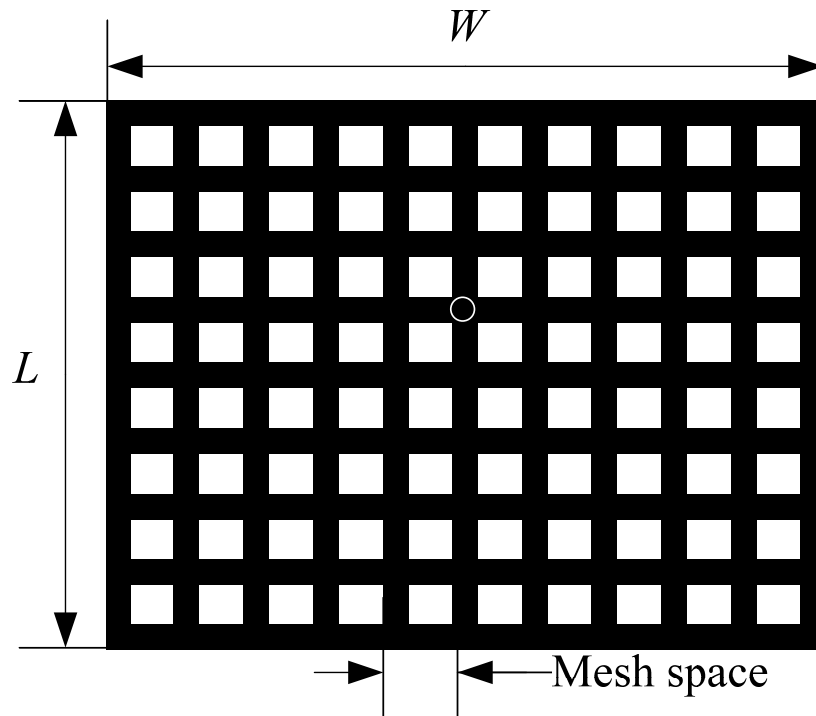
In this chapter, the meshed microstrip antennas which can potentially save a large amount of conductive materials for antenna fabrication is presented. The metal coverage can be further reduced by using non-uniform meshes which will be shown in Section 5.2. The simulations including surface current distribution, antenna mode analysis, antenna gain and efficiency of the meshed patches will be represented in Section 5.3. The meshed patch antenna has comparable gain to the solid patch but with much lower metal coverage. The factors affecting the loss of the meshed patch antennas will be discussed in Section 5.5 and the solutions for improving antenna efficiencies of the meshed patch antennas will be presented. Representative measurements have been carried out for verifying the simulations, the results will be shown in Section 5.6. The skin effect on the embroidered patch antennas due to the thin metallization of conductive thread will be analysed in Section 5.7. Embroidered meshed patch antennas on the flexible fabric substrate with improved antenna efficiency will be presented in Section 5.8.

### 5.1 Introduction

The conductive layers of patch antennas can be created on the fabric surface by flexible conductive materials and there are several methods to attach the conductive materials on normal fabric clothes permanently such as embroidery [1]–[3] and inkjet printing [4]–[6]. However the cost of these specialist materials is expensive. For

instance the cost of conductive thread Amberstrand Silver 66 is approximately £1 per meter. Depending on the stitch spacing, a 2.4 GHz 37 mm × 28 mm rectangular patch antenna may require 6.6 meters of conductive thread for 100% coverage, and therefore it will be over £6.6 per antenna for the material cost alone. Reducing the price of manufacturing textile antennas will boost the development of wearable technology. Meshing the patch antennas reduces the material requirements and therefore lowers the costs. Furthermore, the meshed patch is more flexible than a solid patch where the surface is completely covered.

Meshed patch antennas originally attracted the researchers' attentions due to its optically transparency [7]–[11]. They are composed of numerous crossed orthogonal parallel lines, and the apertures are distributed on the surface uniformly. The metal structure is shown in Figure 5-1 (the mesh space and line width vary by design). When the transparent substrate is used, the whole microstrip patch antenna is see-through. Clasen *et al.* analysed the surface current distribution of uniform meshed patch antennas [12]. The current flows in both vertical and horizontal directions and it has similar performance as the conventional rectangular patch antenna. It was observed that the current path is longer on the meshed structures than on the solid patches and therefore the resonant frequency of the meshed patch antenna is lower than the same size solid patch antenna [12], [13].



**Figure 5-1 Sketch of uniform meshed patch structure**

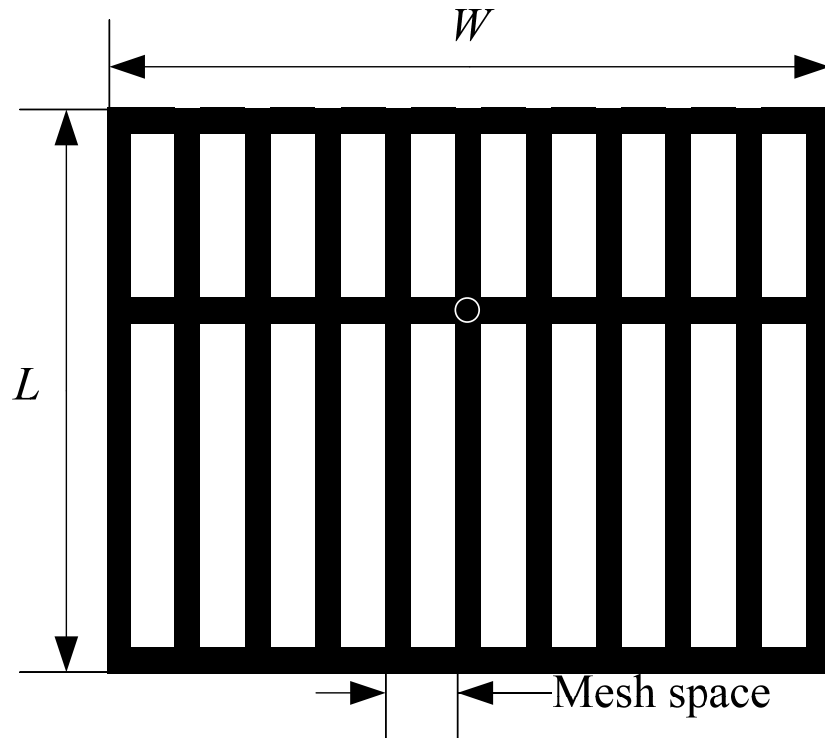
The effect of the meshes on resonant frequency of meshed patch antenna is similar to slots in slotted microstrip antennas. The slotted patch antennas generally have another lower resonant frequency which widens the antenna bandwidth or create dual-band patch antennas [14]–[17]. Hofer indicated that a narrow transverse slot in the transmission line can be treated as adding a series inductor [18]. This method can also be used for analysing the effect of the slots in microstrip antennas [19]. The currents travel around the slots or the mesh holes and have longer electrical length. As the microstrip patch antenna can be modelled as  $LC$  resonant circuit [20], the extended electrical length due to the slots or the meshes increases the inductance and results in lower resonant frequency.

However, compared with the slot patch antenna, the frequency shift of meshed patch antenna is less significant. This is because there are no cut slots in the edges of the patch. Patch antennas has strong electric fields on the radiation edges and highest current density on non-radiating edges. The complete structure of these edges

maintains the radiation behaviours such as resonant frequency and antenna modes. Furthermore, the uniform meshed patch is divided into a number of small square segments by the mesh lines. Each segment is framed by the four mesh lines. These segments are distributed evenly on the patch surface. As a result the surface current direction on uniform meshed patch is similar to the solid patch.

## 5.2 Non-Uniform Meshed Microstrip Antennas

It is known that at  $TM_{01}$  mode the current distribution on the rectangular patch antenna is mainly dominated by the vertical direction current with the feed indicated in Figure 5-1. As shown in Chapter 4, with the same ratio of high and low conductivity area, the vertical zigzag patch has higher antenna efficiency than the horizontal zigzag patch. Therefore the vertical conductor paths are more important than the horizontal paths for the  $TM_{01}$  mode. A non-uniform meshed patch was designed based on this concept. The structure is shown in Figure 5-2. The number of vertical lines is the same as for the meshed patch in Figure 5-1. However there are only three horizontal lines: two along the top and bottom, and the third line crosses the feed point and creates a path that allows current flow from feed point into the vertical lines. Due to the reduction of the horizontal lines, this non-uniform meshed patch minimises the usage of the conductive materials, and it is more flexible than the uniform meshed patch. In Chapter 4, the low conductivity “gaps” reduces the antenna efficiency but does not change the antenna resonant frequency [21]. However for the uniform and non-uniform meshed patches, the conductive lines are separated by nonconductive gaps, i.e. air. As a result, the resonant frequency of the meshed patch antenna is affected by the mesh space between mesh lines. In this chapter the mesh space includes the width of the mesh line, shown in Figure 5-2.



**Figure 5-2 Sketch of non-uniform meshed patch structure**

The metal coverage of a solid 2.4 GHz, 37 mm  $\times$  28 mm rectangular patch antenna is 1036 mm<sup>2</sup>. Figure 5-3 shows the trend of reducing the surface metal coverage by increasing the mesh space. The uniform meshed patch has the same spacing between the horizontal and vertical lines. 0.2 mm width lines were applied on both the vertical and horizontal mesh lines. It is clear that the metal coverage is reduced significantly with enlarged mesh size. For instance, the solid patch surface area is 1036 mm<sup>2</sup> and the coverage can be reduced to 82 mm<sup>2</sup> if the 4 mm spacing non-uniform mesh is employed. Furthermore, the non-uniform meshed patch requires less metal coverage than the same sized uniform meshed patches due to fewer horizontal lines. This figure demonstrates the area reduction and lower cost by using the non-uniform mesh with three horizontal lines.

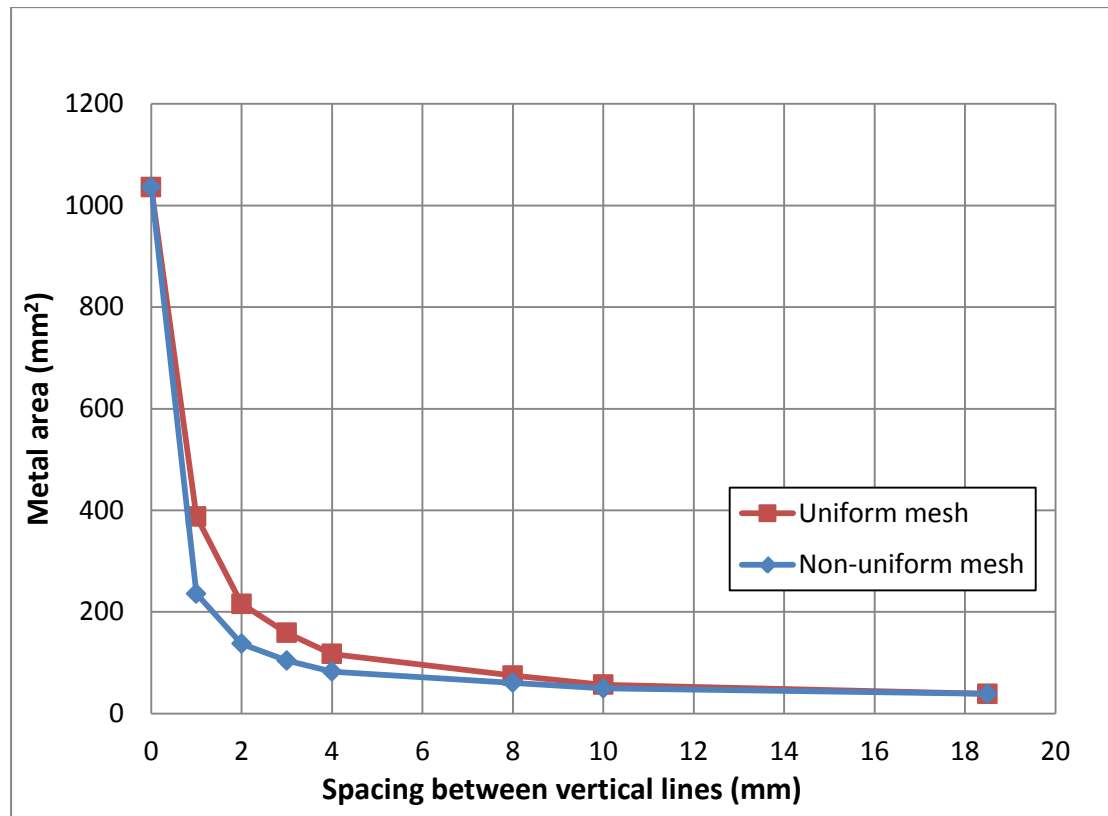


Figure 5-3 Metal coverage of meshed patch with different mesh sizes

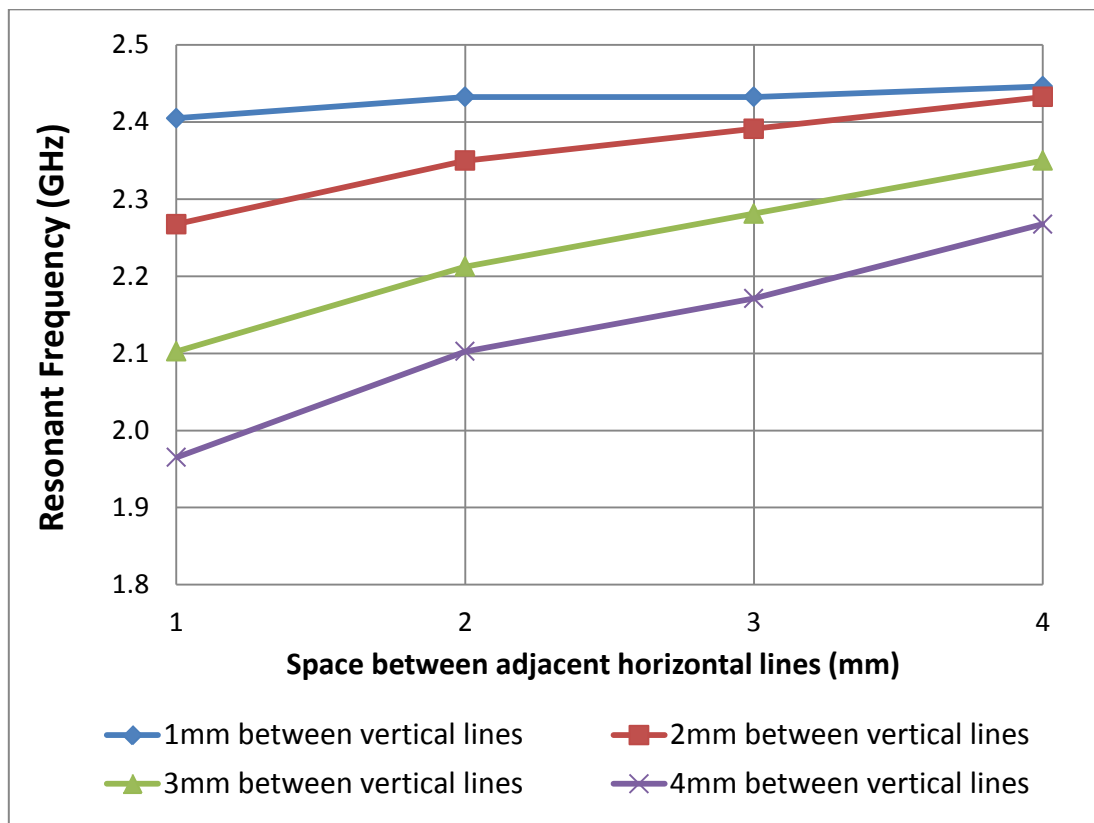
## 5.3 Antenna Modes and Surface Current Distribution

### 5.3.1 Resonant Frequency of Meshed Microstrip Antennas

Previous research only showed that the resonant frequency of meshed patch antenna was reduced by increasing the horizontal and vertical mesh space with fixed ratio [12], [13]. In other words, only the uniform meshed patch antennas were discussed. In fact, the influences of vertical lines and horizontal lines on the resonant frequency of meshed patch antennas are different. More precisely, larger space between vertical lines reduces the resonant frequency of the meshed patch antenna, larger space between horizontal lines, per contra, increases the resonant frequency. Figure 5-4 shows the simulated results of the resonant frequencies with different mesh sizes of uniform meshed patches. The exterior dimensions of all the patches are equal ( $W =$

37 mm and  $L = 28$  mm). The  $x$  axis in Figure 5-4 represents the distance between adjacent horizontal lines, from 1 mm to 4 mm. The four curves represent the increased resonant frequency with larger distances between vertical lines. In this simulation, as the exterior dimensions of the patches are fixed, the greater distance between adjacent lines means fewer mesh lines.

Figure 5-4 indicates that with the same space between horizontal lines, larger spaces between vertical lines lead to lower resonant frequency. By contrast, with the same space between vertical lines, larger space between horizontal lines increases the resonant frequency. Therefore, it can be concluded that the non-uniform meshed patch antennas have higher resonant frequency than the uniform meshed patch antennas with the same horizontal mesh spaces.



**Figure 5-4 Simulation of changes in resonant frequency with different mesh sizes of uniform meshed patch antennas**

To analyse the effect of the mesh spaces on the resonant frequency of the meshed patch antennas, the uniform meshed and non-uniform meshed patch antennas with different horizontal mesh spaces were simulated. The mesh cells in the uniform meshed patch are square. The same exterior dimension solid patch antenna was simulated for a comparison. All the patches were placed on solid dielectric substrates with solid copper ground planes. The dielectric constant of the substrate is 4.5, loss tangent equals to 0.0037, and the thickness is 1.57 mm. The outline dimensions of all the patches are 37 mm  $\times$  28 mm. The ground plane is 90 mm  $\times$  70 mm solid copper. Metallization thicknesses of all the patches are 0.01 mm. The solid copper patch with this dimension works at 2.43 GHz. For the meshed patches, the mesh line width was set to 0.2 mm which approximately equalled to the width of the flattened embroidered Amberstrand Silver 66 threads.

The simulation results demonstrate that the resonant frequency of the uniform meshed patch antenna is determined by the mesh size. The reduced resonant frequencies with larger mesh sizes are shown in Figure 5-5. The black curve in Figure 5-5 is the S11 of the solid patch which has the highest resonant frequency.

Figure 5-6 shows the S11 results of non-uniform meshed patch antennas. It proves that the resonant frequency of non-uniform meshed patch is also decreased by larger mesh space. It also shows that the non-uniform meshed patch has higher resonant frequency than the uniform meshed patch with the same mesh space. In addition, it can be seen that when the mesh space is smaller than 3 mm, the resonant frequencies of non-uniform meshed patches are very close to the solid patch. The variation is less than 20 MHz. When the mesh space increases to 4 mm, the variation is approximately 60 MHz. Therefore, the resonant frequencies of non-uniform meshed patches are closer to the same sized solid patch than the uniform meshed patch with the same horizontal mesh space.



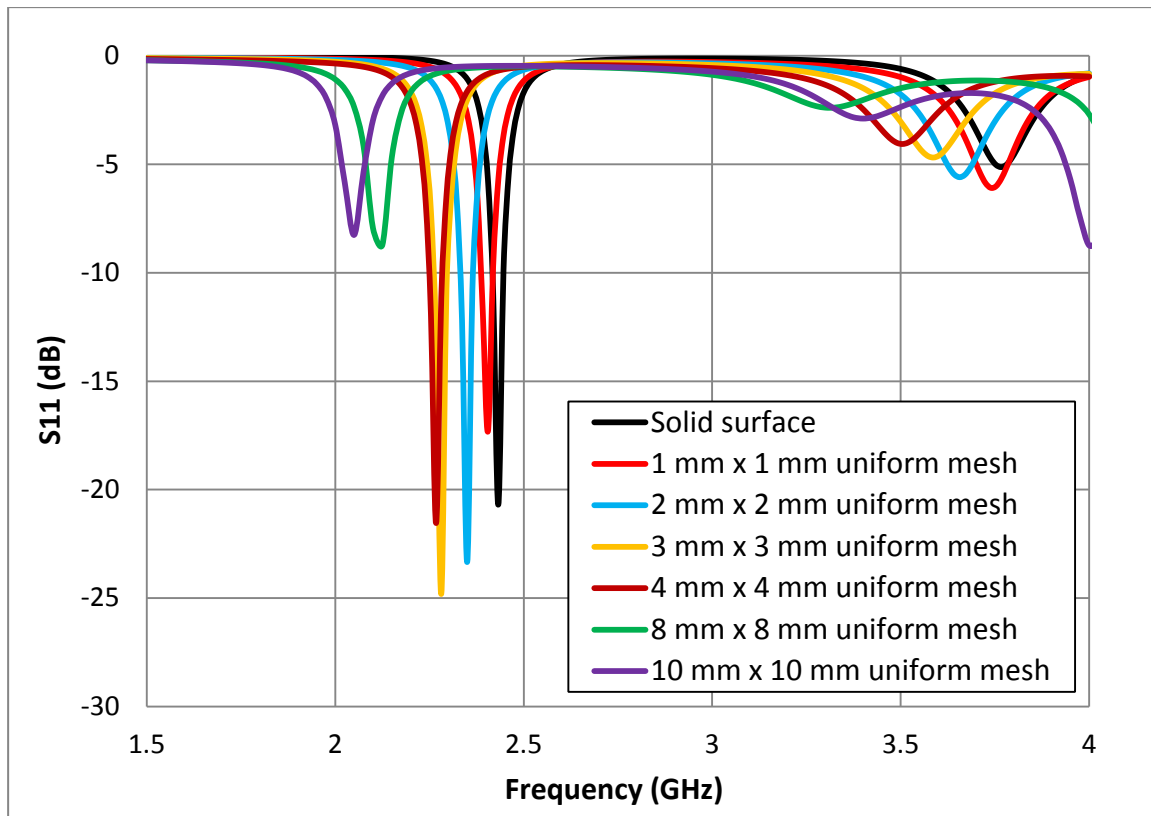


Figure 5-5  $S_{11}$  of uniform meshed patch antennas with different mesh spaces

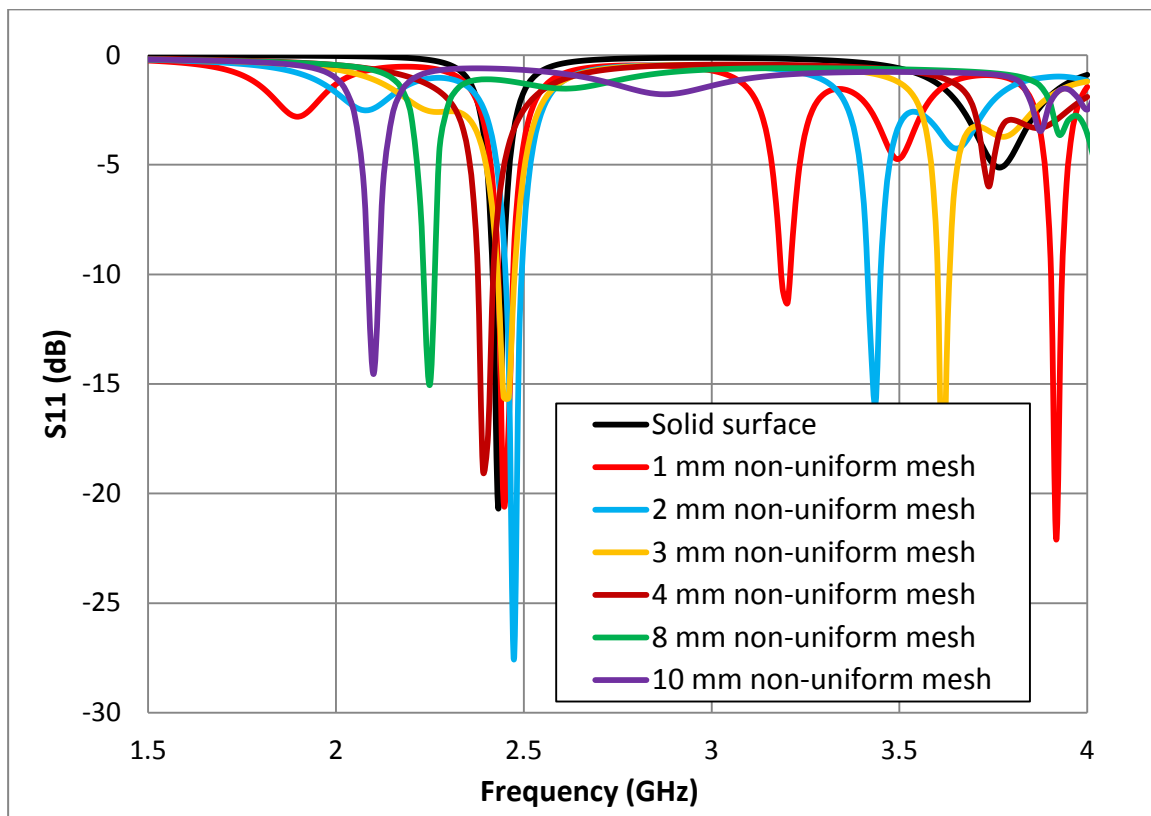
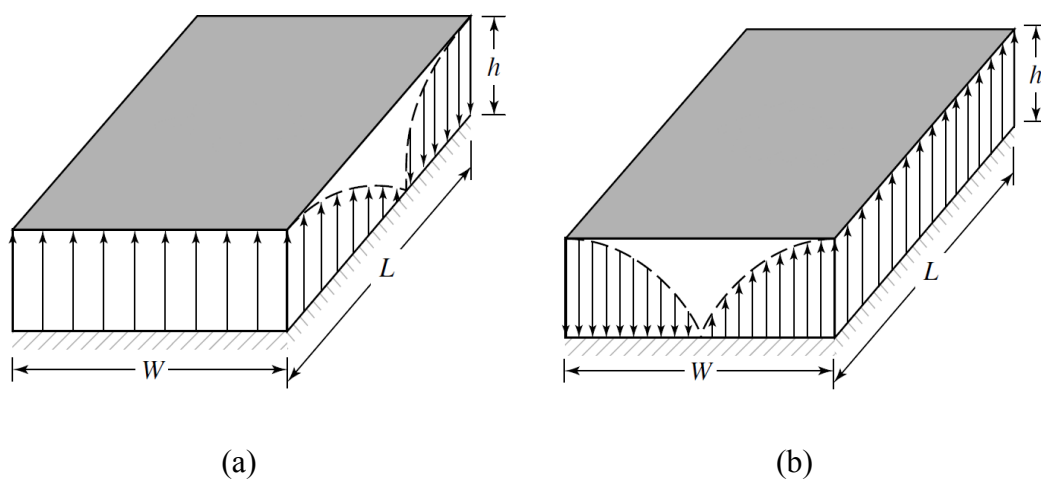


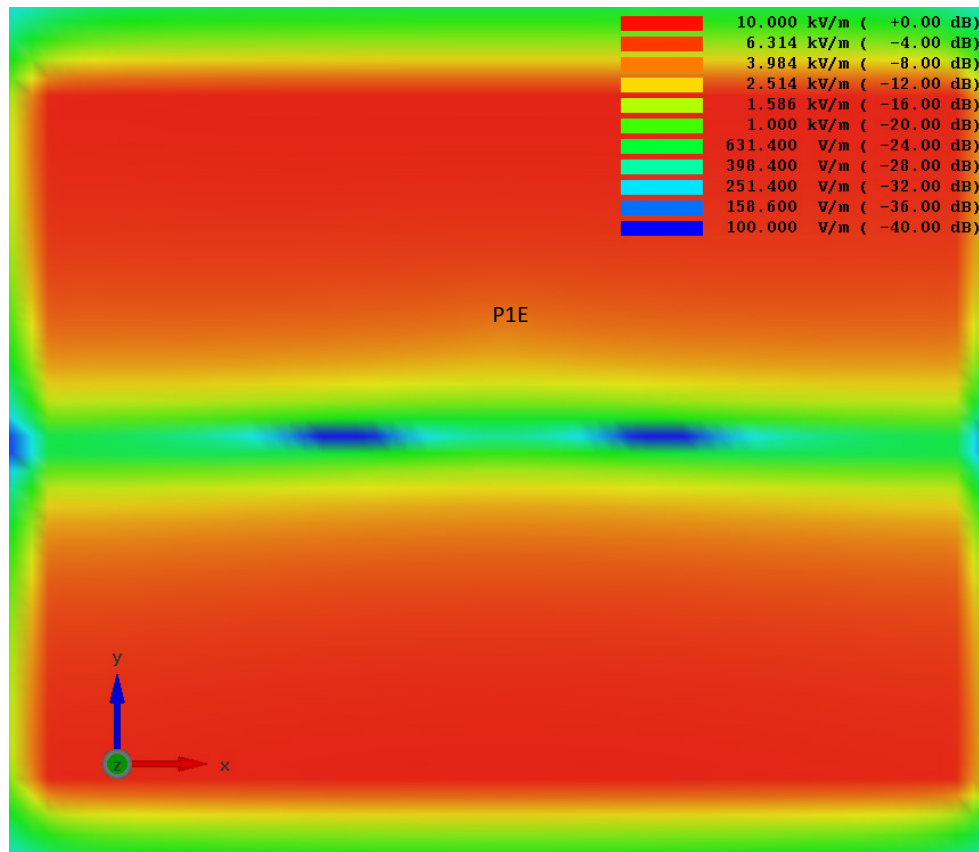
Figure 5-6  $S_{11}$  of non-uniform meshed patch antennas with different mesh spaces

### 5.3.2. $TM_{01}$ Mode of Meshed Microstrip Antennas

Simulated results have shown that the resonant frequencies of meshed patches are lower than the equally dimensioned solid copper patch. It is also essential to understand the antenna modes of meshed patches. The TM mode of microstrip antenna can be defined in the cavity mode [20]. The field configuration modes for rectangular patches are shown in Figure 5-7. The resonant frequency of the solid patch at  $TM_{01}$  mode is determined by the antenna length  $L$ . Figure 5-8 shows the electric field of the solid patch antenna at the  $TM_{01}$  mode at 2.43 GHz when looking on the above. The red colour indicates the highest electric field value whilst blue is lowest. It can be seen that at the  $TM_{01}$  mode, the highest electric field magnitude value is observed at the top and bottom edges of the patch antenna which are the radiating slots. At the two non-radiating slots, the electric field strength at the centre is a minimum.



**Figure 5-7** Electric field distribution for the (a)  $TM_{01}$  and (b)  $TM_{10}$  mode in the microstrip cavity (picture from [20])



**Figure 5-8 Electric fields of solid patch antenna at  $TM_{01}$  mode**

The 3 mm uniform and non-uniform meshed patches are taken as examples. The electric fields of the uniform and non-uniform meshed antenna at the resonant frequencies are shown in Figure 5-9 to Figure 5-10 respectively. The electric field plots of the meshed patches antennas are similar to the solid patch at the  $TM_{01}$  mode apart from the weak electric field in the apertures of the meshed holes. High electric fields are observed underneath the conductors.

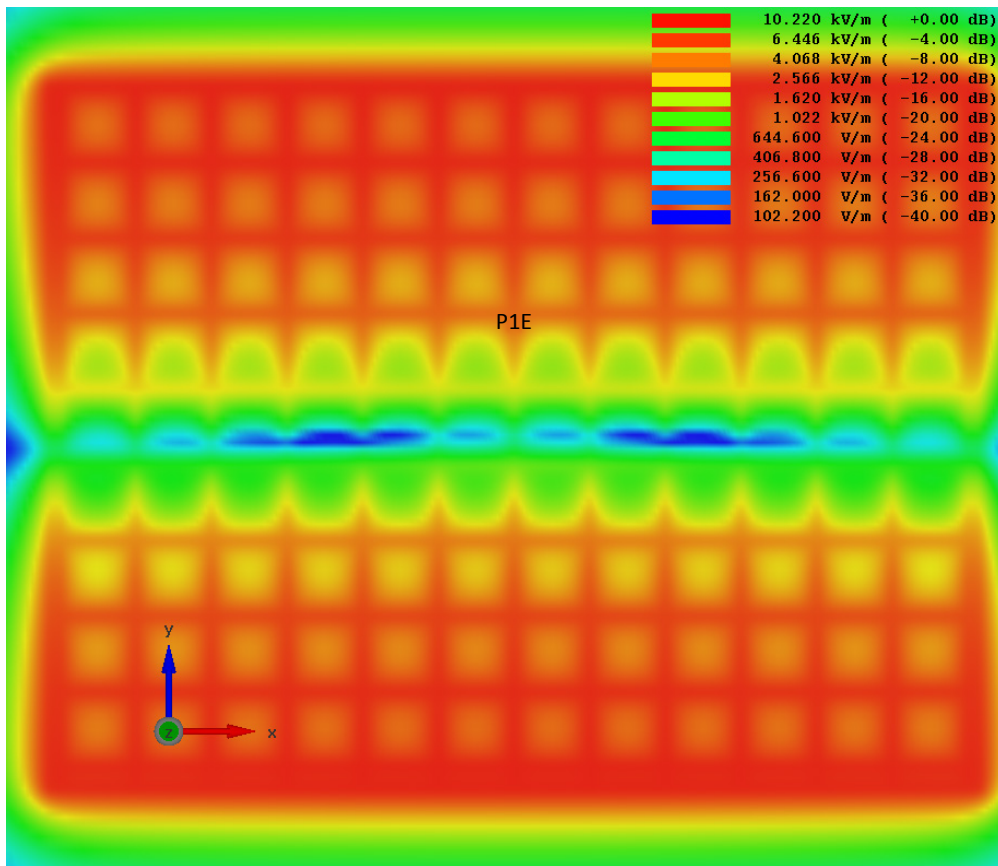


Figure 5-9 Electric fields of 3 mm uniform meshed patch at  $TM_{01}$  mode

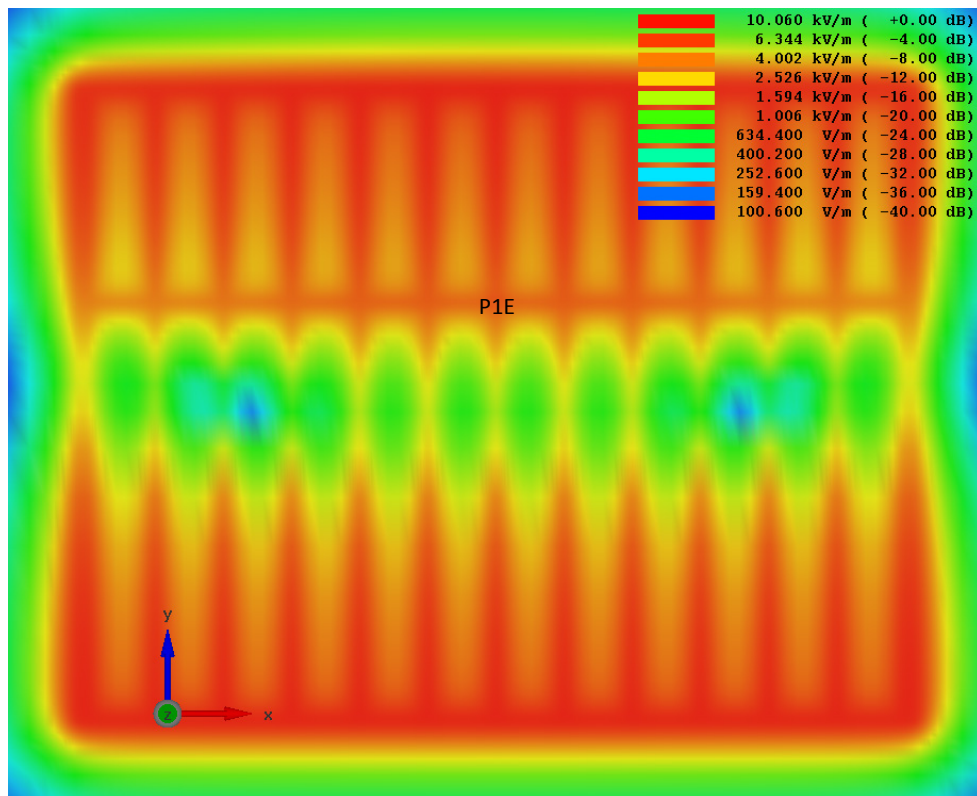


Figure 5-10 Electric fields of 3 mm non-uniform meshed patch at  $TM_{01}$  mode

### 5.3.3. Surface Current Distribution of Meshed Microstrip Antennas at $TM_{01}$ Mode

Figure 5-11 to Figure 5-13 show the surface current in the  $x$ ,  $y$  and  $x&y$  directions on the solid copper patch at the  $TM_{01}$  mode. The arrows indicate the direction of the currents. It can be seen that the current in  $y$  direction is significantly stronger than in  $x$  direction which results in the major current flows in the  $y$  direction. The highest current density (red colour) is observed at the left and right edges which are the non-radiating slots in Figure 5-13.

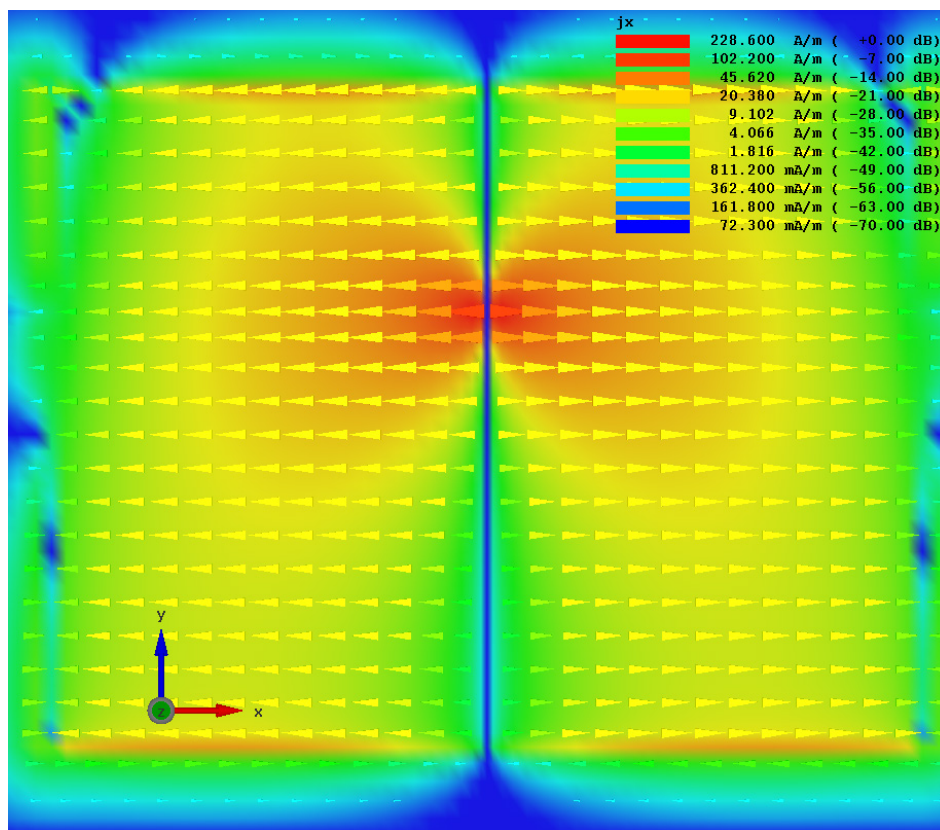


Figure 5-11  $x$  direction component of surface current distribution in a solid patch at  $TM_{01}$  mode



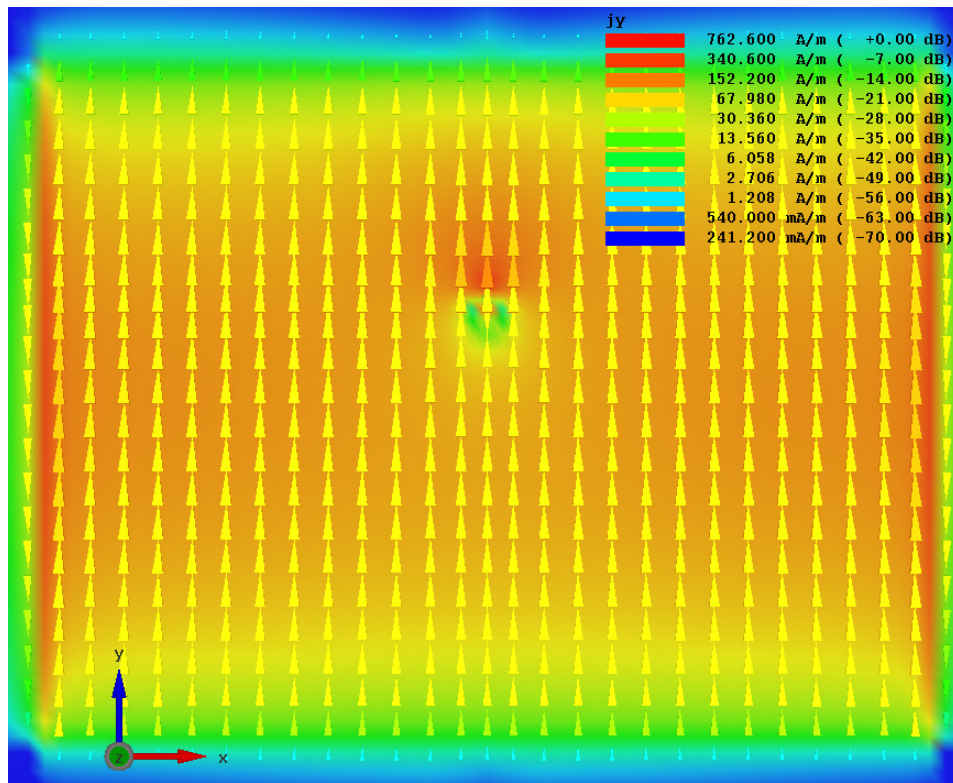


Figure 5-12 y direction component of surface current distribution in solid patch at  $TM_{01}$  mode

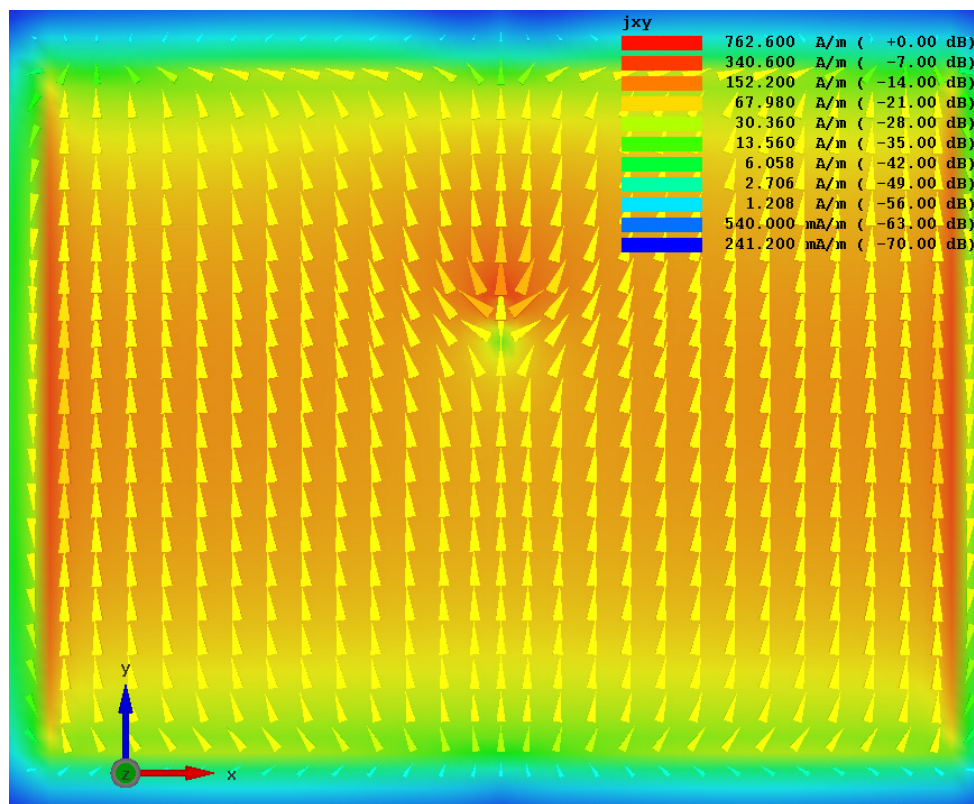
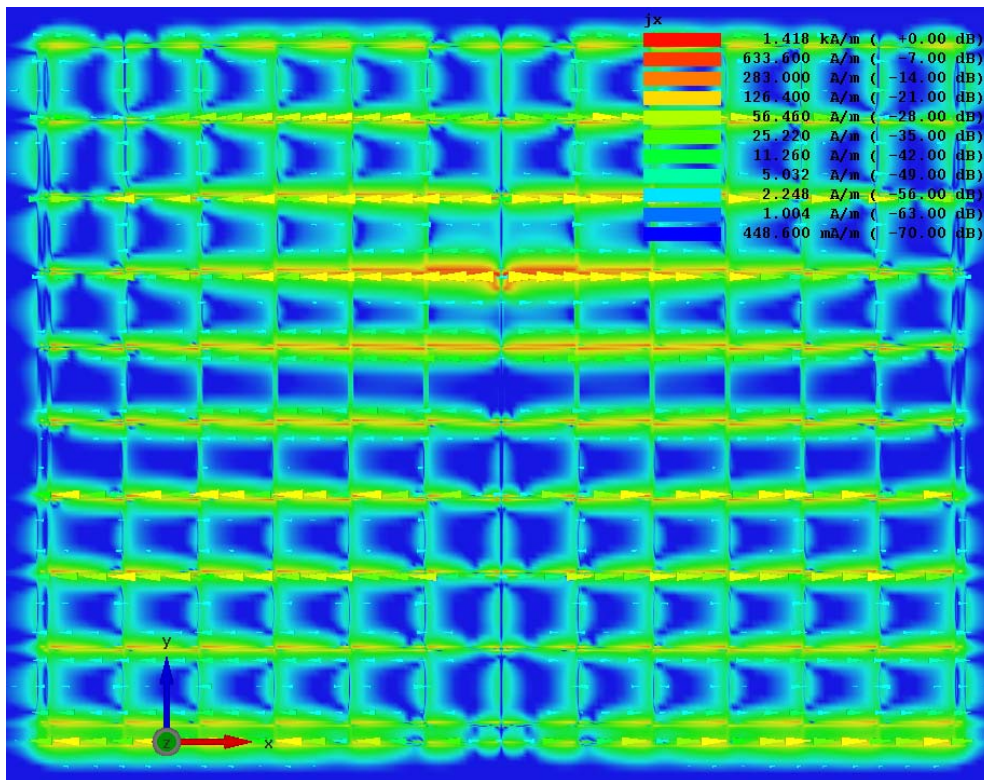


Figure 5-13 Surface current distribution on solid patch in x & y directions at  $TM_{01}$  mode

Figure 5-14 to Figure 5-16 show the surface current distribution on  $3 \text{ mm} \times 3 \text{ mm}$  uniform meshed patch. The current direction and highest density position are very similar to the solid copper at the  $\text{TM}_{01}$  mode: the major current is dominated by the current in  $y$  direction. But the current is distorted in both  $x$  and  $y$  directions by the mesh holes. It bypasses the mesh holes and results in longer electrical length. The larger mesh size results in longer current paths. Consequently, the resonant frequency of the meshed patch antenna will be lower than the same size solid patch due to the extended current paths.



**Figure 5-14  $x$  direction component of surface current distribution in  $3 \text{ mm} \times 3 \text{ mm}$  uniform meshed patch at  $\text{TM}_{01}$  mode**



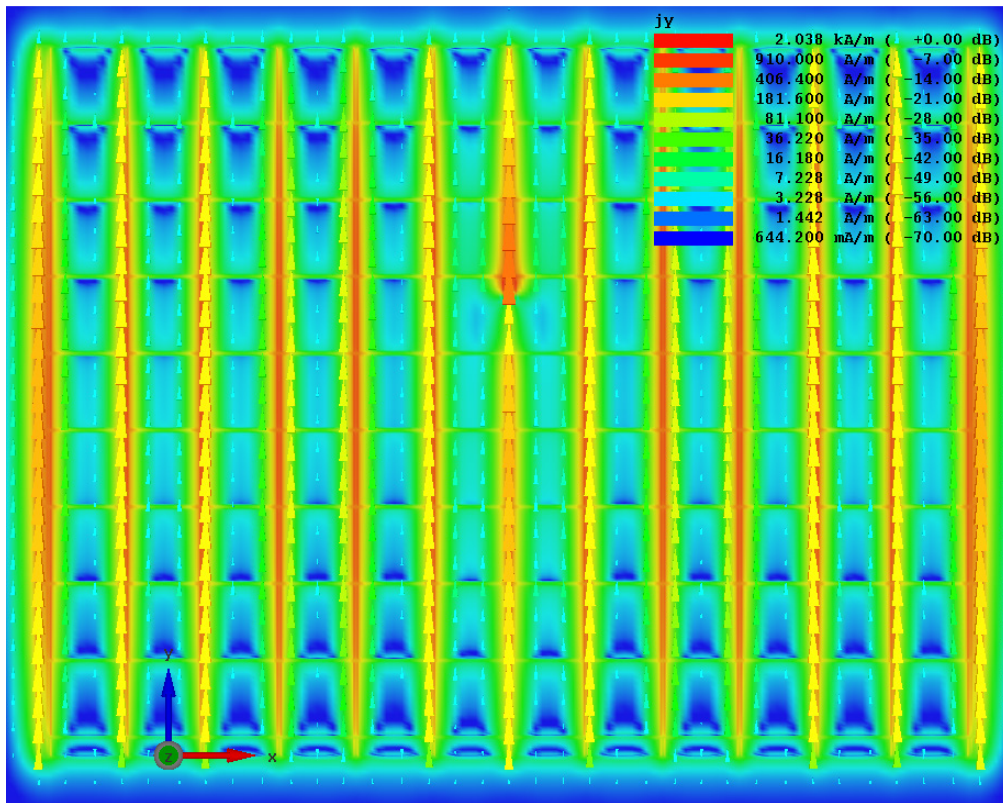


Figure 5-15  $y$  direction component of surface current distribution in  $3\text{ mm} \times 3\text{ mm}$  uniform meshed patch at  $\text{TM}_{01}$  mode

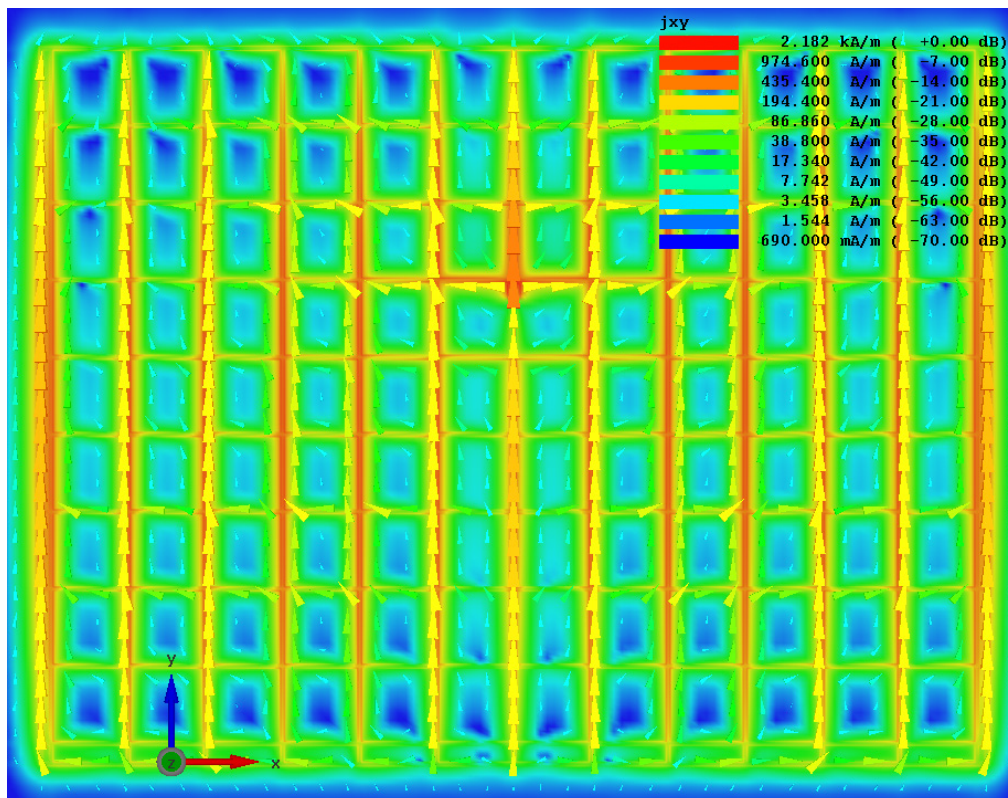


Figure 5-16 Current distribution on  $3\text{ mm} \times 3\text{ mm}$  uniform meshed patch in  $x$  &  $y$  directions at  $\text{TM}_{01}$  mode



Although current in the  $y$  direction is more important than in the  $x$  direction for the  $TM_{01}$  mode, the number of paths in the  $x$  direction also affects the antenna resonant frequency. With smaller number of horizontal lines, there are fewer current paths available in  $x$  direction. This raises the resonant frequency. The concept of the non-uniform meshed patch is to remove all the horizontal current paths except the top and the bottom strip which providing the completed radiation edges. The horizontal conductor in the middle connects the feed point and all the vertical lines.

Figure 5-17 to Figure 5-19 show the surface current on the non-uniform meshed patch. It can be observed that the middle horizontal line directs the current from the feed point to both left and right sides of the patch antenna, and the current flows into the vertical lines at the junctions with the horizontal lines. The largest current still flows in the  $y$  direction. The current distribution of non-uniform patch antenna is similar to the vertical directional zigzag patch which was shown in Chapter 4. However, since there is no low conductivity material filled in the gaps between mesh lines, the three horizontal lines lead the current flow into all the vertical lines at their junctions. Therefore, as seen in Figure 5-17 to Figure 5-19, higher current values appear not only on the two side edges of the non-uniform patch, but also on the three horizontal lines. This indicates that all the three horizontal lines are important for guiding the current.

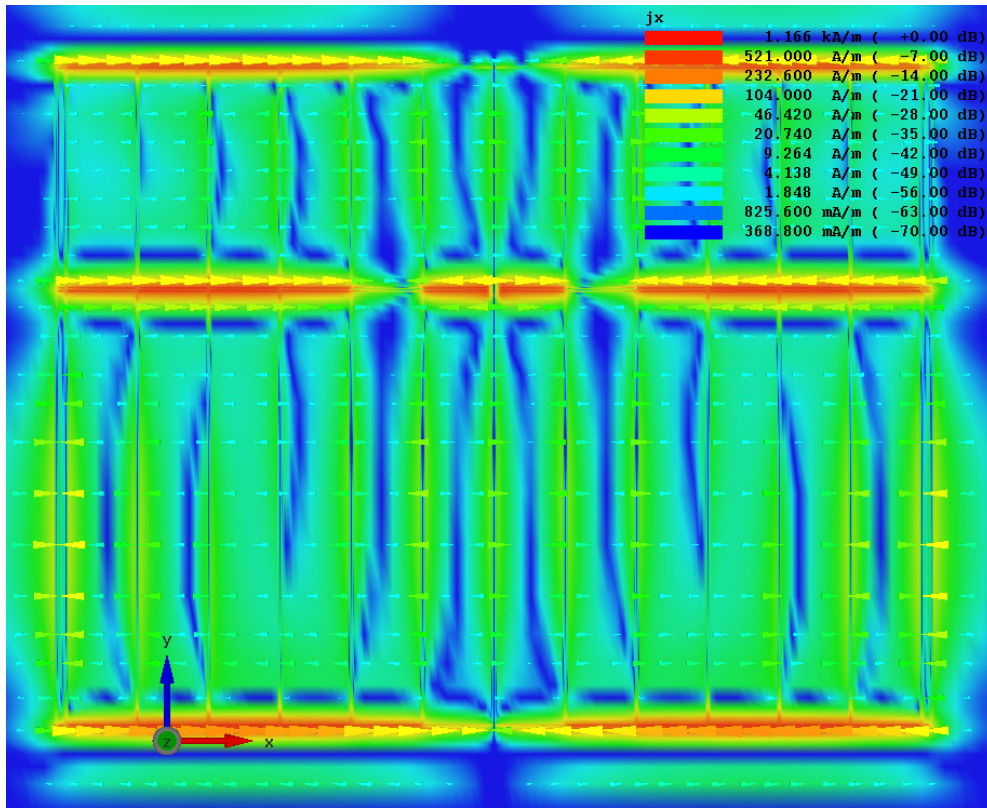


Figure 5-17  $x$  direction component of surface current distribution in 3 mm space non-uniform meshed patch at  $TM_{01}$  mode

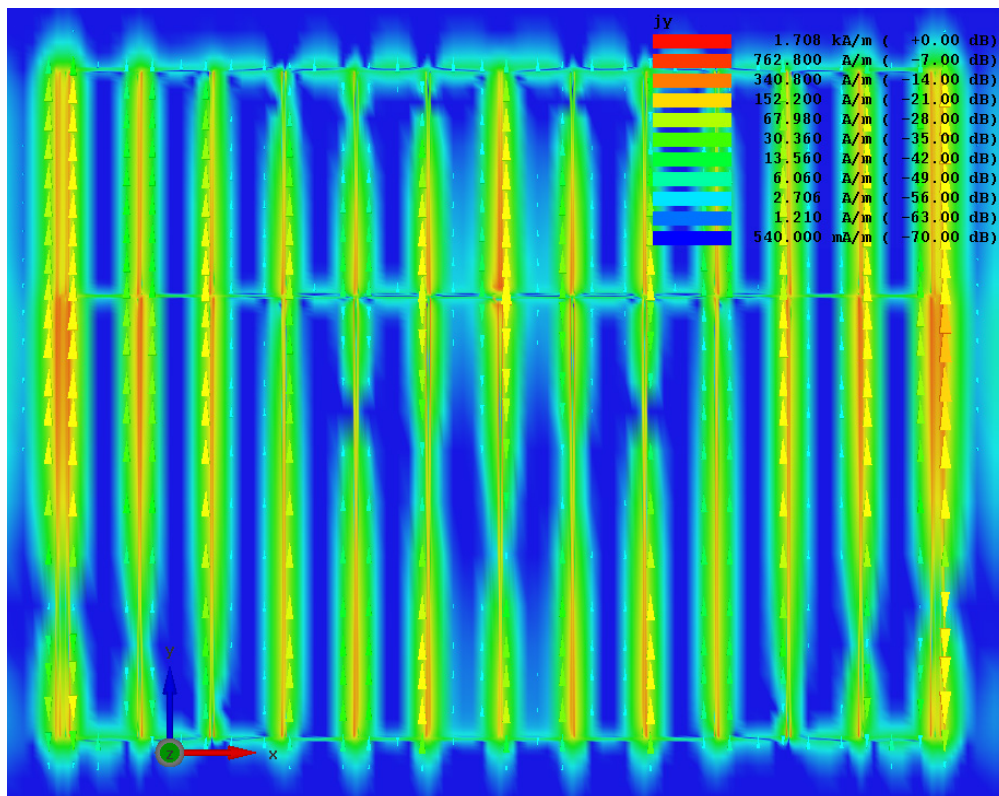
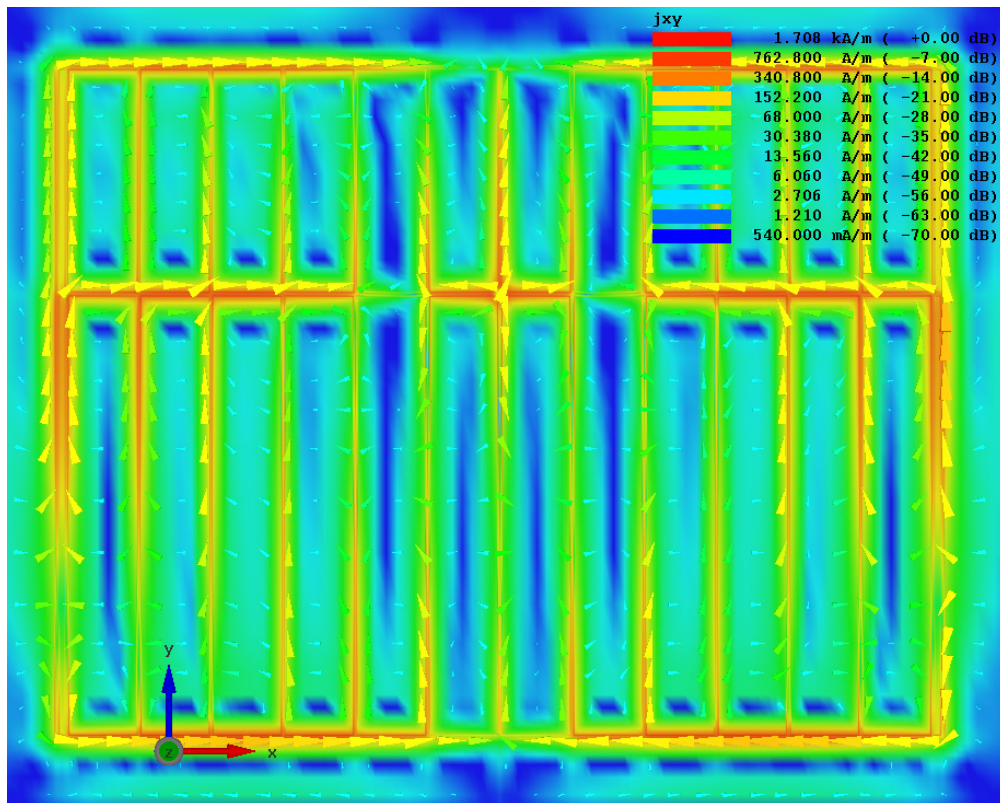


Figure 5-18  $y$  direction component of surface current distribution in 3 mm space non-uniform meshed patch at  $TM_{01}$  mode

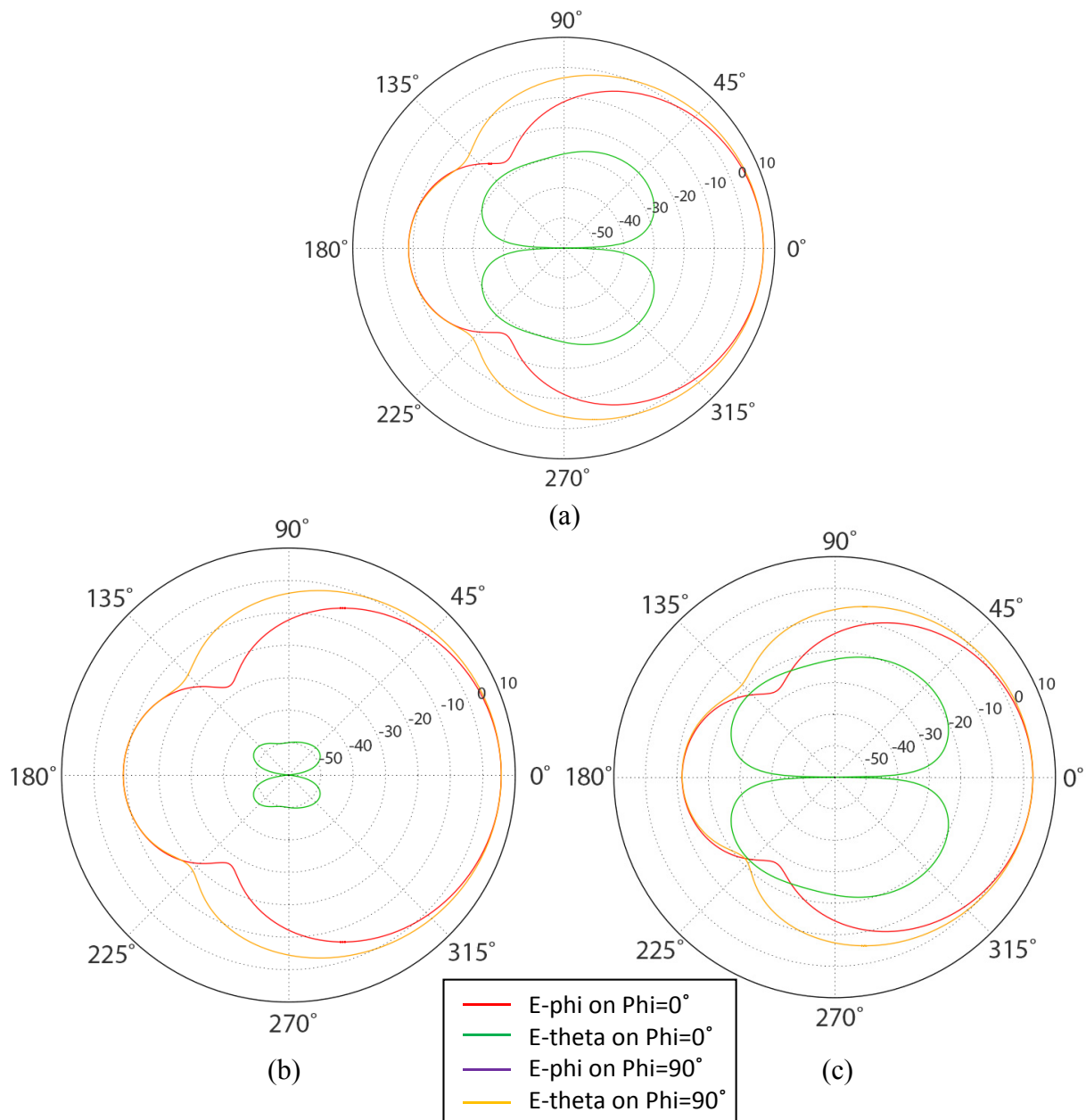


**Figure 5-19** Current distribution on 3 mm space non-uniform meshed patch in  $x$  &  $y$  directions at  $TM_{01}$  mode

#### 5.3.4. *Cross Polarization of Non-Uniform Meshed Microstrip Antennas*

Since the current is always in the same direction on two parallel mesh lines, the vertical lines can be treated as even mode coplanar microstrip lines. For the even mode, the electric field has even symmetry between adjacent lines, and the gap between the two strip conductors is effectively open-circuit [22], the current flows between the two strip conductors across the gap can be neglected. As a result, the cross-polarization level of non-uniform meshed patch antennas will be smaller compared with the solid and uniform meshed patch antennas. Figure 5-20 (a) and Figure 5-20 (b) show the simulated radiation pattern of the solid copper and 1 mm non-uniform meshed patch respectively. Comparing with the solid copper patch, the 1 mm non-uniform meshed patch has lower cross polarization level, the difference is approximately 22 dB. However, with larger mesh space, the ratio of  $y$  directional to  $x$  directional current paths will be smaller. This results in higher cross polarization level.

When the mesh spacing is larger than 4 mm, the cross polarization of non-uniform meshed patch is larger than the solid copper patch. The simulated radiation pattern of 4 mm non-uniform meshed patch is shown in Figure 5-20 (c). This indicates that the larger mesh spacing reduces polarization purity of the non-uniform meshed patch antenna. Wearable devices may benefit from a dual polarised antenna due to the dynamic position and orientation.



**Figure 5-20 Simulated electric field gain patterns (in dBi) of**

**(a) Solid copper patch antenna**

**(b) 1 mm non-uniform meshed patch antenna**

**(c) 4 mm non-uniform meshed patch antenna**

## 5.4 Effect of Metal Coverage of Meshed Microstrip Antennas

A range of simulations were compared with different mesh sizes with uniform and non-uniform meshed patch antennas. The material of the patches is copper (conductivity  $5.8 \times 10^7$  S/m) with 0.01 mm thickness. A 90 mm  $\times$  70 mm and 1.57 mm thick Taconic RF-45 substrate with  $\epsilon_r = 4.5$ , loss tangent = 0.0037 was used. The ground planes are solid copper. The width of the mesh lines is chosen as 0.2 mm which is equal to the flattened width of the Amberstrand Silver 66 thread. All the meshed patches have fixed size of 37 mm  $\times$  28 mm. The mesh spacing indicates the space between two parallel lines. The mesh spacing between the two lines at the edges may be smaller than the claimed mesh spacing in order to maintain the exterior dimension. The uniform meshed patches have the same mesh spacing between horizontal and vertical lines. All the patches were fed 9.5 mm away from the long edge.

The simulated results for the uniform and non-uniform meshed patch antennas are shown in Table 5-1 and Table 5-2 respectively. The metal coverage percentage is the ratio of the area that is covered by conductive material compared to 37 mm  $\times$  28 mm area. The thread length is the estimation of the total length of conductive thread if the patch was to be embroidered but excludes the extra length due to lock stitch. The gain and total antenna efficiency values include the loss due to the mismatch.

Table 5-1 Simulation results of uniform meshed patch antenna


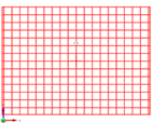
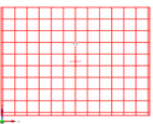
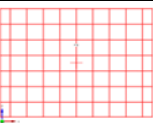



Mesh spacing (mm)	Metal area (mm <sup>2</sup> )	Metal coverage (%)	Thread length (mm)	Resonant frequency (GHz)	S11 (dB)	10dB BW (MHz)	Gain (dBi)	Directivity (dBi)	Radiation efficiency (%)	Total efficiency (%)
Solid Patch	1036.00	100.00	5180	2.43	-16.4	31.2	6.3	7.3	80.7	78.7
1mm 	387.76	37.43	2165	2.41	-17.3	31.7	5.6	7.3	68.1	66.8
2mm 	216.00	20.85	1143	2.35	-23.3	35.3	4.4	7.3	51.8	51.6
3mm 	158.80	15.33	827	2.28	-24.8	36.8	3.6	7.3	42.8	42.7
4mm 	117.28	11.32	604	2.27	-21.5	36.0	3.1	7.3	38.8	38.6
8mm 	74.80	7.22	381	2.13	-8.7	n/a	1.4	7.1	31.0	26.8
10mm 	56.80	5.48	288	2.05	-8.3	n/a	0.1	7.0	23.9	20.3
18.5mm 	38.64	3.73	195	1.73	-13.3	18.6	-3.6	6.6	10.0	9.6



Table 5-2 Simulation results of non-uniform meshed patch antennas

Mesh spacing in vertical direction(mm)	Metal area (mm <sup>2</sup> )	Metal coverage (%)	Thread length (mm)	Resonant frequency (GHz)	S11 (dB)	10dB BW (MHz)	Gain (dBi)	Directivity (dBi)	Radiation efficiency (%)	Total efficiency (%)
Solid Patch	1036.00	100.00	5180	2.43	-16.4	31.2	6.3	7.3	80.7	78.7
1mm 	235.92	22.77	1203	2.43	-20.4	39.7	5.7	7.4	68.8	68.1
2mm 	137.28	13.25	699	2.47	-27.6	45.6	5.2	7.4	60.2	60.1
3mm 	104.40	10.08	531	2.46	-15.6	46.1	4.6	7.4	53.6	52.1
4mm 	82.48	7.96	518	2.39	-18.9	40.9	2.8	7.3	36.5	36.0
8mm 	60.56	5.85	307	2.25	-15.0	27.4	2.2	7.2	32.1	31.1
10mm 	49.60	4.79	251	2.10	-14.6	26.8	0.9	7.1	25.0	24.0
18.5mm 	38.64	3.73	195	1.73	-13.3	18.6	-3.6	6.6	10.0	9.6

For the same mesh spacing, the non-uniform mesh structure requires less metal than the uniform meshes due to the reduced number of horizontal lines. Comparing the data in Table 5-1 with Table 5-2, it is noticed that the antenna efficiencies of uniform meshed patches and the same spacing non-uniform meshed patches are very similar at their resonant frequencies. But the efficiencies of non-uniform meshed patches are slightly higher (apart from the 4 mm mesh spacing). According to the surface current analysis in Section 5.3.3, the reason that is these non-uniform meshed patches have higher efficiencies is because they have less horizontal currents paths. Nevertheless, the meshed patch structure can save more than 3/4 of the materials at the cost of dropping the total efficiency by 10%. For instance, the 1 mm space non-uniform meshed patch only has 22.77% metal coverage of the patch surface but has 68.1% total efficiency (a solid copper patch has 78.7% efficiency). Overall, comparing with the uniform meshed patches with the same mesh space, the non-uniform meshed patch has higher antenna efficiency but with less metal coverage. Figure 5-21 shows the total antenna efficiencies of both non-uniform meshed patches and uniform meshed patches at their resonant frequencies as a function of the metal coverage. It also noticed that the non-uniform meshed patch antenna has wider bandwidth than the uniform meshed patch antenna with the same mesh space.

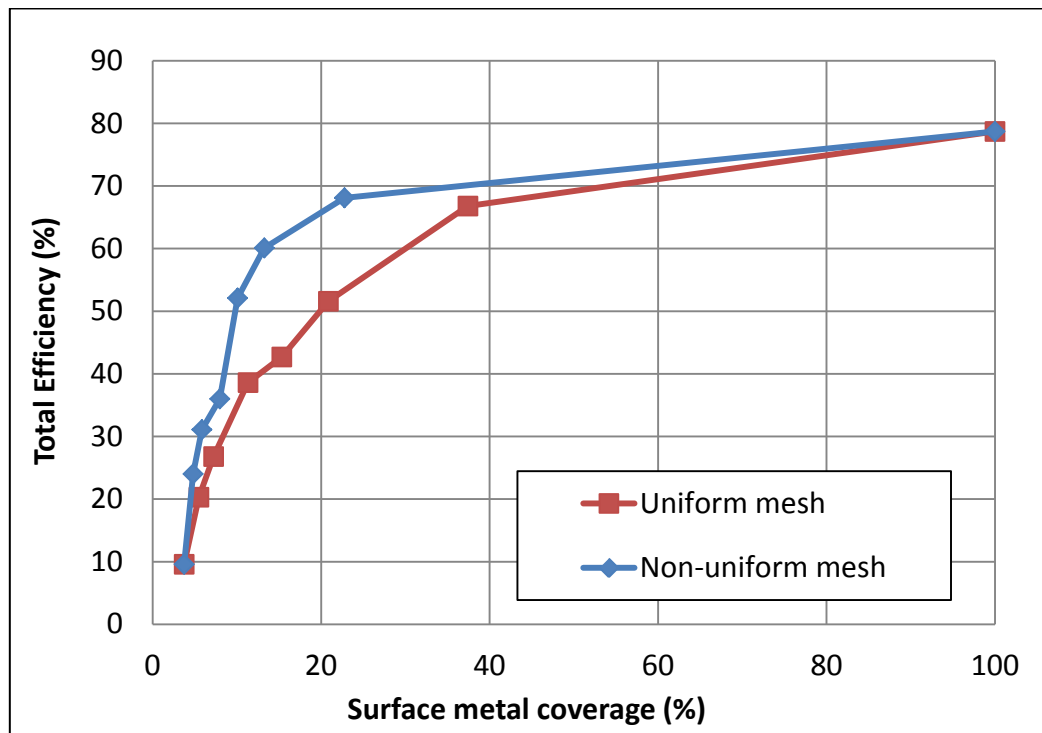


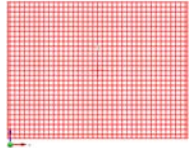
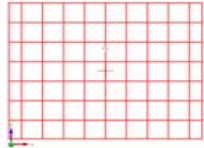
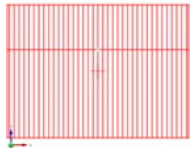
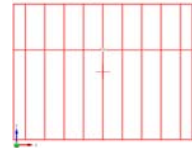
Figure 5-21 Simulated total efficiency as a function of metal surface coverage



## 5.5 Factors of Losses in Meshed Microstrip Antennas

A further set of simulations was carried out to analyse the factors of losses in meshed patch antennas. The conduction loss and the dielectric loss were considered as the two major factors of loss in this analysis. To eliminate these two factors, perfect electric conductor (PEC, conductivity =  $\infty$ ) and lossless dielectric substrate (loss tangent = 0) were also simulated. Therefore there were four combinations: i) copper (conductivity =  $5.8 \times 10^7$  S/m) on the lossy dielectric substrate (loss tangent = 0.0037); ii) copper on lossless substrate; iii) PEC on lossy substrate; and iv) PEC on lossless substrate. The fully covered solid patch, 1 mm non-uniform meshed patch, 1 mm uniform meshed patch, 4 mm non-uniform meshed patch and 4 mm uniform meshed patch have been analysed. 10  $\mu\text{m}$  metallization thickness was used for the conductors in these simulations. The simulated results are shown in Table 5-3. It can be seen that the changes of conductivity and loss tangent have little effect on resonant frequency. Furthermore the directivities of all the antennas are very similar. However, the gain values varied with the different mesh sizes and mesh structures.

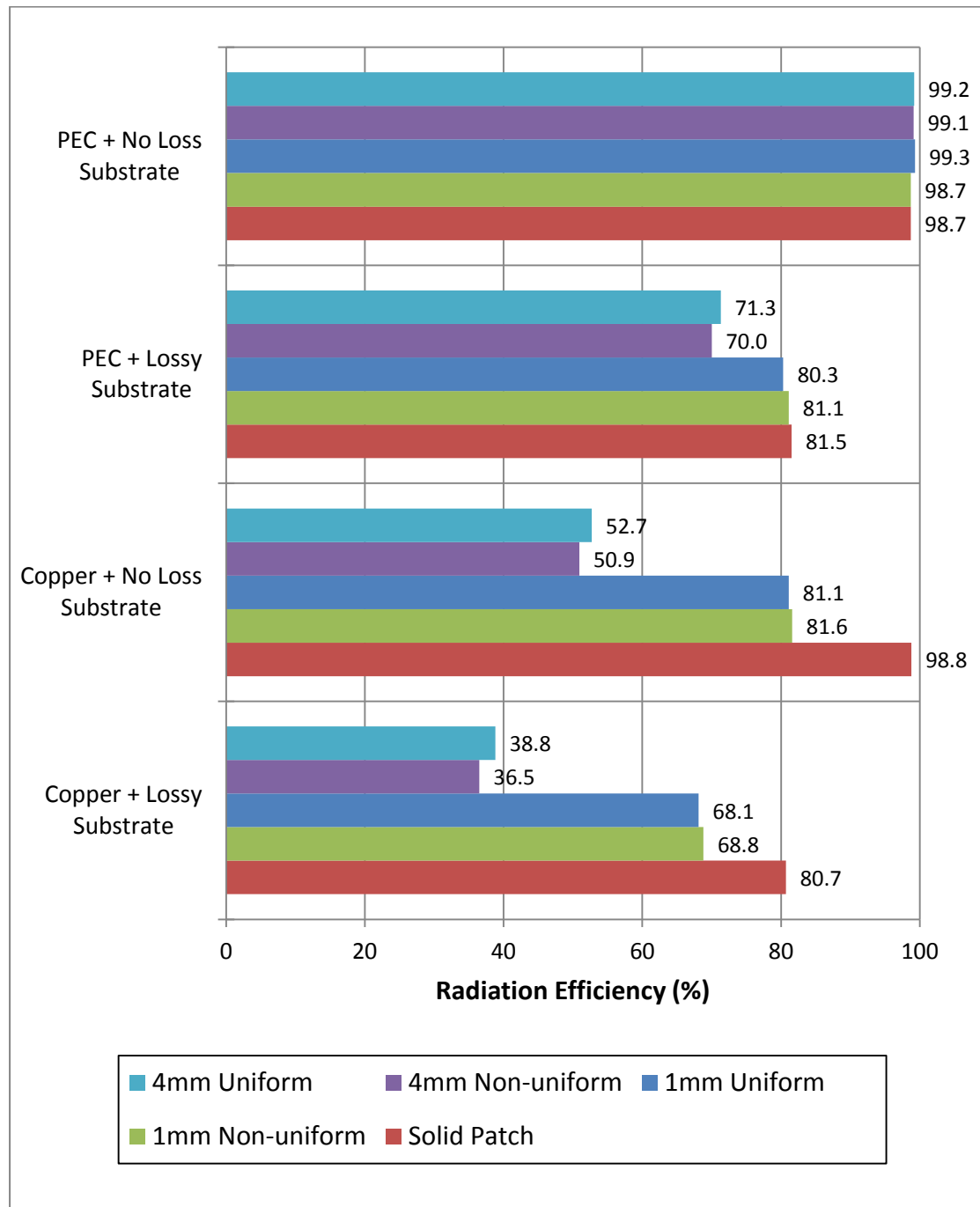
Table 5-3 Effects of conduct loss and dielectric loss to meshed patch antennas

	Solid patch				1mm uniform 				4mm uniform 				1mm non-uniform 				4mm non-uniform 			
	Copper & Lossy	Copper & No loss	PEC & Lossy	PEC & No loss	Copper & Lossy	Copper & No loss	PEC & Lossy	PEC & No loss	Copper & Lossy	Copper & No loss	PEC & Lossy	PEC & No loss	Copper & Lossy	Copper & No loss	PEC & Lossy	PEC & No loss	Copper & Lossy	Copper & No loss	PEC & Lossy	PEC & No loss
<b>Metal area (mm<sup>2</sup>)</b>	1036.00				387.76				117.28				235.92				82.48			
<b>Resonant frequency (GHz)</b>	2.43	2.43	2.43	2.43	2.41	2.39	2.41	2.39	2.27	2.27	2.28	2.27	2.43	2.43	2.44	2.43	2.39	2.39	2.41	2.41
<b>S11 (dB)</b>	-16.4	-21.8	-16.5	-21.8	-17.3	-24.3	-23.9	-21.7	-21.5	-14.3	-9.3	-7.2	-20.4	-25.1	-20.0	-16.0	-18.9	-21.2	-17.3	-11.0
<b>Gain (dBi)</b>	6.3	7.3	6.4	7.3	5.6	6.4	6.4	7.3	3.1	4.3	5.2	6.3	5.7	6.5	6.4	7.2	2.8	4.3	5.8	6.9
<b>Directivity (dBi)</b>	7.3	7.3	7.3	7.3	7.3	7.3	7.3	7.3	7.3	7.3	7.2	7.2	7.4	7.4	7.4	7.3	7.3	7.3	7.3	7.3
<b>Total efficiency (%)</b>	78.7	98.2	79.7	98.0	66.8	80.8	80.0	98.6	38.6	50.8	62.2	80.2	68.1	81.4	80.2	96.2	36.0	50.5	68.7	91.2
<b>Radiation efficiency (%)</b>	80.7	98.8	81.5	98.7	68.1	81.1	80.3	99.3	38.8	52.7	71.3	99.2	68.8	81.6	81.1	98.7	36.5	50.9	70.0	99.1

As shown in Table 5-3, using perfect conductor and lossless substrate can increase the antenna gain and efficiencies. Comparing radiation efficiencies can eliminate the impacts due to the return loss. Figure 5-22 shows the variation of radiation efficiencies with different patch surface structures and loss factors. For the solid patch, the difference of copper and PEC materials is very small, and the efficiency variation is less than 1%. Comparing the efficiencies results of PEC with copper for the meshed patches, the conduction loss is more significant with larger mesh spacing. More precisely, on the lossy substrate, when PEC replaces copper as the conductor material, the increases of antenna efficiency for both the 4 mm uniform and non-uniform meshed patches (32.5% and 33.5% respectively) are larger than the 1 mm uniform and non-uniform meshed patches (12.2% and 12.3% respectively). Similarly on the lossless substrate, the increased efficiency of using PEC on both the 4 mm uniform and non-uniform meshed patches are greater than the 1 mm uniform and non-uniform meshed patches. Larger mesh space means lower metal coverage area which results in higher surface resistance and more conduction loss. If the antenna is made from PEC and lossless substrate, all the patch antennas efficiency are close to 99% regardless the mesh sizes.

The dielectric loss reduces the efficiency of both the meshed and the solid patch antennas. When copper is used as the conductive material, the efficiency of the 1 mm uniform meshed patch antenna on a lossless substrate is 81.1% and it is reduced to 68.1% if a lossy substrate is used for the same meshed patch antenna. The reduction due to the lossy material is 13%. Similarly, the efficiency reductions due to the lossy substrate of the 1 mm non-uniform meshed patch, 4 mm uniform meshed patch and 4 mm non-uniform meshed patch antennas can be obtained as 12.8%, 13.9% and 14.4% respectively. It can be seen the dielectric losses of the meshed patch antennas are similar when copper is used as conductor. However, the difference of dielectric loss is greater when PEC is used. The impact of the dielectric loss is more significant on patches with larger mesh spaces.

Therefore, the meshes increase both conduction and dielectric losses. Larger mesh space results in more conduction loss. The dielectric loss is more significant on larger mesh space when non-PEC material is used. This simulation shows the ratio of performance to cost for the meshed microstrip antenna design.



**Figure 5-22 Effects of conduction loss and dielectric loss on meshed patch antennas**

## 5.6 Etched Meshed Microstrip Antennas

Four etched copper meshed microstrip antennas were fabricated. They are 1 mm and 4 mm space uniform/non-uniform meshed patch antennas. Their specifications are the same as the simulation. The line width is 0.2 mm. Figure 5-23 and Figure 5-24 show the 1 mm space uniform and non-uniform meshed patches respectively. A solid copper patch with the same dimensions (37 mm  $\times$  28 mm) was made as a reference. The measured S11 of the five antennas are shown in Figure 5-25. The S11 results agree with simulation results of the frequency shift in Figure 5-5 and Figure 5-6, i.e. the resonant frequencies were lowered by the increased the mesh spacings. Furthermore, the resonant frequencies of the non-uniform meshed patches are closer to the solid copper patch than the uniform meshed patches. Particularly the 1 mm non-uniform meshed patch has the same resonant frequency as the solid one. Therefore, by reducing the number of the horizontal lines reduces the shift of the resonant frequency of the meshed patch antennas, this agrees with the simulated results.

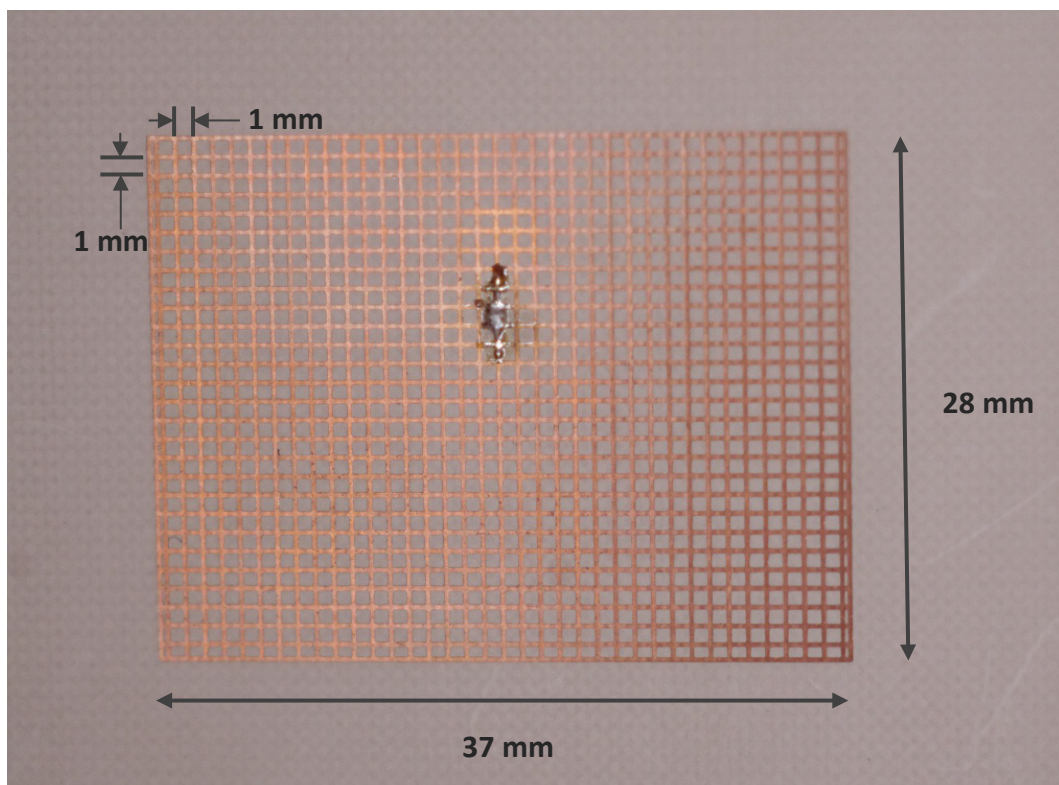


Figure 5-23 Etched 1 mm spacing uniform meshed patch antenna

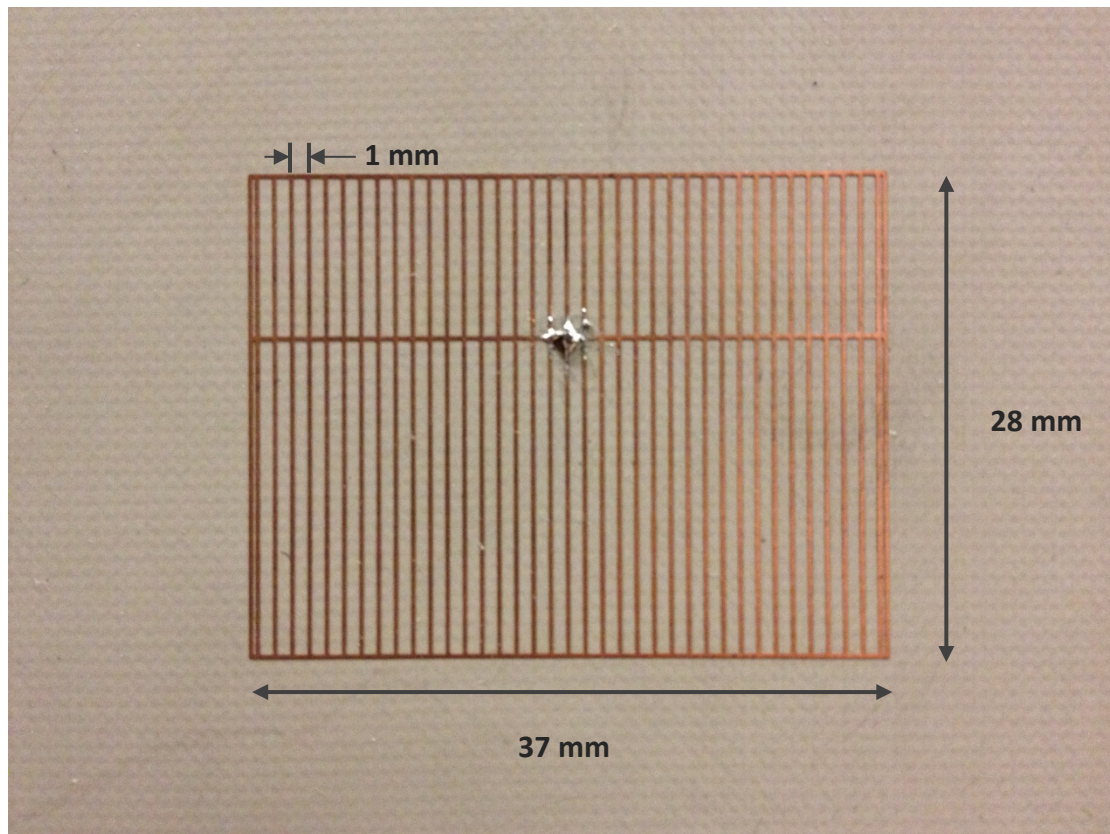


Figure 5-24 Etched 1 mm spacing non-uniform meshed patch antenna

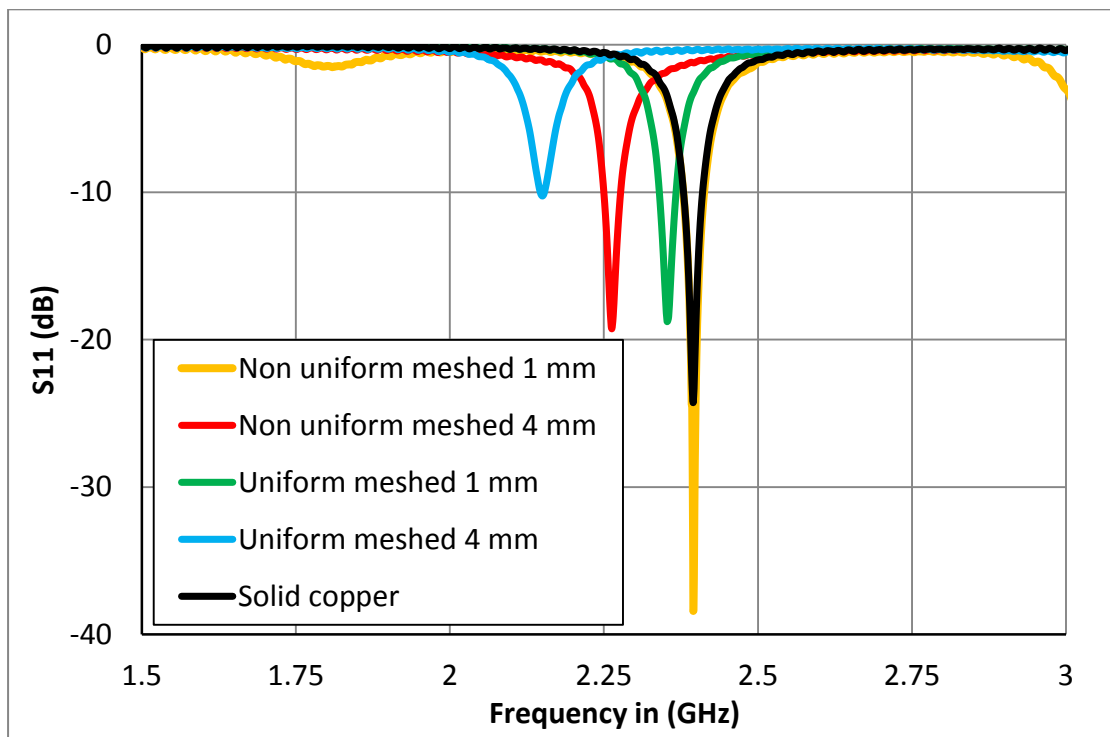
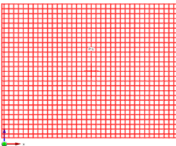
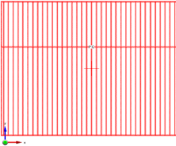
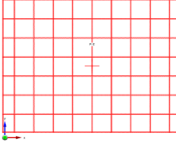
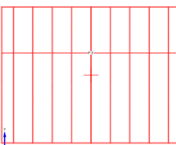


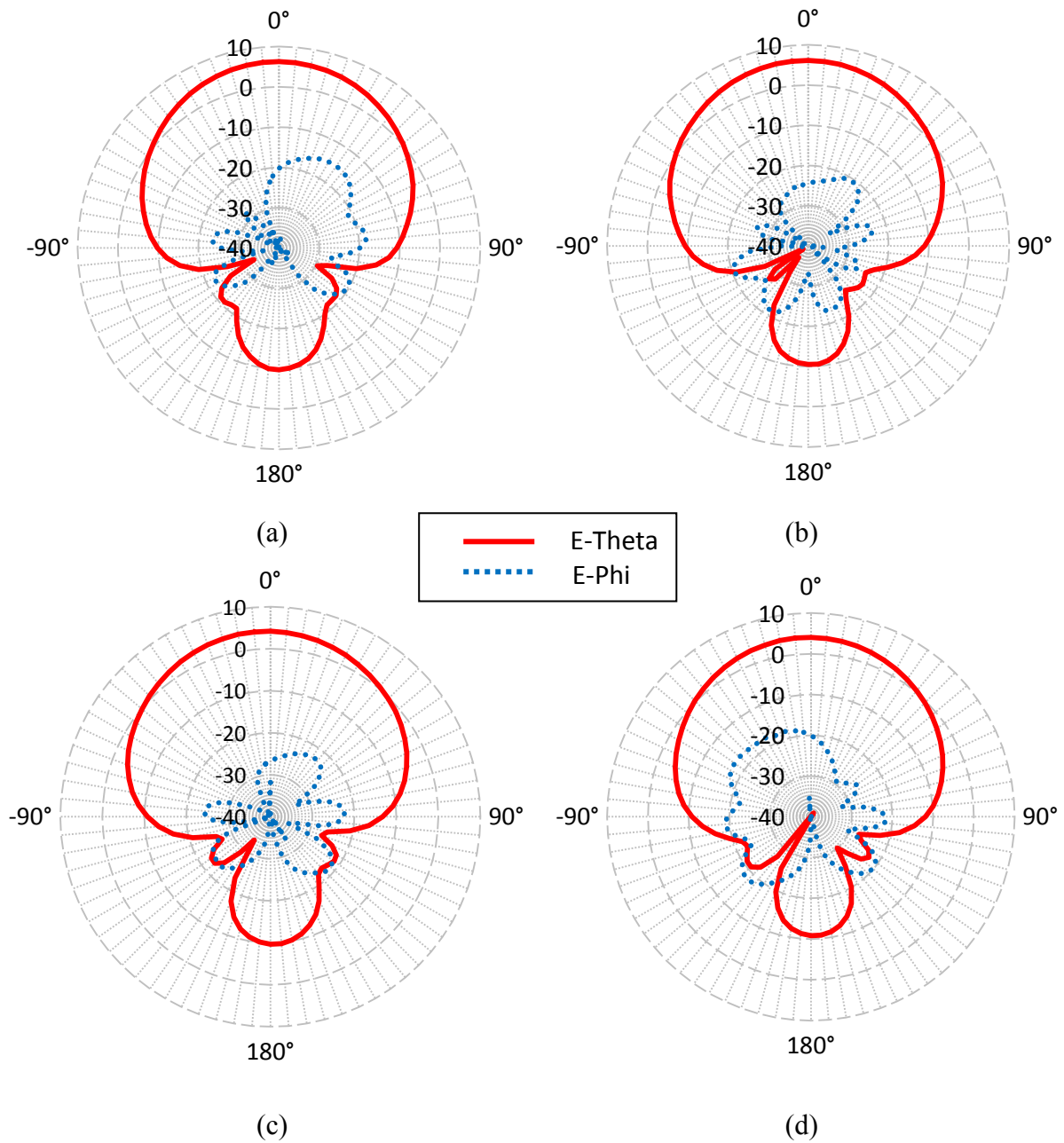
Figure 5-25 Measured S<sub>11</sub> of etched copper meshed patch antennas

The measured results including the antenna gains and efficiencies are shown in Table 5-4. All the meshed patches have similar directivity values compared with the solid patch. The gain values are smaller with larger mesh spacing. However the gain of the 1 mm uniform meshed patch is only 0.4 dB less than the solid copper but the metal coverage is almost 1/3 of the solid copper. The coverage can be reduced to 23% when applying the 1 mm non-uniform meshed structure with the total efficiency only 5.3% lower than the solid copper patch antenna. The 4 mm uniform and non-uniform meshed patches have approximately 4 dBi antenna gain but the metal coverage are only 11% and 8 % of respectively. The measured radiation patterns of etched meshed patch antennas are shown in Figure 5-26.

**Table 5-4 Measured results of meshed patch antennas**

	Metal coverage (%)	Resonant frequency (GHz)	S11 (dB)	10 dB BW (MHz)	Gain (dBi)	Directivity (dBi)	Total efficiency (%)	Radiation efficiency (%)
<b>Solid copper</b>	100.00	2.40	-24.5	30.0	6.5	7.4	80.4	80.7
<b>1mm uniform</b> 	37.43	2.35	-18.8	27.5	6.1	7.5	72.9	73.8
<b>1mm non-uniform</b> 	22.77	2.40	-38.4	35.0	6.2	7.4	75.1	75.2
<b>4mm uniform</b> 	11.32	2.15	-10.2	n/a	4.2	7.5	42.5	47.0
<b>4mm non-uniform</b> 	7.96	2.26	-19.1	27.5	4.0	7.3	45.6	46.2





**Figure 5-26** Measured electric field gain patterns (in dBi) on  $\phi=0^\circ$  plane of etched

**(a)** 1 mm uniform meshed patch antenna at 2.35 GHz

**(b)** 1 mm non-uniform meshed patch antenna at 2.40 GHz

**(c)** 4 mm uniform meshed patch antenna at 2.15 GHz

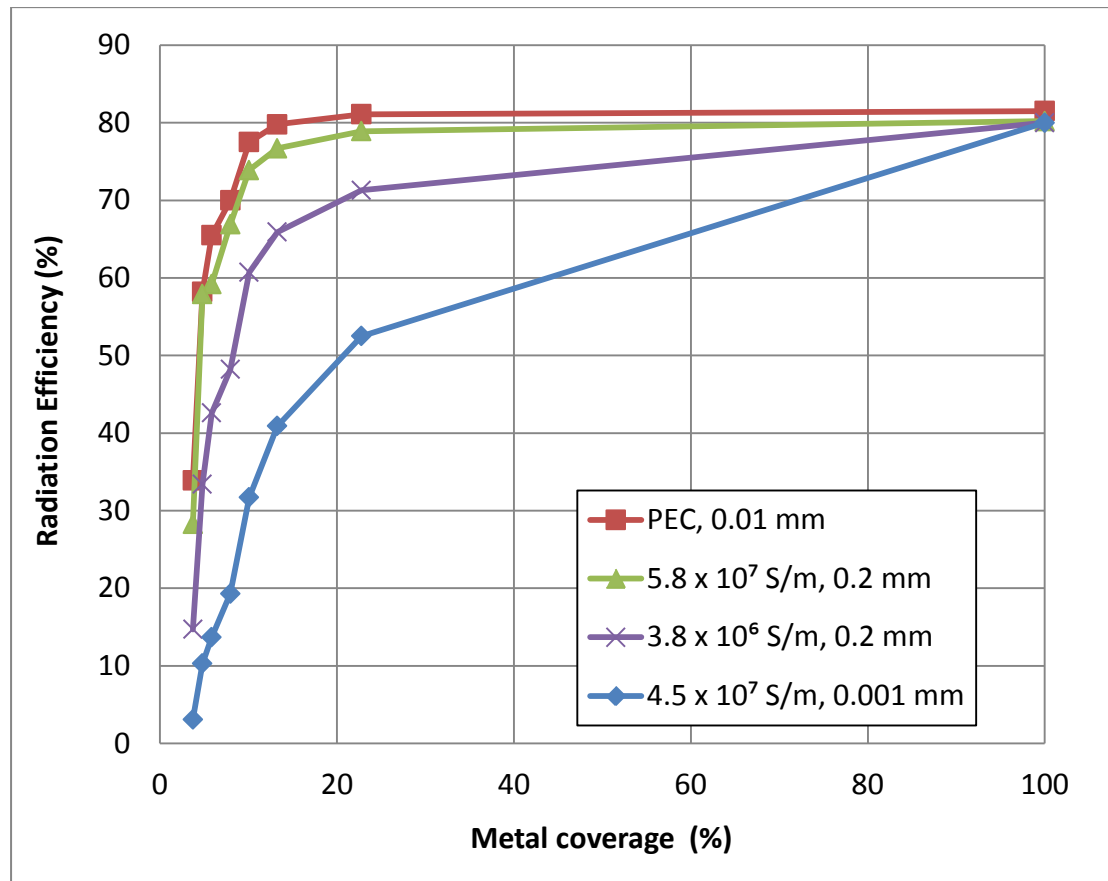
**(d)** 4 mm non-uniform meshed patch antenna at 2.26 GHz



## 5.7 Embroidered Non-Uniform Meshed Microstrip Antennas

### 5.7.1 Skin Effects of Conductive thread on Antenna Efficiency

Chapter 4 has revealed that the thin metallization of Amberstrand Silver thread reduced the embroidered patch antenna efficiency. Likewise, the performance of the non-uniform meshed patch antennas are affected by the skin effect of the conductive thread. In Chapter 2, the equivalent conductivity of the Amberstrand Silver thread is obtained approximately  $4.5 \times 10^7$  S/m. The value is lower than annealed copper ( $5.8 \times 10^7$  S/m). Simulations were made to analyse the effects of the lowered conductivity and the thin coating layer on the non-uniform meshed patch antennas. Four different conductors were used for simulating the non-uniform meshed patch antennas: i) PEC with 0.01 mm thickness, ii) 0.2 mm copper ( $5.8 \times 10^7$  S/m), iii) 0.2 mm low conductivity material ( $3.8 \times 10^6$  S/m) and iv) 0.001 mm Amberstrand Silver ( $4.5 \times 10^7$  S/m). To eliminate the influence of the dielectric loss, all the meshed patches were placed on the same substrate with  $\epsilon_r = 4.5$ , loss tangent = 0.0037 and solid copper ground planes. The radiation efficiencies of different conductive materials are shown in Figure 5-27. The mesh spacing is converted into metal coverage area compared with a solid patch. Clearly, the PEC yields the highest efficiency. The efficiency of the non-uniform meshed patch decreases with lowered conductivities. The thin metallization of Amberstrand Silver results in further reduction of the efficiency. Although the conductivity of Amberstrand Silver is higher than the low conductivity material, the efficiency of Amberstrand Silver meshed patches are lower than the low conductivity material meshed patches with the same metal coverage due to the thinner metallization. It is worth noting that the efficiency of the 1  $\mu\text{m}$  Amberstrand Silver solid patch (100% metal coverage) is very close to the PEC conductor. This indicates the 1  $\mu\text{m}$  metallization has little effects on the solid patch antenna as the conductor surface is continuous. This simulation shows that the thickness of cladding layer is the major limitation on the efficiency of embroidered meshed patch antennas.



**Figure 5-27 Simulation non-uniform meshed patch antennas with different conductive materials and metallization thickness**

Figure 5-27 presents the trade-off between antenna efficiency, conductivity of the thread and metal area coverage. The total thread length usage for embroidering the meshed patch antennas can be easily calculated from the metal coverage. Assuming that the patch surface is entirely covered by the Amberstrand Silver 66 threads i.e. 0 mm mesh spacing, then the thread usage is approximately 7.9 meters if it is embroidered on a 0.5 mm thickness base fabric using 2 mms lock stitches. The thread usage can be reduced by more than 75% if the non-uniform meshing is applied. The cost can be simply estimated by the total thread usage multiplied by the price per unit length. It can provide a guideline for embroidered antenna design. It should be pointed out that this guideline is based on a specific material with rigid substrate and solid copper ground plane. The results will vary with different conductors or dielectric materials.

### **5.7.2 Measured Results of Embroidered Non-uniform Meshed Microstrip Antennas**

The embroidery machine at Loughborough University (see Figure 2-15) was used for fabricating the embroidered meshed patch antennas. A 1 mm spacing non-uniform meshed patch antenna (37 mm × 28 mm) was embroidered onto denim fabric using Amberstrand Silver 66 with 2 mm lock stitches. The embroidered 1 mm spacing non-uniform meshed patch is shown in Figure 5-28. This embroidered patch was placed on the 1.57 mm thick Taconic RF-45 substrate ( $\epsilon_r = 4.5$ , loss tangent = 0.0037) with the same feeding method in Chapter 4. The thermal melt hemming web made from copolyamide was used for the adhesive. The measured antenna performance is shown in Table 5-5. The etched non-uniform meshed copper patch antenna with the same specification (i.e. dimension, mesh spacing) is added as a comparison. As shown in Table 5-5, the resonant frequency of embroidered patch antenna is 60 MHz lower than the equivalent etched copper patch. In addition, the total efficiency of the embroidered meshed patch antenna is 35.8% lower than meshed copper patch. This is partly due to the Amberstrand Silver conductivity and cladding layer thickness. The broken filaments due to the friction during the embroidery are observed (see Figure 5-28). The breakages of the filaments result in higher resistance of the thread which increase the conduction loss. Nevertheless, the denim and hemming web may also introduce losses and changed the dielectric constant value of the substrate. The measured radiation patterns of the embroidered 1 mm non-uniform meshed patch are shown in Figure 5-30.



Figure 5-28 Embroidered 1 mm spaced non-uniform meshed patch on denim fabric

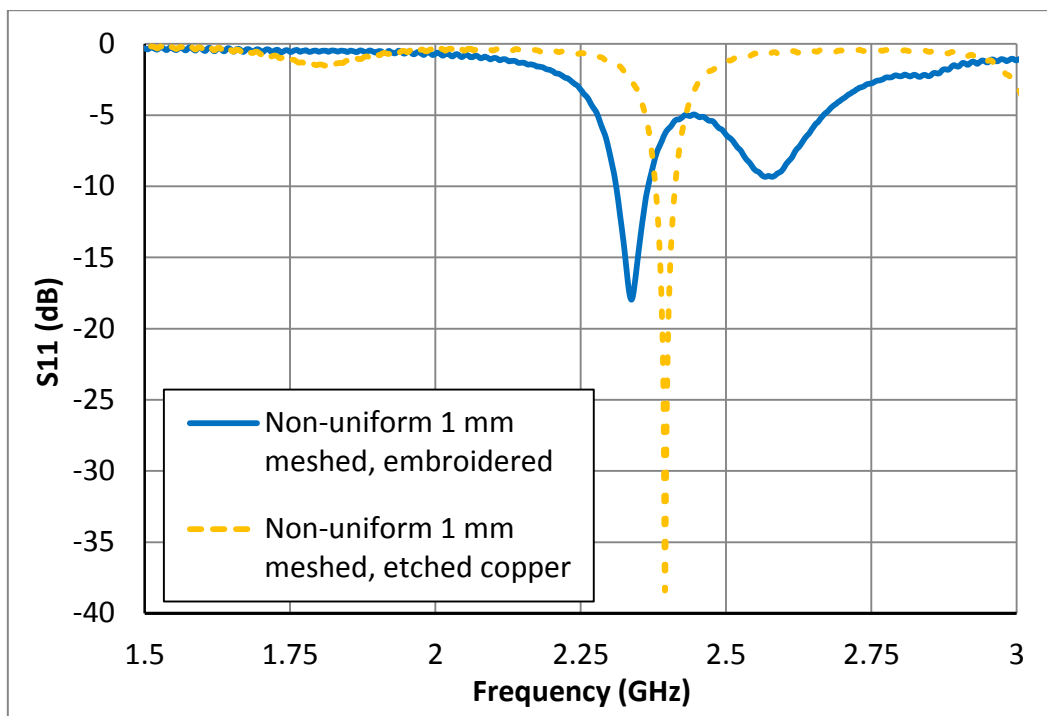
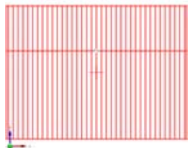
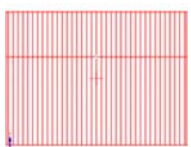
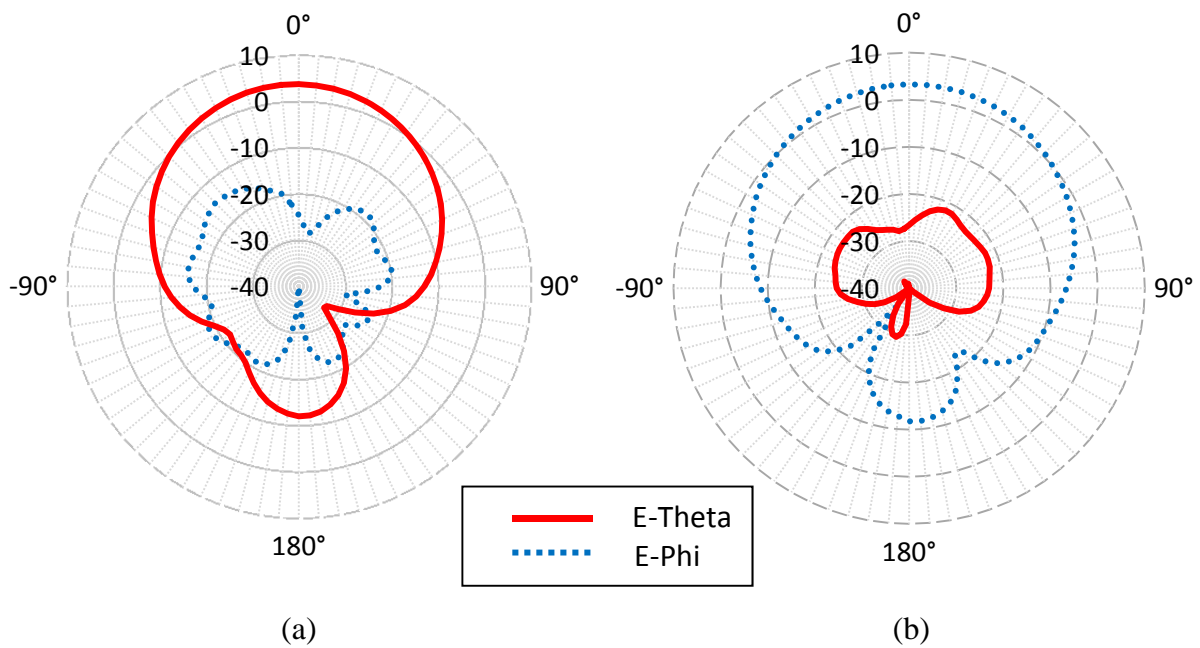


Figure 5-29 Measured S11 results of embroidered and etched 1 mm non-uniform meshed patch antennas

**Table 5-5 Measured results of etched and embroidered 1 mm non-uniform meshed patch antennas**

	Resonant frequency (GHz)	S11 (dB)	10 dB BW (MHz)	Gain (dBi)	Directivity (dBi)	Radiation efficiency (%)	Total efficiency (%)
<b>Embroidered 1mm</b> 	2.34	-18.0	55.0	3.5	7.6	40.0	38.9
<b>Etched copper 1mm</b> 	2.40	-38.4	35.0	6.2	7.4	75.1	75.2



**Figure 5-30 Measured electric field gain patterns (in dBi) of embroidered 1 mm non-uniform meshed patch antenna on (a)  $\phi=0^\circ$  and (b)  $\phi=90^\circ$  planes**

## 5.8 Low Loss Flexible Dielectric Substrate Materials

Section 5.5 showed that there were two way to improve efficiencies of meshed patch antennas: higher conductivity metal and lower loss dielectric substrate. Section 5.7.1 indicated the thin metallization of the conductive thread reduces the embroidered antenna efficiency. Sourcing a dielectric material with low loss factor can overcome the loss that was introduced by the low conductivity and thin cladding layers of the conductive thread.

In Chapter 2 the dielectric properties of several flexible nonconductive fabrics were examined. The structure of the hair-like fibres in textiles creates millions of microscopic holes which are distributed in the fabric. The air gaps are introduced by those holes and the dielectric loss is reduced. Moreover this structure makes the whole fabric soft and flexible, which is suitable for wearable applications. However the disadvantage of the introduced air holes is the reduction of the relative permittivity, which means the geometry sizes of microstrip antennas on these materials will be larger than on the high permittivity substrates.

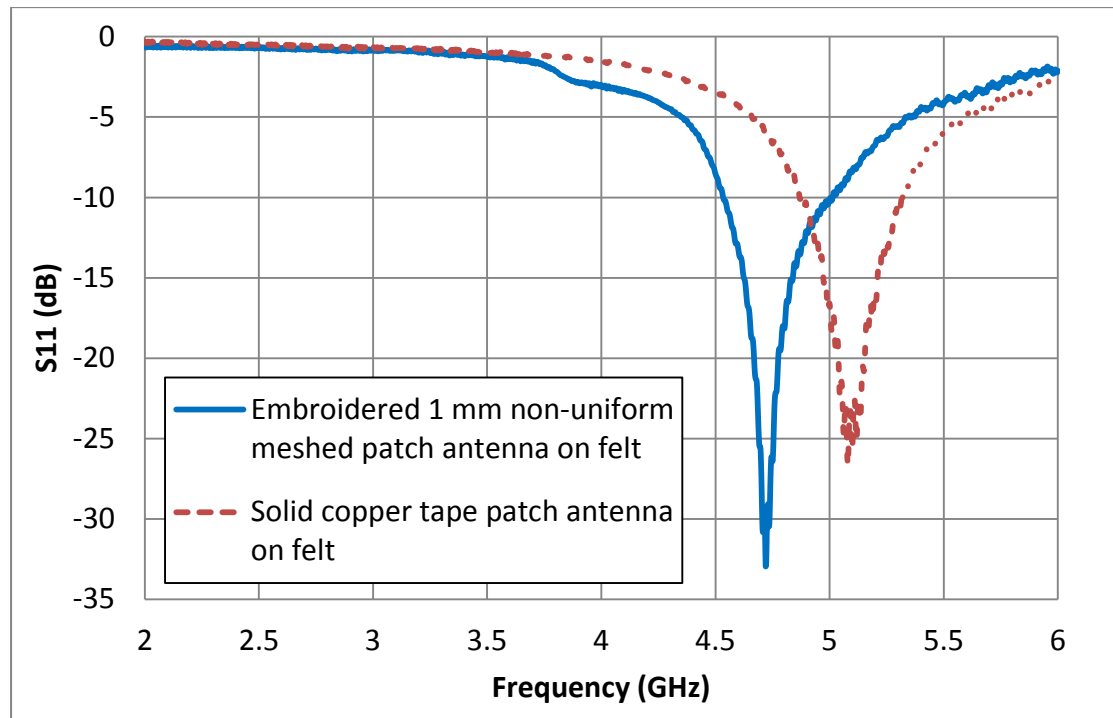
The felt was chosen as dielectric substrate because of its low loss tangent. However due to its low relative permittivity value and thickness, the antenna size had to be increased to work at 2.4 GHz. Due to the limitation of materials, the antennas were re-designed with reduced size to work at 5 GHz band for WLAN application. One 1 mm spacing non-uniform meshed patch was embroidered on denim fabric using Amberstrand Silver 66, and placed on 4.6 mm thick felt substrate using copolyamide hemming web. The exterior dimension of the patch antenna is 28 mm  $\times$  24 mm. The ground plane was made by the copper tape. The embroidered patch is shown in Figure 5-31.



**Figure 5-31 Embroidered 1 mm non-uniform meshed patch antenna on flexible felt substrate**

An equally sized solid copper tape patch on the same felt substrate with copper tape ground plane was made for a comparison. The measured  $S_{11}$  results are shown in Figure 5-32 and antenna efficiencies are shown in Table 5-6. Compared with the solid copper patch on the same felt substrate, the embroidered non-uniform meshed patch has lower resonant frequency. The difference of resonant frequency is 360 MHz, which is larger than the variation of embroidered 1 mm non-uniform meshed 2.4 GHz patch (60 MHz). However, the antenna efficiency of this embroidered non-uniform meshed patch on felt is 60% which is the highest efficiency embroidered patch antenna in this thesis. The 1 mm non-uniform meshed patch has approximately 21.38% metal coverage compared with the solid copper surface area. The total thread usage for embroidering this patch is approximately 1.1 meters includes the extra length due to the lock stitches.



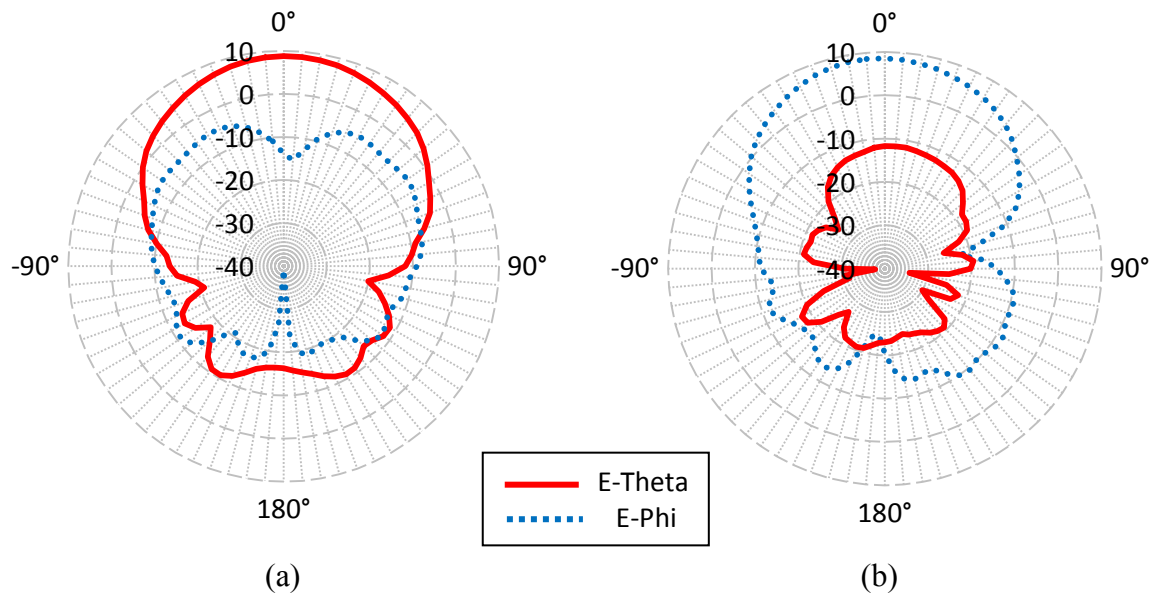


**Figure 5-32 Measured S11 of embroidered non-uniform meshed and solid copper tape patch antennas on felt substrate**

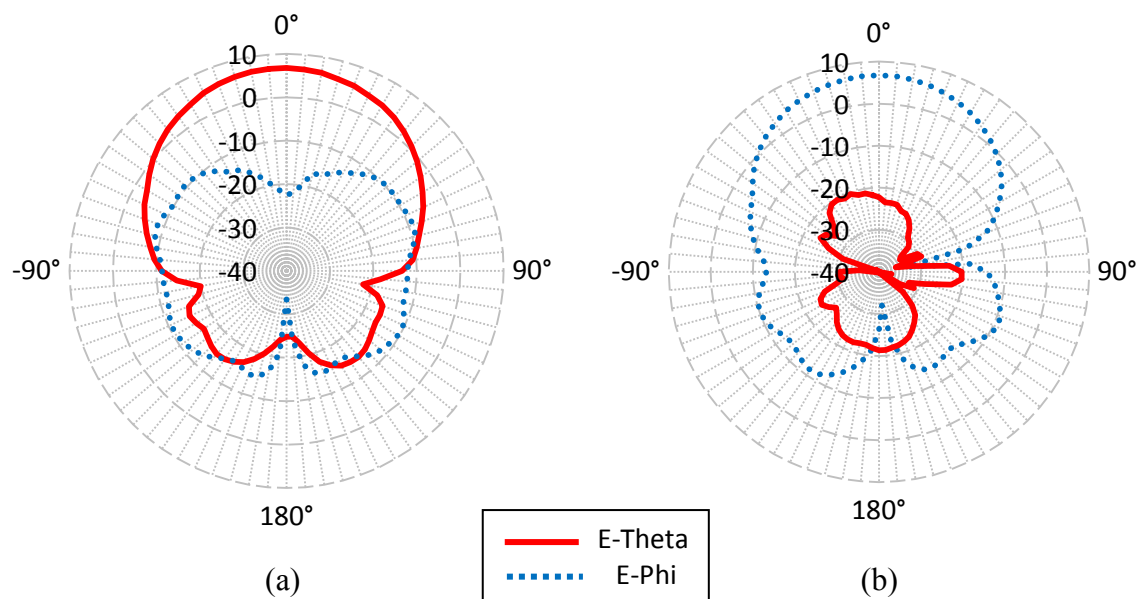
**Table 5-6 Measured copper and embroidered patch antennas on felt substrate**

	Metal coverage (%)	Resonant frequency (GHz)	S11 (dB)	10 dB BW (MHz)	Gain (dBi)	Directivity (dBi)	Radiation efficiency (%)	Total efficiency (%)
Embroidered 1 mm spacing non-uniform mesh on felt	21.38	4.72	-32.9	467.5	6.8	9.0	60	59.8
Solid copper tape on felt	100.00	5.08	-26.4	447.5	8.8	9.1	93	92.8





**Figure 5-33** Measured electric field gain patterns (in dBi) of copper tape patch antenna with felt substrate at 5.08 GHz on (a)  $\phi=0^\circ$  and (b)  $\phi=90^\circ$  planes



**Figure 5-34** Measured electric field gain patterns (in dBi) of embroidered 1 mm non-uniform meshed patch antenna with felt substrate at 4.72 GHz on (a)  $\phi=0^\circ$  and (b)  $\phi=90^\circ$  planes

The radiation patterns of the two patch antennas are very similar (see Figure 5-33 and Figure 5-34). The copper tape patch has slightly larger cross polarization levels at

boresight than the meshed patch. The measured results verified the simulation results in Section 5.3.4. From previous simulation, it is assumed that this decreased polarization level is due to the reduced current paths in the direction perpendicular to the dominant current on the embroidered non-uniform meshed patch.

## 5.9 Conclusions

This chapter presents two meshed structures for patch antenna design: the uniform mesh and the non-uniform mesh. Compared with the same exterior dimension solid patch antenna, the resonant frequencies of the meshed patch antennas are lower due to the meshes. The apertures created by the mesh holes on the patch surface lengthen the electrical length which results in lower resonant frequency. Compared with the uniform meshed patches with the same mesh space, the non-uniform meshed patches have higher resonant frequencies and closer to the resonant frequency of the same sized solid patch antenna. This frequency shift must be considered for meshed patch antenna design.

The non-uniform meshed patch has similar RF performances with the same uniform mesh spacing patch. The current distribution analysis reveals the major current direction for meshed patches is in  $y$  direction at the  $TM_{01}$  mode. The antenna gain and efficiencies between the uniform and non-uniform meshed patches with the same mesh space are very similar. However, the non-uniform meshed patches have slightly higher gain than the uniform meshed patches with the same mesh space. This indicates that the reduction of the current paths which are orthogonal with major current direction does not affect the non-uniform meshed patch antenna performance.

The conductor material usage of meshed patch antennas can be reduced at the cost of decreasing antenna efficiencies. The non-uniform meshed patch gives the advantage in

reducing material cost due to fewer horizontal lines. The etched 1 mm spacing non-uniform meshed patch with the metal coverage less than 1/4 of the solid patch still has 75.2% efficiency which is 5.3% lower than the etched solid patch antenna with 100% metal coverage. This will benefit potential wearable antenna applications since the cost of manufacturing and materials can be reduced.

The embroidered patch antenna has lower antenna efficiency than the etched copper patch due to the low equivalent conductivity value of the conductive thread and the metal thickness. Using high conductivity material which reduces the ohmic loss and low loss substrate which improves the dielectric loss can enhance the antenna efficiency of meshed patches. Flexible fabric substrate materials such as denim and felt were used as the dielectric substrate for the embroidered microstrip antennas. The lower relative permittivity and loss tangent of the felt fabric are capable to improve the loss and achieve high efficiency fabric antennas. A 60% efficiency embroidered flexible fabric patch antenna has been achieved with 21% of the material costs when applying the non-uniform meshes. This is the highly satisfaction outcome in terms of costs, flexibly and antenna performance.

## References

- [1] S. Zhang, A. Chauraya, W. Whittow, R. Seager, T. Acti, T. Dias, and Y. Vardaxoglou, “Embroidered wearable antennas using conductive threads with different stitch spacings,” in *Loughborough Antennas & Propagation Conference (LAPC)*, 2012, pp. 1–4.
- [2] J. L. Volakis, L. Zhang, Z. Wang, and Y. Bayram, “Embroidered flexible RF electronics,” in *IEEE International Workshop on Antenna Technology (iWAT)*, 2012, pp. 8–11.
- [3] Y. Kim, K. Lee, Y. Kim, and Y. C. Chung, “Wearable UHF RFID tag antenna design using flexible electro-thread and textile,” in *IEEE Antennas and Propagation International Symposium*, 2007, pp. 5487–5490.
- [4] A. Chauraya, W. G. Whittow, J. C. Vardaxoglou, Y. Li, R. Torah, K. Yang, S. Beeby, and J. Tudor, “Inkjet printed dipole antennas on textiles for wearable communications,” *IET Microwaves, Antennas & Propagation*, vol. 7, no. 9, pp. 760–767, Jun. 2013.
- [5] Y. Li, R. Torah, S. Beeby, and J. Tudor, “Inkjet printed flexible antenna on textile for wearable applications,” in *Textile Institute World Conference, Selangor, Malaysia*, 2012.
- [6] M. M. Tentzeris, R. Vyas, V. Lakafosis, A. Traille, H. Lee, E. Gebara, and M. Marroncelli, “Inkjet-printed RFIDs for wireless sensing and anti-counterfeiting,” in *6th European Conference on Antennas and Propagation (EuCAP)*, 2012, pp. 3481–3482.
- [7] K. Ito and M. Wu, “See-through microstrip antennas constructed on a transparent substrate,” in *Antennas and Propagation, ICAP 91., Seventh International Conference on (IEE)*, 1991, vol. 1, pp. 133 – 136.
- [8] T. W. Turpin and R. Baktur, “Meshed Patch Antennas Integrated on Solar Cells,” *IEEE Antennas and Wireless Propagation Letters*, vol. 8, pp. 693–696, 2009.

- [9] J. Hautcoeur, L. Talbi, and K. Hettak, "Feasibility Study of Optically Transparent CPW-Fed Monopole Antenna at 60-GHz ISM Bands," *IEEE Transactions on Antennas and Propagation*, vol. 61, no. 4, pp. 1651–1657, Apr. 2013.
- [10] J. R. Saberlin and C. Furse, "Challenges with optically transparent patch antennas," *IEEE Antennas and Propagation Magazine*, vol. 54, no. 3, pp. 10–16, Jun. 2012.
- [11] S. Ahn and H. Choo, "A Systematic Design Method of On-Glass Antennas Using Mesh-Grid Structures," *IEEE Transactions on Vehicular Technology*, vol. 59, no. 7, pp. 3286–3293, Sep. 2010.
- [12] G. Clasen and R. Langley, "Meshed Patch Antennas," *IEEE Transactions on Antennas and Propagation*, vol. 52, no. 6, pp. 1412–1416, Jun. 2004.
- [13] T. Chang, C. Lan, and J. Kiang, "Mesh antennas with reduced size," in *IEEE Antennas and Propagation Society Symposium*, 2004, vol. 4, pp. 3832–3835.
- [14] K. F. Lee and T. Huynh, "Single-layer single-patch wideband microstrip antenna," *Electronics Letters*, vol. 31, no. 16, pp. 1310–1312, Aug. 1995.
- [15] K. F. Lee, K. M. Luk, K. F. Tong, S. M. Shum, T. Huynh, and R. Q. Lee, "Experimental and simulation studies of the coaxially fed U-slot rectangular patch antenna," *IEE Proceedings - Microwaves, Antennas and Propagation*, vol. 144, no. 5, pp. 354–358, 1997.
- [16] R. Bhalla and L. Shafai, "Resonance behavior of single U-slot microstrip patch antenna," *Microwave and Optical Technology Letters*, vol. 32, no. 5, pp. 333–335, Mar. 2002.
- [17] A. A. Deshmukh and K. P. Ray, "Formulation of Resonance Frequencies for Dual-Band Slotted Rectangular Microstrip Antennas," *IEEE Antennas and Propagation Magazine*, vol. 54, no. 4, pp. 78–97, Aug. 2012.

- [18] W. J. R. Hofer, "Equivalent Series Inductivity of a Narrow Transverse Slit in Microstrip," *IEEE Transactions on Microwave Theory and Techniques*, vol. 25, no. 10, pp. 822–824, Oct. 1977.
- [19] X. Zhang and F. Yang, "Study of a slit cut on a microstrip antenna and its applications," *Microwave and Optical Technology Letters*, vol. 18, no. 4, pp. 297–300, Jul. 1998.
- [20] C. A. Balanis, *Antenna Theory: Analysis and Design*, 3rd ed. New York: Wiley, 2005.
- [21] R. Seager, S. Zhang, A. Chauraya, W. Whittow, Y. Vardaxoglou, T. Acti, and T. Dias, "Effect of the fabrication parameters on the performance of embroidered antennas," *IET Microwaves, Antennas & Propagation*, vol. 7, no. 14, pp. 1174–1181, Nov. 2013.
- [22] D. M. Pozar, *Microwave Engineering*, 3rd ed. New York: Wiley, 2005.

# Chapter 6

## Conclusions and Future Work

---

### 6.1 Summary of Research Novelty

This thesis has theoretically, numerically and experimentally investigated the effect of the embroidery parameters on the DC and RF performance of embroidered microstrip transmission lines and antennas using conductive threads. Different embroidery parameters including stitch direction, stitch spacing and the number of filaments in conductive threads has been critically analysed and evaluated. Embroidered low-profile, light-weight and discrete wearable antennas can be integrated into ordinary clothing. State of the art embroidery machines have been used which demonstrates applicability of mass manufacturing wearable textile antennas. This will reduce the cost of manufacturing and boost the acceptance of wearable technologies. The repeatability of embroidered patch antennas has been measured and the effects of stitch spacing on the performance have been analysed.

This thesis has introduced a simulation methodology for realising the anisotropic nature of the embroidered stitches on microstrip antennas. Previously, researchers had only considered the conductive textile as continuous and uniform sheets with low equivalent conductivities. In this thesis, the direction of embroidered stitches and spacing between them were modelled. The embroidered stitches resulted in an anisotropic conductor surface on the microstrip antennas. The simulated results illustrated the distortion of surface currents due to the anisotropic embroidered conductors.

Based on the anisotropic conductor model, a novel non-uniform meshed microstrip antenna has been designed. Patch antennas with the non-uniform mesh structure have a significant reduction of metal coverage but has comparable efficiency to the same exterior sized solid patch antenna. Embroidered non-uniform meshed patch antenna on flexible low loss fabric substrate with improved gain and efficiency has also been fabricated.

A detachable and flexible RF connector made by hook and loop has been designed and measured. This hook and loop connector can be used as ‘switch’ or ‘plug’ for wearable electronics. Electroplating has been applied on the hook and loop connectors to lower the DC resistance and improve the RF performance.

## 6.2 Summary of Results

In Chapter 2, the current techniques of fabricating electro-textiles have been summarised and compared. Embroidery has been chosen to fabricate wearable textile antennas in this thesis due to its high resolution and fabrication advantages applicable to bespoke or mass manufactureable designs. The availability of commercial conductive threads and state of the art embroidery machines can reduce the cost of manufacture. Multifilament conductive thread Amberstrand was chosen as the embroidery thread. The SEM image indicates that the metal coating layer on a single filament is approximately 1  $\mu\text{m}$ . The conductivity of the metal coating layer is estimated as approximately  $4.5 \times 10^7$  S/m. The skin effect should be considered for RF applications. The schematics of embroidered stitches are shown in Chapter 2. The total length of the embroidered thread is determined by the thickness of the base fabric and the stitch length. Optimum fabric thickness and stitch length provides high quality and cost ratio. In addition, the dielectric properties of fabric materials have been examined by using the split post dielectric resonator. The flexible fabric dielectric substrates with low loss tangent were chosen to reduce the dielectric loss of fabric patch antennas.



The DC and RF performances of embroidered transmission lines have been examined in Chapter 3. Conductive threads with more filaments along with close stitch spacing are desirable for low DC resistance and good RF performance. However, stitch direction is the most important fabrication parameter in embroidered transmission lines. Stitch direction that is parallel with the transmission line is recommended to achieve optimal RF performance of the embroidered transmission lines. The detachable and flexible hook and loop connector has also been presented in this Chapter. The reusable connector allows electronics to be removed from the fabric RF system. The improvement of electroplated hook and loop connectors has been presented. Measured results showed that the insertion loss of electroplated hook and loop connectors can be reduced to 1 dB up to 2 GHz.

In Chapter 4 the effects of embroidered stitch direction and spacing on patch antenna performance have been analysed. Close stitch spacing and stitch direction parallel to the dominant current direction results in the highest antenna efficiency. The embroidered patch antenna with 0.4 mm stitch spacing and parallel direction has a 52.5% total efficiency. The same stitch spacing with the stitch direction perpendicular to the current reduces the efficiency by 15%. The 0.4 mm spacing diagonal stitch direction antenna produces 30% efficiency. The diagonal stitches allow vertical and horizontal directed current components which produced a high cross polar component. The zigzag embroidered stitches have been simulated and the results were presented in this chapter. The patch antenna was composed of zigzag conductor and low conductivity “gaps”. The zigzag conductor represented the embroidered thread and the low conductivity “gaps” simulated the contacted filaments between adjacent stitches. The simulated surface current flow indicated that the current followed the direction of the stitches. Various conductivities of the contacting filaments have been simulated and shown the correlation between measurements and simulations. The repeatability of embroidered patch antennas has been examined and the results showed that with the advanced embroidery manufacture technique the embroidered antennas have the potential to be mass manufactured.

Chapter 5 presented the uniform and non-uniform meshed patch antennas. The meshed conductor reduced the metal coverage of the patch antennas and therefore the usage of thread for embroidering could be saved. The non-continuous conductor surface of the meshed patches lowers the resonant frequency. Compared with the uniform meshed patch with the same mesh spacing, the non-uniform meshed patch antenna had a higher resonant frequency. The current distribution analysis revealed that the major current direction on the meshed patches followed the  $TM_{01}$  mode. Although the non-uniform meshed patch has lower metal coverage, the antenna efficiencies of the same mesh spacing uniform and non-uniform meshed patches are very similar. This indicated that the conductor paths in the direction perpendicular to the current can be removed without affecting antenna performance. The measured results indicated that the conductor material usage of meshed patch antennas can be reduced to less than 1/4 at the cost of 5.3% reduction of antenna efficiency.

The non-PEC conductors of the conductive thread lowered the antenna efficiency of embroidered antennas. This conduction loss can be reduced by using high conductivity thread material. On the other hand, fabric materials with large number of air voids have low loss tangent and they can be used as dielectric substrate to reduce the dielectric loss of patch antennas. The embroidered non-uniform patch antennas with 21% metal coverage area on the low loss flexible felt substrate were fabricated. The antenna efficiency was achieved as 60% at 4.7 GHz.

### **6.3 Implications for Industry**

This thesis has shown the feasibility of fabricating wearable fabric antennas using state of the art embroidery technology. The flexible embroidered antennas will not only meet the requirements of the end users but also be capable of meeting industrial manufacture requirements. The capability of the embroidered fabric based antennas including transmission lines and low profile detachable connectors has been presented.

The effects of embroidery parameters on the antenna performance and the optimum embroidery design have been stated. This allows industry to evaluate the cost and performance ratio. These results have implications for many different industrial areas, particular for the manufactures of fabric based wearable antennas. The detailed process will feed into manufacturing and the results will be used to inform the development of representative products that can be potentially mass manufactured.

Many sources estimate that there will be more than 160 million wearable devices in the world in the next three years. Smart textile with mass-manufactureable embroidered wearable antennas will reduce the manufacturing cost and promote the wearable technology market. The fabric antennas will be no longer be limited to specialised applications such as aerospace or military, an affordable price will make them suitable for personal use. For instance, the market of health and fitness monitoring will be benefitted from the fabric based on-body antennas.

The cost of the embroidered antennas will be lowered by applying the non-uniform meshed antennas. Embroidered meshed antenna could produce cost savings compared with using conventional flexible conductors such as Nora Dell. The usage of specialised conductive threads can be further reduced by applying this non-uniform meshed structure, which may reduce the cost of embroidered patch antennas by 75%. This will boost the development of textile wearable technology. The application of the non-uniform meshed structure is not just limited to the embroidered antennas but also can be applied to the inkjet printing for saving the expensive conductive ink.

## **6.4 Future Work**

This thesis has mainly focused on the microstrip antennas. However, other types of antennas such as monopole or dipole can also be considered as embroidered wearable

antennas. The monopole and dipole antenna may suffer from the effects of human body proximity. The body will detune the on-body antennas and result in a resonant frequency shift. Human tissue may absorb a part of the radiated energy and therefore the antenna efficiency will be lower than in free space. Embroidery may be particularly suited to the planar antenna geometry. Further investigation is required to consider other structures of antennas.

In this research a coaxial probe feed was generally used for feeding the microstrip antennas due to the mismatch of embroidered microstrip fed lines. However, the probe feed increases the complexity of manufacture and is inconvenient for low-profile on-body antennas. Alternative feed methods should be investigated in future research to produce thinner antennas and reduce the manufacture processes. The hook and loop connectors can be used combined with planar feed structures to function as switches or transmission line feedings.

The meshed patch antenna showed that the current will be guided by the direction of conductive threads. This feature might be useful in circular polarized antennas such as GPS antennas. The GPS antenna integrated into clothing will be suitable for outdoor activities. Further research could exploit the anisotropic current flow on the orthogonal fibres in the fabric to generate circular polarization.

Embroidery is not only limited to fabricating radiating elements of antennas. It can also be used for directive elements or reflection planes in reflector antennas. The foldable and portable corner reflector or parabolic antennas can be realised by the embroidered fabric reflectors which can be folded like an umbrella when not in use. This light-weight and portable reflector antennas will be appropriate for applications which require both mobility and functionality. In addition, embroidery is also potentially capable of creating RF printed circuit boards. Making fully fabric and flexible electronic system using embroidery will realise the fully flexible fabric

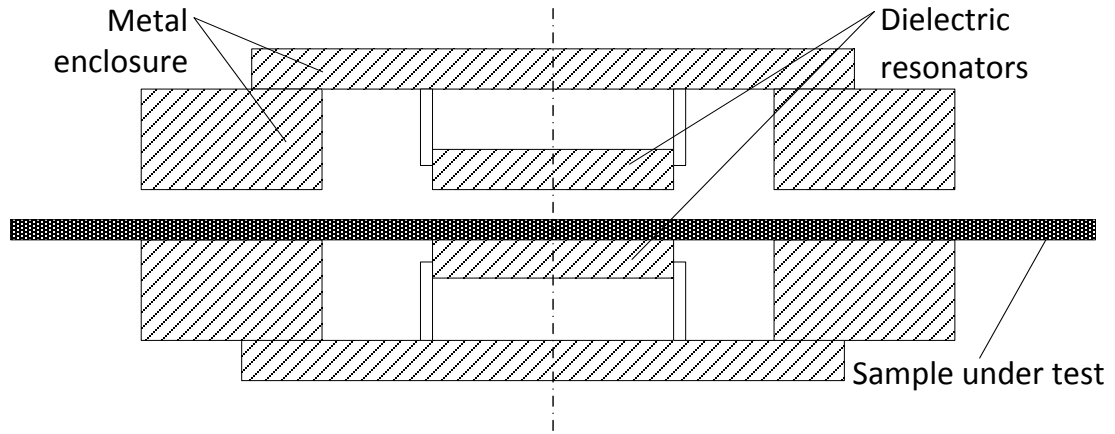
wearable electronics. Investigation of electromagnetic properties of embroidered coplanar circuit board is required for this development.

# Appendix A

## Split Post Dielectric Resonator

---

This appendix summarise the method for using dielectric properties in the Section 2.4. The microwave Q meter can be used to measure the S21 results of split post dielectric resonator without vector network analyser (VNA). By measuring the quality factors (Q) of the empty resonator and with the dielectric material in the resonator, the permittivity and loss tangent can be calculated [1], [2].



**Figure A-1 Schematic diagram of a split post dielectric resonator (redrawn from [2])**

The real part of the permittivity of the fabric material under test can be obtained by

$$\epsilon'_r = 1 + \frac{f_0 - f_s}{hf_0 K_\epsilon(\epsilon'_r, h_s)} \quad (\text{A.1})$$

Where  $f_0$  is the resonant frequency of empty resonator,  $f_s$  is the resonant frequency with fabric sample,  $h_s$  is the thickness of the fabric sample and  $K_\epsilon$  is the function of  $\epsilon'_r$  and  $h_s$ . By definition  $K_\epsilon$  function values were found for a given resonator and fixed  $\epsilon'_r$  and  $h_s$  as

$$K_\epsilon(\epsilon'_r, h_s) = \frac{f_0 - f_s}{(\epsilon'_r - 1)h_s f_0} \quad (\text{A.2})$$

Exact resonant frequencies and the values of  $K\varepsilon$  are computed for a number of  $\varepsilon'_r$  and  $h_s$  for a given resonator and in tabulation. Interpolation will be used to compute  $K\varepsilon$  for other values of  $\varepsilon'_r$  and  $h$ . The initial value of  $K\varepsilon$  in permittivity evaluation (using (1)) is taken to be the value for  $\varepsilon'_r = 1$  and a given thickness of sample. Subsequent values of  $K\varepsilon$  can be found for the subsequent dielectric constant values obtained in the iterative procedure. Because  $K\varepsilon$  is a slowly varying function of  $\varepsilon'_r$  and  $h_s$  so the iterations using equation (1) converge rapidly.

The loss tangent of the fabric sample can be determined by (A.3)

$$\tan\delta = \frac{Q^{-1} - Q_{DR}^{-1} - Q_c^{-1}}{P_{es}} \quad (\text{A.3})$$

where the  $Q$  is the unloaded Q factor of the resonator containing the fabric sample under test,  $Q_c$  is the Q factor depending on metal losses for the resonator containing the fabric sample.

$$Q_c = Q_{c0} K_2(\varepsilon'_r, h_s) \quad (\text{A.4})$$

where  $Q_{c0}$  is the Q factor depending on metal losses for empty resonator.

$P_{es}$  is the electric energy filling factor of the fabric sample defined as

$$P_{es} = h\varepsilon'_r K_1(\varepsilon'_r, h_s) \quad (\text{A.5})$$

$Q_{DR}$  is the Q factor depending on dielectric losses in the resonator

$$Q_{DR} = Q_{DR0} \frac{f_0 P_{eDR0}}{f_s P_{eDR}} \quad (\text{A.6})$$

$P_{eDR}$  and  $P_{eDR0}$  is the electric energy filling factors for the resonator that contained the fabric sample and empty respectively.  $Q_{DR0}$  is the Q factor depending on dielectric losses in empty resonator. Similar to the function  $K\varepsilon$ ,  $K_1$  and  $K_2$  are the functions of  $\varepsilon'_r$

and  $h_s$  and are also in tabulation. Interpolation is used to compute the values of these functions for specific values of  $\epsilon_r^*$  and  $h$ .

The Q factor is obtained by measuring the -3 dB bandwidth of the S21 using either network analyser or the Q meter.

$$Q = \frac{f_r}{\Delta f} \quad (\text{A.7})$$

Where  $f_r$  is the resonant frequency and the  $\Delta f$  is the -3 dB bandwidth.

The specifications of the empty split post dielectric resonator are included in the file of the resonator and the functions above have been integrated into the software. After measuring the thickness of the sample and the Q factors for the loaded and empty resonator, the permittivity and loss tangent can be obtained using the microwave Q meter software.

## References

- [1] J. Krupka, "Measurements of the complex permittivity of microwave circuit board substrates using split dielectric resonator and reentrant cavity techniques," in *Seventh International Conference on Dielectric Materials, Measurements and Applications*, 1996, pp. 21–24.
- [2] J. Krupka, A. P. Gregory, O. C. Rochard, R. N. Clarke, B. Riddle, and J. Baker-Jarvis, "Uncertainty of complex permittivity measurements by split-post dielectric resonator technique," *Journal of the European Ceramic Society*, vol. 21, no. 15, pp. 2673–2676, Jan. 2001.